BEACH HYDROLOGY:

IMPLICATIONS FOR BEACH QUALITY ALONG SOUTHERN GEORGIAN BAY, CANADA

BEACH HYDROLOGY:

IMPLICATIONS FOR BEACH QUALITY ALONG SOUTHERN GEORGIAN BAY, CANADA

By

NATALIE E. SPINA, B.Sc

A Thesis

Submitted to the School of Graduate Studies

In Partial Fulfillment of the Requirements

For the Degree

Master of Science

McMaster University

MASTER OF SCIENCE (2011) **McMaster University**

Earth and Environmental Science **Hamilton, Ontario**

TITLE: Beach Hydrology: Implications for Beach Quality Along Southern Georgian Bay, Canada

AUTHOR: Natalie E. Spina, B.Sc. (McMaster University)

SUPERVISOR: Professor James E. Smith

NUMBER OF PAGES: xvi, 198

ABSTRACT

Recreational beaches of the Great Lakes play a critical role in the quality of life for beach goers and contribute to the economic and environmental health of the Great Lakes region. Over the past decade, concerned local residents, municipalities, and public beach goers have observed the deteriorating beach quality along the shores of the Great Lakes. Numerous problems exist at these beaches including: high levels of *E.coli*, encroachment of invasive and non-native vegetation, iron staining, loss of sand. However, the more pervasive problem appears to be increased wet conditions at beaches that use to be dry. This study was undertaken to investigate the physical and hydrological factors that control wet and dry beaches, in order to determine why these beaches exist. Combined field, laboratory, and modelling methodologies were used to characterize four beach sites and calibrate beach models along southern Georgian Bay in Tiny Township, ON. The results of this research indicate that there are three interconnected factors that influence wet and dry beaches, including: (1) texture of a beach, (2) depth to the water table, and (3) elevation of the ground surface. Texture is the primary factor that controls the moisture conditions at a beach even though all beaches were classified as sands. This is a consequence of the fact that fine grained sands have significantly higher capillary rise and retain higher moisture contents above the water table compared to coarse grained sands. Depth to the water table influences the moisture conditions at a beach through its association with the relative position of the top of the capillary rise within respect to the surface of the beach. Ground surface elevation influences the depth of sand above the water table at a beach; lower and flatter surface elevations have the water table (and capillary rise) closer to the beach surface than at beaches with steeper elevations. In summary, wet beaches have high moisture contents at and near the surface of a beach (> 10 %), shallow water tables (~ < 50 cm), and flat ground surface elevations. Dry beaches have low moisture contents at and near the surface of a beach (< 10 %), deep water tables (~ > 50 cm), and steep ground surface elevations. Using the numerical model HYDRUS-2D, four calibrated beach models provide a framework for beach managers to gain insights into beach quality issues through scenario testing. Beaches with shallow water tables and flat surface elevations (either natural or human-induced) are at greater risk of becoming wet under high lake level scenarios than beaches with steeper surfaces (dry beaches). Heavy precipitation events are temporary and do not convert dry beaches into wet beaches and high evaporation rates do not convert wet beaches into dry beaches; conversion of beaches is mainly influenced by beach surface alterations (e.g. bulldozing and removing sand dunes). The conclusion of this study is that hydrological factors are primary controls on the quality of the beaches and the associated problems along the shores of the Great Lakes.

Keywords: hydrology, sand texture, Great Lakes, beaches, beach management, numerical modelling

ACKNOWLEDGEMENTS

I would first and foremost like to thank my supervisor Dr. James E. Smith for his mentoring and ongoing support throughout my many years at McMaster University. I have thoroughly enjoyed this learning opportunity and developed a skill-set and confidence that I will be able to apply well beyond my world of academia. I would like to also thank Dr. Allan S. Crowe from the National Water Research Institute of Environment Canada for providing me with the opportunity to collaborate on this project. Thank you for your guidance, support, and helpful words of encouragement throughout this experience.

Thank you to my lab-mates for creating a fun and enjoyable work environment. A special thanks to Heather McLeod for her helpful advice and detailed edits on my thesis, to Kevin Evelegh for his encouragement and sense of humor during the challenging moments, and also to Jennie Kirby for her moral and technical support during this project.

I would like to thank the NSERC Discovery Grant to James E. Smith and Environment Canada for their financial support for this project. My appreciation goes to Andreanne Barnes and Charles Talbot from the Environment Canada Technical Operations team who provided me with a valuable skill-set and assistance with fieldwork.

Last but not least, thanks to my friends and family for their understanding and endless patience, especially to my mom and dad for their love and continuous words of encouragement; I can see the light at the end of the tunnel.

TABLE OF CONTENTS

LIST OF FIGURES

LIST OF TABLES

LIST OF APPENDIXES

1.0 INTRODUCTION

1.1 Problem Scope

Recreational beaches of the Great Lakes are critical to the quality of life for beach goers and local residents. Beaches play a significant role in the economic and environmental health of the Great Lakes region (IJC Report, 2011). Over the past decade however, the quality and aesthetics of the beaches along the Great Lakes has been deteriorating. Several persistent problems are observed along the beaches, including: high levels of *Escherichia coli* (*E. coli*) (Whitman and Nevers, 2003), invasive species (e.g. Phragmities, sedges, and rushes) (Crowe and Milne, 2007), septic system contamination (Robertson *et al.*, 1991), iron staining, loss of sand (erosion), and wet conditions (wet sand, ponding water, and surface runoff). In addition, there has been an increase in human activity altering the beaches including: bulldozing the sand dunes, installing break walls, installing sewer and tile drains that redirect runoff and groundwater to the lake, ATVing on the beaches, paved parking lots adjacent to beaches, and also planting nonnative species (i.e. turf grass). These activities may be factors contributing to the degrading quality of beaches of the Great Lakes. As a result, concerned public beach visitors, local residents, and municipalities are demanding actions and answers on why their beaches are deteriorating.

Several studies have focused their research on one of the beach problems: *E. coli* contamination, due to the human health implications associated with high levels (Whitman and Nevers, 2003; Alm *et al.*, 2006; Beversdorf *et al.*, 2006). The other beach problems however, have received little or no attention, and continue to degrade the quality of the beaches of the Great Lakes. Recently, Crowe and Milne (2007) characterize the beaches of the Great Lakes into two categories: wet beaches (natural and degraded) and dry beaches (natural). The characteristics of wet beaches include wet sand at and near ground surface, ponded water after a heavy rainfall, a

shallow water table, and hydrophytic vegetation (e.g. sedges, rushes, and cattails). Wet beaches are typically associated with various beach problems such as *E. coli* in the groundwater, wet conditions, and the presence of invasive vegetation (i.e. *Phragmites australis*). Dry beaches are characterized by dry sand at and near the surface, sand dunes that contain native beach grass (*Ammophila breviligulata*), and a deep water table. Beach problems are rarely present at dry beaches (Crowe and Milne, 2007). This study suggested that wet beaches provide conditions suitable for the infiltration of water and contaminants (e.g. *E. coli)* to the groundwater, and retention of water near the surface that provides suitable conditions for hydrophytic vegetation and turf grass. Crowe and Milne (2007) also suggested that dry beaches with deep water tables do not permit infiltration to the water table nor do dry beaches retain water in the sand close to ground surface. It is currently unclear why wet and dry beaches exist and also why the quality of several of the beaches around the Great Lakes are deteriorating.

1.2 Research Objectives and Hypotheses

1.2.1 Objectives

From a practical perspective, the knowledge gained in this study will provide the scientific basis for understanding why problems exist only at wet beaches, and for the restoration and sustainability of beaches of the Great Lakes. This study will focus on investigating the backshore area of beaches of the southern Georgian Bay. In this thesis the backshore area of a beach is defined as the area of sediment from the swash zone inland to the base of the foredunes (Figure 2.1). Specific field and laboratory objectives of this study are:

1. Determine if depth of the water table and elevation of the ground surface influence whether a beach is a wet beach or a dry beach

2. Determine if there are textural (grain size distributions) and structural (porosity, saturated hydraulic conductivity, bulk density, and moisture content) factors controlling whether a beach is wet or dry

Numerical modeling objectives of this study are:

1. Determine how lake level fluctuations along with beach topography influence wet and dry beach conditions using HYDRUS-2D simulations
2. Determine how precipitation events affect the moisture contents at wet and dry beaches using HYDRUS-2D simulations
3. Determine how evaporation affects the moisture contents at wet and dry beaches using HYDRUS-2D simulations
4. Determine if the removal or addition of sand converts a dry beach into a wet beach, and vice versa using HYDRUS-2D simulations

1.2.2 Hypotheses

1. The moisture content of beaches are due to:
    i. the depth to the water table
    ii. the grain size distribution of the sand and associated water retention characteristics
2. The textural and structural properties of the sand at wet and dry beaches promote or restrict infiltration
3. Evaporation only influences the moisture contents at the surface of wet and dry beaches
4. Adding or removing sand influences the moisture conditions at a beach

This study will use a combination of field, laboratory, and modelling methodologies. Field and laboratory techniques will be used to characterize the physical and hydrological properties of wet and dry beaches at four beach sites along the shore of southern Georgian Bay. Modelling simulations will be used to provide insight and a better understanding of the fundamental processes and factors controlling the existence of wet and dry beaches, as well as, associated beach management issues.

2.0 BACKGROUND LITERATURE

2.1 History of Beaches of the Great Lakes: Formation and Management

A beach is defined as "*the gently sloping shore of a body of water which is washed away by waves or tides, especially the parts covered by sand or pebbles*" (Figure 2.1) (AGI, 1962). The formation of a beach is the result of waves, currents, and/or tides that deposit, erode, and sort sediments, and in turn control to the character of a beach (Trenhaile, 2007). The beaches of the Great Lakes were formed at the end of the Wisconsinan Episode glaciation, when melt water from the retreating glaciers created large glacial lakes and streams, depositing sediments (Chapman and Puntman, 1984). Post-glacial isostatic rebound of the earth's crust formed the present basins of the Great Lakes and their drainage systems (Chapman and Putnam, 1984). The beaches of the Great Lakes formed as a result of breaking waves eroding and depositing the glacial sediments along the shores of the former post glacial lakes and present Great Lakes (Chapman and Putnam, 1984).

Management of the Great Lakes region, including its waters and beaches, is necessary in order to sustain healthy beaches and water quality. Existing management and planning policies focus their efforts on protecting the water quality of the Great Lakes. There is been less focus pertaining to the rise and root cause of the beach problems that are located in the backshore area

of beaches. Several challenges arise in managing and governing the vast region of the Great Lakes, due to the large size of the Great Lakes basin and the interconnection of the shorelines among several different jurisdictions. As such, in 1909, the International Joint Commission (IJC) was formulated to assist governments from Canada and the United States to collectively manage, protect, and find solutions to problems of the Great Lakes region (IJC Report, 2011). The IJC however, mainly focuses on addressing concerns of the nearshore environment instead of the backshore environment of beaches, including: eutrophication, groundwater quality, fish consumption, and invasive aquatic species (IJC Report, 2011). More effort is required in monitoring and managing the backshore area of beaches in order to restore and protect the quality of the beaches along the shores of the Great Lakes.

2.2 Groundwater Dynamics at Beaches

Numerous studies have investigated groundwater conditions below beaches in marine environments (*see reviews by* Baird and Horn, 1996; Horn, 2002 & 2006). However, these studies focus on the effects of waves and tides on groundwater conditions and swash zone dynamics. Currently, there is a lack of literature that investigates groundwater dynamics below the beaches of the Great Lakes. In fact, there is only one study by Crowe and Meek (2009) that characterize the groundwater conditions below the beaches of the Great Lakes. Although beaches in marine environments are influenced by different processes (salt-water intrusions, tides, large scale waves, sea level changes), than at fresh water beaches (fresh water, small-scale waves, fluctuating lake levels, seasonal influences such as snow melt) some processes that affect groundwater conditions at marine beaches can be applied to the beaches of the Great Lakes; these processes will be discussed in this section.

2.2.1 Groundwater Flow below the Backshore Area of Beaches

The groundwater system at a beach is a dynamic, shallow, unconfined aquifer system that is influenced by atmospheric exchanges, waves, swash, tides (Horn, 2002) and/or lake level changes (Crowe and Meek, 2009). Within a beach, the water table (where pore pressures equal atmospheric pressure) and it's shape and elevation is controlled by the physical characteristics of the porous medium, tides, waves, and precipitation (Gourlay, 1992). Below the beach, the water table slopes towards the adjacent water body, and given the high hydraulic conductivity of the sand, groundwater flow is essentially one-dimensional (horizontal) towards the lake (Crowe and Meek, 2009).

Under hydrostatic conditions (when the lake is calm), groundwater exits the beach and discharges vertically (upward) into the lake (Figure 2.2a) (Cherkauer and McKereghan 1991; Baird and Horn, 1996; Ullman *et al.*, 2003; Crowe and Meek, 2009). Under hydrodynamic conditions (wave runup) (Figure 2.2b) however, lake water infiltrates into the swash zone (see *Section 2.2.2*), and hence a localized and short-term reversal in the direction of groundwater flow occurs but only at the swash zone (Turner and Nielsen, 1997; Horn, 2002 & 2006; Austin and Masselink, 2006; Cartwright *et al.*, 2006; Meek, 2007).

2.2.2 The Swash Zone

The swash zone is defined as the nearshore zone of a beach, where the beachface is exposed to the continuous uprush and downrush from waves (Trenhaile, 2004) (Figure 2.2b). Several studies have investigated the complexities of groundwater flow within the swash zone at beaches (Horn, 2002 & 2006; Austin and Masselink, 2006; Cartwright *et al.*, 2006). Field evidence has indicated that the water table often fluctuates and becomes disconnected in this zone from the

adjacent water body (Horn, 2002 & 2006; Meek, 2007). Then when this occurs, a seepage face develops and the groundwater discharges above the adjacent water body at the shoreline (Horn, 2002 & 2006). In addition, a seepage face can also develop when a well-developed capillary fringe (defined as saturated pores above the water table under negative pressure) intersects the surface (Neba *et al.*, 2002). Within the swash zone, waves continuously runup and rundown the beachface, allowing water to infiltrate into the unsaturated zone (above the water table) and exfiltrate through the seepage face (Grant, 1948; Turner and Masselink, 1998; Austin and Masselink, 2006). Infiltration of lake water into the swash zone by waves has been observed to generate a groundwater divide (water table mound) that forces inland flow (Figure 2.2b) (Meek, 2007).

2.2.3 The Capillary Fringe and Capillarity

Above the water table, there is a zone of saturated porous media with pore pressure less than zero, known as the capillary fringe (Figure 2.2). The capillary fringe is examined in beach studies due to its role in water table fluctuations (Gillham, 1984; Hegge and Masselink, 1991; Turner, 1993a & b; Li *et al.*, 1997; Debrasch *et al.*, 1999). The capillary fringe forms as a result of multiphase flow, where a wetting fluid (water) displaces a nonwetting fluid (air) through imbibition (defined as the process of wetting) (Ronen *et al.*, 2000). Moisture is thereby held within the individual pore spaces by the phenomenon of capillarity (Hillel, 1998). At the pore scale, pressure (capillary pressure) exists at the air-water interface (Figure 2.3), which is explained through the following capillarity equation:

$$\psi = -\frac{2\gamma \cos\theta}{\rho g r} \qquad (2.1)$$

where; ψ represents soil water pressure in head units [L], γ represents the interfacial tension between both fluids [F/L], θ represents the contact angle [degree], r represents the radius of curvature of the curved menisci [L], ρ represents the density of water [M/L^3], and g represents the

gravitational constant [L/t^2] (Bear, 1979). Because capillarity is controlled by the radius of curvature of the curved menisci between soil grains (*r*), the physical characteristics (texture and structure) of a soil play an important role in controlling the amount of moisture retained within that soil.

Small additions of water from waves and/or precipitation that infiltrate to the capillary fringe have been found to create an instantaneous rise of the water table at beaches (Hegge and Masselink, 1991; Turner, 1993a & b; Li *et al.*, 1997; Debrasch *et al.*, 1999). This phenomenon was first recognized by Gillham (1984) who applied small additions of water to the ground surface and observed a water table rise of 30 cm within the first 15 seconds of application. Because the capillary fringe holds pore water under negative pressure (suction) and is saturated; small additions of water releases the tension within the pores, increasing pore pressure (from negative to positive pore pressure), therefore inducing a water table rise (Gillham, 1984; Hegge and Masselink, 1991; Turner 1993a & b; Li *et al.*, 1997; Debrasch *et al.*, 1999). Furthermore, the height of water table rise is controlled by the physical characteristics of the porous medium (grain size distribution, bulk density, porosity heterogeneities). Fine grains have smaller pores and as a result in a larger rise of the water table through capillarity compared to coarse grains (Gillham, 1984; Abdul and Gillham, 1984; Turner, 1993a; Debrasch *et al.*, 1999).

2.2.4 Beach Water Table Fluctuations

i. Tidal Influences (Coastal Beaches)

The influence of tides on water table elevations has been extensively studied on coastal beaches (Emery and Foster, 1948; Nielsen, 1990 & 1999; Turner, 1993a, b, c; Turner and Nielsen, 1997; Jackson *et al.*, 1999). During a rising tide (flood tide), water infiltrates into the beachface causing the water table to rise, where as, during a falling tide (ebb tide), water will drain from the

beachface and will fall (Jackson *et al.*, 1999). Emery and Foster (1948) was the first study to observe a lag in response time of the water table due to tidal forcing. During a falling tide, field evidence indicated that the water table continued to rise (forming a mound shape), instead of instantaneously falling with the tide. The response of the water table to the tide was controlled by the physical characteristics (e.g. grain size, bulk density, porosity, and permeability) of the beach sand (Emery and Foster, 1948). Fine-grained sands generally have high bulk densities, smaller pore spaces, and low permeabilities compared to coarse-grained sands, therefore, a water table mound occurs because the rate of drainage from the beachface is slower compared to the rate of the falling tide (Emery and Foster, 1948). Consequently, a water table mound acts as a groundwater divide, reversing the flow of groundwater (Figure 2.2b) (Freeze and Cherry, 1979; Abdul and Gillham, 1989; Nielsen, 1990; Turner and Nielsen, 1997; Nielsen, 1999). As a result, contaminants from the adjacent water body can travel inland, contaminating the beach aquifer (Nielsen, 1990 & 1999).

ii. Seasonal Variations (Beaches of the Great Lakes)

Although groundwater flow at beaches has been extensively studied in coastal environments, a lack of information has been presented quantifying the groundwater flow conditions below the beaches of the Great Lakes. Crowe and Milne (2007) investigated water table positions at wet and dry beaches of the Great Lakes. The depth of the water table at wet beaches is approximately 0.5 m or less, measured about 20 m from the lake, and the depth to the water table at dry beaches is approximately 1.0 m or more, measured about 20 m from the lake. Crowe and Meek (2009) found water tables fluctuated as a result of seasonal changes in lake levels and infiltrating precipitation and snow melt. Because the lake acts as the point of discharge for groundwater below the beach, the water table will fluctuate proportionally to the lake level changes

(rise and fall of the discharge point) (Crowe and Meek, 2009). Furthermore, the position of the water table at these beaches is highest in the spring due to increased infiltration from snowmelt and high lake levels, and lowest in the winter due to reduced infiltration and low lake levels (Crowe and Meek, 2009).

It was also noted that water does not flow from the lake into the groundwater below a beach during a seasonal or long-term rise in the lake level because these lake level changes are relatively slow compared to the rate of groundwater flow/discharge into the lake. Hence, seasonal and long-term lake level changes do not cause a reversal in the direction of groundwater flow or a water table mound at the groundwater-lake interface. However, as discussed in the previous section, short term lake-level changes due to wave runup during storms will cause the movement of lake water into the aquifer, reversals in the direction of groundwater flow, and the formation of a groundwater mound at the shore (Figure 2.2b) (Meek, 2007).

2.3 The Role of Texture and Structure in Soil Hydrology

The beaches of the Great Lakes are predominantly classified as sand and/or gravel beaches, which are typical textural characteristics along the shores of glacial lakes (Trenhaile, 2004). There is a lack of information presented in literature regarding a detailed analysis of the grain size distribution of beaches of the Great Lakes. Studies of these beaches generally provide a qualitative observation of the average textural class of the beach sediment, rather than providing a detailed and quantitative range of the variations in grain sizes from the beaches (Crowe and Milne, 2007; Darke and McKenna-Newman, 2008; Crowe and Meek, 2009; Skalbeck *et al.*, 2010). Crowe and Milne (2007) characterized the average texture of the beaches along southern Georgian Bay as well-

sorted coarse sand, with fine to medium grained sand comprising the sand dunes on the leeward side of the beach.

The textural (grain size distribution) and structural (bulk densities, porosity, and moisture content) properties of a porous media influence capillarity, and hence the moisture content of the porous medium (Luthin and Miller, 1953; Bear, 1979; Gillham, 1984; Hillel, 1998; Romano *et al.*, 1999; Silliman *et al.*, 2002; Dunn and Silliman, 2003). Specifically, textural and structural properties influence the ability of a soil to retain moisture. As shown in Figure 2.4, fine-grained soils have a high ability to retain moisture under low pressures (high capillary pressures) compared to coarse grained soils (Schwartz and Zhang, 2003; Yang *et al.*, 2004). Hence a beach composed of fine sand will contain higher moisture contents than a beach composed of coarse sand. Also, soils with large pores (e.g. coarse grained sands) preferentially drain as a result of weak capillarity between large pores (Luthin and Miller, 1953). Furthermore, heterogeneities within a soil can also influence the moisture-retention properties. For instance, a soil with a mean grain size distribution of a coarse grained sand that is poorly sorted, can in fact resemble the soil moisture retention characteristics of a fine sand (Romano *et al.*, 1999). This is because the poorly sorted grains can fill the pore spaces around larger grains, affecting the capillarity of that soil. When assessing the moisture content of the sand at beaches, it is therefore important to not only characterize the texture of the sand, but also to understand the heterogeneities present within the sand at the beach.

2.4 Beach Topography

2.4.1 Influences of Sediment Erosion and Deposition

It is well known that beaches are dynamic and rarely reach an equilibrium state, because they are continuously exposed to erosion and depositional processes. The morphology of beaches of

the Great Lakes are also highly variable even though they formed during the same glaciation event. Flat and sloped surface topographies of beaches exist within close proximities to each other along the shores of the Great Lakes (Crowe and Milne, 2007). Once a beach is altered, whether by natural (wind and wave erosion and deposition) or anthropogenic influences (e.g. bulldozing), the topography will change until a new state of equilibrium is reached (if ever) (Lundgren, 1986). Figure 2.5 provides a schematic overview of the varying surface topographies observed at beaches, which will be discussed in this section.

Sand dunes form as the result of wind erosion and deposition (Aeolian sediment transport) and are present on the leeward side of several beaches surrounding the Great Lakes (Crowe and Milne, 2007; Crowe and Meek, 2009). Studies have investigated the relationship between surface moisture content and Aeolian sand transport (erosion and deposition) at beaches (Wiggs *et al.*, 2004; Oblinger and Anthony, 2008; Darke and McKenna-Newman, 2008). As the moisture content of the sand at ground surface increases, the rate of sand removal by wind decreases because high moisture contents increase the bulk mass and cohesion of the sand. As a result, very high wind energy is required to remove, transport, and deposit the sand grains to another location on the beach (Jackson and Cooper, 1999; Yang and Davidson-Arnott, 2005). Furthermore, moisture content heterogeneities present in beaches can result in an alternating bar and trough (also known as dune and swale) surface topography; where bars are comprised of dry sand and troughs are comprised of wet sand (Oblinger and Anthony, 2008).

In addition to the transport of beach sand by wind, studies have investigated the removal and deposition of sediment as a result of the uprush and downrush of waves in the swash zone (Lundgren, 1986). Sediment erosion is promoted by high water tables and deposition by low water tables, where high water tables enhance the downrush of waves, creating turbulent flow, thereby

causing erosion (Grant, 1948; Baird and Horn, 1996; Horn, 2002). Inversely, sediment deposition is enhanced by low water tables on the beachface, promoting infiltration and deposition of sediments carried by the uprush of waves (Grant, 1948; Baird and Horn, 1996; Horn, 2002). Sediment transport (deposition and erosion) by waves has been found to influence the slope of the beachface (Austin and Masselink, 2006; Cartwright *et al.*, 2006). In addition, waves also are responsible for shaping beaches because they are a movement of energy which transfers that energy to the beachface once it runs up in the swash zone (Lundgren, 1986).

2.4.2 Human Induced Beach Profile Alterations

Beach topography is also influenced by human activities. Crowe and Meek (2009) reported that there has been an increase in residential development along the shores of the Great Lakes. Local beach residents have bulldozed the sand dunes and beach sand, and also installed break walls along the beaches. Installing break walls can help protect buildings adjacent to the beach, however, these break walls generally accelerate erosion close by or along the adjacent shoreline to the structures (Lundgren, 1986). An investigation characterizing the surface topography of the beaches of the Great Lakes is important in order to understand the natural and anthropogenic influences that may contribute to the degrading quality of beaches.

2.5 Modelling of Beach Hydrology

Several studies have undertaken numerical modelling investigations to gain insight on the dynamic behaviour of groundwater flow below beaches. These numerical models provide an efficient and cost effective means of gaining insight into the complex processes that occur in the real field setting at beaches (Crowe *et al.*, 2004). Groundwater modelling studies below beaches focus on

investigating the dynamics of flow in the saturated zone below the water table (Cheng and Anderson, 1993; Hunt *et al.*, 2003; Townley and Trefry, 2000; Crowe *et al.*, 2004; Meek, 2007). As such, several studies have focused on the influence of tides and waves on water table fluctuations, and also decoupling of the water table at the seepage face, in coastal environments (Baird and Horn, 1996; Li *et al.*, 1997; Baird *et al.*, 1998; Li *et al.*, 2000; Teo *et al.*, 2003). Few investigations have focused on the groundwater flow below beaches adjacent to lakes (Cheng and Anderson, 1993; Crowe *et al.*, 2004; Meek, 2007).

Modelling saturated groundwater flow below beaches is generally 1D horizontal in the saturated zone (Baird and Horn, 1996; Crowe et al., 2004). Beach models commonly use one assumed value for the saturated hydraulic conductivity (K_{sat}), an impermeable boundary layer below the beach, and either a constant head, constant flux, or variable flux as the inland boundary condition to calibrate the water table (Baird and Horn, 1996). Water flow above the water table is rarely considered in beach modelling studies because it is generally 1D vertical, however, recent studies investigating the complex 2D flow within the swash zone at the groundwater-lake interface, have accounted for the capillary fringe and it's influence on groundwater flow and water table fluctuations (Parlange 1987; Li *et al.*, 1997; Nielsen and Perrochet, 2000; Jeng *et al.*, 2005). Additional modelling that incorporates both saturated and unsaturated zone flow of groundwater at beaches is required to fully understand the processes that occur within these dynamic systems.

2.6 Infiltration Dynamics

2.6.1 Infiltration below the Beaches of the Great Lakes

Infiltration refers to the process of water entering a soil from available surface water (Philip, 1956a) and is an important phenomenon to investigate due to its influences on groundwater

recharge, transport of contaminants, and also available water for plants (Geiger and Durnford, 2000). Unlike groundwater flow through the saturated zone, groundwater flow through the vadose zone has been under studied at beaches. Previous beach studies have focused on investigating infiltration dynamics in the swash zone, because these processes contribute to sediment transport (Grant, 1948; Turner and Masselink, 1998; Horn, 2002; Austin and Masselink, 2006). Other studies at beaches (as previously discussed) investigated the response of the capillary fringe to infiltration as a mechanism for water table fluctuations (Hegge and Masselink, 1991; Turner, 1993a & b; Li *et al.*, 1997; Debrasch *et al.*, 1999). Recently, Tan *et al.* (2007) investigated the meteorological and hydrological factors influencing groundwater recharge along a marine beach. Water table depth and rainfall intensity were found to influence groundwater recharge; an increase in rainfall intensity and shallow water table depth resulted in increased groundwater recharge (Tan *et al.*, 2007). More research needs to focus on investigating infiltration and recharge processes below the backshore area of beaches of the Great Lakes. Understanding the movement of water within the vadose zone will provide better insight on groundwater flow and retention within wet and dry beaches.

2.6.2 Theory of Infiltration

The theory of infiltration is well understood and has been documented in literature (*reviewed by* Hillel, 1982 & 1998). An early seven part series by Phillip (1956a & b), made a significant scientific contribution to understanding the mathematical solutions and theories behind the infiltration equation. Philip (1956a) incorporated important components of the medium (i.e. hydraulic conductivity, suction, hydraulic diffusivity) that influence infiltration, into a mathematical solution for vertical infiltration into a semi-infinite homogeneous porous medium under transient conditions:

$$\frac{\partial \theta}{\partial t} = \frac{\partial}{\partial z}\left(D\frac{\partial \theta}{\partial z}\right) - \frac{\partial K}{\partial z} \quad (2.2)$$

where; θ is the volumetric moisture content [L^3/L^3], t is time [t], D is the hydraulic diffusivity of the medium [L^2/t], z is the vertical direction [L], and K is the hydraulic conductivity of the medium [L/t] (Philip, 1956a). The left side of the equation represents the change in moisture content (storage) of the medium, and the right side represents the influence of soil suction/capillarity (wetness gradient) and gravity forces during infiltration. It should be noted that these two terms dominate during different times of infiltration. During early times of infiltration, suction gradients dominate compared to gravitational forces. However, during late times, the wetting front penetrates deeper into the profile decreasing suction gradients; therefore, gravity forces control the movement of the wetting front (Philip, 1956b; Hillel, 1982).

Several studies have investigated the process of infiltration through sandy soils and have found that the ability of sand to infiltrate water is dependent on several factors including: duration and intensity of the precipitation event (Rubin *et al.*, 1964; Tymchak and Torres, 2007; Chiu *et al.*, 2009), initial moisture content (Garder and McLaren, 1999; Chiu *et al.*, 2009), saturated hydraulic conductivity (Dincer *et al.*, 1973), physical properties (e.g. texture and structure) (Dincer *et al.*, 1973; Yang *et al.*, 2004), presence of vegetation (Garder and McLaren, 1999; Wang *et al.*, 2007; Wang *et al.*, 2008) and heterogeneity of the medium (Hillel, 1998). These factors describe the "infitrability" of a soil which is a term coined by Hillel (1982) to describe the infiltration capacity of a soil, when water at atmospheric pressure is available at the ground surface (Hillel, 1998). Understanding the factors that control infiltration through sands can provide insight on the process of infiltration at beaches, however, more research is needed to quantify the process of infiltration at wet and dry beaches, in order to gain better insight on their associated problems.

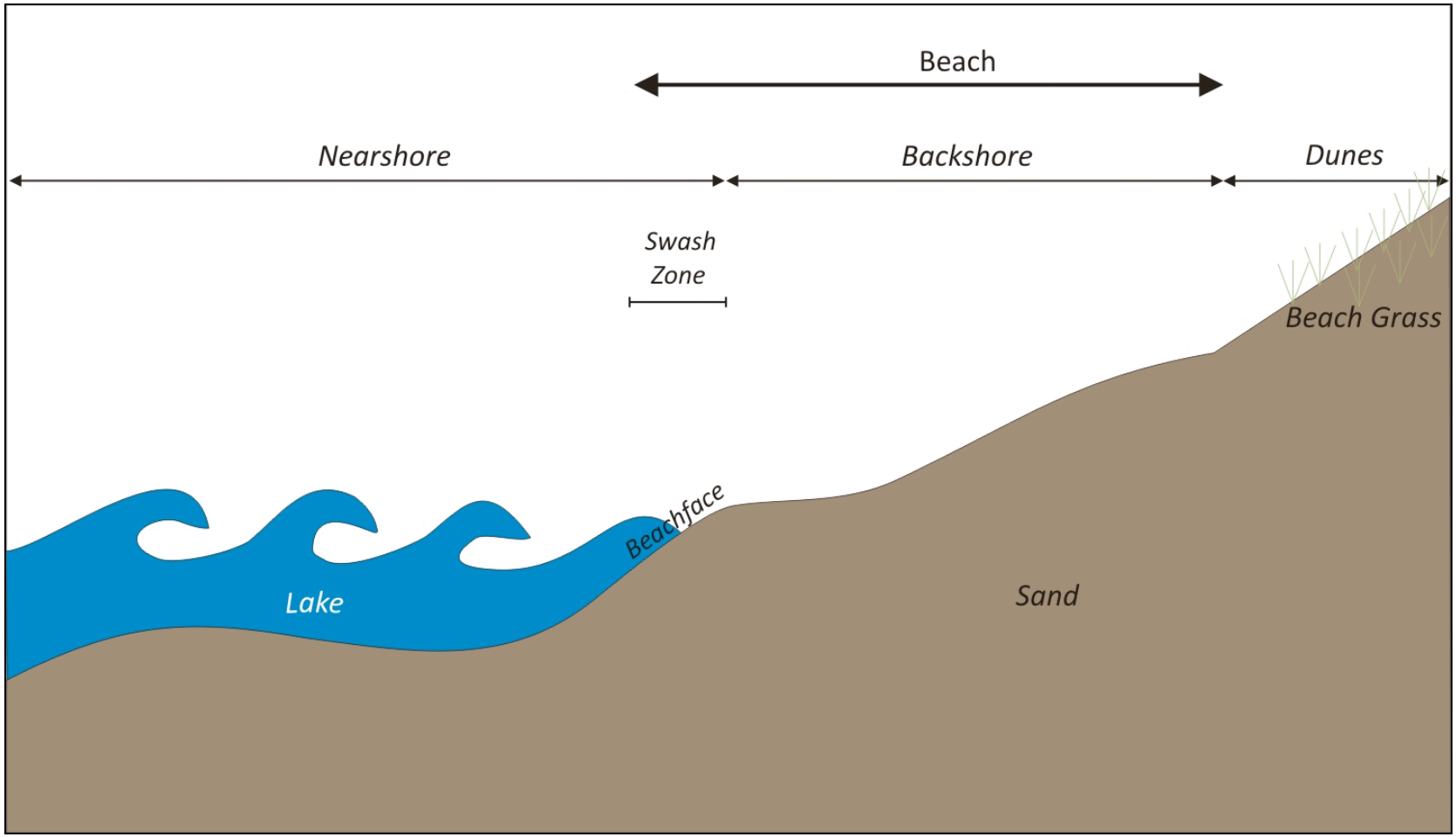

Figure 2.1: Schematic defining the profile of a beach (*modified from* Davis and Fitzgerald, 2004).

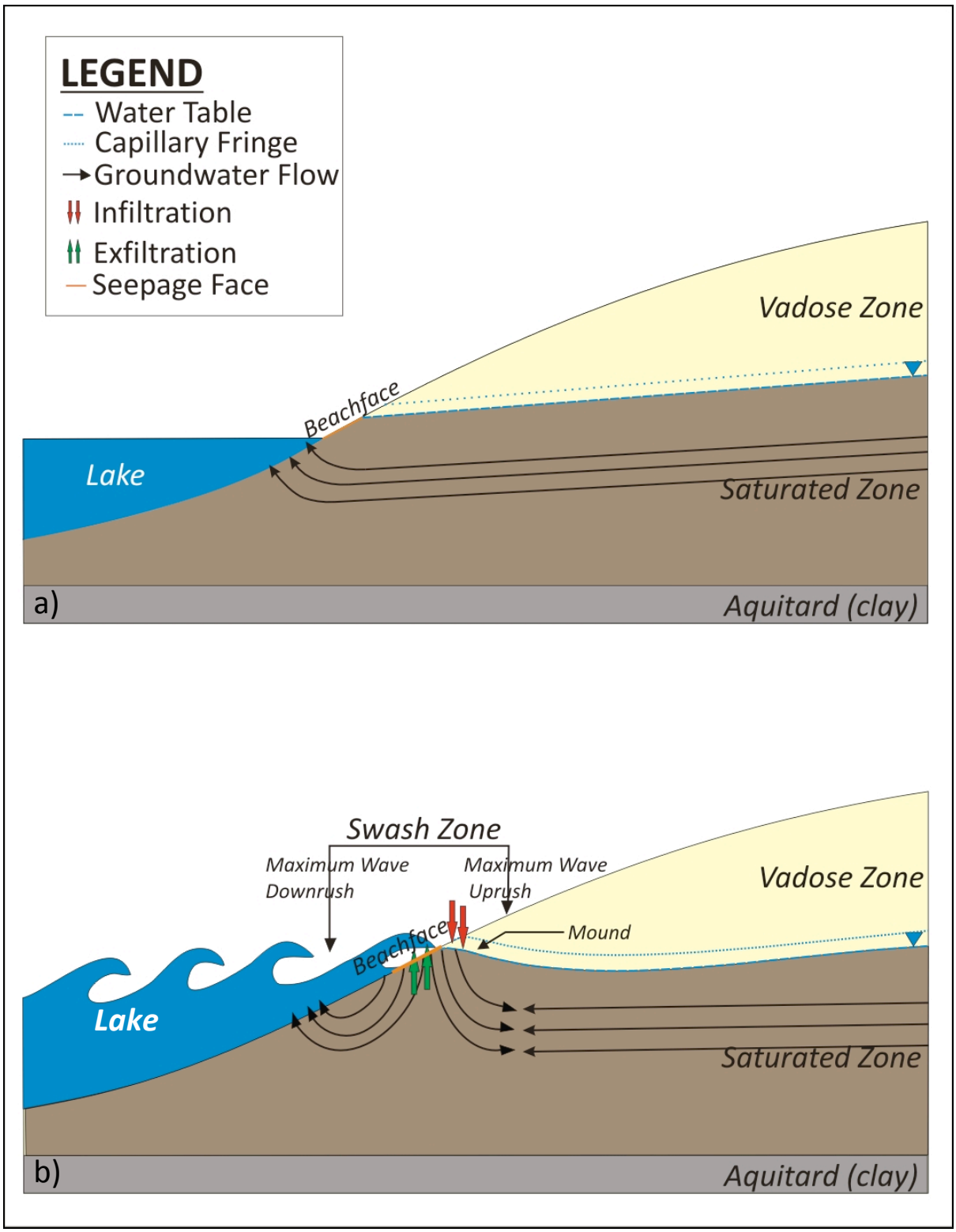

Figure 2.2: Typical groundwater flow below beaches (a) under hydrostatic conditions (calm lake) and (b) under hydrodynamic conditions (wave runup, stormy conditions).

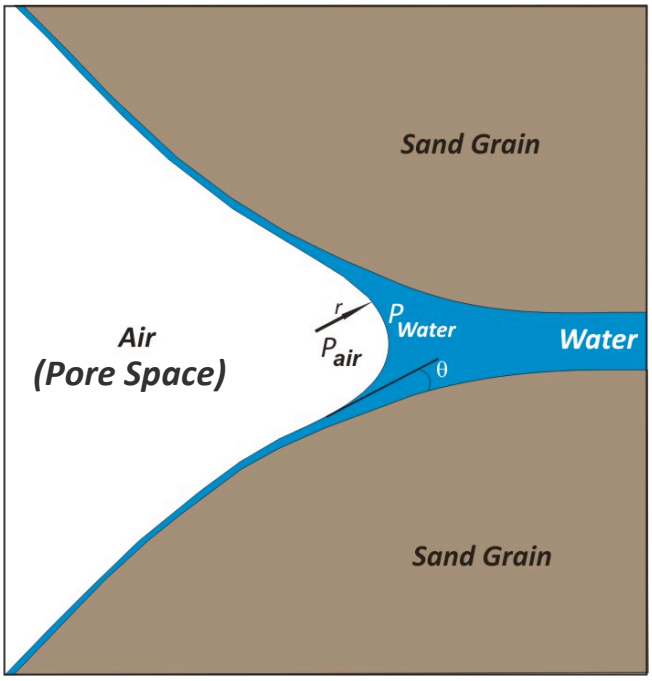

Figure 2.3: Schematic showing water retention between two sand grains by capillarity, where *P* is capillary pressure of the pore fluid, *r* is the radius of the curved meniscus, and θ is the contact angle (*modified from* Fetter, 1999).

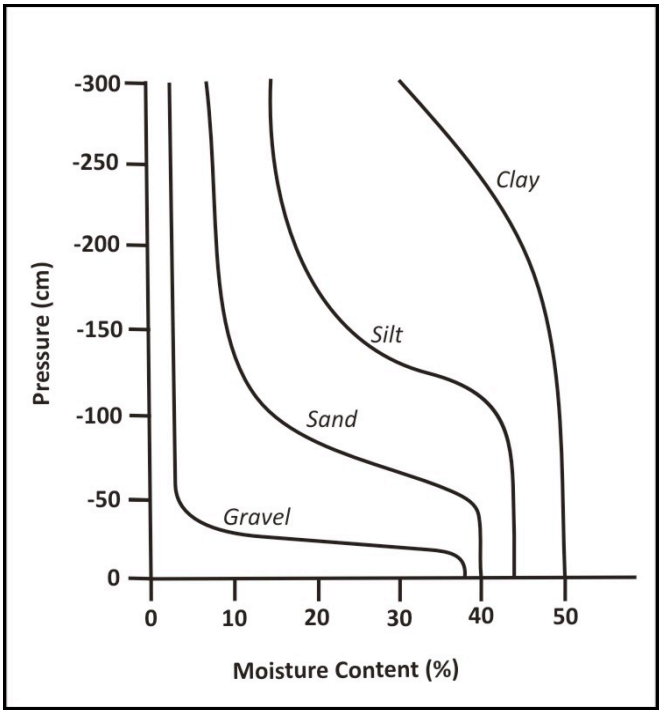

Figure 2.4: Soil moisture retention curves for different soils. Demonstrates that under a specific applied pressure, different soils will retain various moisture contents (*modified from* Stephens, 1996).

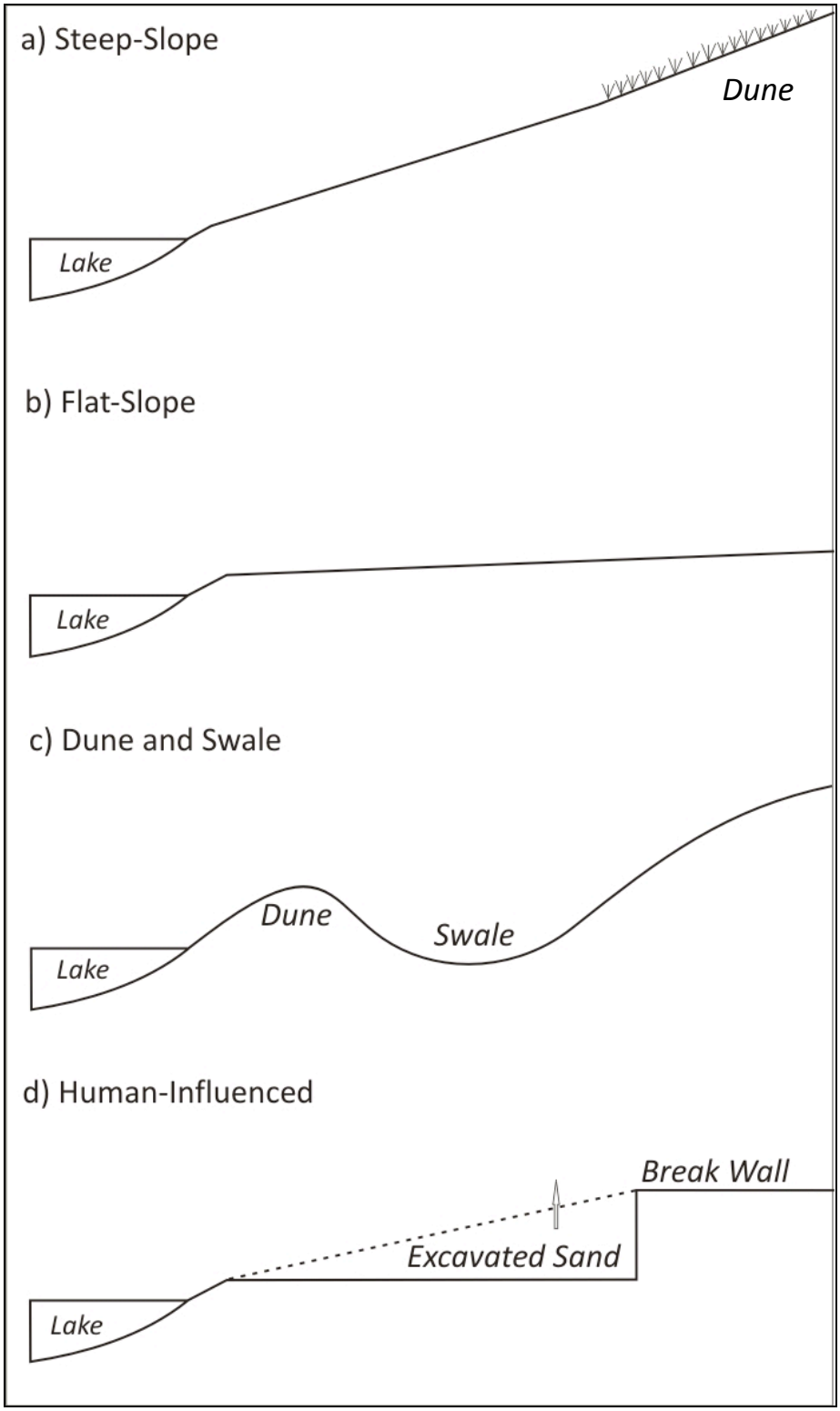

Figure 2.5: Schematics of natural and human-induced surface topographies of beaches surrounding the Great Lakes.

3.0 METHODOLOGIES: Field, Laboratory and Modelling Methods and Analyses

3.1 Field Methods

3.1.1 Site Description and Field Set-Up

A total of four beaches were investigated along the shores of southern Georgian Bay, in Tiny Township, ON (Figure 3.1). Following Crowe and Milne (2007) definitions of wet and dry beaches, two wet beaches (natural and degraded) and two dry beaches (natural) were selected. The beaches are located within a close proximity of each other (approximately 13 km) and were selected because they represent the typical conditions of beaches in this area.

The two wet beaches selected for this study were Jackson Park Beach (JPB) (44°40'28.4"N, 79°59'14.3"E) and Woodland Beach South (WBS) (44°34'12.5"N, 79°59'42.5"E). Both beaches exhibit typical conditions of wet beaches including: wet sand, ponding surface water, invasive and non-native vegetation, and previous tests by *Environment Canada* detected elevated levels of *E. coli* in the groundwater below. Jackson Park Beach is a natural wet beach because it has not been altered by human activities, whereas, Woodland Beach South is a degraded wet beach because local residents have and continue to, altered the beach by bulldozing the natural sand dunes and also installing break walls.

The two dry beaches selected in this study were Balm Beach South (BBS) (44°40'59.7"N, 79°59'40.7"E) and Woodland Beach North (WBN) (44°34'24.8"N, 79°59'35.8"E). Both beaches are natural dry beaches because they have not been altered by humans. These beaches exhibit typical conditions of dry beaches including: dry sand, sand dunes on the leeward side of the beach, natural beach grass in the sand dunes, and do not contain *E. coli* in the groundwater below, as previously detected by *Environment Canada*. BBS is located north of JPB, followed by WBN, and WBS. WBS is a

former continuation of WBN (< 500 m apart), however, due to human induced alterations; both beaches appear very different.

All four field sites were initially set-up by measuring a transect from the lake to a reference point using a standard 100 m measuring tape. Sampling pits were dug along the transect (perpendicular to the lake), spaced approximately 10 m apart, in order to best represent the physical and hydrological conditions at each beach. Additional pits were dug in between the sampling pits for additional measurements of surface and water table elevations. A handheld GPS (Garmin Rino 130) was used to record locations of the first and forth sampling pits along the transect as a reference for future field sampling. Figure 3.2a, b and Figure 3.3a, b summarize the field set-up at all four beaches.

3.1.2 Ground Surface and Water Table Elevations

Ground surface and water table elevations were collected in the summer (August 2009) at BBS, JPB, WBN and WBS and in the fall (October 2009 and November 2010) at BBS, JPB, and WBS. Sampling pits were dug along the transect to obtain a complete profile of the water table and surface elevations at each beach. Once the pits were dug, they were left for approximately 5 minutes to allow the water to completely fill and stabilize (approach a dynamic equilibrium).

A wood plank (3.7 cm x 3.7 cm) was placed over each borehole and was used as a reference point to measure the ground surface elevations and water table depths. The centre of the wood plank was marked with a line to indicate the exact location of where to measure the ground surface elevations and water table depths. Ground surface elevations were measured using an electronic level (Leica Wild-NA2000 Auto Level). Temporary benchmarks were used at each beach site as a reference point for leveling. A leveling rod was placed directly on the top of the reference line on

the wood plank and the elevation of the ground surface was measured. Using a standard measuring tape, the depth of the water table was measured from the reference line to the top of the water table in each pit. After the water table depths were taken, the water table elevations were calculated by subtracting the water table depth to the ground surface elevation.

3.1.3 Particle Sampling

At each beach, three to four sampling pits were along the transect were used to collect particle samples. The wood planks that were previously used as reference points for the ground surface and water table elevations were also used as references for the depths of the particle samples. Wood pegs were inserted into the wall of the sampling pit at 5 cm increments from the surface to the water table, to indicate sampling locations (Figure 3.4). Particle samples were collected using a custom made sand sampler (Figure 3.5). The sand sampler was designed to collect a sample of approximately 100 g of sand, including fine grains to small pebbles, and has dimensions of 6 cm (length) by 6 cm (with) by 2 cm (height). The sand sampler was wiped clean with a *Kimwipe* before and after each sample was collected. For the collection of each sample, the sampler was inserted horizontally into the wall of each pit, carefully removed, and emptied into a zip-lock bag for grain size analyses in the laboratory.

3.1.4 Bulk Density, Porosity, and Volumetric Moisture Contents: Short-Cores

Bulk density samples were collected at 5 cm increments, adjacent to the particle sample locations, in the wall of the sample pit. Samples were collected using the "*Short-Cores"* method as outlined in Dane and Topp (2002). Short cylindrical metal cores with dimensions of 4.8 cm (diameter) by 3.3 cm (height) were used to obtain both bulk density and volumetric moisture

content (VMC) samples and also to calculate porosities. Prior to sample collection, the wall of the borehole was scraped with a metal spatula to minimize moisture loss due to evaporation. This would affect the VMC results and also helped to ensure that the samples collected represent natural field conditions. Once the wall of the sample pit was prepped, the short cylindrical core was pushed into the face of the wall and the sample was collected. Excess sand that extended beyond the edges of the core was scraped away with the spatula. The sample was emptied into a zip-lock bag, triple bagged, stored in a cooler to minimize evaporation losses, and transported to the laboratory for analysis.

3.1.5 *In Situ* Volumetric Moisture Contents: Time Domain Reflectometry (TDR)

A Time Domain Reflectometry (TDR) was used to measure *in situ* measurements of volumetric moisture contents at each site. A TDR measures the dielectric constant of soil, as this constant is influenced by the volume of moisture within the soil (Stephens, 1996). To obtain volumetric moisture contents, the TDR uses a universal calibration curve that is insensitive to the type of soil. Variations in moisture content are averaged over the length of the TDR probes (Stephens, 1996). The TDR is most reliable in soils with high moisture contents because as the moisture contents become low in a soil, the water absorbed onto the soil grain transform into a crystalline structure, thereby, lowering the dielectric content (Stephens, 1996).

The TDR used in this study is the Moisture-Point MP-917 model made by *Environmental Sensors Inc*. It contains two parallel metal probes (20 cm in length) that are attached by wires to a signal receiver (Figure 3.6). TDR measurements were taken at 5 cm increments in each sampling pit from the surface to the water table. The probes were carefully inserted horizontally into the wall of the sampling pit (Figure 3.6). It was important to minimize wobbling the probes when inserting them

into the sand, because this would create air pockets adjacent to the probe that could influence the moisture readings. A hammer was used to gently tap the TDR probes completely into the pit wall and the instrument was turned on. An electrical signal sent by the signal receiver was sent to the ends of the probes, and returned back to the receiver which produced a volumetric moisture content reading of the volume of sand surrounding the probes. The moisture content of the sand was recorded and the TDR was removed and wiped clean for the next test.

3.1.6 Field-Saturated Hydraulic Conductivity

i. Guelph Permeameter

The Guelph Permeameter (Soil Moisture Equipment Corp (SMEC), model 2800K1) Single-Head method was used to determine field saturated hydraulic conductivity (K_{fs}) measurements in the vadose zone at each beach in June, 2010. This method involves measuring the continuous infiltration necessary to maintain a constant head of water in a cylindrical borehole dug above the water table (Reynolds and Elrick, 1987). Approximately 2 cm to 5 cm of the dry surface sand was scraped away to prevent sand from falling into the hole. A soil auger was used to dig a 6 cm diameter hole to the depth of interest. A wood plank (3.7 cm x 3.7 cm) was placed over top of the hole and was used as a reference to measure the depth of the hole. Once the hole was dug, a sizing auger was used to smooth the walls and base of the hole. The Guelph Permeameter was then filled with tap water to the zero mark on the reservoir. Tap water was used instead of distilled water because there are no clay particles present at the beach sites (SMEC, 1993). The Guelph Permeameter was carefully placed into the hole and the test was ready to begin (Figure 3.8). The hydraulic head for each test was set to 5 cm and the time for every 5 cm drop of water in the

reservoir was recorded. A minimum of three Guelph Permeameter tests were conducted on each type of sand (fine, medium, and/or coarse sand) present at each beach.

Field saturated hydraulic conductivities were calculated by:

$$K_{fs} = \frac{CAR}{\left[2\pi H^2 + C\pi a^2 + \frac{2\pi H}{\alpha *}\right]} \quad (3.1)$$

where; *C* is a dimensionless shape factor, *A* is the cross sectional area of the Guelph Permeameter reservoir [L^2], *R* is the steady state fall of water level in the Guelph Permeameter reservoir [$L.T^{-1}$], *H* is steady depth of water in the well [L], a is the radius of the well [L], and α* is the soil texture / structure parameter [L^{-1}] (SMEC, 1993). The value of *C* is 0.87 and was determined by reading the graph of *C* versus H/α provided in the Soil Moisture Equipment Corp (1993) user's manual. The cross sectional area of the two chambers (*A*) was 35.39 cm^2 and the radius of the hole (*a*) was 3.0 cm. '*R*' was calculated by dividing the length of water fall in the reservoir, by the time interval when steady state was reached. The soil texture/structure parameter, α*, was 0.12 cm^{-1} for fine and medium sands, and 0.36 cm^{-1} for coarse sands (SMEC, 1993).

ii Minidisk Infiltrometer

A minidisk infiltrometer (MDI), also known as a tension infiltrometer, is used to determine the K_{fs} of a soil (or sand). It is comprised of a polycarbonate tube attached to a porous plate. The polycarbonate tube is split into two chambers; a bubble chamber and a water reservoir (Figure 3.9). The bubble chamber controls the applied suction at the porous plate and the water reservoir supplies the water that infiltrates through the porous plate, into the sand (Decagon Devices, 2009).

The MDI was used in June 2010 to determine the K_{fs} of the surface sand at all four beaches, following the methods described in the Minidisk Infiltrometer user's manual (Decagon Devices,

2009). Both chambers were filled with water and the suction was set to 2 cm, 4 cm, and 6 cm for each test. The applied suctions used during the MDI tests are typical suctions that are applied to sands (Decagon Devices, 2009). The initial volume of water in the water reservoir was recorded prior to each test. The MDI was then firmly placed on a flat spot on the surface of the beach (adjacent to each sampling pit) to ensure good contact between the surface sand and the porous plate. The initial time was recorded (time zero) when the porous plate made contact with the sand and a stop watch was turned on to record time. During the test, the water level in the reservoir continuously lowered as the water was infiltrating and being wicked by the sand. For every 10 mL of water that infiltrated into the sand, a corresponding time was recorded during the test. The test was completed once the water reservoir was empty. The MDI test was conducted three times at the same location on the surface of the beach (adjacent to each sampling pit), using a different applied suction during each test.

The volumes of water and corresponding times recorded during the infiltration tests were input into a basic *Microsoft Excel* spread sheet provided by Decagon Devices (2009). The spread sheet contained a macro to calculate infiltration as a depth of water using the following formula:

$$I = \frac{V_i - V_t}{15.9} \tag{3.2}$$

where; I is the depth of infiltration of water (cm), V_i is the initial volume (L^3), V_t is the volume recorded (L^3) corresponding with a time (t), and 15.9 is cross-sectional area of the porous plate (Decagon Devices, 2009). Plots of infiltration versus the square root of time were also created using the Excel macro and a second order polynomial function was fit through the cumulative infiltration points (*see example graph below*).

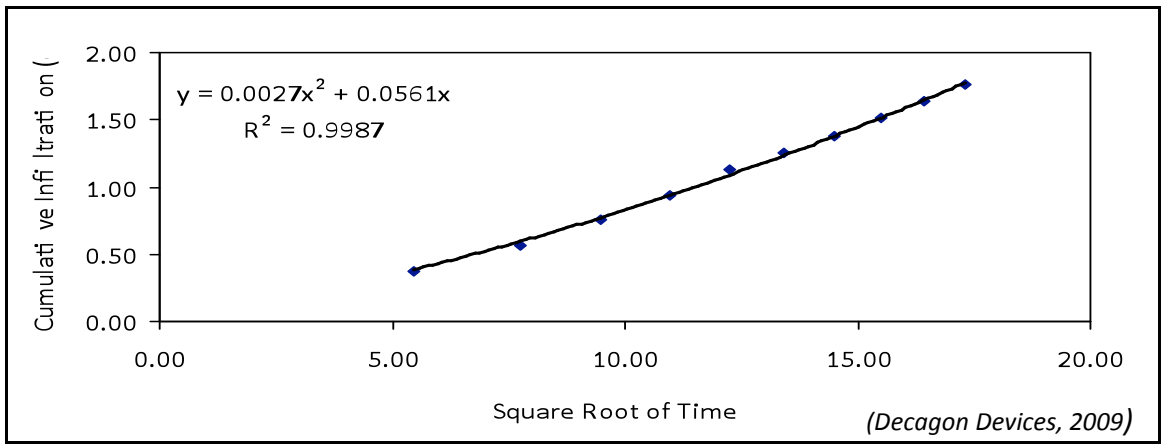

K_{fs} for the surface sands at the beaches were calculated using the MDI by:

$$K_{fs} = \frac{C1}{A} \tag{3.3}$$

where K_{fs} is the field-saturated hydraulic conductivity of the sand (cm.s^{-1}), $C1$ is the first coefficient of the 2nd order polynomial forced through the origin (cm·s$^{-1/2}$) A is a coefficient calculated by Equation 3.4 [dimensionless] (Decagon Devices, 2009):

$$A = \frac{11.65(n^{0.1} - 1)\exp[2.92(n - 1.9)\alpha h_o]}{(\alpha r_o)^{0.91}} \tag{3.4}$$

where n and α are the van Genuchten parameters for sands under different applied suctions (2.68 and 0.145, respectively) [dimensionless], r_o is the radius of the minidisk (2.2 cm), and h_o is the applied suction (2 cm, 4 cm, or 6 cm) (Decagon Devices, 2009).

3.1.7 Vibracoring

Vibracoring is a technique used to obtain cores of sand by forcing a metal core into the ground using vibration and gravity. The vibra-corer used in this study was made by Vi-Cor Technologies Inc. The vibra-corer consisted of a lexan tube (2 3/16" or 5.56 cm inside diameter) inside a metal core barrel that was capped at the bottom with a cutting section containing a

sediment catcher (Figure 3.7). The metal core is attached to a power source which drives the core into the ground. As the core is forced into the ground, the sediment catcher opens on the way down and closes on the way up. Vibracoring took place in October 2009 at JPB (hole 1 and 3), BBS (hole 1 and 3), and WBS (hole 1) in order to obtain particle samples below the elevation of the August 2009 water table, in the saturated zone. A second vibracoring trip took place in November 2010 to obtain additional saturated zone samples from WBS (hole 4) and JPB (lake). A hand held GPS (Garmin Rino 130) was used to locate pre-existing boreholes from field sampling in August 2009. Two boreholes were dug at each beach using a posthole digger until a depth of approximately 5 cm above the water table. Once the depth of the hole was measured, the metal core was placed inside the borehole and vibracoring began. When the core could not move any further into the ground, vibracoring ceased. The length of the core above the bottom of the borehole was measured and the core was then hoisted out of the ground. The lexan tube inside the metal core was removed, excess tubing was cut away, and finally the tube was capped at both ends for grain size analysis in the laboratory.

3.2 Laboratory Analyses

3.2.1 Sample Preparation

Prior to oven drying, the Short-Cores samples were initially weighed in crucibles, using a scale (Mettler Toledo Balance, model PG5002-S DR) to obtain a wet mass (discussed in *Section 3.2.3*). All sand samples (Particle, Short-Cores, Guelph Permeameter (grab) samples) were oven dried in an oven (Fisher Scientific Isotemp Oven, model 650G) at 105°C for 24 h to remove moisture (Dane and Topp, 2002). Finally, the samples were cooled in a desiccator, weighed, and prepared for analyses.

3.2.2 Grain Size Distribution Analyses

i. Mechanical Sieving

The mechanical sieving method was used to obtain grain (particle) size distributions, following the Soil Science Society of America (SSSA) method (Dane and Topp, 2002). Once the samples were prepared (*refer to Section 3.2.1*), aggregates within the samples were separated using a mortar and pestle and pre-sieved using a 2 mm US Standard stainless steel (8" or 20.32 cm diameter) test sieve (A.S.T.M. 2000d Specifications). Pre-sieving the samples removes large pebbles (> 2 mm) and/or organic material (e.g. fine roots and twigs). For the purpose of this study, grains > 2 mm were not considered because the beaches investigated are composed of mainly sand which are defined by grain sizes from 0.0625 mm to 2 mm. Using a sediment splitter (Caprco Inc. Microsplitter, model SS-16-3X) to avoid sample biases, sand samples were split evenly to obtain approximately 45 to 55 g of sand samples. 45 to 55 g of sand was used for the sieving analysis instead of 75 to 100 g because 8" diameter sieves were used instead of 20" diameter sieves, therefore, less mass was required. Once the samples were split, contents were emptied into a stack of sieves (2.0 mm to 0.020 mm) and placed on a mechanical shaker (Humbolt Mfg. Co., model H-4325) for 10 minutes. Contents in each sieve were then emptied and weighed, and were gently brushed to remove any sand grains caught in the sieve. The percent of sand caught on each sieve was then calculated by:

$$\%Caught = \frac{M_T}{M_S} \times 100\% \qquad (3.5)$$

where; M_T is the total mass of the sample and M_s is the mass of the sample on each sieve (Brady and Weil, 2002). Finally, sieves were cleaned with methanol to remove fine particles, and the next sample was prepared.

ii. Grain Size Distribution and Texture Classification

The percent of sand caught on each sieve (*% Caught*) was converted into a percent cumulative passing *(CP)* value by:

$$\% CP = 100 - (\% \text{ Caught in 2 mm sieve}) \quad (3.6)$$

$$\% CP = (\% \text{ CP from top sieve}) - (\% \text{ Caught in current sieve}) \quad (3.7)$$

For the purposes of this study, the percent caught in the 2 mm sieve was set to zero. The *% CP* for each sample was plotted on grain size distribution curves. Grain size distribution curves are plots of cumulative passing (%) versus grain size diameter (mm) and show the distribution of grains present within a sample. According to the US Department of Agricultural classification of grain sizes, silts are defined between 0.2 to 0.05 mm, very fine sands are defined between 0.05 to 0.10 mm, fine sands are defined between 0.10 to 0.25 mm, medium sands are defined between 0.25 to 0.5 mm, coarse sands are defined between 0.5 to 1.0 mm, and very coarse sands are defined between 1.0 to 2.0 mm (Brady and Weil, 2002).

The textures of the Tiny Township beaches were classified using the grain size information from the mechanical sieving analyses and the soil textural triangle:

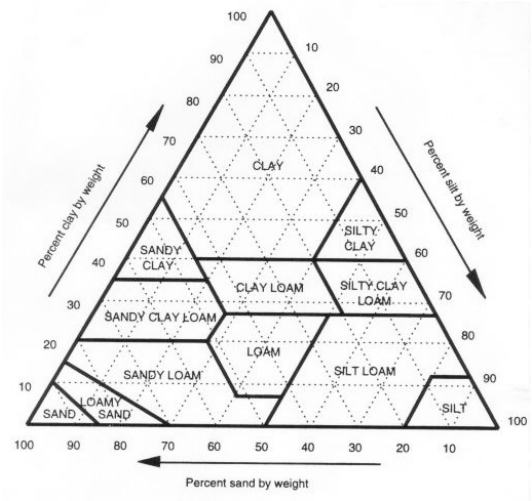

where the percent caught from the sand, silt, and clay sieves were used with the textural triangle to determine the overall classification of the samples (Brady and Weil, 2002).

Using the grain size distribution curve, the mean grain size was obtained graphically and calculated by the following equation:

$$M = \frac{\phi 16 + \phi 50 + \phi 84}{3} \tag{3.8}$$

where *M* is the mean grain size (phi), and ϕ is the corresponding grain size at 16, 50, and 84 percent passing (phi) (Reineck and Singh, 1980). For unit consistency, the following equation was used to convert millimeters into phi units:

$$\phi = -\left(\frac{Log_{10} d}{Log_{10} 2}\right) \tag{3.9}$$

where ϕ is the grain size (phi) and *d* is the grain size (mm) (Reineck and Singh, 1980).

To determine homogeneity/heterogeneity within each sample, the uniformity coefficient (C_u) was calculated. The C_u is essentially a ratio that describes the slope of the grain size distribution curve. The C_u was calculated by:

$$C_u = \frac{d_{60}}{d_{10}} \tag{3.10}$$

where C_u is the uniformity coefficient [dimensionless], d_{60} is the grain diameter at 60 percent cumulative passing (mm), and d_{10} is the grain diameter at 10 *% CP* on the grain size distribution curve (mm). A small coefficient defines a well sorted soil, a large coefficient defines a poorly sorted soil, and a coefficient of unity defines a perfectly sorted soil (Kasenow, 2002).

3.2.3 Bulk Density, Porosity, and Volumetric Moisture Contents: Short-Cores

The samples from the Short-Cores field method were prepared in the laboratory according to *Section 3.2.1*. Bulk densities were calculated by:

$$\rho_b = \frac{M_d}{V} \tag{3.11}$$

where; ρ_b is the dry bulk density [M/L^3], M_d is the dry mass of sample [M], and V is the short core volume [L^3] (Brady and Weil, 2002). Using the same sample, volumetric moisture contents were calculated by:

$$VMC = \frac{V_w}{V_b} \times 100\% \tag{3.12}$$

where; VMC is the percent volumetric moisture content, V_w is the volume of water in the sample [L^3], and V_b is the bulk sample volume [L^3] (Brady and Weil, 2002). Porosities were calculated by:

$$n = \frac{1 - \rho_b}{\rho_s} \tag{3.13}$$

where; n is the percent porosity, ρ_b is the bulk density [M/L^3], and ρ_s is the particle density (Brady and Weil, 2002). The sand grains around Lake Huron (including Georgian Bay) are mainly composed of quartz (LHCCC, 2011), therefore, the particle density of a quartz sand (2.65 g/cm^3) was used (Brady and Weil, 2002).

3.2.4 Vibracore Sample Preparation and Analyses

The lexan vibracore tubes that collected in the field were sectioned and analyzed in the laboratory. Compaction was assumed to occur evenly throughout the entire core and was calculated by:

$$C = \frac{(L_b - L_r)}{L_b} \times 100\% \tag{3.14}$$

where; C is the percent compaction of the core, L_b is the length of the core below the bottom of the borehole [L], and L_r is the length of the recovered core [L]. When sectioning the cores to obtain the

sand samples, each section was cut using gardening sheers to represent a depth interval of 10 cm at each beach. For example, if a core compacted by 25 %, the entire core was evenly sectioned in intervals of 7.5 cm which represented an *in situ* depth 10 cm. Once each section was cut, the sand was scooped out of the core and prepared following the methods described in *Section 3.2.1*. In addition, the samples were then processed and analyzed for grain size distributions following the methods described in *Section 3.2.2*.

Due to compaction during vibracoring, bulk density and porosity measurements were not directly measured. Instead, porosities were first estimated using the uniformity coefficient for each sand sample (*refer to Section 3.2.2*) presented in Odong (2007):

$$n = 0.255 \times \left(1 \pm \left(0.83^{C_u}\right)\right) \tag{3.15}$$

where; n is the predicted porosity and C_u is the uniformity coefficient (Odong, 2007). Bulk densities were then estimated by rearranging Equation 3.9:

$$\rho_b = (1 - n) \times \rho_s \tag{3.16}$$

where; ρ_b is the bulk density [M/L^3], n is the porosity, and ρ_s is the particle density (quartz sand = 2.65 g/cm^3).

3.3 Modelling Methodologies

3.3.1 Empirical Methods to Predict Saturated Hydraulic Conductivities

There are several empirical methods that are used as standard estimation techniques to predict the saturated hydraulic conductivities of soils, including: Hazen (1892), Slitcher (1897), Kozeny-Carmen (1956), Beyer (1964), and Terzaghi (1964) (Kasenow, 2002; Odong, 2007; Song *et al.*, 2009). Four empirical methods were selected in this study to determine the saturated hydraulic conductivities (K_{sat}) of the sand at the Tiny Township beaches; Hazen, Slitcher, Kozeny-Carman, and

Beyer. Table 3.1 presents the empirical formulas for these methods, including their assumptions. These four methods were selected because they are commonly used to predict the K_{sat} of sands ranging between 0.0625 mm to 2 mm (very fine sands to very coarse sands) (Vukovic and Soro, 1992; Kasenow, 2002; Odong, 2007; Song *et al.*, 2009).

The four empirical methods incorporate textural data (i.e. d_{10}, n, and/or C_u) to determine the K_{sat}. The Hazen, Slitcher, and Kozeny-Carman methods commonly use the value of d_{10} from a particular sample which is obtained from the grain size distribution curve (*refer to Section 3.2.2*). In addition, these methods also use the value of n, however, this value is expressed differently between all three methods (*refer to Table 3.1*). The most recent method presented by Beyer uses the C_u, instead of n, along with the d_{10} value to predict the K_{sat} of a sample. The C_u represents how well or poorly sorted a material is, whereas, n represents the porosity of a material. Both parameters represent different textural properties, thereby expressing different heterogeneities (variability) within a sample. In addition, the value of the β-parameter is unique to each method because it was originally calibrated specifically to each method, in order to better predict the K_{sat} of a soil sample.

3.3.2 Applied Numerical Modelling Using HYDRUS-2D

i. Model Justification

HYDRUS-2D is a *Microsoft Windows* based model that was developed by the U.S Salinity Laboratory, U.S Department of Agriculture, Agriculture Research Service. The model analyzes 2D water flow and solute transport in variably saturated porous media (Simunek *et al.*, 1999). The numerical model was used in this study to simulate saturated and unsaturated zone flow at wet and dry beaches in order to understand the controlling factors and processes that influence the moisture

conditions at the Tiny Township beaches. The model was chosen because it has extensive capabilities in modelling saturated-unsaturated water flow; specifically because it can simulate 1D and 2D flow and can also handle irregular shaped grids (non-rectangular), such as beaches.

The governing equations for the HYDRUS-2D code numerically solves for the Richards' equation for saturated-unsaturated water flow and also the convection-dispersion equation for heat and solute transport. The governing equations are solved by using a Galerkin type linear finite element method (Simunek *et al.*, 1999). For this study, HYDRUS-2D was used to solve water flow in 2D using the Richards' equation:

$$\frac{\partial \theta}{\partial t} = \frac{\partial}{\partial x_i}\left[K\left(K_{ij}^{A}\frac{\partial h}{\partial x_j} + K_{iz}^{A}\right)\right] - S \qquad (3.17)$$

where; θ is the volumetric moisture content [$L^3.L^{-3}$], h is the pressure head [L], S is the sink term [T^{-1}], x_i are the spatial coordinates (i = x,z) [L], t is time [T], $K_{ij}{}^{A}$ is the anisotropy tensor [dimensionless], K is the unsaturated hydraulic conductivity [LT^{-1}].

ii. Grid Design and Initial and Boundary Conditions

Two dimensional flow domains were set up for each beach (BBS, JPB, WBN, and WBS) (Figure 3.10 and Figure 3.11). To eliminate boundary value problems, the dimensions of the domains were extended in the vertical and horizontal direction compared to the cross-sectional area (below the transect) that was measured in the field. Using the MESHGEN-2D grid generator installed in HYDRUS-2D, a finite element grid was generated for each beach. The MESHGEN-2D grid generator applies an irregular and unstructured triangular mesh to an irregular shaped domain. Because unsaturated groundwater flow requires smaller nodal spacing compared to saturated groundwater flow, the nodal density was higher (about 5 cm to 10 cm) in the vadose zone, below the surface, and

also adjacent to the boundaries of each domain. In addition, the density of the nodal spacing were lower (about 30 cm spacing) in the saturated zone, below the water table.

Table 3.2 provides a summary of the boundary conditions and data sources used in each beach model. Figures 3.10 and 3.11 provide a 2D view of the set up of each model, along with the assigned initial and boundary conditions. All models were set up with a constant head boundary on the left-side of the model, which represented the lake (Georgian Bay). In addition, all models were assigned a no flux boundary surrounding the bottom of the domains to represent the impermeable layer that exists below beaches (Baird and Horn, 1996; Crowe and Meek, 2009). A constant head boundary was also set on the right-side of the models (BBS, JPB, and WBN) to maintain the elevation of the water tables, consistent with field measurements. The WBS model had a constant flux boundary instead of the constant head boundary. The constant flux boundary would allow the water table to respond accordingly to the variations in K_{sat} across this beach. Finally, the top boundary condition in each model was assigned an atmospheric boundary condition, which provided the option of adding precipitation, evaporation, and/or transpiration to the simulations.

iii. Model Calibration and Sensitivity Analyses

Table 3.3 provides an overview of the input parameters used to initially set up the HYDRUS-2D beach models. The models were calibrated to field measurements in order to represent the field conditions at the Tiny Township beaches. The four models were calibrated specifically to the August 2009 measurements of water table elevations and also the moisture content profiles above the water tables at each beach. When calibrating the models to the measurements from August 2009, the assumption was made that field the measurements represent steady state or dynamic equilibrium conditions at beaches.

Water table positions were calibrated by adjusting the constant head boundary condition on the right-side of the BBS, JPB, and WBN models. The boundary was adjusted until the slopes of the water tables (hydraulic gradients) were consistent with field measurements in August 2009. In addition, the water table in the WBS model was calibrated by adjusting the constant flux boundary and also by adjusting the K_{sat} of the material layers until the two water table slopes in the model were consistent with field conditions. The calibrations were complete when the water table elevations were within ± 5 cm of the field measurements.

In order to calibrate the moisture content profiles above the water tables in the models to field measurements, the soil hydraulic parameters: α, n, θ_s, θ_r, and K_{sat}, were adjusted. The hydraulic parameter '*l*' was assumed the value of 0.5 which is commonly used for most soils (Simunek *et al.*, 1999). The soil hydraulic parameters are used in HYDRUS-2D by van Genuchten (1980) and Mualem (1976) functions:

$$\theta(h) = \begin{cases} \theta_r + \dfrac{\theta_s - \theta_r}{\left[1 + (\alpha|h|)^n\right]^m} & h < 0 \\ \theta_s & h \geq 0 \end{cases} \tag{3.18}$$

$$K(h) = K_s S_e^{0.5}\left[1 - (1 - S_e^{1/m})^m\right]^2 \tag{3.19}$$

where; $$m = 1 - \frac{1}{n}; \qquad S_e = \frac{\theta - \theta_r}{\theta_s - \theta_r} \tag{3.20}$$

where; θ is the volumetric water content [$L^3.L^{-3}$], h is the pressure head [L], θ_r is the residual water content [$L^3.L^{-3}$], θ_s is the saturated water content [$L^3.L^{-3}$], α is a soil water retention fitting parameter[L^{-1}], K is the unsaturated hydraulic conductivity [L..T^{-1}], K_s is the saturated hydraulic conductivity [L..T^{-1}], S_e is the effective water content, and m, n are soil water retention fitting parameters. Equation 3.18 is used to predict the soil moisture retention curve (SMRC); the relationship between moisture held within the pores of a soil under a give pressure head (analogous

to the height above the water table at steady state conditions. Equation 3.19 is used to predict the unsaturated hydraulic conductivities in the vadose zone, which expresses the unsaturated hydraulic conductivities as a function of pressure heads.

Soil hydraulic parameters were first predicted using the Neural Network Prediction (Rosetta) option provided within the HYDRUS-2D model. This option uses pedotransfer functions (PTFs) to predict moisture retention parameters and saturated hydraulic conductivity using soil textural (percent sand, silt, and clay) and structural (bulk density) data (Rassam *et al.*, 2003). The Neural Network Prediction provided a reference point to adjust and calibrate the water retention fitting parameters: α and *n*. The soil hydraulic properties were calibrated to the field moisture data by inputting the volumetric moisture content from just below the beach surface as θ_r, the average porosity as θ_s, the mean saturated hydraulic conductivity (empirically predicted) for each material as K_s. Finally, α and *n* parameters were adjusted to yield soil moisture retention curves that fit the average moisture content profiles measured at each beach.

Once the calibrations were successful, a sensitivity analysis was conducted on the soil hydraulic parameters:α, *n*, θ_s, and K_{sat} in the flat sloped, wet beach model (JPB) and in the steep sloped, dry beach model (WBN). The purpose of the sensitivity analyses is to reduce any uncertainties with the calibrated parameters that were used in the models, and also to validate the four beach models (Rocha *et al.*, 2006). Table 3.5 provides an overview of the parameters tested (θ_s, K_s, α, and *n*) including their values and data sources. All parameters were varied over a reasonable range of expected values for sands.

Figure 3.1: Regional map of Lake Huron and Georgian Bay, Ontario, Canada. Field sites investigated in this study (●) with respect to neighboring towns (■).

Figure 3.2a: Aerial and panoramic view of Jackson Park Beach field site and sampling transect.

Figure 3.2b: Aerial and panoramic view of Woodland Beach South field site and sampling transect.

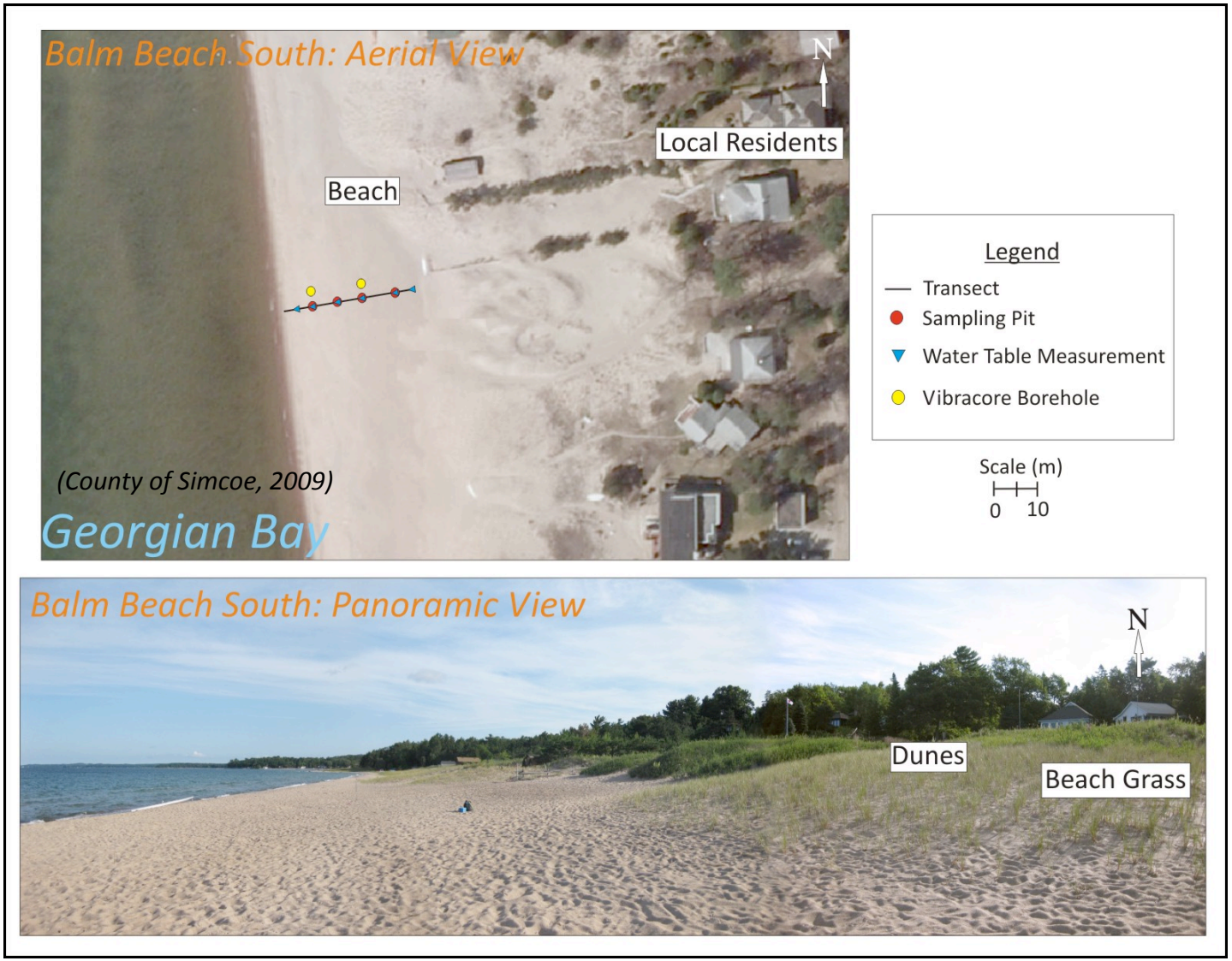

Figure 3.3a: Aerial and panoramic view of Balm Beach South field site and sampling transect.

Figure 3.3b: Aerial and panoramic view of Woodland Beach North field site and sampling transect.

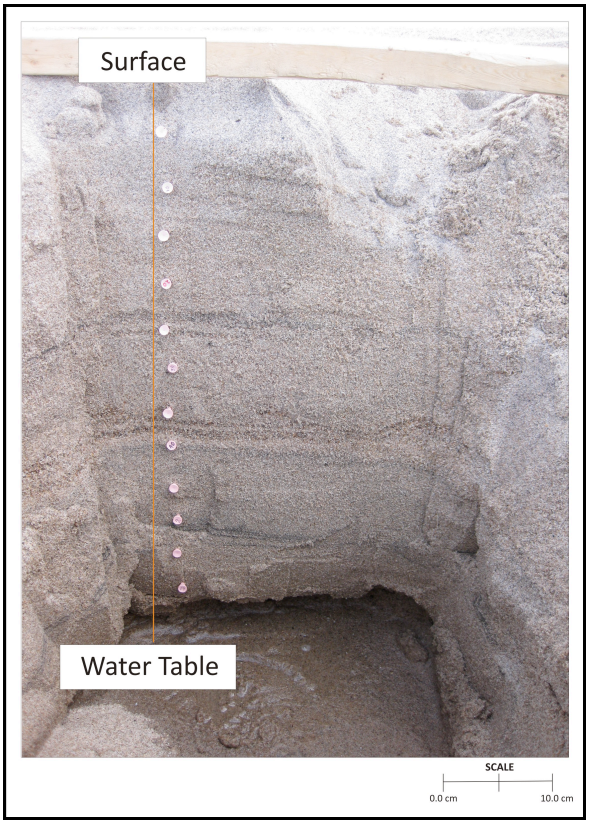

Figure 3.4: Example of sampling pit set-up for water table depth, moisture content, bulk density, and particle sampling, August 2009. Pink pins are spaced at 5 cm intervals.

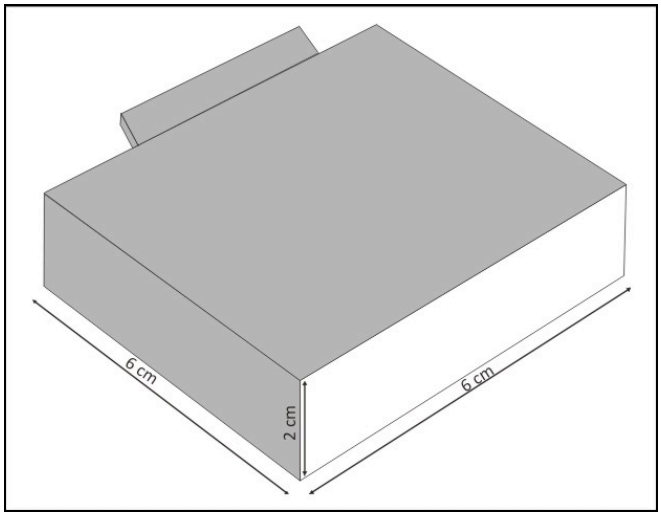

Figure 3.5: Schematic of sand sampler used to collect vadose zone grain samples, August, 2009.

Figure 3.6: Collection of *in situ* volumetric moisture contents within sampling pit (top) and close-up of Time Domain Reflectometry (TDR) probe used (bottom), August 2009.

(a)

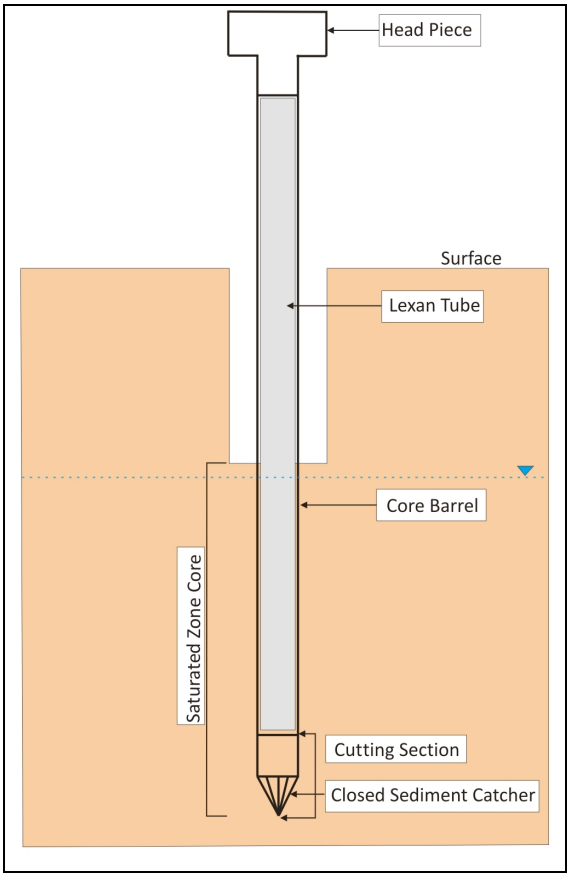

(b)

Figure 3.7: (a) Diagram of the vibra-corer, (b) example of vibracoring to obtain particle samples in the saturated zone, October 2009.

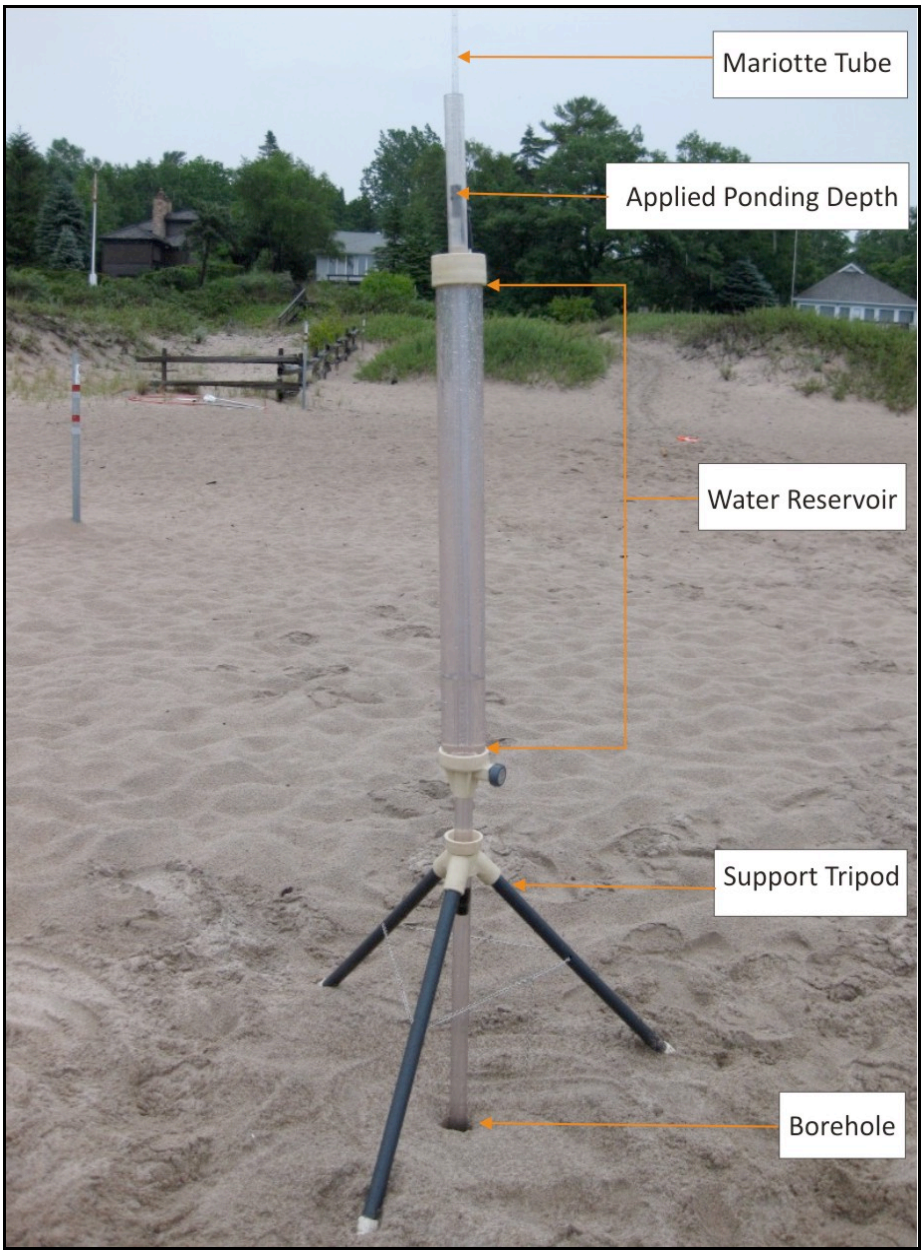

Figure 3.8: Guelph Permeameter used at the Tiny Township beaches to obtain field-saturated hydraulic conductivity measurements below beach surface, June 2010.

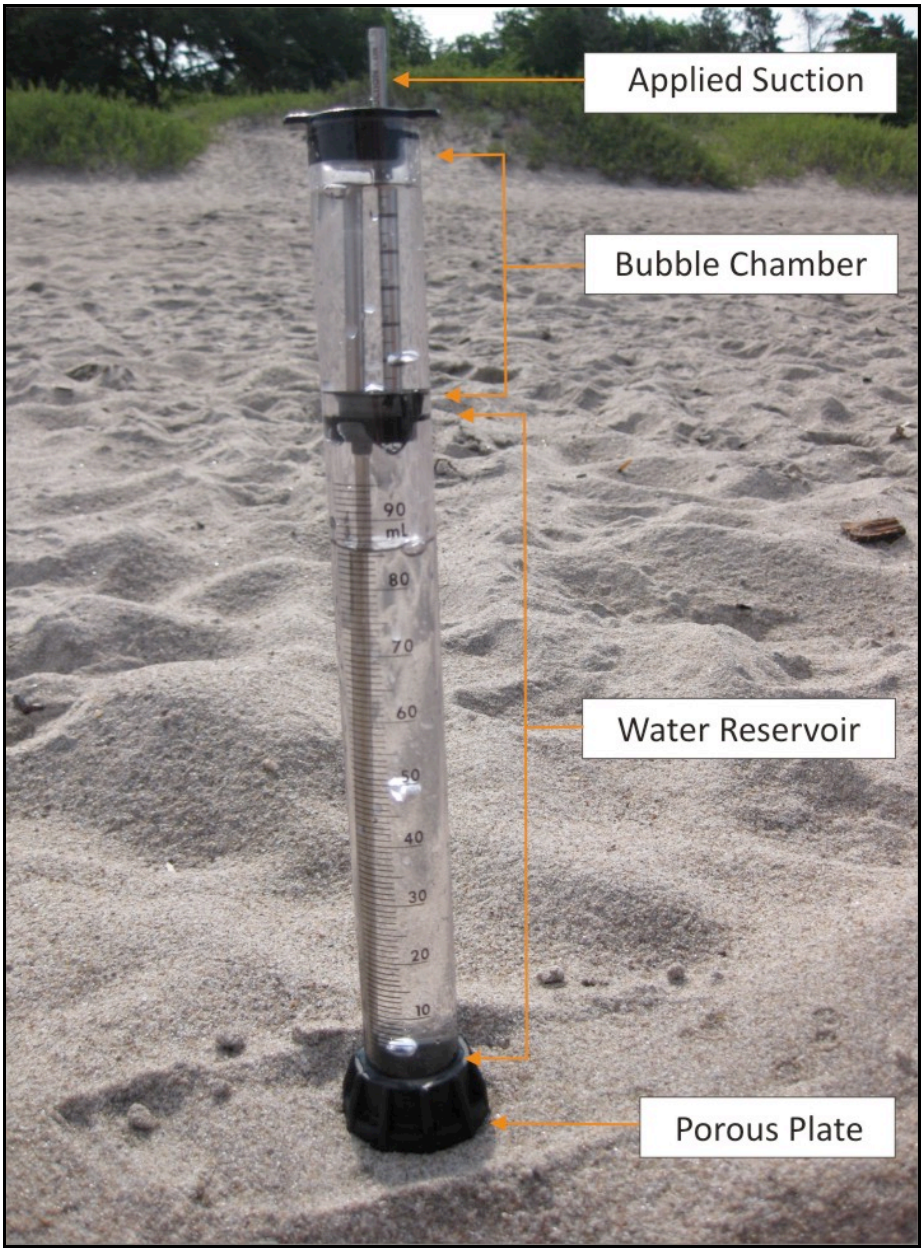

Figure 3.9: Minidisk Infiltrometer (MDI) used at the Tiny Township beaches to obtain field-saturated hydraulic conductivity measurements at beach surface, June 2010.

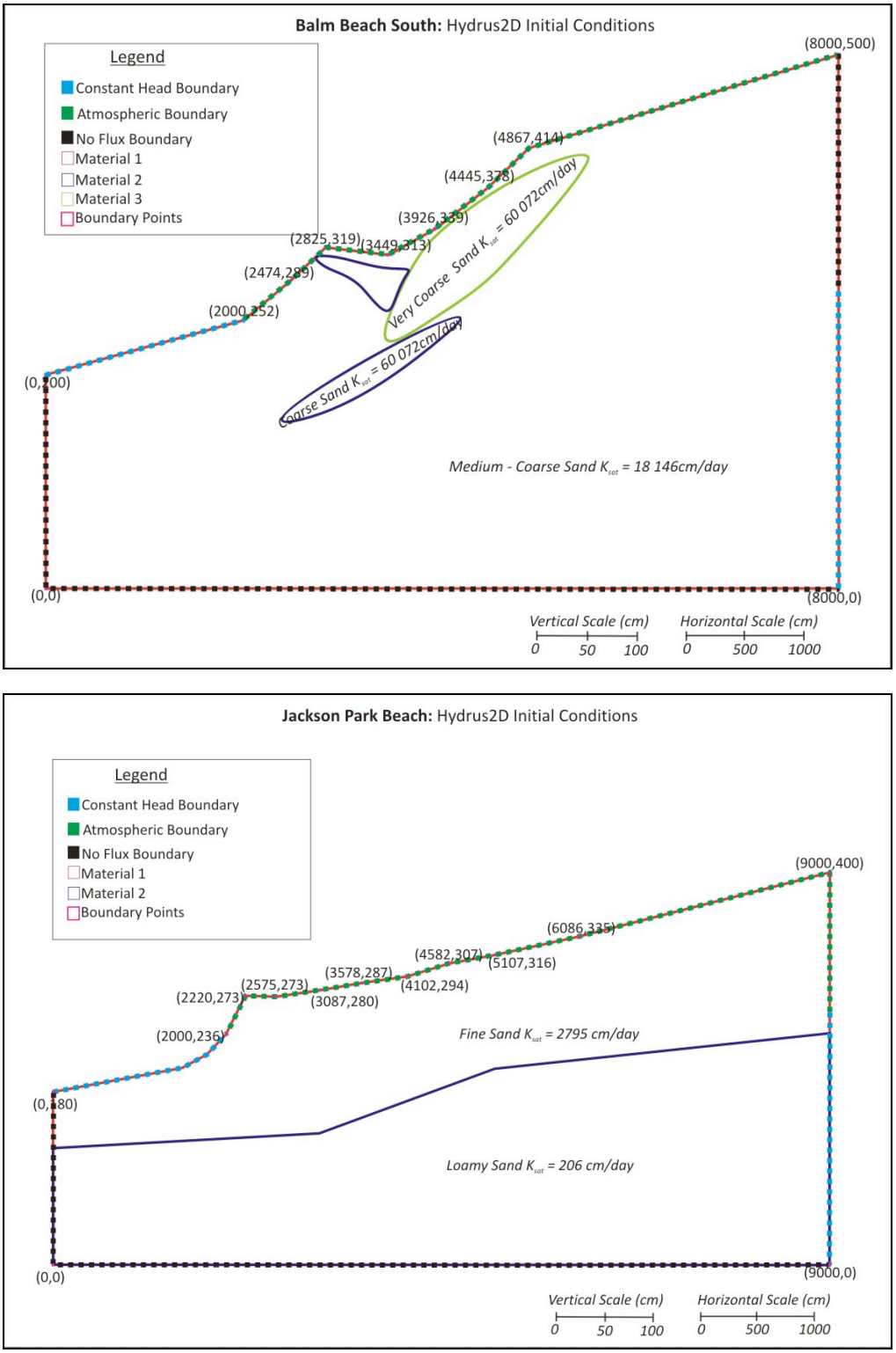

Figure 3.10: Profile of HYDRUS 2D flow domain and boundary conditions for Balm Beach South (top) and Jackson Park Beach (bottom).

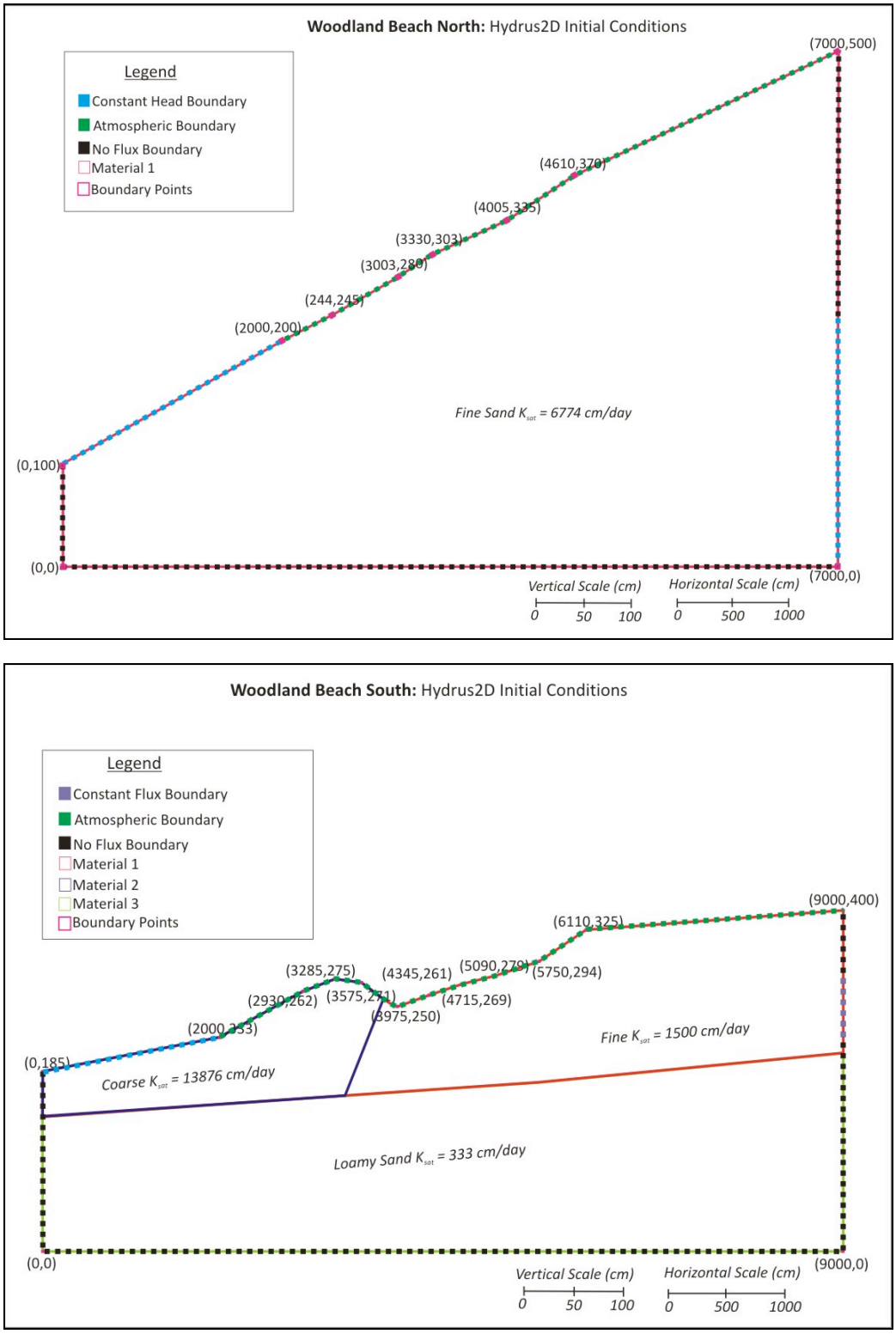

Figure 3.11: Profile of HYDRUS 2D flow domain and boundary conditions for Woodland Beach North (top) and Woodland Beach South (bottom).

Table 3.1: Summary of empirical methods used to predict the K_{sat} of the beach sand

Method	Equation	Parameters	Assumptions
HAZEN (1892) [1]	$K_{sat} = \frac{g}{\upsilon}(\beta_H)(1+10(n-0.26))d_{10}^2$	K_{sat}= saturated hydraulic conductivity (m/sec) g = acceleration of gravity (9.81m/sec^2) υ = kinematic viscosity (m^2/sec) β_H = 6 x 10^{-4} [--] n = porosity [--] d_{10} = effective diameter (m)	0.1mm < d_e< 3 mm[1] Fine grained sands to gravel
SLITCHER (1897) [1]	$K_{sat} = \frac{g}{\upsilon}\beta_S(n^{3.287})d_{10}^2$	K_{sat}= saturated hydraulic conductivity (m/sec) g = gravitational constant (9.81m/sec^2) υ = kinematic viscosity (m^2/sec) β_S = 0.01 [--] n = porosity [--] d_{10}= effective diameter (m)	0.01 < d_e < 5.00[1] Very fine sands to gravel
KOZENY - CARMEN (1956) [1]	$K_{sat} = \frac{g}{\upsilon}(B_{KZ})\left(\frac{n^3}{(1-n)^2}\right)d_{10}^2$	K_{sat}= saturated hydraulic conductivity (m/sec) g = gravitational constant (9.81m/sec^2) υ= kinematic viscosity (m^2/sec) β_{KZ} = 9.61 x 10^{-3} [--] n = porosity [--] d_{10} = effective diameter (m)	Large grained sands[1] Not appropriate for soils above 3 mm [2]
BEYER (1964) [1]	$K_{sat} = \frac{g}{\upsilon}\beta_B\left(\log\frac{500}{C_u}\right)d_{10}^2$	K_{sat}= saturated hydraulic conductivity (m/sec) g = gravitational constant (9.81m/sec^2) υ= kinematic viscosity (m^2/sec) β_B = 6.0 x 10^{-4} [--] C_u= uniformity coefficient [--] d_{10}= effective diameter (m)	0.06 mm < d_{10} < 0.6 mm[1] Fine grained sands to coarse grained sands 1 < C_u 20[1]

[1]Kasenow (2002) [2]Odong (2007)

Table 3.2: Boundary conditions and data sources for each beach model

Beach Domain	Boundary	Condition	Data Source
BBS, JPB, WBN, WBS	Upper boundary – surface	Atmospheric	Assumed steady stated conditions – set evaporation and precipitation to zero
BBS, JPB, WBN, WBS	Left boundary – lake	Constant head	Set as position of the lake-shoreline intersection point measured in the field
BBS, JPB, WBN, WBS	Left boundary – below lake	No flux	Assumed vertical upward flow towards the lake (Crowe and Meek, 2007)
BBS, JPB, WBN, WBS	Lower boundary – silt/clay	No flux	Assumed impermeable boundary 2-3 m below beach (Baird and Horn, 1996)
BBS, JPB, WBN	Right boundary – saturated zone	Constant head	Maximum water table position measured in the field (assumed hydrostatic equilibrium)
WBS	Right boundary – saturated zone	Constant flux	Calculated from K_{sat} and hydraulic gradient
BBS, JPB, WBN, WBS	Right boundary – vadose zone	No flux	Vadose zone - no flow (assumed hydrostatic equilibrium)

Table 3.3: HYDRUS-2D input parameters used to set up the beach models

Beach	**BBS**	**JPB**	**WBN**	**WBS**
Main Process				
o Water Flow	✓	✓	✓	✓
Geometry Information				
o Length Units	cm	cm	cm	Cm
o Geometry Type	General	General	General	General
o Type of Flow	Vertical	Vertical	Vertical	Vertical
Soil Profile				
o Number of Materials (Heterogeneity)	4	2	1	3
o Number of Layers (Mass Balance)	1	1	1	1
Time Information				
o Time Units	days	days	days	Days
Time Discretization				
o Initial Time	0	0	0	0
o Final Time	25	25	25	25
o Initial Time Step	5e-05	5e-05	1e-05	5e-05
o Minimum Time Step	1e-05	1e-05	0.0001	1e-05
o Maximum Time Step	0.1	0.1	0.1	0.1
Boundary Conditions				
o Number of Time-Variable Boundary Conditions	0	0	0	0
Print Information				
Print Output				
o Number of Print Times	10	10	10	10
Iteration Criteria				
Iteration Criteria				
o Maximum Number of Iterations	50	50	50	50
o Water Content Tolerance	0.005	0.005	0.005	0.001
o Pressure Head Tolerance	0.5	0.5	0.5	0.1
Time Step Control				
o Lower Optimal Iteration Range	3	3	3	3
o Upper Optimal Iteration Range	7	7	7	7
o Lower Time Step Multiplication Factor	1.1	1.1	1.1	1.1
o Upper Time Step Multiplication Factor	0.7	0.9	0.9	0.7
Internal Interpolation Tables				
o Lower Limit of the Tension Interval	1e-006	1e-006	1e-006	1e-006
o Upper Limit of the Tension Interval	10000	10000	10000	10000
Initial Conditions				
o In the Pressure Head	✓	✓	✓	✓
Soil Hydraulic Model				
o van Genuchten-Mualem	✓	✓	✓	✓
o Hysteresis	No	No	No	No

Table 3.4: Soil hydraulic parameters (for material 1) and data sources used in the sensitivity analyses for the JPB (flat-sloped, wet beach) and WBN (steep-sloped, dry beach) models

Soil Hydraulic Parameter	Value	Data source
	Jackson Park Beach (material 1)	
θ_s	0.49	Maximum field porosity value (increased by 0.02)
	0.47[1]	Average field porosity value
	0.45	Lowered field by 0.02
K_s ($cm \cdot day^{-1}$)	4147	Maximum empirically estimated K_s from field data
	2795[1]	Average empirically estimated K_s from field data
	1287	Minimum empirically estimated K_s from field data
α	0.0126	Increased α by 0.01[2]
	0.0226[1]	Estimated by HYDRUS-2D neural network prediction
	0.0326	Decreased α by 0.01[2]
n	5.0789	Increased n by 1.0[2]
	4.0789[1]	Estimated by HYDRUS-2D neural network prediction
	3.0789	Decreased n by 1.0[2]
	Woodland Beach North (material 1)	
θ_s	0.47	Maximum field porosity value (increased by 0.06)
	0.41[1]	Average field porosity value
	0.35	Lowered field by 0.06
K_s ($cm \cdot day^{-1}$)	21600	Maximum empirically estimated K_s from field data
	6774[1]	Average empirically estimated K_s from field data
	2652	Minimum empirically estimated K_s from field data
α	0.0430	Increased α by 0.01[2]
	0.0330[1]	Estimated by HYDRUS-2D neural network prediction
	0.0230	Decreased α by 0.01[2]
n	6.0	Increased n by 1.0[2]
	5.0[1]	Estimated by HYDRUS-2D neural network prediction
	4.0	Decreased n by 1.0[2]

[1] Best fit parameters
[2] Similar magnitude of parameter variation for a HYDRUS-2D sensitivity analysis for a sand as reported in Albright *et al.* (2002)

4.0 RESULTS & DISCUSSIONS: Physical and Hydrogeological Characterization of Wet & Dry Beaches

4.1 Beach Surface and Water Table Elevations

The elevation of the ground surface of all four beaches increase with increasing distance inland from the lake (Figure 4.1). Elevations were not referenced to a common datum, but to the lake level elevation at each site. Figure 4.1 provides a profile of the surface and water table elevations for the Tiny Township beaches that were measured in August 2009. Beach surface and water table elevations measured in August 2009. Seasonal measurements of beach surface and water table elevations collected in August 2009, October 2009, and November 2010 are presented in Table A1.1 (*Appendix 1)*. It is evident that BBS and WBN have higher surface elevations above the lake compared to JPB and WBS, 1.25 m, 1.60 m, 0.72 m, and 0.42 m, respectively measured approximately 25 m from the lake at each beach. BBS and WBN also have steeper-sloped surfaces with sand dunes on the leeward side of the beach, compared to the flat-sloped surface at JPB which does not have sand dunes. The backshore area of WBS is also flat-sloped, however, the nearshore area contains a small sand dune. Therefore, WBS has a dune and swale beach topography (Oblinger and Anthony, 2008). Although the beach surfaces are continuously exposed to erosional and depositional processes (e.g. Aeolian sediment transport, waves, storms, and ice), the surface elevations in the backshore area of the beaches generally remained consistent (unchanged) throughout all sampling dates (Figure 4.2).

Studies characterizing groundwater conditions below the beaches of the Great Lakes have identified a link between beach topography and water table depths; dry beaches typically have steeper slopes, and deeper water tables, and wet beaches typically have flatter slopes and shallower water tables (Crowe and Milne, 2007; Crowe and Meek, 2009). The positions of the water tables at all four beaches do not follow the slope of the ground surface (Figure 4.1). At all four beaches, the

depth to the water table increases with increasing distance inland from the lake. However, the rate of increase in the depth to the water table across a beach changes among the beaches. At BBS and WBN, the depth to the water table rapidly increases to over a meter within 25 m of the lake. At JPB and WBS the depth to the water is consistent less than 0.7 m up to 40 m from the lake. For example, the depths to the water table measured 25 m from the lake on August 2009 are approximately 1.10 m, 1.44 m, 0.61 m, and 0.25 m at BBS, JPB, WBN, and WBS, respectively.

The hydraulic gradients or slopes of the water tables were calculated from Figure 4.1 as the change in hydraulic head with the change in distance and are presented in Table 4.1. The water tables at BBS, WBN and JPB at all sampling dates have a fairly consistent slope across the beach. The water table at WBS appears to have two distinct slopes; a flatter water table near the lake (< 10 m), and a steeper water table position away from the lake (> 10 m). In August 2009, hydraulic gradients for BBS, JPB, and WBN, were: 0.0086, 0.0075, and 0.0063, respectively. Two hydraulic gradients were calculated for WBS because the water table exhibited two slopes: 0.0073 near the lake and 0.0210 away from the lake. All hydraulic gradients are similar to hydraulic gradients reported by Crowe and Meek (2009) for beaches along the shores of Lake Huron and Georgian Bay.

Seasonal hydraulic gradients and the range of water table elevations from October 2009 and November 2010 are also presented in Table 4.1. The depths to the water tables and corresponding hydraulic gradients were not measured at WBN in October 2009 and BBS and WBN in November 2009 (Figure 4.1). Similar to Crowe and Meek (2009), the hydraulic gradients are consistent seasonally at a specific site, and fluctuate proportionally with lake level fluctuations. The hydraulic gradient near the lake at WBS during August 2009 is not consistent with the hydraulic gradients in October 2009 and November 2010 because of the impact of a storm event during August 2009. The elevation of the lake at WBS in August 2009 was higher (~ 0.15 m) relative to the lake level the day

before (*see difference between August 2009 and October 2009 lake levels in Figures 4.1c and 4.1d*). This storm event caused high waves that infiltrated and raised the water table at the shoreline and caused the water table near the shore to rise.

It is evident that a relationship exists between the surface elevation and water table positions at a beach. Steep-sloped beaches (BBS, WBN) have deeper water tables compared with flat-sloped beaches (JPB, WBS) that have shallower water tables (Table 4.1). This relationship remains consistent seasonally as the surface elevations remain consistent in the backshore area of the beaches and the position of the water tables fluctuate in response to the rise and fall of lake levels. In addition, according to the Crowe and Milne (2007) definition of wet and dry beaches, the deep water table (> 50 cm) below BBS and WBN classify these beaches as dry beaches and the shallow water table (< 50 cm) below JPB and WBS classify these beaches as wet beaches.

4.2 Texture and Structure of the Tiny Township Beaches

4.2.1 Textural Characterization

A detailed textural characterization of the grain distribution and variation along the shores of the Great Lakes has not been presented in literature. The texture of the beach sediment was investigated in this study because it is hypothesized to control the wet and dry conditions of the Tiny Township beaches. Results from the mechanical sieving analysis are plotted as grain size distribution curves (*Appendix 2*). The beaches are classified as sandy beaches, comprised of approximately 100 percent sand (Table 4.2). Well below the beach surface at JPB and WBS, 110 and 120 cm respectively (~ 10 m inland), high percentages of silt particles were detected. Therefore, the textural classifications well below the surface at these beaches are loamy sands and sandy loams at JPB, and loamy sands, sandy loams, and silty loams at WBS.

In total, two hundred and sixty five field samples were sieved and analyzed from the vadose and saturated zone at all four beaches. The large number of field samples for grain size analysis is unique to this study and provides detailed information on the variability in grain sizes present below the surface at each beach. Mean grain sizes for each field sample were calculated graphically from the grain size distribution curves using Equation 3.8. A statistical summary of the arithmetic mean, median (d_{50}), range, variance, standard deviation, coefficient of variation, and uniformity coefficient for samples collected in the vadose and saturated zone are presented in Table 4.3. All four beaches are comprised of different sized sand grains, with the exception of JPB and WBS which also contain silt grains at depth. Figure 4.3 summarizes mean grain size distribution curves for the materials characterized at each beach. BBS is comprised of coarse sand (M = 0.647 mm), with a range of medium to very coarse sand. JPB is comprised of fine sand (M = 0.167 mm), with a range of silt to medium sand. WBN is also comprised of fine sand (M = 0.231 mm), with a range of fine to medium sand. WBS is comprised of medium sand (M = 0.283mm), with a range of silt to coarse sand. According to Table 4.3, WBS contains the highest variation, standard deviation, and coefficient of variation of all the beaches: 0.0176 mm^2, 0.133 mm, and 47 %, respectively. In addition, the average uniformity coefficient is highest for WBS (2.459), which further supports the high variability present within WBS compared to the other beaches. From the plots of the grain size distributions (Figure 4.3) and the uniformity coefficients presented in Table 4.3, it is evident that the slopes of the curves are not uniform (uniformity coefficient is greater than unity). This suggests that sands are a mixture of grain sizes (not well sorted) at all four beaches and variation exists.

The variation of grain size distributions within the beach profiles, based on individual 5 cm samples are presented in Figure 4.4.1 and Figure 4.4.2. Statistical analyses were conducted on the log transformed mean grain size data, using a single-factor ANOVA to determine if there are

statistically significant differences among the mean grain size distributions within each beach (i.e., the four sampling pits) and also among the four beaches (*refer to Appendix 2 for grain size distribution curves from all samples*). Results (Table 4.4) show JPB contains no statistically significant differences in mean grain sizes among sampling pits. BBS and WBN contain two sampling pits that are statistically significantly different and WBS has one sampling pit that is statistically significantly different within the beach. Results of significant differences among beaches are presented in Table 4.5. All beaches are statistically significantly different from each other, with the exception of WBN and WBS where no statistical significantly difference was detected. A possible explanation for this finding is attributed to the fact that these two beaches are in fact part of the same continuous section of beach (WBN and WBS are separated by less than 500 m) and hence it is likely that both were exposed to common sediment depositional and erosional processes. In addition, local residents stated that 30 years ago WBS was a dry beach with essentially the same characteristics as WBN. However, currently these beaches have very different appearances because beach-front residents have, and continue to, altered the beach profile by bulldozing the surface of the beach and sand dunes, in addition to installing break walls.

In summary, results of the grain size distributions below the Tiny Township beaches show that although the overall textures of these beaches are classified as sand, textural variations exist, ranging from fine sand to very coarse sand, both within a specific beach and also among the four beaches. Furthermore, statistically significant differences exist within and also among beaches, even though these beaches are within approximately 13 km along southern Georgian Bay. Previous studies have generally under classified or assumed that the textures within a beach are relatively homogeneous sands (e.g. Crowe and Milne, 2007; Darke and McKenna-Newman, 2008; Crowe and Meek, 2009; Skalbeck *et al.*, 2010), however, results from this study prove otherwise.

4.2.2 Volumetric Moisture Content, Bulk Density, and Porosity of the Tiny Township Beaches.

The structural properties, including bulk density and porosity of the beaches are known to affect the moisture retention of sand, and thus affect whether or not a beach is effectively a wet or a dry beach. Table 2A.1 (*Appendix 2*) summarizes the structural properties measured in August 2009 at the Tiny Township beaches. Above the water table, bulk densities and porosities were measured from the short-cores samples collected in the pits. However, below the water table, bulk densities and porosities were estimated from grain size data (Equations 3.15 and 3.16) due to methodology limitations (e.g. compaction and sediment loss), as previously discussed in *Chapter 3.0, Section 3.2.4.*

Bulk densities are plotted against depth below ground surface at the Tiny beaches (Figure 4.5). Bulk density estimates (from the vibracore samples) are presented in Figure 4.5 at depths of 95 – 205 cm and 90 – 200 cm at BBS1 and BBS3 respectively, 45 – 170 cm and 60 – 190 cm at JPB1 and JPB3 respectively, 80 – 155 cm and 90 – 155 cm at WBS1 and WBS4 respectively. The maximum bulk density is 1.80 $g \cdot cm^{-3}$, at JPB and WBS and the minimum is 1.28 $g \cdot cm^{-3}$, at BBS. No apparent trend is visible between bulk densities and depth below surface at all four beaches. Mean (arithmetic) bulk density values are: 1.47 $g \cdot cm^{-3}$, 1.53 $g \cdot cm^{-3}$, 1.55 $g \cdot cm^{-3}$, and 1.57 $g \cdot cm^{-3}$, respectively at BBS, JPB, WNB, and WBS. These bulk densities fall within the typical range for the bulk densities of sands (1.44 – 1.60 $g \cdot cm^{-3}$) (Solutions Direct, 2011).

Porosities at the Tiny Township beaches are plotted against depth below ground surface in Figure 4.6. Similar to bulk densities, no trend is apparent between porosities and depth below surface. The maximum porosity value is 0.53 at BBS and the minimum porosity is 0.32 at JPB and also WBS. The mean porosity values at each beach are 0.45, 0.42, 0.41, and 0.41 at BBS, JPB, WBN, and WBS, respectively. These porosity values fall within the range of sands, presented in Kasenow

(2002), where: fine sands range between 0.26 and 0.53, medium sands range between 0.29 and 0.49, and coarse sands range between 0.31 and 0.46.

Measurements of volumetric moisture contents were collected in the vadose zone using the TDR method and the short-cores method and are presented in Figure 4.7.1 and 4.7.2 respectively. The two methods did not yield the same volumetric moisture contents for each sample location. Figure 4.8 directly compares the measurements from the TDR method with the measurements from the short-cores method on a 1:1 graph. The TDR method generally measured higher moisture contents compared to the short cores method (approximately ≤ 10 %), with the exception of a few samples at all four beaches. Recall from *Chapter 3.0, Section 3.1.5,* that the TDR method detects volumetric moisture contents by measuring the variations of the bulk dielectric constant of a soil due to changes in the volume of water in the porous medium (Stephens, 1996). TDR provides a value averaged over the length of the sample probe (20 cm in this study) and is accurate to approximately 1 % volumetric water content. The universal calibration curve for TDR works best in sands but is subject to lesser accuracy at lower water contents (approximately < 5 %) due to the relative lack of continuous water filled pore pathways at these lower volumetric water contents. In addition, because the TDR averages moisture contents over the length of the 20 cm probes rather than over 5 cm collected with the short-cores, and the visible stratigraphic variation of the sand is on the centimeter scale, the small cores can be expected to capture more variation in water contents. However, although the measurements from the TDR and short-cores methods did not always coincide (due to methodology differences), the trend of soil moisture contents versus depth was consistent between both methods (Figure 4.7.1 and Figure 4.7.2).

During field collection, a heavy rain event occurred during the sampling of the WBN2 sand pit and just before sampling the WBN3 sand pit. During the rain event, water infiltrated into sand

through the beach surface and the walls of the open sand pits and increased the moisture content near the surface until a depth of approximately 15 – 20 cm below the surface. The increase in volumetric moisture contents is apparent at both WBN2 and WBN3. At WBN2, the TDR measurements were taken before the rain event and exhibit a similar surficial (upper 20 cm) moisture profile that is observed at the other sand pits (Figure 4.7.1c). But the short-cores data at WBN2, collected after the rain event, shows increased moisture content near surface due to infiltration (Figure 4.7.2c). At WBN3, also sampled just after the rain event, both the TDR and short-cores methods show an increased surficial moisture contents due to infiltration (Figure 4.7.1.c and Figure 4.7.2c).

Below the surface (approximately > 10 cm), the moisture contents measured by the TDR method decrease compared with the moisture contents measured by the short-cores method, where the moisture contents increase until 20 cm below the surface. This may be attributed to small scale heterogeneity captured by the short-cores method which directly measured the moisture content over a 5 cm length scale at intervals along the wall of the sampling pit. Such small-scale variations would not be directly detected by the TDR as a result of averaging moisture contents over the 20 cm length of the probes.

Although the measurements of the TDR and short-cores methods did not always coincide (due to methodology differences), both methods showed that the distribution of soil moisture with depth exhibited two distinct trends among all sites; a stepwise change in moisture content and a continuous decrease in moisture content. For example, the volumetric moisture contents (both TDR and short-cores) are stepwise in nature at BBS and WBN. The moisture contents remain less than 10 % well below the surface of the beach until approximately 15 – 20 cm above the water table, where the moisture contents increase linearly, and approach saturation at the water table. The moisture

contents at JPB and WBS exhibit a continuous increase with depth from ground surface to the water table water table.

Common at wet beaches, volumetric moisture contents decrease proportionally inland from the lake, as the elevation of the ground surface and depth to the water table increase. However, this trend is not observed below WBS1. The moisture contents at WBS1 are drier at and below the surface and appear stepwise in nature, similar to BBS and WBN. At this beach, WBS1 has the largest depth to the water table (0.537 m) along the transect. In addition, the volumetric moisture contents of the surface sands are drier (approaching residual saturation) at all beaches due to the influence of evaporation on the surface of the beaches. Moisture contents at the surface of BBS and WBN (and also WBS1) are drier (< 10 %), where as, moisture contents at the surface of JPB and WBS (WBS2-WBS4) are wetter (> 10 %), with the exception of the backshore locations at JPB (JPB3 and JPB4) (< 10 %). As such, it is apparent that moisture contents are lower at and below the surface of a beach when the elevation of the ground surface is high (> 50 cm above the lake) and the depth of the water table below the surface is low (> 50 cm from the surface). In contrast, moisture contents are higher at and below the surface of a beach when the elevation of the ground surface is low (< 50 cm above the lake) and the depth to the water table is close to the surface (< 50 cm from the surface).

In addition, there is a relationship between volumetric moisture content and texture of the beach sand. For example, the beach with the coarsest sand (BBS) contains the lowest volumetric moisture contents from all soil pits, ranging from approximately 1 – 7 % at the surface and also at depths well below the surface of the beach. Where as, higher moisture contents are observed in the beaches comprised of fine sand. For example, at WBS (WBS2 – WBS4), moisture contents ranged from approximately 20 – 34 % at and below the surface of the beach. High moisture contents are also observed at and below the surface of JPB, however, these moisture contents have a larger

range from approximately 12 – 42 %, where the lowest moisture content was measured in the furthest sampling pit (inland) from the lake (JPB4) and the highest moisture content was detected in the sampling pit closest to the lake (JPB1).

In summary, the results of the bulk densities and porosities at the Tiny Township beaches are consistent with the ranges for similar textured sands presented in literature (Kasenow, 2002). Moisture contents are generally lower (< 10%) at and below the surface at BBS and WBN (dry beaches) and increase linearly close to the water table (~ 15 – 20 cm). Moisture contents are generally higher (> 10 %) at and below the surface at JPB and WBS (wet beaches), with the exception of the sand dune at WBS1 (dry section of the wet beach), and increase continuously with depth. Furthermore, the profiles of the moisture contents along each transect of sampling pits show the proportion of the profile that is near residual saturation increases with depth inland from the lake, proportional to the increasing ground surface elevation/increasing depth to the water table. It is also apparent that a relationship between texture and moisture content exists at the Tiny Township beaches; coarse sands are drier compared to fine sands.

4.3 Hydraulic Conductivity of the Tiny Township Beaches

4.3.1 Field Saturated Hydraulic Conductivities

i. Guelph Permeameter

Field-saturated hydraulic conductivities (K_{fs}), were determined through a total of 30 Guelph Permeameter tests conducted in different materials (fine to coarse sand), at various depths below the beaches. To verify that the K_{fs} measurement corresponded to the texture of interest grab samples were collected from the soil auger (used to prepare the hole for the Guelph Permeameter

test) and sieved in the lab to determine the mean grain size. Results from the mechanical sieving analysis of the grab samples are presented as grain size distribution curves in *Appendix 3*.

Table 4.6 presents the field-saturated hydraulic conductivities that were calculated from the Guelph Permeameter measurements using Equation 3.1. The corresponding textural classifications from the grab samples are also presented in this table, at all four beaches. The variations in K_{fs} among beaches range between one to two orders of magnitude. Within a beach however, the range in K_{fs} varies by less than a half an order of magnitude. The geometric means of the K_{fs} are 8.38×10^{-2} $cm.s^{-1}$, 9.07×10^{-3} $cm.s^{-1}$, 2.39×10^{-2} $cm.s^{-1}$, and 2.96×10^{-2} $cm.s^{-1}$, at BBS, JPB, WBN, and WBS, respectively (Table 4.7). WBN, and WBS values are consistent with the range of K_{fs} reported at Lake Huron and Georgian Bay beaches in Crowe and Meek (2009) (2.91×10^{-2} $cm.s^{-2}$ to 8.69×10^{-2} $cm.s^{-1}$). Furthermore, K_{fs} at JPB are similar to the mean hydraulic conductivities of lacustrine sand reported in Crowe *et al.* (2004) (4.17×10^{-3} $cm.s^{-1}$), and WBN and WBS are consistent with the mean conductivities for Aeolian sand reported in that study (2.52×10^{-2} $cm.s^{-1}$). Overall, the variation (coefficient of variation) in field-saturated hydraulic conductivities is relatively small within each beach, by less than a factor of 2 (less than 100%). Although small, variation does exist within these beaches and is highest at WBN (fine sand) and lowest at BBS (coarse sand).

A single-factor ANOVA was conducted on the log transformed field-saturated hydraulic conductivities to test if there are significant differences in K_{fs} among beaches (*Appendix 3, Table 3A.1*). Results show that there is a statistical significant difference in K_{fs} at BBS compared to the other beaches, however, there is no statistical significant difference detected in K_{fs} among JPB, WBN, and WBS. BBS is predominantly coarse sands (K_{fs}) compared to JPB, WBN, and WBS which are predominantly comprised of fine-medium sands (lower K_{fs}). In addition, a single-factor ANOVA was also conducted on the K_{fs} to determine if there is a statistical significant difference between the

corresponding textures (determined from the grab samples) (*Appendix 3, Table 3A.2*). A statistical significant difference was detected among the fine, medium, and coarse textures from all of the beaches.

ii. Minidisk Infiltrometer Measurements

A total of forty-four minidisk infiltrometer (MDI) K_{fs} measurements were taken at the surface of each beach, using multiple applied suctions (2 cm, 4 cm, and 6 cm). Grab samples were not collected (or analyzed for texture) from the surface sand at the beaches, therefore, the K_{fs} measurements correspond to textural data that was collected and analyzed at the surface of the beaches in August 2009. Results are presented in Table 4.8, including geometric mean and K_{fs} values at each beach. Mean K_{fs} values for the surface sands at BBS, JPB, WBN, and WBS are: 4.53×10^{-2} $cm.s^{-1}$, 5.92×10^{-2} $cm.s^{-1}$, 8.33×10^{-2} $cm.s^{-1}$, and 5.07×10^{-2} $cm.s^{-1}$, respectively. Hydraulic conductivities are consistent with the range of the Guelph Permeameter conductivities. Therefore, it can be concluded that there are no surface effects influencing K_{fs} values compared Guelph Permeameter K_{fs} values below the beaches.

In summary, measurements of field-saturated hydraulic conductivities at the beaches are consistent within the range of K_{fs} reported in literature at beaches of the Great Lakes. Although small, variations are present within the measurements of K_{fs} within a particular beach. Statistical significant differences are detected between the K_{fs} of textures; however, these differences are not as apparent among the beaches, with the exception of BBS which is statistically significantly different. Both the Guelph Permeameter and Minidisk Infiltrometer methods yield K_{fs} measurements that are consistent within the same range. These methods are advantageous for determining the K_{fs} at a beach because they provide *in situ* field measurements that capture the effect of local

heterogeneities on K_{fs}. It is important to recognize that both methods provide field-saturated hydraulic conductivity measurements, not saturated hydraulic conductivity measurements, due to the presence of residual air when conducting the tests (Reynolds and Elrick, 1987; Marinas, 2009).

4.3.2 Empirical Methods Predicting Saturated Hydraulic Conductivities

Empirical methods were used to predict the saturated hydraulic conductivities (K_{sat}) of beach sands using textural data. Field methods predicting the K_{sat} of soils are time consuming and costly. Furthermore, field methods used in the vadose zone (e.g. Guelph Permeameter and Minidisk Infiltrometer) do not provide measurements of K_{sat}; instead, they provide field-saturated hydraulic conductivities (K_{fs}), which have been found to be lower than K_{sat} by a factor of 2 to 6, due to the presence of residual air (Marinas, 2009). In addition, field measurements of K_{fs} are affected by local heterogeneities present within porous media; where, groundwater preferentially flows faster along coarser layers (high K_{sat}) and slowly across finer layers (low K_{sat}) (Freeze and Cherry, 1979). As such, empirical methods are at times advantageous because they provide a cost effective and relatively fast means of collecting saturated hydraulic conductivities using only textural data.

Studies have not tested the reliability of empirical methods in predicting K_{sat} below beaches, and in particular below the beaches of the Great Lakes. In this study, empirical methods were investigated to determine the K_{sat} of the beach sand in Tiny Township, using the textural data that was provided from the grain size analyses. In addition, to enhance these estimation techniques, the 'β' parameters embedded within the empirical formulas were calibrated to the mean K_{fs} values that were measured at the beaches using the Guelph Permeameter.

i. Empirical Methods

Four empirical methods (Hazen, Slitcher, Beyer, and Kozeny-Carman) were used to estimate the K_{sat} at the Tiny Township (*see Section 3.3.1, Table 3.1*). A statistical summary conducted on the log transformed K_{sat} data is summarized in Table 4.9, including the geometric mean, range, standard deviation, variance, and coefficient of variation for all empirical methods. The means from the empirical estimates (K_{sat}) are consistent within one order of magnitude of the Guelph Permeameter (K_{fs}) means (*refer to* Table 4.7). It was hypothesized that the variability (coefficient of variation) of the predicted K_{sat} would be high because this method incorporates small scale heterogeneities (i.e. 5 cm increments) that are captured within the textural data. Results show that the variability in K_{sat} estimates predicted by all of the empirical methods is relatively small; less than 100 % or by a factor of 2. The small variability in K_{sat} is consistent among all of the empirical methods, where, WBN has the highest variability, followed by JPB, WBS, and BBS.

Results comparing the empirical estimates (K_{sat}) with the corresponding Guelph Permeameter measurements (K_{fs}) are presented in Table 4.10. It was hypothesized that the empirical estimates would predict higher K_{sat} values compared to the measured K_{fs} values by factors of 2 to 6, due to the presence of residual air. However, results are not consistent with this hypothesis. That is, the empirical methods predicted both higher and lower K_{sat} values compared to the Guelph Permeameter method. The Guelph Permeameter K_{fs} measurements were then adjusted to K_{sat} by multiplying the values by a factor of 3.5 to account for residual air present in soils when using this method (Reynolds and Elrick, 1987). Table 4.11 summarizes the adjusted Guelph Permeameter measurements of K_{fs} to K_{sat}, with the corresponding empirical estimates of K_{sat}. The empirical estimates are generally lower compared to the adjusted Guelph Permeameter (K_{sat}) values, with the exception of WBS3 and WBS4, where the empirical estimates are higher.

A single-factor ANOVA was conducted on the Guelph Permeameter measurements of K_{fs} and the empirical estimates of K_{sat}, to determine if there is a statistical significant difference between the measured and predicted hydraulic conductivities (K_{fs} vs. K_{sat}). Results presented in Table 3A.2 (*Appendix 3*) show that a statistical significant difference was only detected between the Guelph Permeameter method and the Slitcher Method. In addition, a single-factor ANOVA was also conducted on the adjusted Guelph Permeameter measurements (K_{sat}) with the empirical estimates (K_{sat}). A statistical significant difference was detected among the Guelph Permeameter and all of the empirical methods (*Appendix 3, Table 3A.3*).

In summary, the estimates of K_{sat} did not consistently predict higher conductivity estimates compared to the K_{fs} measurements as originally hypothesized. This may be explained due to the differences between techniques, where the empirical methods predict the K_{sat} at a small scale (individual samples), whereas, the Guelph Permeameter method measures *in situ* K_{fs} over a much larger scale which could account for local heterogeneities. Furthermore, the measurements of the adjusted K_{sat} from the Guelph Permeameter method were higher and also statistically significantly different than the estimates of K_{sat} from the empirical methods. Therefore, although the empirical methods provide estimates of K_{sat} that are within the range of the Guelph Permeameter measurements, this study suggests that the Guelph Permeameter method is a superior method in obtaining both the K_{fs} and K_{sat} of sands at these beaches. This is because, the Guelph Permeameter method accounts for entrapped air present during saturation of these sands and also accounts for the influence of local heterogeneities present at these beaches. However, if only textural information is available, this study proves the validity of these methods in predicting reasonable estimates of K_{sat} of sands, consistent with previous studies testing the validity of the estimates on sand in general (Vukovic and Soro, 1992; Kasenow, 2002; Odong, 2007; Song *et al.,* 2009).

ii. Calibrated Empirical Methods

Unique to this study, the four empirical equations were enhanced by modifying their β–parameters in order to accurately represent the K_{sat} (adjusted) values that were provided by the Guelph Permeameter method. β–parameters were initially calibrated to the mean Guelph Permeameter K_{sat} measurements at each beach, followed by conductivity calculations using the four empirical equations. This method forces the empirically predicted means to equal the Guelph Permeameter means, while capturing variability due to textural differences. The empirical equations (*see Table 3.1*) were rearranged to isolate and solve for β and to substitute the 'K_s' term in the equations by the mean Guelph Permeameter K_{sat}. The new (calibrated) β–parameters were calculated by:

$$\beta_{HC} = \frac{K_s}{\left[\frac{g}{\upsilon} \times (1 + 10(n - 0.26))d_{10}^2\right]} \tag{4.3}$$

$$\beta_{SC} = \frac{K_s}{\left[\frac{g}{\upsilon} \times (n^{3.287})d_{10}^2\right]} \tag{4.4}$$

$$\beta_{BC} = \frac{K_s}{\left[\frac{g}{\upsilon} \times (\log\frac{500}{C_u})d_{10}^2\right]} \tag{4.5}$$

$$\beta_{KCC} = \frac{K_s}{\left[\frac{g}{\upsilon} \times \left(\frac{n^3}{(1-n)^2}\right) \times d_{10}^2\right]} \tag{4.6}$$

where β_{HC} is the new Hazen-Calibrated coefficient [dimensionless], β_{SC} is the new Slitcher-Calibrated coefficient [dimensionless], β_{BC} is the new Beyer-Calibrated coefficient [dimensionless], β_{KCC} is the new Kozeny-Carman-Calibrated coefficient [dimensionless], K_s is the empirical saturated hydraulic

conductivity term that was substituted using the mean K_{sat} values from the Guelph Permeameter method ($m \cdot s^{-1}$), g is the gravitational constant (9.81 $m \cdot s^{-1}$), υ is the kinematic viscosity ($m^2 \cdot s^{-1}$), d_{10} is the effective diameter (m), n is the porosity [dimensionless], and C_u is the coefficient of uniformity [dimensionless]. Once all of the β–parameters were calibrated using the corresponding textural data (n, d_{10}, and/or C_u) from the grab samples and mean K_{sat} from the Guelph Permeameter measurements, the arithmetic means were calculated to produce a calibrated β–parameters for each method at each of the beaches.

Calibrated β–parameters are presented in Table 4.12. The β-calibrated empirical equations were used to recalculate the K_{sat} values below the beaches using their corresponding textural data at 5 cm increments. The mean, range, variance, standard deviation, and coefficient of variation for all beaches are summarized in Table 4.13. It is important to note that the means presented in this table are not equal to the Guelph Permeameter means (*presented in* Table 4.9) because the modified equations were not only applied to the textural data from the corresponding Guelph Permeameter grab samples, but were also applied to all of the textural samples that were collected at the beaches. However, when directly comparing the means of the empirical K_{sat} to the Guelph Permeameter (adjusted) K_{sat}, the means are equal as a result of the calibration. Consistent original empirical estimates (Table 4.9), the variability (coefficient of variation) among the calibrated estimates is also small; less than 100 % (or by a factor of 2). Furthermore, the variation present within the K_{sat}-calibrated estimates is highest at WBN and JPB and lowest at BBS and WBS, also consistent with original empirical estimates and Guelph Permeameter measurements. However, because the enhanced empirical methods were calibrated to the Guelph Permeameter K_{sat} (adjusted measurements), the variability is approximately 10 % smaller compared to the original empirical estimates.

Only one empirical method was selected to estimate the K_{sat} of the materials at the beaches for input parameters in the HYDRUS-2D numerical model. In order to select the appropriate method, a single-factor ANOVA test was conducted to test all four methods to see if there is a statistical significant difference in their predicted values of K_{sat}. Results from the ANOVA are presented in *Appendix 3, Table 3A.4*, where no statistical significant difference was detected. As such, all four modified empirical methods are appropriate in predicting the K_{sat} at the Tiny Township beaches. However, the empirical method selected for this study is the Kozeny-Carman-Calibrated method because it is recognized as one of the most commonly accepted empirical methods used in studies as it has been found to accurately predict K_{sat} values closest to those obtained experimentally (Vukovic and Soro, 1992; Odong, 2007).

In summary, this study enhances the estimation techniques of predicting the K_{sat} at the beaches of Tiny Township. The calibrated empirical methods are advantageous to use when predicting the K_{sat} of the beaches of the Great Lakes because they incorporate *in situ* field measurements (expressed within the β–parameter) and also capture variability through textural data. Although the variability expressed by these estimates is relatively small, it is consistent with the variability captured by *in situ* K_{fs} methods. Furthermore, the empirical estimates support field measurements, indicating that the fine grained beaches of Tiny Township (WBN and JPB) are more variable in K_{sat} compared to the medium and coarse grained beaches (WBS and BBS).

4.4 Beach Hydrology: Calibrating Saturated-Unsaturated Beach Models of Tiny Township

Groundwater flow below the water table has been previously simulated at beaches using saturated flow models (Cheng and Anderson, 1993; Townley and Trefry, 2000; Hunt *et al.*, 2003; Crowe *et al.*, 2004; Meek, 2007). Currently, there is a lack of groundwater modelling which includes

both the vadose zone and saturated zone at beaches of the Great Lakes. In this study, the saturated-unsaturated numerical model HYDRUS-2D was used to model the beaches of Tiny Township. Numerical modelling of these beaches has three primary goals: (1) providing insight on why wet and dry beaches exist along the shores of southern Georgian Bay; (2) characterizing the role of various physical and hydrogeological factors on moisture contents of the beaches; and (3) providing a framework for testing beach management scenarios. The following section describes how the four beach models were calibrated to field data and also the sensitivity analysis that was conducted to validate the models for the use at the beaches of the Great Lakes.

4.4.1 Calibrations of the Tiny Township Beach Models

i. Groundwater Flow

Groundwater flow under steady state conditions were examined in models for each of the four beaches to determine appropriate boundary and initial conditions. True steady state conditions do not exist at beaches because they are dynamic systems which are continuously exposed to forces such as waves and lake level fluctuations. This study therefore recognizes this fact, however, assumes that field measurements taken in August 2009 represent dynamic equilibrium conditions that will be referred to and discussed as "steady state conditions" in this section. Steady state conditions were reached approximately 2.5 days, when there was no change of groundwater flux into and out of the beach with time. Groundwater velocity vectors and the hydraulic gradients in the beach models are consistent with field measurements. As such, groundwater within the models flows from the inland constant head boundary horizontally towards the lake, and discharges vertically at the lake. This is also consistent with beach groundwater flow conditions presented in Horn (2002 & 2006), Meek (2007) and Crowe and Meek (2009). Although HYDRUS-2D provides the

option for seepage face boundary conditions, the beach models were not calibrated with seepage face boundaries at the shoreface. As discussed in *Chapter 2.0, Section 2.2.2*, groundwater flow at a beach not only discharges at the lake, but also at the seepage face (Horn, 2002 & 2006). This is attributed to a well developed capillary fringe (above the water table) intersecting the shoreface (Neba *et al.*, 2002). The relatively small scale of the seepage face and localized groundwater conditions compared to the backshore area of a beach is not within the scope of this study and furthermore, would not have a significant influence on the groundwater flow conditions beyond the nearshore environment at a beach. As such, the groundwater flow vectors in the models flow along the shoreface boundary and discharges vertically into the lake.

ii. Water Table Positions

Water table positions in the models were calibrated by adjusting the constant head boundary on the landward boundary of the model domains, until the elevation of the water tables matched the measured elevations of the water tables for August 2009. Figure 4.9 summarizes the calibrated water table elevations compared with the measured (field) elevations for all four beaches. Corresponding data values are presented in Table 4A.1 (*Appendix 4*). Circled in Figure 4.9 are outliers that were measured in the field, compared with the calibrated water table elevations in the models. At BBS, outliers are observed adjacent to the lake, where they are approximately 5 cm lower than the lake level. This is because there were high waves which caused the measured lake level to be higher. At JPB, an outlier exists at the end of the transect, where the measured water table position is 10 cm higher compared with the calibrated water table position. This elevation does not follow the same slope compared with the other water table elevations at JPB. As such, it is possible that local heterogeneities not detected during field sampling are responsible for the higher

water table elevation. That is, materials with lower K_{sat} can induce a steeper water table slope. A similar outlier is observed at the end of the transect at WBS, where the measured water table elevation is 14 cm higher than the calibrated water table elevation. The presence of local heterogeneities not detected during field sampling may also explain the presence of this outlier. Finally, the elevation of the lake measured at WBS appears to be artificially high compared to the adjacent water table elevations. Similar to BBS, rough waves and an incoming storm also recorded in field notes explains the temporary high lake level compared to the adjacent water table elevations (*previously discussed in Section 4.1*).

To further investigate the accuracy of the calibrated water table elevations with measured field elevations, 1:1 plots were created (Figure 4.10). In addition, simulation results were compared with field data by calculating the Root-Mean-Squared (RMS) error between the measured and calibrated water table elevations (Anderson and Woessner, 1992). Comparison of field measurements with simulation results indicates low RMS errors of 1.4 cm, 1.2 cm, 0.4 cm, and 1.9 cm for BBS, JPB, WBN, and WBS, respectively; therefore, the water table calibrations were successful.

The boundary conditions in the WBS model were different from the other beaches because WBS contains the highest heterogeneity as observed due to the presence of two water table slopes and also through high textural variations. In order to account for the influence of textural variations on the position of the water table, a constant flux boundary condition was used instead of a constant head boundary. Theoretically, the slope of the water table is dependent on the K_{sat} of the beach sand. That is, the groundwater flux (Darcy flux, q) is proportional to the saturated hydraulic conductivity (K_{sat}) multiplied by the hydraulic gradient (slope of the water table, $\Delta h/\Delta l$) (Freeze and Cherry, 1979). Therefore, materials with lower K_{sat} restrict groundwater flow, thereby increasing the

hydraulic gradient in this zone relative to zones with a higher K_{sat}. According to the field data for hydraulic gradients (slope of the water table) at WBS, the texture of the sand near the lake should be coarser (lower K_{sat}) than the sand away from the lake (higher K_{sat}). Field textural and K_{sat} data at WBS however, contradicts this; fine and medium sands (lower K_{sat}) were detected near the lake and medium and coarse sands (higher K_{sat}) were detected away from the lake. Therefore, in order to calibrate the water table, the material layers within the model were modified to fit the water table position to field data. A coarse sand layer was substituted for the fine-medium layer (near the lake) and a fine sand layer was substituted for the medium-coarse later (away from the lake). In addition, the bottom loam layer in the WBS model was not adjusted because it is deep enough below the beach, thereby not directly influencing the slope of the water table.

iii. Soil Hydraulic Parameters

Soil hydraulic parameters calculated by the Neutral Network Prediction (Rosetta) method that is built into the HYDRUS-2D model are summarized in Table 4.14. HYDRUS-2D uses van Genuchten (1980) soil hydraulic parameters to calculate soil moisture retention curves presented in Figure 4.11. The moisture curves represent the ability of the sands below each beach (wet or dry) to retain water.

As observed in Figure 4.11, it is evident that predicted soil moisture retention curves do not match the volumetric moisture profiles measured above the water table at the beaches in August 2009. This is because, the Neural Network Prediction method is an approximation method based on using single material properties (e.g. texture (% sand, % silt, and % clay) and bulk density) to predict the soil hydraulic parameters (van Genuchten parameters) of a soil. In order to calibrate the beach models to the field moisture profiles (volumetric moisture contents), soil hydraulic parameters: α, *n,*

θ_r, and θ_s were adjusted to fit the soil moisture retention curves to the field moisture profiles; where α, *n,* are van Genuchten (1980) curve fitting parameters, θ_r and θ_s are the residual and saturated volumetric moisture contents. Recall, that for these calibrations the assumption was made that the moisture profiles from field measurements represented steady state (or dynamic equilibrium) conditions at the Tiny Township beaches. First, the maximum porosity values measured in the field at each beach was used for θ_s. Next, α and *n* parameters were adjusted until the moisture contents within the beach models fit the field moisture profiles. Finally, θ_r values were adjusted to fit the surface moisture contents with the moisture contents that were measured just below the surface in the field. The θ_r that were measured from surface samples in the field were not used as the θ_r value. This is because, the surface samples were exposed to high evaporation rates and are therefore, not representative of true moisture contents that correspond with a particular height above the water table (negative pressures) in the soil moisture retention function. In addition, some beaches contained up to three different material layers, therefore, the layers were individually calibrated to corresponding sample pits that were comprised of the same texture/saturated hydraulic conductivity.

Figure 4.12 presents the calibrated moisture retention curves that best fit the field measurements. Examining the calibrated moisture curves, it is clear that the beaches do not retain moisture above the water table in the same way. For example, BBS holds 15 % moisture up to a depth of 20 cm above the water table, where as, JPB holds the same moisture content but at higher elevations, about 60 cm above the water table. Similarly, the WBN and WBS hold the same moisture (15 %) approximately 35 – 40 cm above the water table. It is therefore evident that the texture comprising each beach plays a role in retaining water which is a defining characteristic of a wet or dry beach.

Saturated hydraulic conductivities influence the hydraulic gradient (slope of the water table) within the beaches and are also considered a soil hydraulic parameter in HYDRUS-2D. The material layers comprising each beach model were assigned a K_{sat}, instead of a textural classification. As such, the empirically predicted K_{sat} (Kozeny-Carman-Calibrated Method) values that were calculated for each sediment sample were divided into material layers by grouping together similar K_{sat} within half of an order of magnitude (e.g. 1 x 10^{-1} to 5 x 10^{-1} cm·s^{-1}, 5 x 10^{-1} – 1 x 10^{-2} cm·s^{-1}, etc.). The geometric mean K_{sat} for each layer was then calculated and used as the final K_{sat} that calibrated the beach models. Because groundwater flow below the water table was being modelled for these calibrations, K_{sat} values were used instead of K_{fs} values. However, if the vadose zone was of particular interest, the K_{fs} would be a better conductivity to use because it accounts for the presence of residual air. Table 4.15 summarizes the calibrated soil hydraulic parameters used in all four calibrated beach models.

4.4.2 Sensitivity Analyses: Validation of Calibrated Beach Models

Sensitivity analyses were undertaken to validate the soil hydraulic parameters (θ_s, K_s, α, and n) that were used to calibrate the beach models. Table 3.5 (*Chapter 3.0*) provides an overview of the soil hydraulic parameters tested including their values and data sources. Soil hydraulic parameters: θ_s and K_s, were varied within the range of measurements for the sands of Tiny Township. α, and n parameters were varied consistent within the range of values reported in the sensitivity analysis presented in Albright *et al.* (2002). The sensitivity analyses were conducted on two of the beach models: JPB (flat-sloped, wet beach) and WBN (steep-sloped, dry beach). Van Genuchten soil moisture retention curves were used to investigate the sensitivity of the models to variations in θ_s,

α, and *n.* Curves of unsaturated hydraulic conductivities (*K*(*h*)) as a function of moisture contents (*q*) were used to investigate the sensitivity of the models to variations in θ_s, K_s, and *n*.

Results are presented in Figure 4.13 (JPB) and Figure 4.14 (WBN), showing the sensitivity of the soil moisture retention curves (SMRC) when varying one parameter at a time, while holding the other parameters constant. The soil moisture retention curves are most sensitive when varying the α parameter, followed by θ_s and *n*. Adjusting the K_s values has no effect on the SMRC because it is not a parameter used within the SMRC function (van Genuchten, 1980). The sensitivity of the SMRC to these parameters is consistent with sensitivity results reported in Albright *et al.* (2002). For example, the α parameter controls the slope of the SMRC, therefore, increasing α results in lower moisture contents retained above the water tables and also throughout the profiles. Decreasing the α parameter results in higher moisture contents retained at the water tables and also at higher elevations above the water tables. Varying the *n* parameter also influences the slope of the SMRC, but results indicate that *n* only influences the slopes near saturation (at the water table) and approaching residual saturation (well above the water table). Because the overall shape of the SMRC is sensitive to adjustments of the α and *n* parameters, the calibrated beach models are thereby validated because the parameters were selected based on fitting the SMRC to the moisture contents that were directly measured in the field. In addition, when varying the θ_s parameter, the SMRC is most sensitive to moisture retained directly above the water table and has no influence well above the water table and also at the surface. Due to the fact that the θ_s does not have a large influence controlling the overall shape of the moisture retention profile and also because this parameter was chosen based on the maximum porosity values that were measured in the field, the final values selected for this parameter validates the models.

In addition, sensitivity results of unsaturated hydraulic conductivities ($K(h)$) as a function of moisture contents (θ) are summarized in Figure 4.15 and Figure 4.16. The shape of the curve is most sensitive to variations in n followed by variations in K_s, and θ_s. The α parameter has no influence on the $K(h)$ function because it is not a parameter used in the equation. In addition, the K_s and θ_s parameters do not significantly influence the sensitivity of the $K(h)$ function because q_s only sets the maximum moisture content and K_s only sets the maximum $K(h)$ within the model. The n parameter however, controls the $K(h)$ of a material under variable θ. In other words, n expresses how well a material conducts at different moisture contents. Sensitivity results for the n parameter are consistent with expectations of the influence of n on $K(h)$. For example, at a moisture content of 30 %, an increase in n indicates that the material does not conduct well in the vadose zone (lower $K(h)$), compared to a decrease in n, which indicates that the material conducts well in the vadose zone (higher $K(h)$). Results from the sensitivity analyses indicate that n accounts for how well sorted particular material is. Well sorted materials consistently conduct well in the vadose zone (high n: uniform pores), whereas, poorly sorted materials (low n: combination of small and large pores) do not conduct well under low moisture contents, instead, conduct well under high moisture contents, once the large pores are filled.

The objective of the sensitivity analyses was to validate the values assigned to the soil hydraulic parameters during the calibration of the beach models. The most sensitive parameter in the soil moisture retention function and also the unsaturated hydraulic conductivity function is α and n, respectively. K_s, and θ_s were not highly sensitive parameters in both functions. Because the beach models were calibrated directly to field measurements (water table elevations and moisture profiles) and the lateral boundary conditions were set far enough away to not influence

groundwater flow conditions, the four beach models thereby validated as they accurately represent field conditions at the Tiny Township beaches.

4.4.3 Calibrated Beach Models of Tiny Township

The calibration of all four beach models was successful in reproducing conditions that correspond with field measurements. In addition, results from the sensitivity analyses validated the models. The final calibrated models for the beaches are presented in Figures 4.17.1, 4.17.2, 4.17.3, and 4.17.4 for BBS, JPB, WBN, and WBS, respectively. The figures show the 2D profiles of water contents (volumetric moisture content) and pressure heads at the beaches. The cross section in each beach model that corresponds to the transect at the field sites is outlined in the figures and should be referred to in this section.

It is evident that the profiles of moisture contents (water contents) and pressure heads are not uniform or consistent among the beaches. The beaches with a deep water table: BBS and WBN are drier (low moisture contents) compared to beaches with a shallow water table: JPB and WBS (high moisture contents). Above the water table (above 0 cm of pressure) at BBS (dry beach), is the smallest transition zone of moisture contents (vertically) before dry conditions are reached. In contrast, at WBN (dry beach) there is a larger transition zone of moisture contents (vertically). Although both beaches are dry with deep water tables, the different transition zones are explained through textural differences between beaches. BBS is comprised of coarse sand grains whereas WBN comprised of fine sand grains, therefore, moisture is retained differently above the water table at both beaches. In addition, the transition zone of moisture contents is highest at JPB and also in the backshore of WBS (shallow water table beaches), where high moisture contents extend from the water table to the surface. Dry conditions are not reached at these beaches until well beyond the

field transect, approximately 5000 cm and 4000 cm inland from the lake at JPB and WBN, respectively and also below the sand dune at WBS, where the depth to the water table is highest.

The 2D pressure head profiles in the beach models are also not consistent among the beaches. BBS and WBS are comprised of the lowest pressure heads across the surface and within the beach profile, where pressure heads are approximately -100 cm to -200 cm (higher suction) above the water table. Corresponding with low moisture contents, BBS and WBN have low pressures above the water table because only residual moisture is present at these beaches, where water is tightly held in pores by capillarity. In contrast, JPB and WBS have higher pressure heads of approximately -50 cm at the surface and also within the beach profile (lower suction). Very low pressures are present only when the surface topography increases at these beaches and when residual moisture contents are present.

In summary, the calibrated models show the continuous and 2D conditions that are present within a beach. The relationship between surface topography and also depth to the water table with moisture contents is evident at all of the beaches, where shallow flat surfaces and shallow water tables are present at wet beaches and steep surfaces and deep water tables are present at dry beaches. In addition, the influence of sand texture on the moisture retained at the beaches is observed through the different transition zones of moisture contents above the water table at each beach. Beach managers, scientists, and consultants could use these beach models to run scenarios to gain insight and a better understanding of the associated problems at beaches of the Great Lakes.

4.5 Discussion and Classification of the Tiny Township Beaches

4.5.1 Physical and Hydrogeological Properties Influencing Moisture Conditions of Beaches

A detailed characterization of the physical and hydrogeolgical properties of wet and dry beaches were investigated in this study to determine why some of the beaches along southern Georgian Bay are wet and others are dry. Following the field, laboratory, and modelling analyses of the Tiny Township beaches, three characteristics were found to influence whether a beach is wet or dry; (1) surface topography of a beach, (2) depth to the water table, and (3) texture of the sand at a beach. These characteristics are interconnected and are summarized in the table below:

(1) Topography + (2) Depth to Water Table	**(3) Texture**		
	Fine Sand	*Medium Sand*	*Coarse Sand*
Steep Surface + Deep Water Table (> 50 cm)	Dry Beach	Dry Beach	Dry Beach
Flat Surface + Shallow Water Table (< 50 cm)	Wet Beach	Wet Beach	Dry Beach

where; a dry beach is defined when the moisture content is < 10 % at and below the surface of the beach until approximately 20 – 25 cm above the water table and a wet beach is defined when the surface moisture content is > 10 % moisture at the surface of the beach and increases linearly with depth to the water table.

i. Surface Topography of a Beach

The surface topography of a beach is controlled both naturally and by human activities. In addition, common among all natural beaches, the surface elevation increases inland from the lake; but the rate of increase in the slope of the surface is different between wet and dry beaches. Natural wet beaches exist when the surface topography is naturally flat-sloped and remains unaltered by human activities. Natural dry beaches exist when the surface topography is naturally

steep-sloped as a result of Aeolian sediment transport processes creating sand dunes on the leeward side of the beach. Wet beaches also exist when natural dry beaches are degraded by human activities (e.g. bulldozing sand dunes and beach sand) having artificially changed the natural topography of the beach by lowering the ground surface.

ii. Depth to the Water Table

A relationship exists between the surface topography of a beach and the depth to the water table where; flat-sloped beaches have shallow water tables and steep-sloped beaches have deep water tables. Hydraulic gradients at wet and dry beaches are not very different and are essentially shallow-sloped, therefore, the depth to the water table is primarily a function of the elevation of the ground surface and not the slope of the water table. A relationship also exists between the depth to the water table and the moisture conditions at beaches. Beaches with shallow water tables have high moisture contents (> 10 %) at and below the surface of the beach, increasing linearly with depth. In contrast, beaches with deep water tables have low moisture contents (< 10 %) at the surface of a beach until approximately 20 – 25 cm above the water table. Moisture contents at the beaches with deep water tables are stepwise in nature. Therefore, beaches with shallow water tables are classified as wet and beaches with deep water tables are classified as dry.

iii. Texture of the Sand at a Beach

Along with influencing the slope of the water table at a beach, the role of texture also influences the moisture content that is retained within the pore spaces above the water table by the phenomenon of capillarity. This fundamental relationship is best described through the soil moisture retention curve of various sediment textures. Figure 4.18 presents a *Type Curve* which summarizes

the moisture retention abilities of different textures present at the beaches of the Great Lakes, ranging from gravel (> 2mm) to very fine sand (0.0625 mm to 0.125 mm). Presented in this study, wet and dry beaches are defined when the moisture content at the surface of the beach is < 10 % moisture. From Figure 4.18, it is evident that different textures do not similarly retain moisture above the water table. For example, at 10 % moisture, a gravel beach would be classified as wet if the depth of the water table was approximately ≤ 8 cm below the surface. In contrast, if the beach was comprised of very fine sand, the beach would be classified as wet if the depth of the water table was approximately > 160 cm below the surface. In general, coarser sands do not retain moisture well above the water table compared to finer sands.

The texture of the beach sand also influences the depth of the water table at beaches because the texture of the sand controls the hydraulic gradient of the water table. This is explained through basic hydrogeological theory (*Darcy's Law*), which indicates that the groundwater flux (q) is proportional to the saturated hydraulic conductivity of a porous medium and also hydraulic gradient. As such, for equally amounts of flux, coarse grained materials (high K_{sat}) induce low hydraulic gradients (flat-sloped water tables) and fine grained materials (low K_{sat}) induce high hydraulic gradients (steep-sloped water tables). As such, beaches with coarse sand have lower water table depths due to lower hydraulic gradients and hence the water table becomes proportionally deeper moving inland. Therefore, a textural analysis classifying the beach material at a particular beach is necessary, in order to understand and explain whether the beach is wet or dry.

4.5.2 Classification of the Tiny Township Beaches

i. Balm Beach South

Balm Beach South (BBS) exhibits typical characteristics of the Crowe and Milne (2007) definition of a dry beach. This beach is comprised of dry surficial sand, does not contain invasive, non-native vegetation encroaching onto the beach and contains sand dunes on the leeward side of the beach, with natural beach grass to prevent sand loss. The surface topography of BBS is a steep-sloped beach from the sand dunes towards the lake. The water table is deep below the beach surface (1.10 m, ~ 25 m inland from the lake) and does not follow the slope of the beach surface, instead extends into the beach from the lake at a low hydraulic gradient (0.0086). The texture of the beach sand is the coarsest (medium to very coarse grains) compared to the other beaches and as a result, the field-saturated and saturated hydraulic conductivities are highest at this beach (mean K_{fs} is 8.38×10^{-2} cm·s^{-1} and mean K_{sat} is 1.35×10^{-1} cm·s^{-1}) compared to the other beaches. Coarse sand is unable to retain moisture as well as fine sand as a result of weak capillarity (Schwartz and Zhang, 2003; Yang *et al.*, 2004) and is observed through the small transition zone of moisture contents above the water table in the 2D BBS model. Therefore, the moisture profile below this beach is relatively dry (< 10 %) from the surface, until about 25 cm above the water table. Furthermore, this beach has not been subjected to human induced changes such as bulldozing sand dunes or installing break walls. Results from this study therefore classify this beach as a naturally dry beach.

ii. Jackson Park Beach

Jackson Park Beach (JPB) exhibits characteristics of a wet beach (Crowe and Milne, 2007) with ponding surface water following a precipitation event, wet surface sand, iron stains, considerable hydrophytic vegetation on the beach and finally no sand dunes on the leeward side of the beach. The surface beach topography is relatively flat and extends inland towards residential lawns (non-native turf grass). The water table below the surface of the beach is shallow (0.61 m, ~

25 m inland from the lake) and extends inland from the lake with a hydraulic gradient of 0.0075. The texture of the sand is finest (fine to medium sand) compared to the other beaches and the field-saturated and saturated hydraulic conductivities are lowest (mean K_{fs} is 9.07x 10^{-3} cm·s^{-1} and mean K_{sat} is 6.94 x10^{-3} cm·s^{-1}) at this beach compared to the others. The moisture profile of this beach is very wet at the surface (> 10 %) and well below the surface (~ 45 % moisture content to about 25 cm above the water table). This was also observed through the large transition zone of moisture contents from the water table to the surface in the JPB beach model. The high moisture contents above the water table at this beach are attributed to the fact that fine sand have a higher ability to retain moisture through capillarity compared to coarse sands (Schwartz and Zhang, 2003; Yang *et al.*, 2004). In addition, this beach has not been subjected to human induced alterations. Therefore, results from this study classify this beach as a natural wet beach.

iii. Woodland Beach North

Woodland Beach North (WBN) exhibits characteristics of a dry beach, as suggested in Crowe and Milne (2007). This beach is comprised of dry surficial sand, and does not contain invasive or non-native vegetation encroaching onto the beach. Sand dunes are present on the leeward side of the beach with natural beach grass to prevent sand loss. The surface topography of WBS is a steep-sloped beach and slopes from the sand dunes towards the lake. The water table is deep; 1.44 m approximately 25 m inland from the lake. The slope of the water table is relatively flat, extending from the lake inland with a hydraulic gradient of 0.0063. The texture of the sand is fine to medium. The mean field-saturated and saturated hydraulic conductivities at this beach are 2.39 x 10^{-2} cm·s^{-1} and 2.29 x 10^{-2} cm·s^{-1} respectively. The fine sand at this beach is also able to retain moisture well above the water table where field data shows that this beach retains high moisture contents (> 10

%) to approximately 50 cm above the water table. This is also observed through the large transition zone of moisture contents (compared to BBS) in the 2D beach model. However, due to the large depth of the water table at this beach (> 50 cm deep), the sand at the surface of the beach remains dry to a depth of several centimeters. This is because the fine grained sand at WBN is unable to retain moisture through capillarity above a depth of ~ 50 cm above the water table. This beach has not been exposed to human alterations and is therefore classified as a naturally dry beach.

iv. Woodland Beach South

Woodland Beach South (WBS) exhibits characteristics of a wet beach (Crowe and Milne, 2007), such as wet sand at the surface, areas of dense invasive and non-native vegetation encroaching onto the beach surface, iron stains, ponding surface water following precipitation events, and contains no sand dunes on the leeward side of the beach. The beach is more complex compared to the other beaches due to the human induced profile changes, affecting the natural features of the beach. WBS once exhibited similar characteristics as WBN (dry sand, sand dunes, higher elevation of the beach surface, steep sloped surface topography, etc.) however, the beach-front residents altered the natural surface of this beach. During the 1970's and 1980's local residents bulldozed and removed the natural sand dunes and installed break walls in their place. At the break wall, the beach/dune surface is now approximately 2 m lower than before the bulldozing occurred. The break walls are still in place and residents still continue to bulldoze sand from the surface of the beach that accumulates against and near to the break wall. The surface topography of this beach is flat (approximately 13 m inland from the lake), with a small sand dune adjacent to the lake, therefore, the surface topography is classified as a dune and swale topography. The depth to the water table is very shallow at this beach (0.25 m, ~ 25 m inland from the lake) and the texture of

this beach is fine to coarse sand (coarser than JPB and WBN). The moisture content of the surface sand is high (~ 20 % moisture) and then mean field-saturated and saturated hydraulic conductivity of this beach is 2.99 x 10^{-2} cm·s^{-1} and 1.58 x10^{-2} cm·s^{-1}, respectively (higher than JPB and WBN). Thus, although this beach has coarser sand than WBN and JPB, the shallow depth to the water table is the cause of this beach being a wet beach. Had the former natural conditions (i.e. those still present at WBN) been retained by the residents, this beach would have a deep water table and would contain low moisture contents above the water table, currently exhibited by WBN. Hence, this beach would have been classified as a dry beach. But because the bulldozing has lowered the ground surface and created a shallow water table and wet conditions, this beach is classified as a degraded wet beach.

Results from the Tiny Township beach investigation were successful in characterizing and classifying the physical and hydrological conditions that control the wet and dry beaches. It is evident that wet and dry beaches are controlled by several interacting factors: (1) Beach surface topography/elevation, (2) Depth to the water table, and (3) Texture of the beaches. When assessing whether or not a beach is wet or dry, all three primary factors need to be investigated as they are interconnected in controlling the conditions at a beach. Furthermore, beach managers can use the calibrated Tiny Township beach models by conducting scenario tests on the beaches in order to address public concerns and beach management implications.

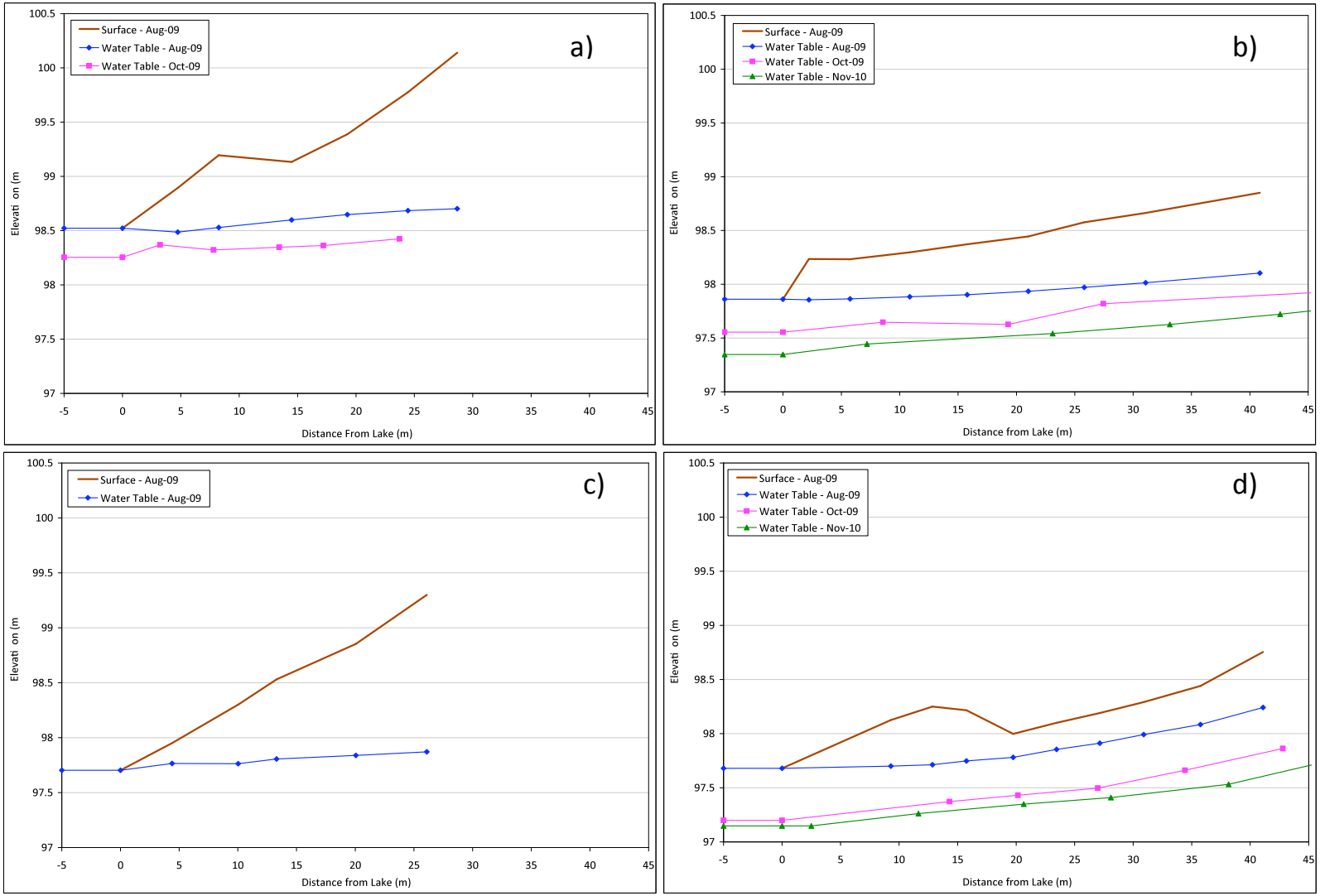

Figure 4.1: Beach surface and water table elevations for (a) BBS, (b) JPB, (c) WBN, and (d) WBS. Seasonal water table measurements (pink and green data sets) were taken at BBS, JPB, and WBS only.

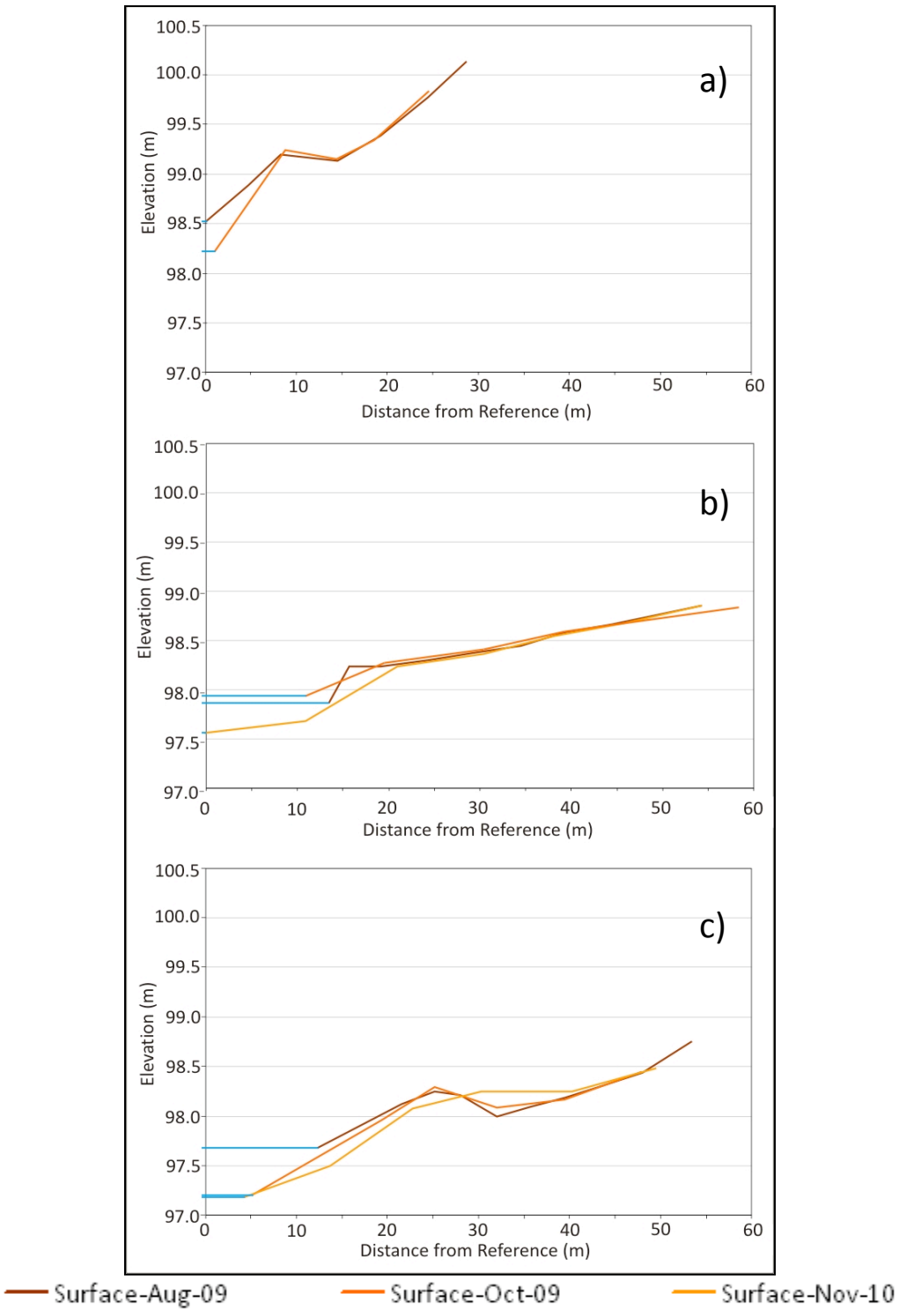

Figure 4.2: Seasonal beach surface elevations collected at (a) BBS, (b) JPB, and (c) WBS only.

Table: 4.1: Water table depths and hydraulic gradients below the beach sites in Tiny Township, August, October 2009, and November 2010

Beach	Date Measured	Ground Surface Elevation (m)[1]	Water Table Depth (m) [1]	Distance from Shore (m) (# of boreholes)	Hydraulic Gradient
BBS	Aug – 09	100.14	1.09	8.25 – 28.67 (4)	0.0086
	Oct – 09	99.88	1.49	7.8 – 23.73 (4)	0.0063
	Nov – 10	--	--	--	--
JPB	Aug – 09	98.85	0.61	10.87 – 40.86 (6)	0.0075
	Oct – 09	98.88	0.62	8.56 – 47.5 (4)	0.0082
	Nov – 10	98.85	0.14	7.20 – 50.30 (5)	0.0085
WBN	Aug – 09	99.30	1.43	10.03 – 26.1 (4)	0.0063
	Oct – 09	--	--	--	--
	Nov – 10	--	--	--	--
WBS	Aug – 09	--	--	9.3 – 15.75 (3)	0.0073[2]
(near lake)	Oct – 09	--	--	14.31-26.98 (3)	0.0099
	Nov – 10	--	--	11.65-28.1 (3)	0.0090
WBS	Aug – 09	98.75	0.25	19.75 – 41.10 (6)	0.0210
(away from	Oct – 09	98.45	0.59	26.98 – 42.79 (3)	0.0232
lake)	Nov – 10	98.45	0.64	28.1– 50.30 (4)	0.0282

[1] Measured ~ 25 m from the lake, [2] Temporary high lake level recorded in field notes due to an incoming storm

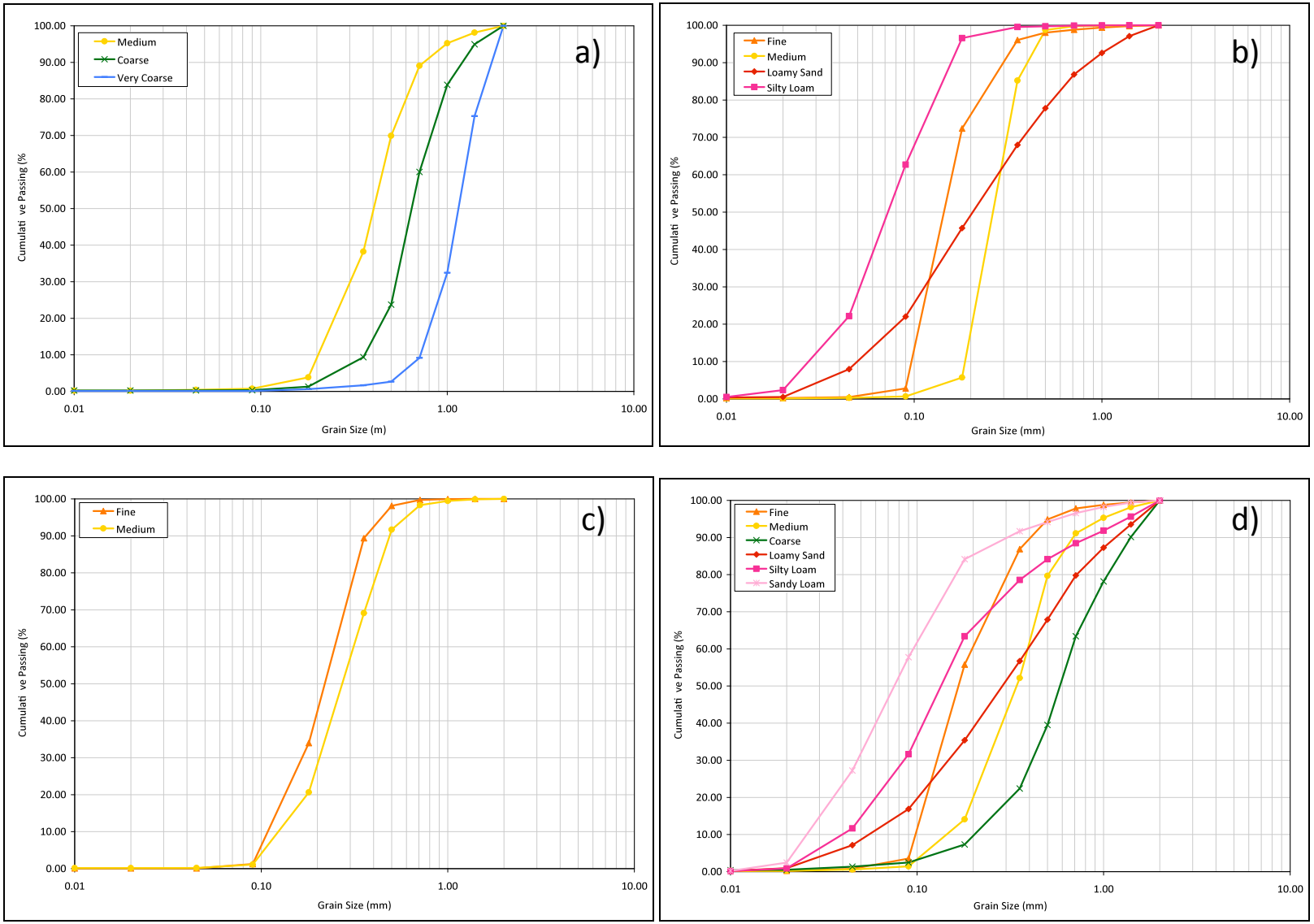

Figure 4.3: Mean grain size distribution curves of sands at each beach: (a) BBS, (b) JPB, (c) WBN, and (d) WBS.

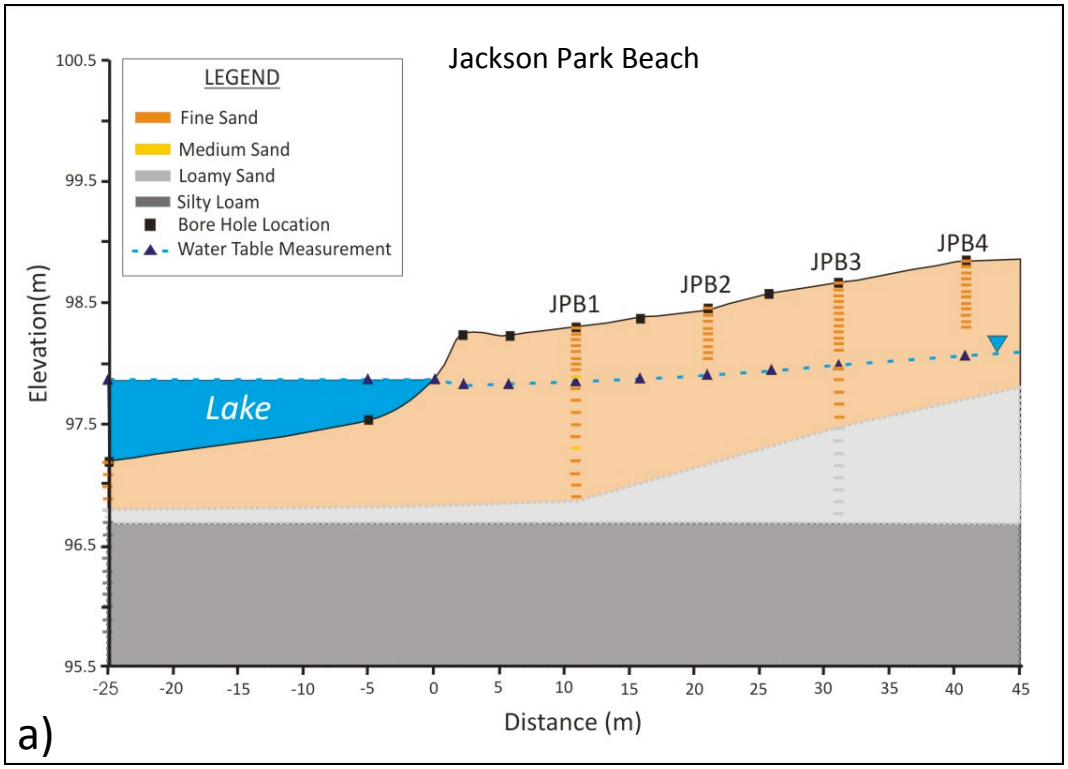

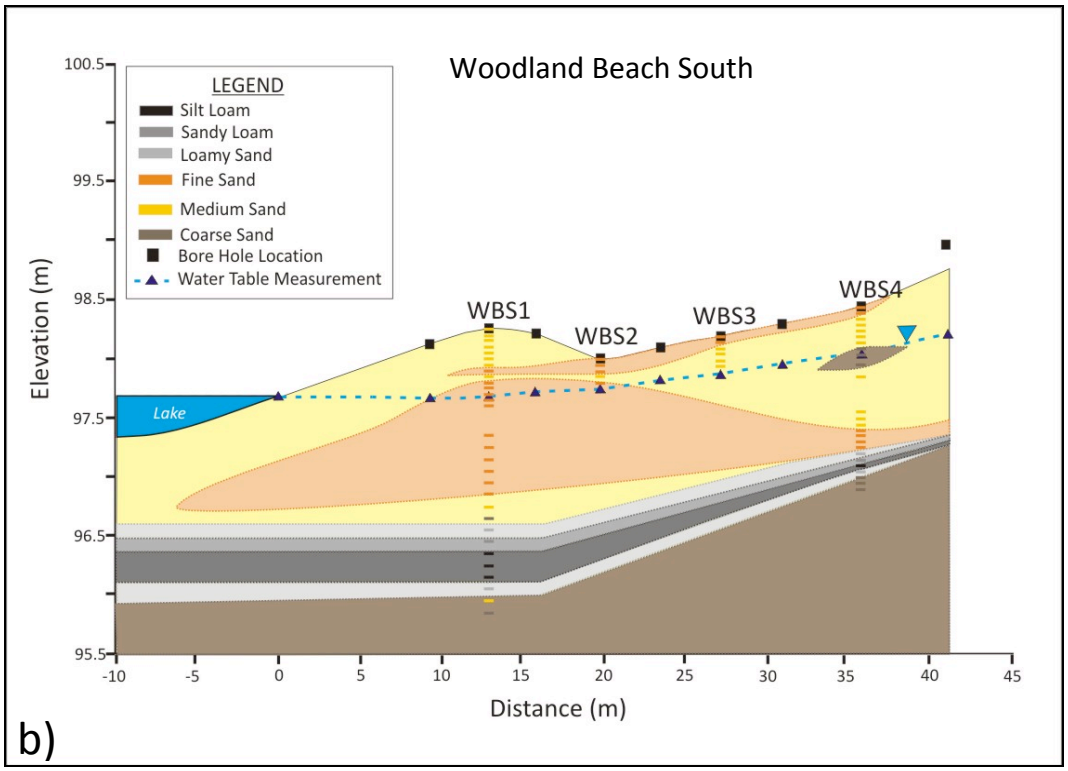

Figure 4.4.1: Overall textural profiles of wet beaches along transect perpendicular to the lake: (a) Jackson Park Beach (b) Woodland Beach South. Rectangles indicate field measurements and slightly lighter shaded areas indicate associated inferred measurements.

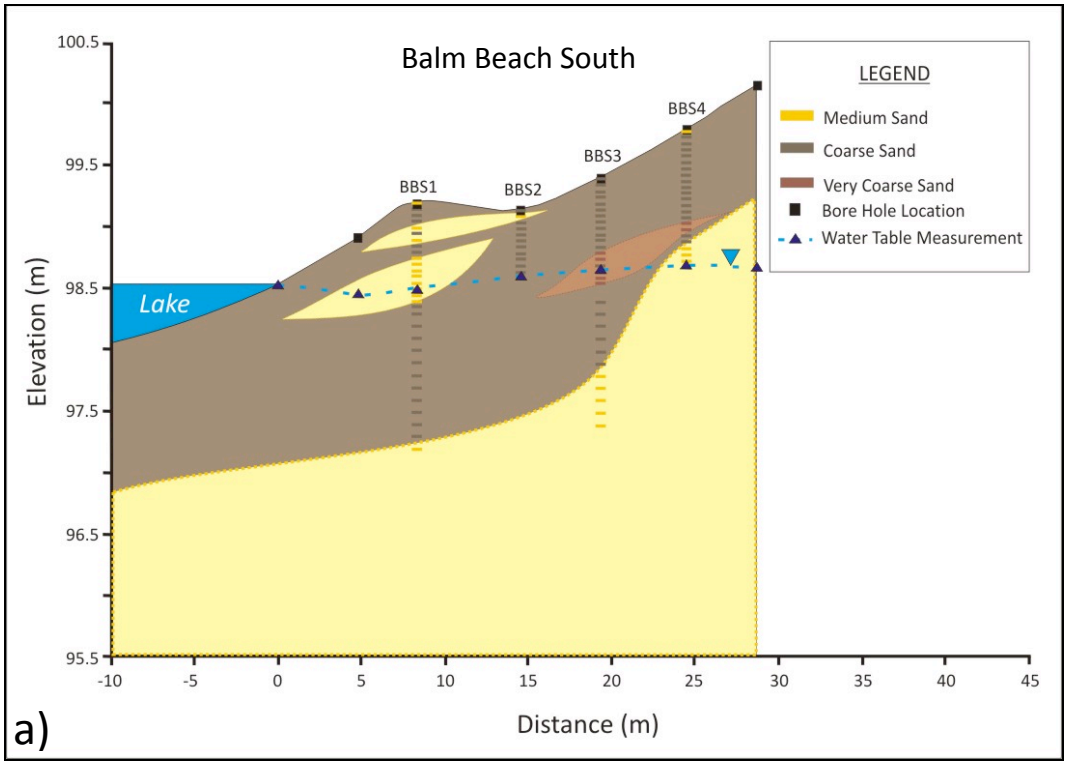

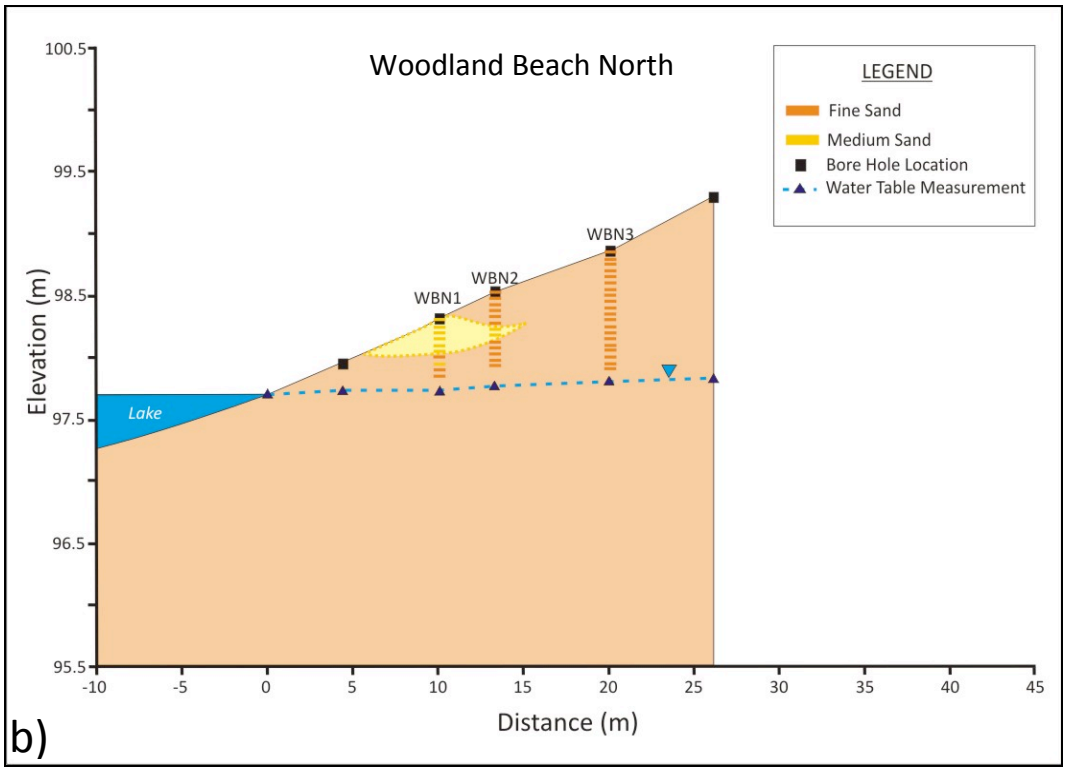

Figure 4.4.2: Overall textural profiles of dry beaches along transect perpendicular to the lake: (a) Balm Beach South (b) Woodland Beach North. Rectangles indicate field measurements and slightly lighter shaded areas indicate associated inferred measurements.

Table 4.2: Textural characterization of materials comprising the beaches of Tiny Township

Textural Class	% Sand	% Silt	% Clay
Balm Beach South			
Sand (Medium)	99	1	0
Sand (Coarse)	100	0	0
Sand (Very Coarse)	100	0	0
Jackson Park Beach			
Sand (Fine)	97	3	0
Sand (Medium)	99	1	0
Loamy Sand	78	22	0
Silty Loam	37	63	0
Woodland Beach North[1]			
Sand (Fine)	99	1	0
Sand (Medium)	99	1	0
Woodland Beach South			
Sand (Fine)	96	4	0
Sand (Medium)	98	2	0
Sand (Coarse)	98	2	0
Loamy Sand	83	17	0
Sandy Loam	42	58	0
Silty Loam	68	32	0

[1]Due to limited site access through residential property with the vibracore equipment, no particle samples were collected below the water table

Table 4.3: Summary of grain size statistics

	BBS	**JPB**	**WBN**	**WBS**
Mean (mm)	0.647	0.167	0.231	0.283
mean texture	*coarse*	*fine*	*fine*	*medium*
Median (d_{50}) (mm)	0.599	0.162	0.233	0.252
Range (mm)	0.26-1.27	0.14-0.50	0.18-0.29	0.07-0.65
Variance (mm^2)[1]	0.0520	0.00295	0.000725	0.0176
Standard Deviation (mm)[1]	0.228	0.0543	0.0269	0.133
Coefficient of Variation (%)	35.22	32.50	11.68	46.89
Uniformity Coefficient (d_{60}/d_{10})	1.922	1.947	2.069	2.459

Table 4.4: Summary of single-factor ANOVA tests on significant differences in grain sizes among sampling pits within a beach. Sample sizes (n) include both vadose and saturated zone samples at ~ 5 cm depth increments.

Critical Value = 3.704				
	BBS1 (n=29)	BBS2 (n=11)	BBS3 (n=29)	BBS4 (n=22)
BBS1		2.266	***4.595**	***5.728**
BBS2			1.142	2.213
BBS3				1.460
BBS4				

Critical Value = 3.729				
	JPB1 (n=23)	JPB2 (n=9)	JPB3 (n=25)	JPB4 (n=12)
JPB1		2.670	0.605	3.318
JPB2			2.251	0.299
JPB3				2.866
JPB4				

Critical Value = 3.442			
	WBN1 (n=10)	WBN2 (n=13)	WBN3 (n=20)
WBN1		***5.911**	***5.629**
WBN2			0.860
WBN3			

Critical Value = 3.751				
	WBS1 (n=30)	WBS3 (n=5)	WBS3 (n=6)	WBS4 (n=16)
WBS1		0.641	2.041	***4.560**
WBS2			2.018	3.359
WBS3				1.042
WBS4				

*** Statistically significantly different**

Table 4.5: Single-factor ANOVA test of significant differences of grain sizes among beaches

Critical Value = 3.670				
	BBS (n=91)	JPB (n=69)	WBN (n=43)	WBS (n=57)
BBS		***34.588**	***22.489**	***22.109**
JPB			***6.997**	***9.982**
WBN				2.115
WBS				

*** Statistically significantly different**

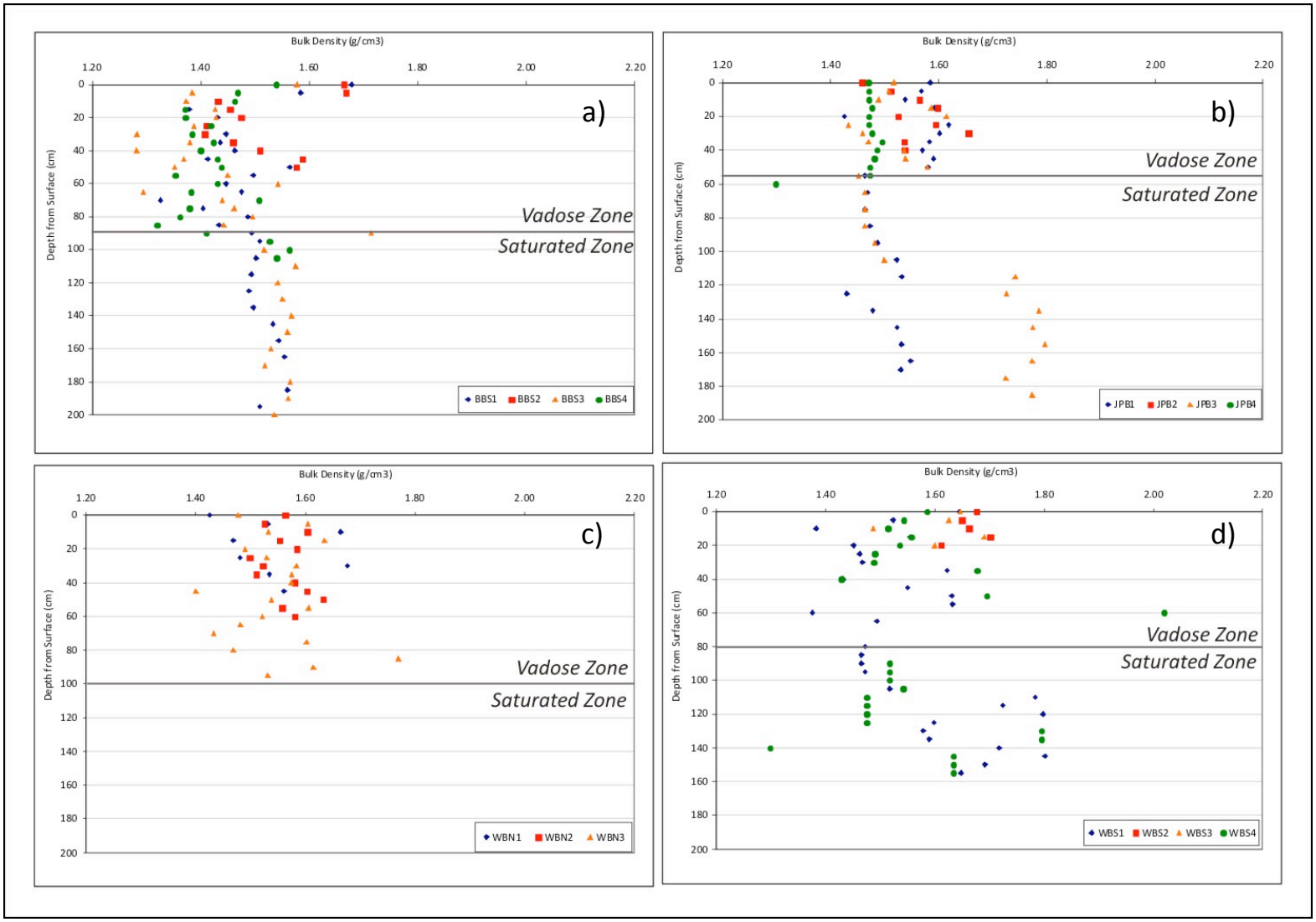

Figure 4.5: Bulk densities for (a) Balm Beach South, (b) Jackson Park Beach, (c) Woodland Beach North, and (d) Woodland Beach South, August 2009 and October 2009.

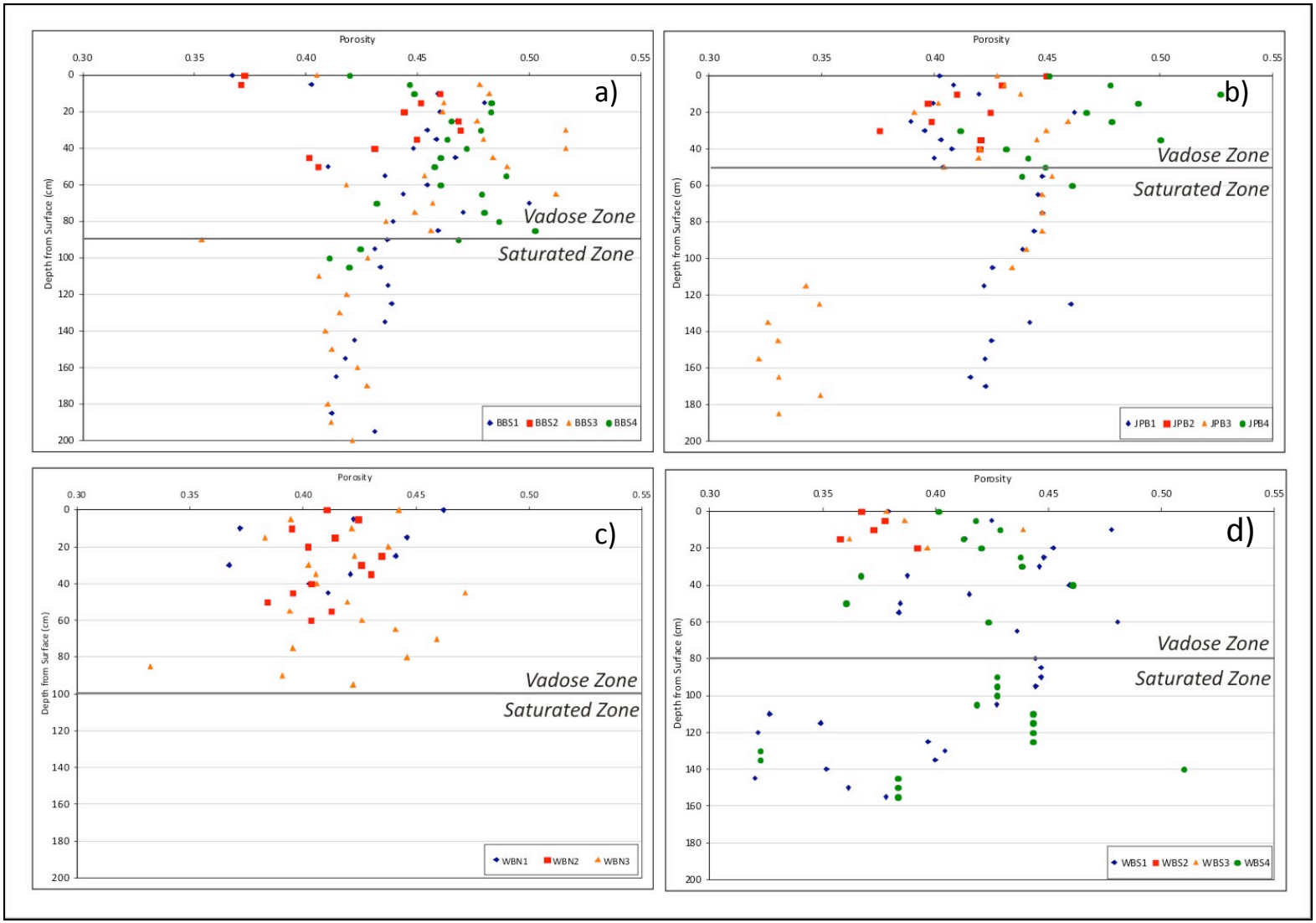

Figure 4.6: Porosities for (a) Balm Beach South, (b) Jackson Park Beach, (c) Woodland Beach North, and (d) Woodland Beach South, August 2009 and October 2009.

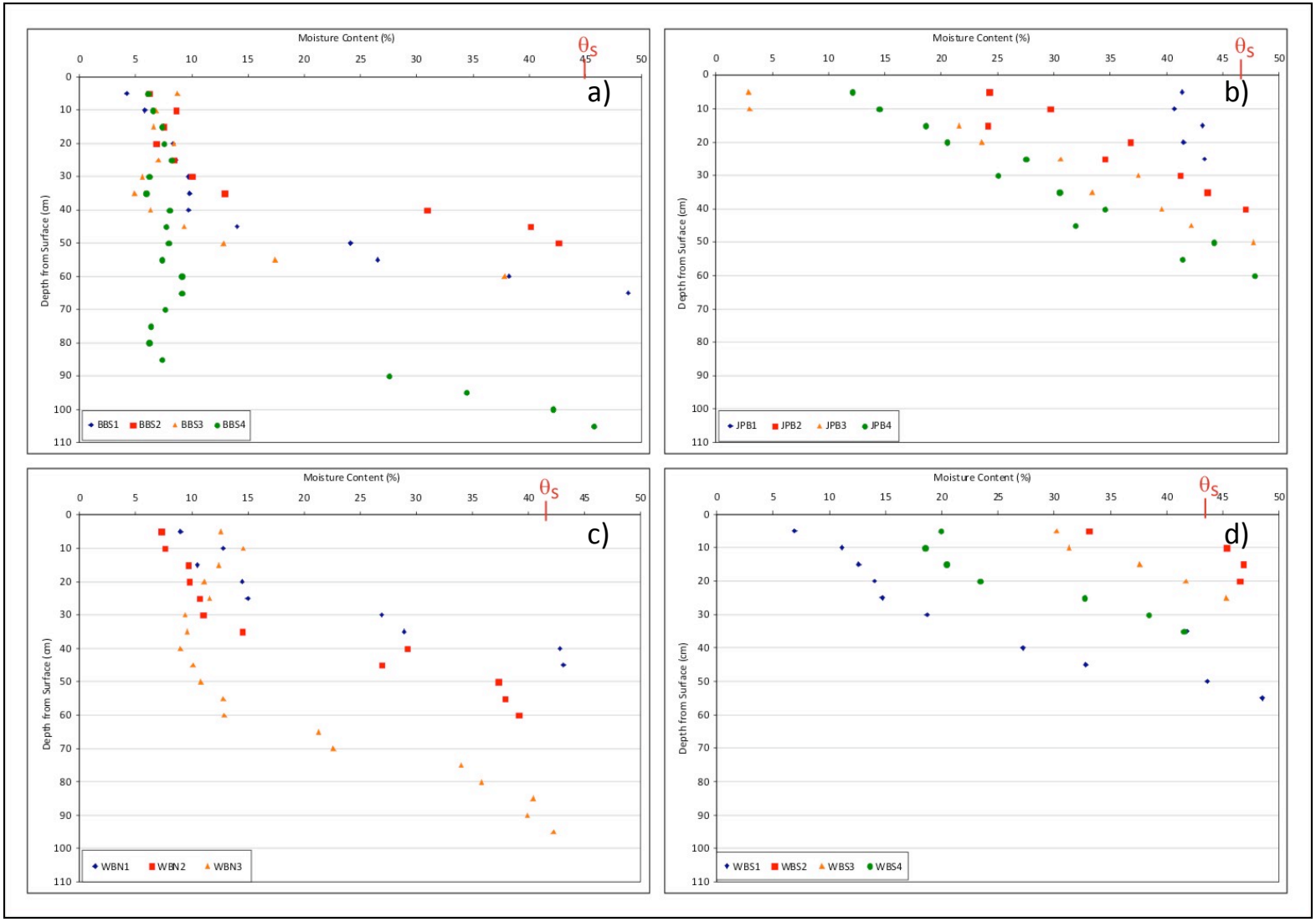

Figure 4.7.1: Volumetric moisture contents measured from TDR probe for (a) Balm Beach South, (b) Jackson Park Beach, (c) Woodland Beach north, and (d) Woodland Beach South, August 2009.

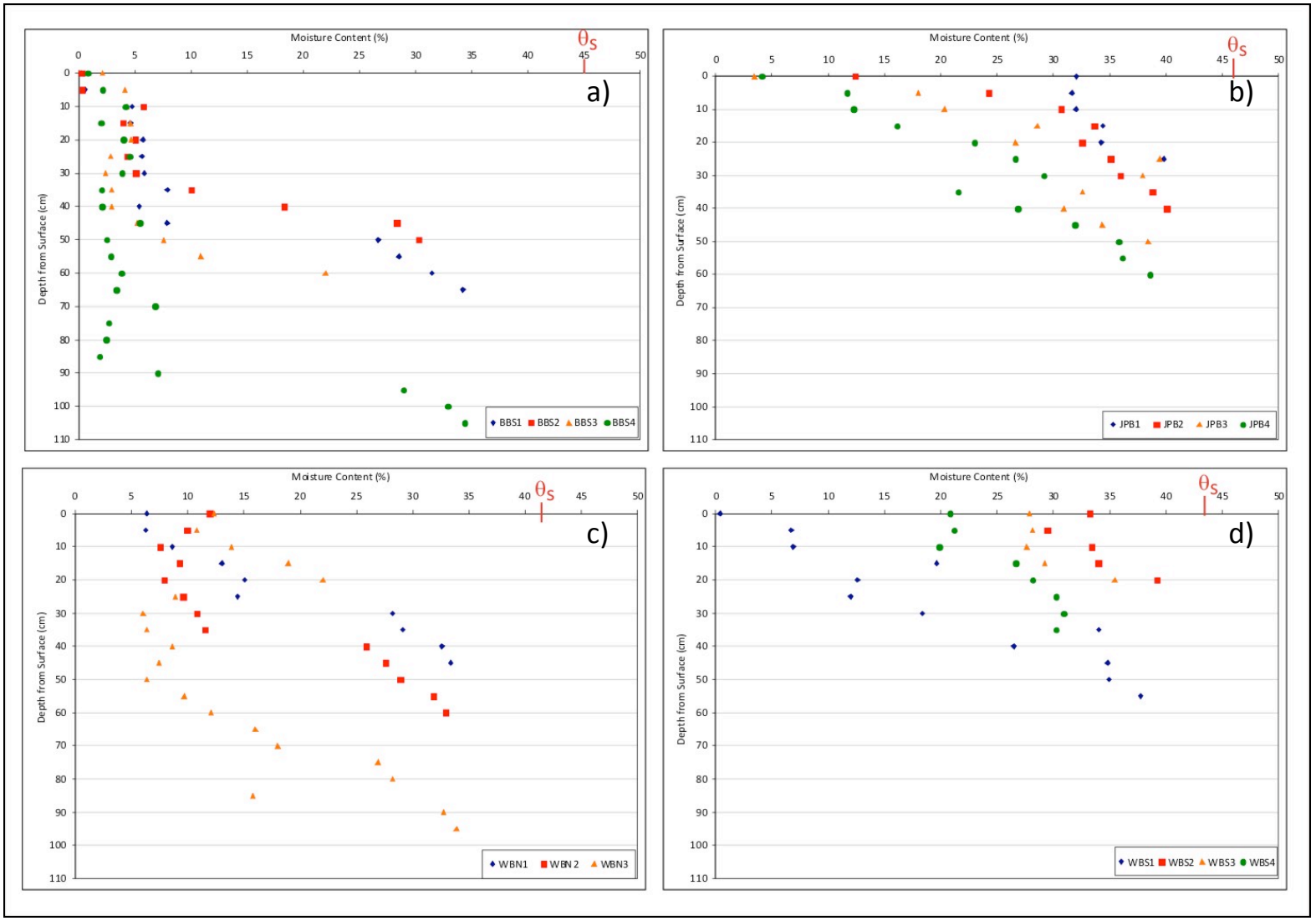

Figure 4.7.2: Short-Cores volumetric moisture contents for (a) Balm Beach South, (b) Jackson Park Beach, (c) Woodland Beach North, and (d) Woodland Beach South, August 2009.

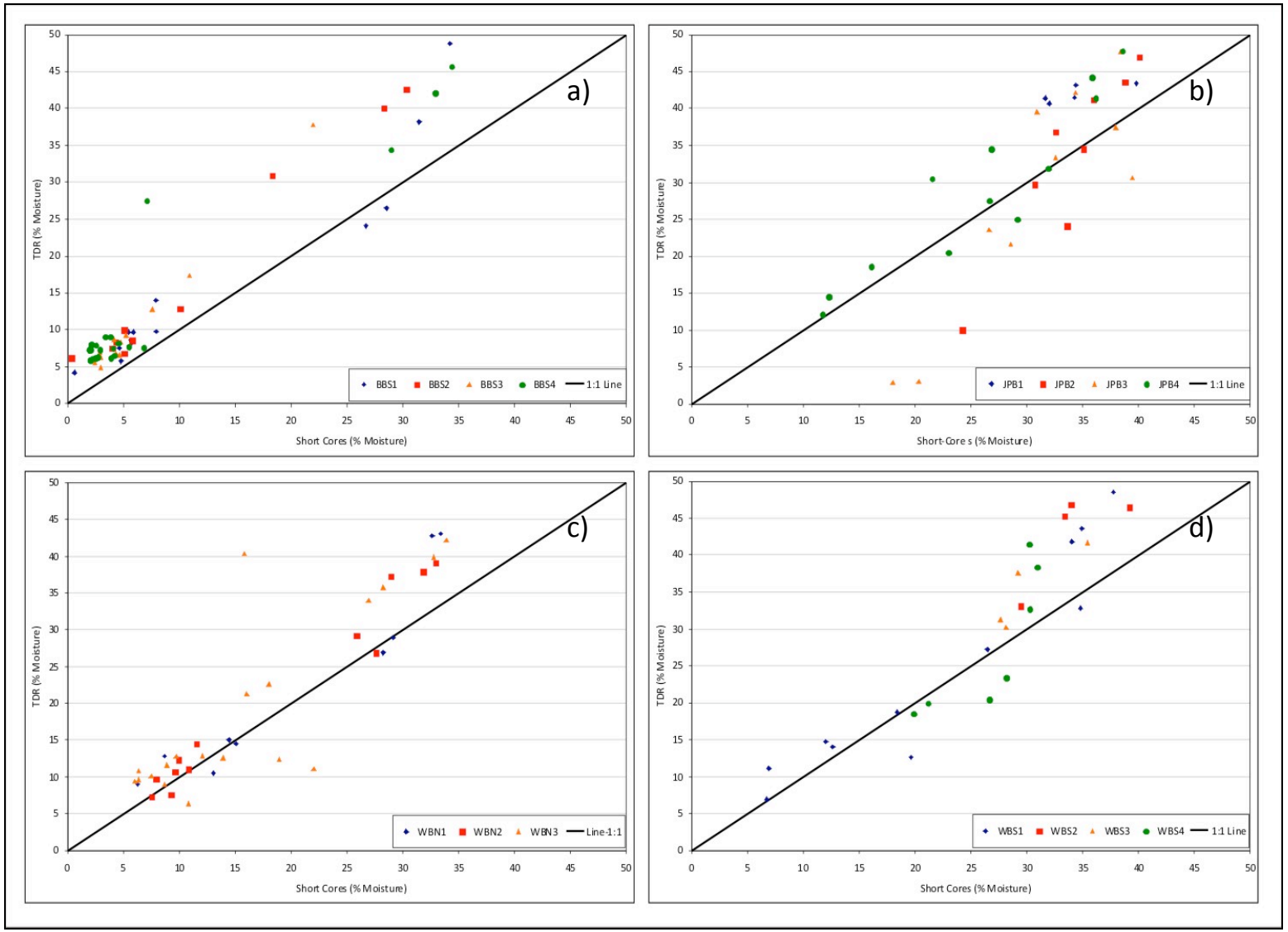

Figure 4.8: Comparing the volumetric moisture contents measured using the TDR Method to the Short-Core Method at (a) BBS, (b) JPB, (c) WBN, and (d) WBS.

Table 4.6: Calculated field-saturated hydraulic conductivity values using a Guelph Permeameter for different grain sizes at the Tiny Beaches field sites, June 2010

Location	Distance from Reference (cm)	Depth of Ponded Water (cm)	Depth from Surface (cm)	Grain Size	K_{fs} (cm/s)
JPB1	35.72	5	20	Fine Sand	1.21E-02
JPB1	35.72	5	20	Fine Sand	1.13E-02
JPB2	25.58	5	20	Fine Sand	1.07E-02
JPB3	15.52	5	30	Fine Sand	7.31E-03
JPB3	15.52	5	30	Fine Sand	6.34E-03
JPB3	15.52	5	20	Fine Sand	9.47E-03
JPB4	5.73	5	30	Fine Sand	7.85E-03
WBS1	34.85	5	25	Medium Sand	2.71E-02
WBS1	34.85	5	25	Medium Sand	2.67E-02
WBS2	27.95	5	15	Fine Sand	2.38E-02
WBS2	27.95	5	15	Fine Sand	2.70E-02
WBS3	20.55	5	25	Medium Sand	3.21E-02
WBS4	11.95	5	10	Fine Sand	2.94E-02
WBS4	11.95	5	25	Medium Sand	4.82E-02
BBS1	8.25	5	30	Medium Sand	5.34E-02
BBS1	8.25	5	20	Medium Sand	6.61E-02
BBS1	8.25	5	30	Medium Sand	6.57E-02
BBS2	14.49	5	25	Coarse Sand	7.63E-02
BBS3	19.26	5	30	Coarse Sand	1.27E-01
BBS3	19.26	5	30	Coarse Sand	1.15E-01
BBS4	24.45	5	25	Coarse Sand	1.15E-01
WBN1	40.32	5	25	Medium Sand	2.55E-02
WBN1	40.32	5	20	Medium Sand	2.39E-02
WBN1	40.32	5	25	Medium Sand	2.17E-02
WBN2	37.05	5	15	Fine Sand	1.76E-02
WBN2	37.05	5	10	Fine Sand	2.52E-02
WBN2	37.05	5	10	Fine Sand	2.71E-02
WBN3	30.30	5	35	Fine Sand	2.07E-02
WBN3	30.30	5	35	Fine Sand	2.93E-02
WBN3	30.30	5	35	Fine Sand	2.67E-02

Table 4.7: Statistical summary of field saturated hydraulic conductivity measurements from the Guelph Permeameter measurements

	BBS	JPB	WBN	WBS
Mean (cm/s)	8.38E-02	9.07E-03	2.39E-02	2.96E-02
Range (cm/s)	5.34E-02 – 1.27E-01	6.34E-03 – 2.14E-02	1.76E-02 – 2.93E-02	2.38E-02 – 4.82E-02
Standard Deviation (cm/s)	1.01	1.01	1.01	1.01
Variance $(cm/s)^2$	1.01	1.03	1.02	1.01
Coefficient of Variation (%)	72.86	88.72	90.66	85.19

Table 4.8: Field-saturated hydraulic conductivity values using a Minidisk Infiltrometer, June 2010

Location	Grain Size (sand)	Applied Suction (cm)	A	C1	Hydraulic Conductivity (cm/s)	Mean (cm/s)
JPB1	Fine	2	1.8	0.064	3.56E-02	5.92E-02
JPB2	Fine	2	1.8	0.068	3.76E-02	
JPB3	Fine	2	1.8	0.084	4.67E-02	
JPB4	Fine	2	1.8	0.116	6.44E-02	
JPB1	Fine	4	0.9	0.055	6.13E-02	
JPB2	Fine	4	0.9	0.042	4.71E-02	
JPB3	Fine	4	0.9	0.040	4.47E-02	
JPB4	Fine	4	0.9	0.074	8.24E-02	
JPB1	Fine	6	0.5	0.047	9.44E-02	
JPB2	Fine	6	0.5	0.025	5.00E-02	
JPB3	Fine	6	0.5	0.048	9.60E-02	
JPB4	Fine	6	0.5	0.048	9.60E-02	
WBS1	Medium	2	1.8	0.102	5.65E-02	5.07E-02
WBS2	Fine	2	1.8	0.100	5.53E-02	
WBS3	Fine	2	1.8	0.069	3.86E-02	
WBS4	Fine	2	1.8	0.081	4.52E-02	
WBS1	Medium	4	0.9	0.058	6.39E-02	
WBS2	Fine	4	0.9	0.044	4.87E-02	
WBS3	Fine	4	0.9	0.044	4.83E-02	
WBS4	Fine	4	0.9	0.051	5.62E-02	
WBS1	Medium	6	0.5	0.029	5.74E-02	
WBS2	Fine	6	0.5	0.020	4.00E-02	
WBS3	Fine	6	0.5	0.032	6.34E-02	
WBS4	Fine	6	0.5	0.022	4.30E-02	
BBS1	Medium	2	1.8	0.124	6.88E-02	4.53E-02
BBS2	Coarse	2	1.8	0.078	4.33E-02	
BBS4	Medium	2	1.8	0.084	4.66E-02	
BBS1	Medium	4	0.9	0.069	7.68E-02	
BBS2	Coarse	4	0.9	0.043	4.82E-02	
BBS3	Coarse	4	0.9	0.032	3.57E-02	
BBS4	Medium	4	0.9	0.034	3.74E-02	
BBS1	Medium	6	0.5	0.026	5.28E-02	
BBS2	Coarse	6	0.5	0.025	5.00E-02	
BBS3	Coarse	6	0.5	0.020	4.08E-02	
BBS4	Medium	6	0.5	0.011	2.24E-02	
WBN1	Medium	2	1.8	0.213	1.18E-01	8.33E-02
WBN2	Fine	2	1.8	0.125	6.97E-02	
WBN3	Fine	2	1.8	0.188	1.05E-01	
WBN1	Medium	4	0.9	0.073	8.14E-02	
WBN2	Fine	4	0.9	0.071	7.91E-02	
WBN3	Fine	4	0.9	0.036	4.00E-02	
WBN1	Medium	6	0.5	0.057	1.14E-01	
WBN2	Fine	6	0.5	0.040	7.92E-02	
WBN3	Fine	6	0.5	0.048	9.64E-02	

Table 4.9: Statistical summary of results from empirical predictions of K_{sat} values using the corresponding textural data from the Tiny Township beaches

	Hazen				**Slitcher**			
	BBS ***n = 95***	**JPB** ***n = 71***	**WBN** ***n = 48***	**WBS** ***n = 51***	**BBS** ***n = 95***	**JPB** ***n = 71***	**WBN** ***n = 48***	**WBS** ***n = 51***
Mean (cm/s)	1.52E-01	1.04E-02	1.87E-02	1.38E-02	6.10E-02	4.23E-03	6.73E-03	6.86E-03
Range (cm/s)	2.40E-02 - 7.87E-01	1.02E-03 - 6.59E-02	1.02E-02 - 4.19E-02	5.43E-04 - 7.09E-05	1.93E-04 - 3.76E-01	7.04E-05 - 5.17E-02	3.15E-03 - 1.83E-02	6.93E-04 - 3.83E-02
Variance $(cm/s)^2$	1.38	1.24	1.05	1.58	1.96	1.93	1.07	1.39
*Standard Deviation (cm/s)	2.37	2.03	1.40	2.79	3.48	3.42	1.47	2.39
Coefficient of Variation (%)	34.95	70.03	82.34	57.63	35.87	59.57	83.64	66.82
	Beyer				**Kozeny-Carman**			
	BBS ***n = 95***	**JPB** ***n = 71***	**WBN** ***n = 48***	**WBS** ***n = 51***	**BBS** ***n = 95***	**JPB** ***n = 71***	**WBN** ***n = 48***	**WBS** ***n = 51***
Mean (cm/s)	1.30E-01	9.64E-03	1.76E-02	1.32E-02	2.40E-01	1.45E-02	2.43E-02	1.70E-02
Range (cm/s)	2.13E-02 - 6.01E-01	1.08E-03 - 5.77E-02	1.03E-02 - 3.71E-02	5.61E-04 - 7.96E-02	3.50E-02 - 1.68E+00	8.30E-04 - 1.18E-01	9.32E-03 - 7.58E-02	4.70E-04 - 7.78E-02
Variance $(cm/s)^2$	1.35	1.20	1.05	1.56	1.53	1.46	1.09	1.77
*Standard Deviation (cm/s)	2.29	1.91	1.39	2.75	2.69	2.54	1.54	3.15
Coefficient of Variation (%)	39.21	72.50	83.05	58.45	20.26	60.22	76.44	52.35

**Parametric statistics were conducted on the log-transformed K_{sat} data, therefore, when the standard deviation is converted back into anti-log values, the numbers do not equal the square root of the variance*

Table 4.10: Comparing empirical estimates (K_{sat}) to corresponding Guelph Permeameter measurements (K_{fs})

Location	Depth from Surface (cm)	Grain Size	Guelph Permeameter K_{fs} (cm/s)	Hazen K_{sat} (cm/s)	Slitcher K_{sat} (cm/s)	Beyer K_{sat} (cm/s)	Kozeny-Carman K_{sat} (cm/s)
BBS1	30	Medium Sand	5.34E-02	2.79E-02	1.09E-02	2.47E-02	4.16E-02
BBS1	20	Medium Sand	6.61E-02	2.39E-02	9.19E-03	2.12E-02	3.46E-02
BBS1	30	Medium Sand	6.57E-02	2.39E-02	9.19E-03	2.12E-02	3.46E-02
BBS2	25	Coarse Sand	7.63E-02	3.45E-02	1.15E-02	3.71E-02	3.95E-02
BBS3	30	Coarse Sand	1.27E-01	1.53E-02	5.13E-03	1.53E-02	1.76E-02
BBS3	30	Coarse Sand	1.15E-01	2.01E-02	7.56E-03	1.80E-02	2.79E-02
BBS4	25	Coarse Sand	1.15E-01	1.74E-02	6.07E-03	1.67E-02	2.14E-02
JPB1	20	Fine Sand	1.21E-02	1.26E-02	5.50E-03	1.05E-02	2.28E-02
JPB1	20	Fine Sand	1.13E-02	1.26E-02	5.50E-03	1.04E-02	2.28E-02
JPB2	20	Fine Sand	1.07E-02	1.15E-02	4.63E-03	1.01E-02	1.80E-02
JPB3	30	Fine Sand	7.31E-03	1.19E-02	4.74E-03	1.05E-02	1.83E-02
JPB3	30	Fine Sand	6.34E-03	1.26E-02	5.24E-03	1.07E-02	2.09E-02
JPB3	20	Fine Sand	9.47E-03	1.26E-02	5.24E-03	1.07E-02	2.09E-02
JPB4	30	Fine Sand	7.85E-03	1.09E-02	3.91E-03	1.08E-02	1.40E-02
WBN1	25	Medium Sand	2.55E-02	1.60E-02	5.59E-03	1.52E-02	1.97E-02
WBN1	20	Medium Sand	2.39E-02	1.60E-02	5.59E-03	1.54E-02	1.97E-02
WBN1	25	Medium Sand	2.17E-02	1.65E-02	5.98E-03	1.50E-02	2.15E-02
WBN2	15	Fine Sand	1.76E-02	1.78E-02	6.34E-03	1.61E-02	2.27E-02
WBN2	10	Fine Sand	2.52E-02	1.78E-02	6.34E-03	1.61E-02	2.27E-02
WBN2	10	Fine Sand	2.71E-02	2.10E-02	7.61E-03	1.90E-02	2.75E-02
WBN3	35	Fine Sand	2.07E-02	4.67E-02	1.81E-02	4.14E-02	6.86E-02
WBN3	35	Fine Sand	2.93E-02	2.45E-02	9.00E-03	2.20E-02	3.27E-02
WBN3	35	Fine Sand	2.67E-02	4.54E-02	1.80E-02	4.87E-02	6.93E-02
WBS1	25	Medium Sand	2.71E-02	7.48E-02	2.82E-02	6.67E-02	1.04E-01
WBS1	25	Medium Sand	2.67E-02	6.99E-02	2.67E-02	6.21E-02	1.00E-01
WBS2	15	Fine Sand	2.38E-02	6.30E-02	2.36E-02	5.63E-02	8.72E-02
WBS2	15	Fine Sand	2.70E-02	6.72E-02	2.46E-02	6.04E-02	8.96E-02
WBS3	25	Medium Sand	3.21E-02	1.85E-01	7.48E-02	1.62E-01	2.93E-01
WBS4	10	Fine Sand	2.94E-02	1.85E-01	7.48E-02	1.62E-01	2.93E-01
WBS4	25	Medium Sand	4.82E-02	2.26E-01	8.97E-02	2.00E-01	3.45E-01

Table 4.11: Comparing empirical estimates (K_{sat}) to corresponding Guelph Permeameter measurements adjusted to K_{sat}

Location	Depth from Surface (cm)	Grain Size	Guelph Permeameter K_{sat} (cm/s)	Hazen K_{sat} (cm/s)	Slitcher K_{sat} (cm/s)	Beyer K_{sat} (cm/s)	Kozeny-Carman K_{sat} (cm/s)
BBS1	30	Medium Sand	2.31E-01	2.79E-02	1.09E-02	2.47E-02	4.16E-02
BBS1	20	Medium Sand	1.87E-01	2.39E-02	9.19E-03	2.12E-02	3.46E-02
BBS1	30	Medium Sand	2.30E-01	2.39E-02	9.19E-03	2.12E-02	3.46E-02
BBS2	25	Coarse Sand	2.67E-01	3.45E-02	1.15E-02	3.71E-02	3.95E-02
BBS3	30	Coarse Sand	4.45E-01	1.53E-02	5.13E-03	1.53E-02	1.76E-02
BBS3	30	Coarse Sand	4.01E-01	2.01E-02	7.56E-03	1.80E-02	2.79E-02
BBS4	25	Coarse Sand	4.01E-01	1.74E-02	6.07E-03	1.67E-02	2.14E-02
JPB1	20	Fine Sand	4.25E-02	1.26E-02	5.50E-03	1.05E-02	2.28E-02
JPB1	20	Fine Sand	3.97E-02	1.26E-02	5.50E-03	1.04E-02	2.28E-02
JPB2	20	Fine Sand	3.73E-02	1.15E-02	4.63E-03	1.01E-02	1.80E-02
JPB3	30	Fine Sand	3.31E-02	1.19E-02	4.74E-03	1.05E-02	1.83E-02
JPB3	30	Fine Sand	2.56E-02	1.26E-02	5.24E-03	1.07E-02	2.09E-02
JPB3	20	Fine Sand	2.30E-02	1.26E-02	5.24E-03	1.07E-02	2.09E-02
JPB4	30	Fine Sand	2.75E-02	1.09E-02	3.91E-03	1.08E-02	1.40E-02
WBN1	25	Medium Sand	8.93E-02	1.60E-02	5.59E-03	1.52E-02	1.97E-02
WBN1	20	Medium Sand	8.38E-02	1.60E-02	5.59E-03	1.54E-02	1.97E-02
WBN1	25	Medium Sand	6.15E-02	1.65E-02	5.98E-03	1.50E-02	2.15E-02
WBN2	15	Fine Sand	8.80E-02	1.78E-02	6.34E-03	1.61E-02	2.27E-02
WBN2	10	Fine Sand	7.59E-02	1.78E-02	6.34E-03	1.61E-02	2.27E-02
WBN2	10	Fine Sand	9.49E-02	2.10E-02	7.61E-03	1.90E-02	2.75E-02
WBN3	35	Fine Sand	7.23E-02	4.67E-02	1.81E-02	4.14E-02	6.86E-02
WBN3	35	Fine Sand	1.03E-01	2.45E-02	9.00E-03	2.20E-02	3.27E-02
WBN3	35	Fine Sand	9.35E-02	4.54E-02	1.80E-02	4.87E-02	6.93E-02
WBS1	25	Medium Sand	9.49E-02	7.48E-02	2.82E-02	6.67E-02	1.04E-01
WBS1	25	Medium Sand	9.35E-02	6.99E-02	2.67E-02	6.21E-02	1.00E-01
WBS2	15	Fine Sand	8.32E-02	6.30E-02	2.36E-02	5.63E-02	8.72E-02
WBS2	15	Fine Sand	9.44E-02	6.72E-02	2.46E-02	6.04E-02	8.96E-02
WBS3	25	Medium Sand	1.13E-01	1.85E-01	7.48E-02	1.62E-01	2.93E-01
WBS4	10	Fine Sand	1.03E-01	1.85E-01	7.48E-02	1.62E-01	2.93E-01
WBS4	25	Medium Sand	1.69E-01	2.26E-01	8.97E-02	2.00E-01	3.45E-01

Table 4.12: New β--parameters calibrated to the mean Guelph Permeameter K_{sat} (adjusted) measurements from the Tiny Township beaches

Beach	Hazen-Calibrated β_{HC}	Slitcher-Calibrated β_{SC}	Beyer-Calibrated β_{BC}	Kozeny-Carman-Calibrated β_{KCC}
BBS	1.69E-03	7.37E-02	1.90E-03	1.89E-02
JPB	1.62E-03	6.59E-02	1.86E-03	1.61E-02
WBN	2.53E-03	1.18E-01	2.68E-03	3.16E-02
WBS	2.62E-03	1.19E-01	2.84E-03	3.14E-02

Table 4.13: Statistical summary of the predicted K_{sat} using the β-calibrated empirical methods

	Hazen-Calibrated				**Slitcher- Calibrated**			
	BBS ***n = 95***	**JPB** ***n = 71***	**WBN** ***n = 48***	**WBS** ***n = 51***	**BBS** ***n = 95***	**JPB** ***n = 71***	**WBN** ***n = 48***	**WBS** ***n = 51***
Mean (cm/s)	4.28E-01	2.81E-02	7.86E-02	6.01E-02	4.52E-01	2.57E-02	7.92-02	5.70E-02
Minimum (cm/s)	6.77E-02	2.73E-03	4.28E-02	2.37E-03	6.83E-02	1.81E-03	3.71E-02	1.81E-03
Maximum (cm/s)	2.22E+00	1.77E-01	1.77E-01	3.09E-01	2.77E+00	1.88E-01	2.15E-01	2.51E-01
Variance $(cm/s)^2$	1.38	1.248	1.058	1.58	1.46	1.36	1.07	1.68
Standard Deviation (cm/s)	2.37	2.03	1.40	2.79	2.53	2.32	1.47	2.99
Coefficient of Variation (%)	9.69	63.45	73.78	43.19	6.80	58.96	70.29	41.51
	Beyer- Calibrated				**Kozeny-Carman- Calibrated**			
	BBS ***n = 95***	**JPB** ***n = 71***	**WBN** ***n = 48***	**WBS** ***n = 51***	**BBS** ***n = 95***	**JPB** ***n = 71***	**WBN** ***n = 48***	**WBS** ***n = 51***
Mean (cm/s)	4.19E-01	2.99E-02	7.87E-02	6.23E-02	4.72E-01	2.43E-02	7.99E-02	5.54E-02
Minimum (cm/s)	6.75E-02	3.35E-03	4.62E-02	2.66E-03	6.88E-02	1.39E-03	3.07E-02	1.53E-03
Maximum (cm/s)	1.91E+00	1.79E-01	1.66E-01	3.77E-01	3.31E+00	1.97E-01	2.50E-01	2.54E-01
Variance $(cm/s)^2$	1.35	1.20	1.05	1.56	1.53	1.46	1.09	1.77
Standard Deviation (cm/s)	2.29	1.91	1.39	2.75	2.69	2.54	1.54	3.15
Coefficient of Variation (%)	11.55	65.35	74.44	43.27	4.82	56.12	67.34	40.18

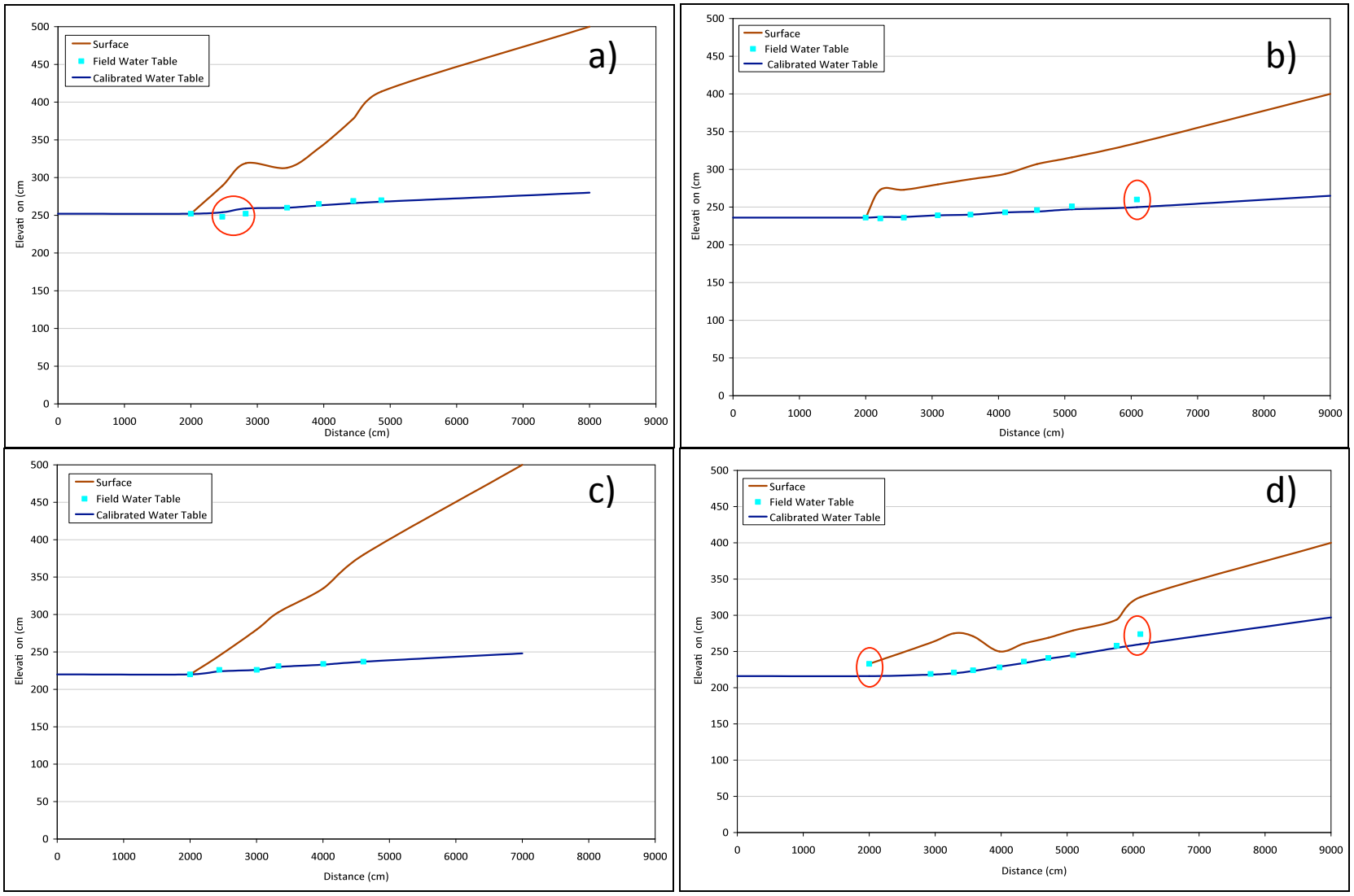

Figure 4.9: Calibrated water table elevations to measured field data at (a) BSB, (b) JPB, (c) WBN, and (d) WBS. Outliers are circled in red and correspond with Figure 4.10.

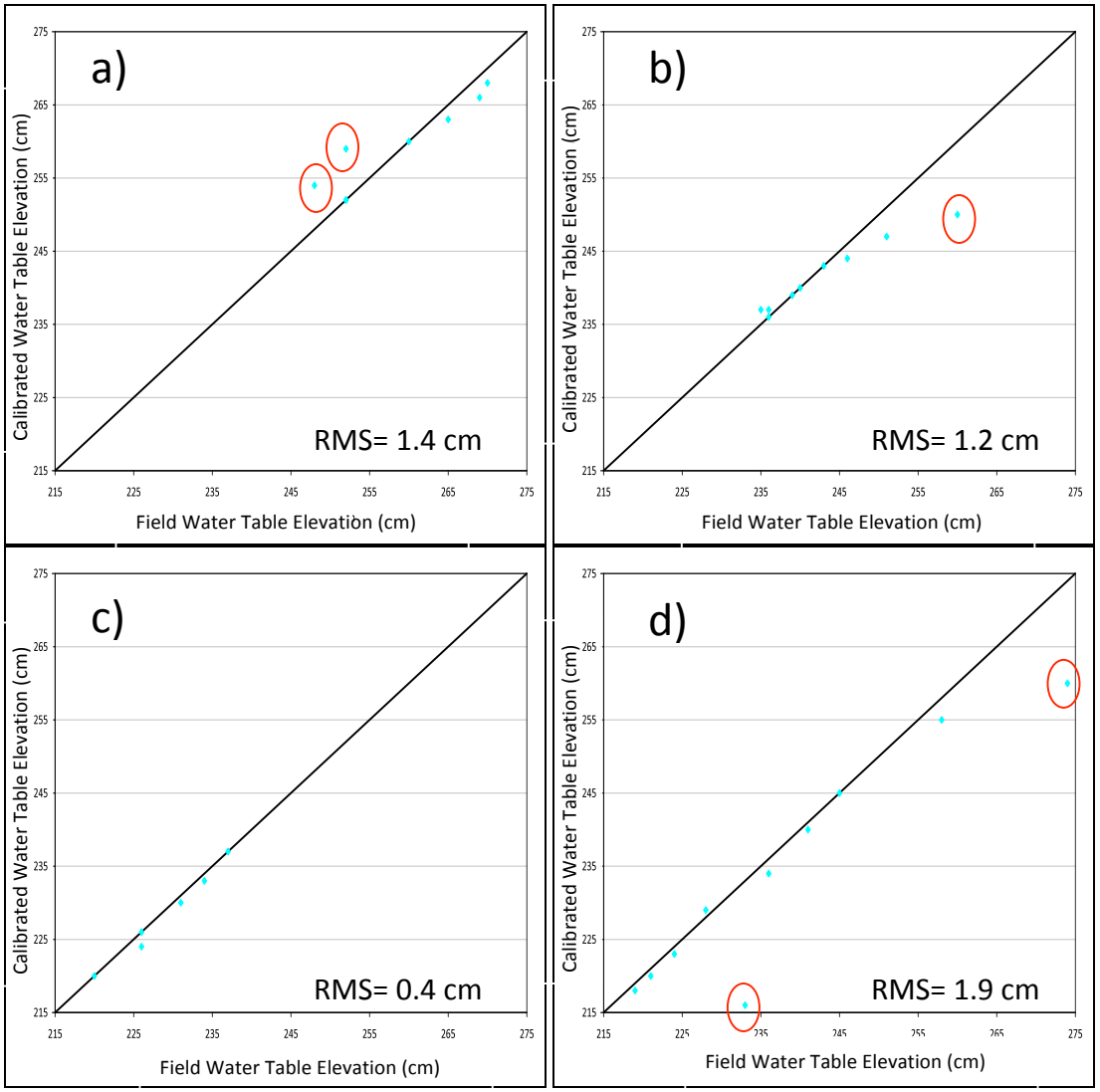

Figure 4.10: 1:1 plots comparing calibrated water table elevations with measured field data (a) BBS, (b) JPB, (c), WBN, and (d) WBS. Outliers are circled in red.

Table 4.14: Soil hydraulic parameters predicted by the Neural Network Predictions (Rosetta) package built into HYDRUS-2D

Soil Hydraulic Parameter	**BBS**	**JPB**	**WBN**	**WBS**
Material 1	Medium-Coarse Sand	Fine Sand	Fine Sand	Fine Sand
o θ_r	0.0531	0.0511	0.0525	0.0467
o θ_s	0.3779	0.3836	0.3686	0.3380
o α	0.0309	0.0326	0.0309	0.0348
o n	4.4866	4.0789	4.4533	3.5396
o $K_s\,(cm.d^{-1})$	1372.94	1116.82	1315.52	628.02
o l	0.5	0.5	0.5	0.5
Material 2	Coarse sand	Loam	--	Medium-Coarse Sand
o θ_r	0.0537	0.0259	--	0.0529
o θ_s	0.3934	0.3054	--	0.3748
o α	0.0312	0.0621	--	0.0309
o n	4.4722	1.4195	--	4.4787
o $K_s\,(cm.d^{-1})$	1445.52	36.77	--	1354.84
o l	0.5	0.5	--	0.5
Material 3	Coarse-Very Coarse Sand	--	--	Loam
o θ_r	0.0554	--	--	0.0243
o θ_s	0.4156	--	--	0.3022
o α	0.0317	--	--	0.0573
o n	4.5279	--	--	1.3574
o $K_s\,(cm.d^{-1})$	1636.24	--	--	32.56
o l	0.5	--	--	0.5

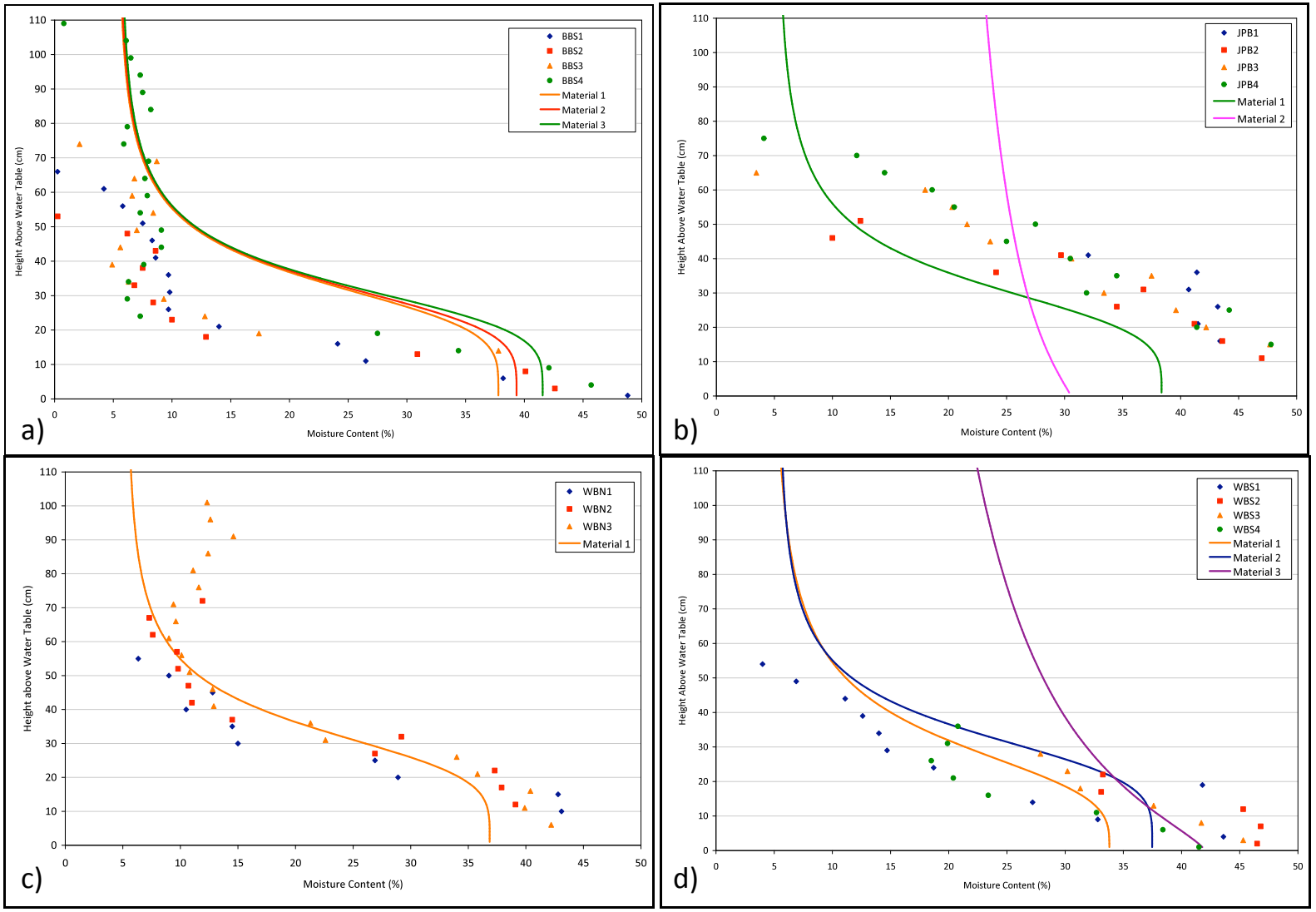

Figure 4.11: Soil moisture retention curves predicted by the van Genuchten (1980) function using soil hydraulic parameters provided by Neural Network Predictions (Rosetta) within HYDRUS-2D at (a) BBS, (b) JPB, (c) WBN, and (d) WBS.

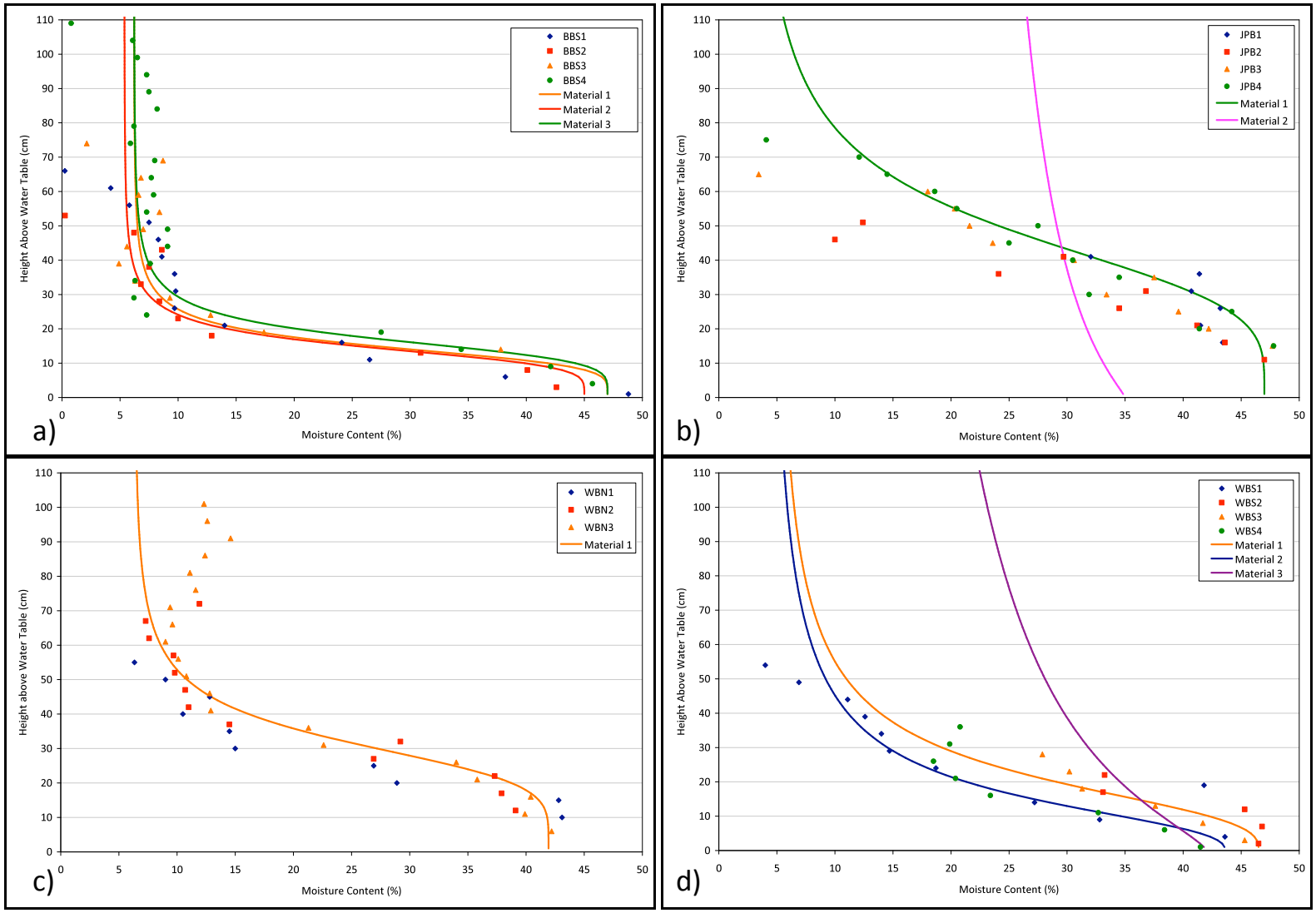

Figure 4.12: Best-fit soil moisture contents above the water table that were calibrated to moisture contents measured at (a) BBS, (b) JPB, (c) WBN, and (d) WBS.

Table 4.15: Summary of best-fit (calibrated) soil hydraulic parameter values used in the calibrated beach models

Soil Hydraulic Parameter	Material 1	Material 2	Material 3
	Balm Beach South		
Texture	*Medium-Coarse*	*Coarse*	*Coarse – Very Coarse*
K_s (cm.s^{-1})	$1.0 \times 10^{-1} – 5.0 \times 10^{-1}$	$5.0 \times 10^{-1} – 1.0 \times 10^{0}$	$1.0 \times 10^{0} – 5.0 \times 10^{0}$
θ_r	0.062	0.0537	0.062
θ_s	0.47	0.45	0.47
K_s (cm.d^{-1})	18146	60072	136107
α	0.0709	0.0712	0.0617
n	4.8866	4.8727	4.9279
l[1]	0.5	0.5	0.5
	Jackson Park Beach		
Texture	*Fine*	*Loam*	--
K_s (cm.s^{-1})	$1.0 \times 10^{-2} – 5.0 \times 10^{-2}$	$1.0 \times 10^{-3} – 5.0 \times 10^{-3}$	
θ_r	0.03	0.0259	--
θ_s	0.47	0.35	--
K_s (cm.d^{-1})	2795	206	--
α	0.0226	0.0621	--
n	4.0789	1.4195	--
l[1]	0.5	0.5	--
	Woodland Beach North		
Texture	*Fine*	--	--
K_s (cm.s^{-1})	$5.0 \times 10^{-2} – 1.0 \times 10^{-1}$		
θ_r	0.06	--	--
θ_s	0.4193	--	--
K_s (cm.d^{-1})	6774	--	--
α	0.0330	--	--
n	5.0000	--	--
l[1]	0.5	--	--
	Woodland Beach South		
Texture	*Fine – Medium*[2]	*Coarse*[2]	*Loam*
K_s (cm.s^{-1})	$1.0 \times 10^{-2} – 5.0 \times 10^{-2}$	$1.0 \times 10^{-1} – 5.0 \times 10^{-1}$	$1.0 \times 10^{-3} – 5.0 \times 10^{-3}$
θ_r	0.0467	0.0400	0.0243
θ_s	0.465	0.436	0.42
K_s (cm.d^{-1})	1500[3]	13876	333
α	0.0548	0.0779	0.0573
n	2.8396	2.4787	1.3574
l[1]	0.5	0.5	0.5

[1] HYDRUS-2D default parameter

[2] WBS – In order to calibrate the water table in HYDRUS-2D to the measured field water table, material 1 was adjusted to a fine-medium sand and material 2 was adjusted to a coarse sand. In other words, the measured grain size data was reversed in the model.

[3] WBS – The predicted saturated hydraulic conductivity for this layer was adjusted (lowered) to calibrate to water table gradients that were measured in the field

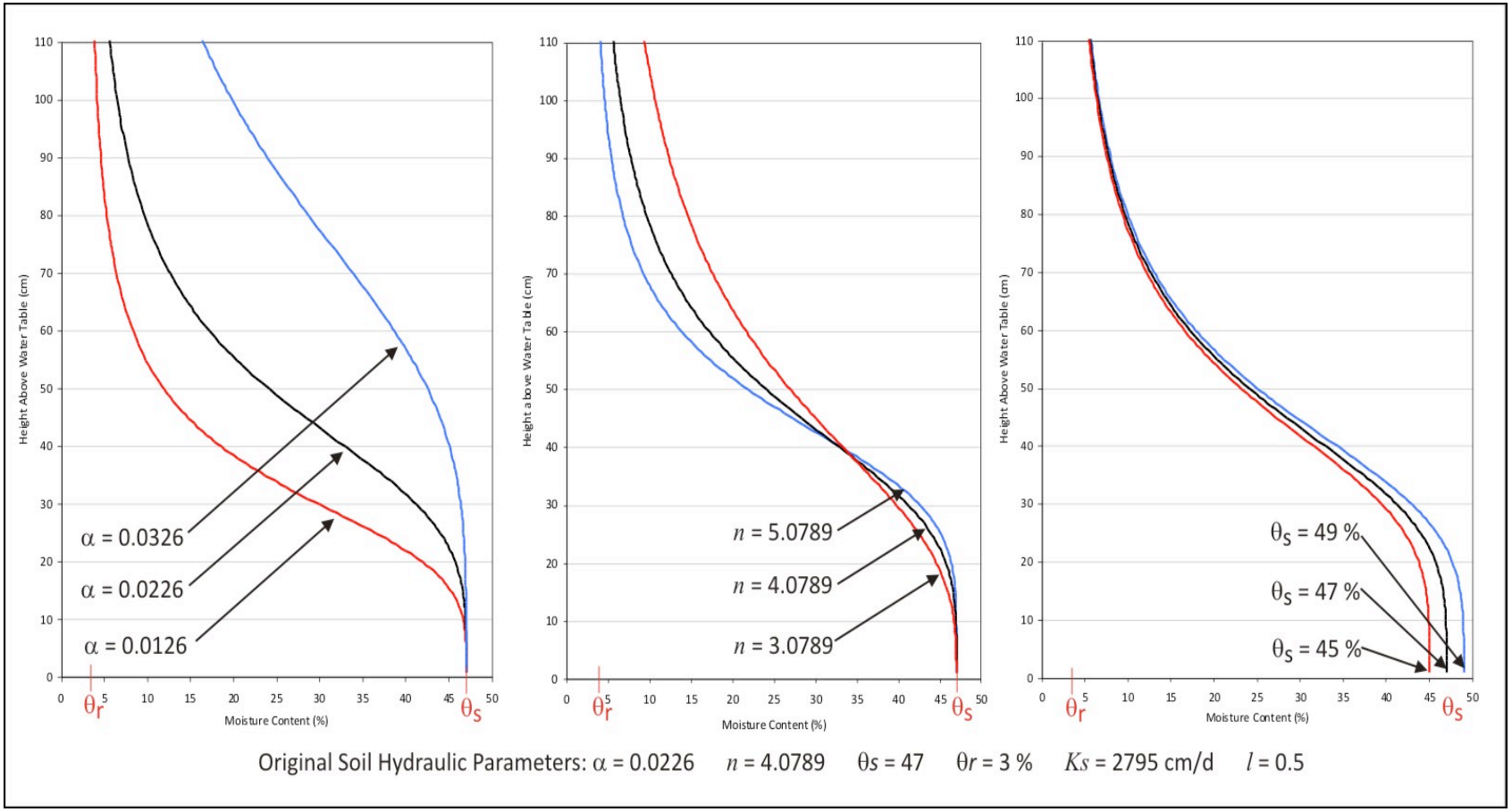

Figure 4.13: Sensitivity analysis of soil hydraulic parameters on the soil moisture retention curve in the JPB model. α and *n* parameters are the most sensitive. Height above the water table represents the absolute pressure head value (cm) at static equilibrium.

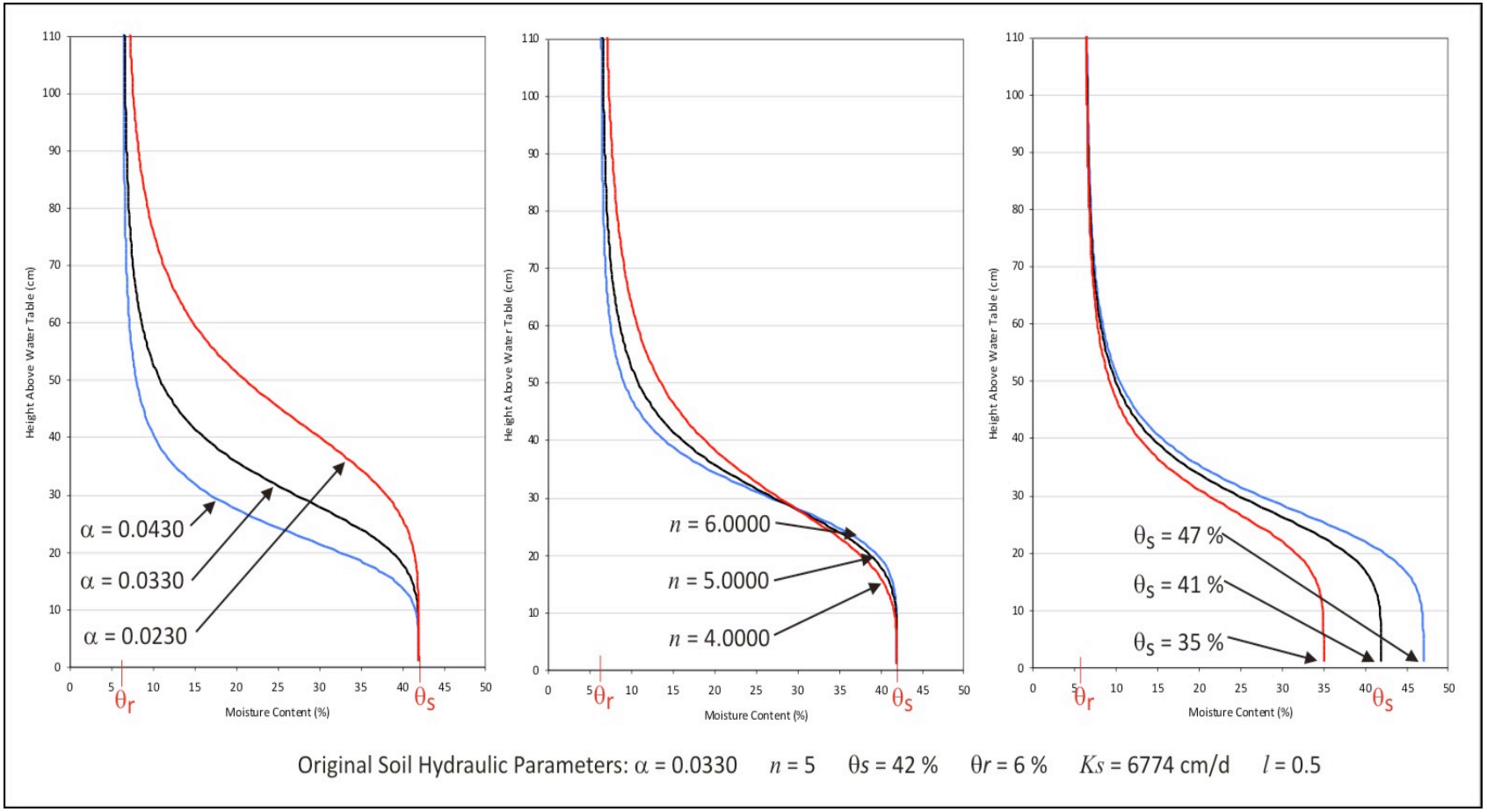

Figure 4.14: Sensitivity analysis of soil hydraulic parameters on the soil moisture retention curve in the WBN model. α and *n* parameters are the most sensitive. Height above the water table represents the absolute pressure head value (cm) at static equilibrium.

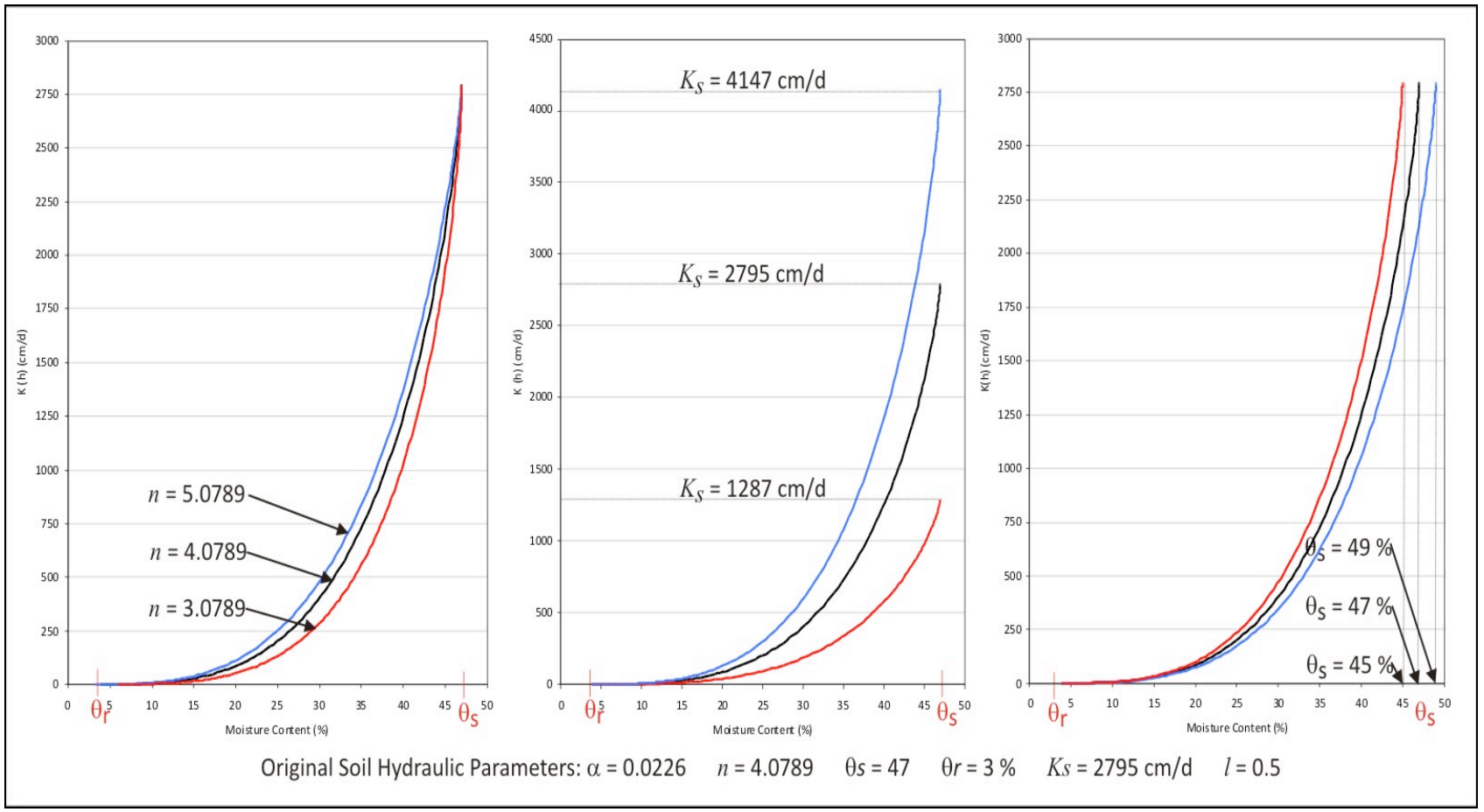

Figure 4.15: Sensitivity analysis of soil hydraulic parameters on the unsaturated hydraulic conductivity ($K(h)$) versus moisture content (θ) function in the JPB model. *n* is the most sensitive parameter.

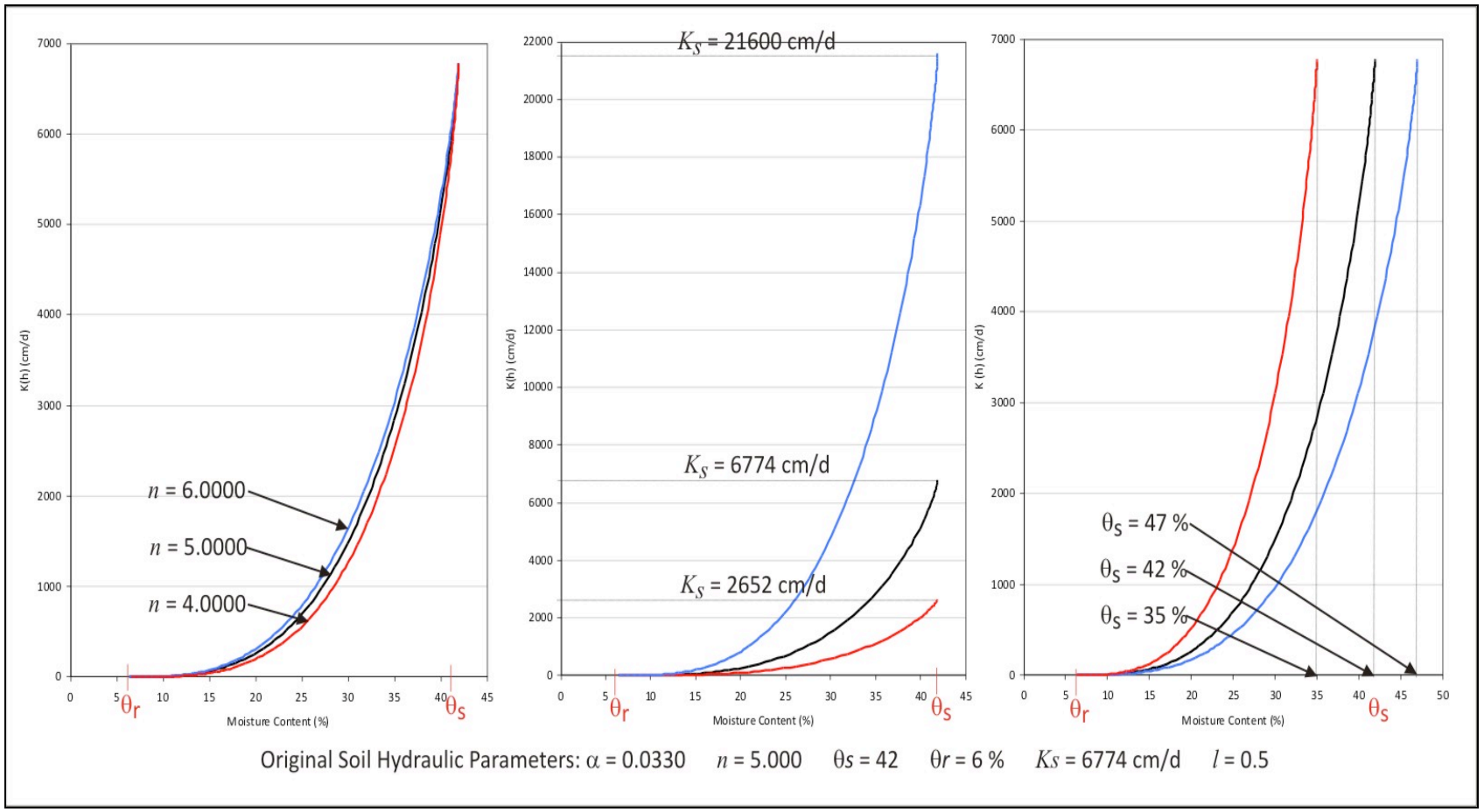

Figure 4.16: Sensitivity analysis of soil hydraulic parameters on the unsaturated hydraulic conductivity ($K(h)$) versus moisture content (θ) function in the WBN model. *n* is the most sensitive parameter.

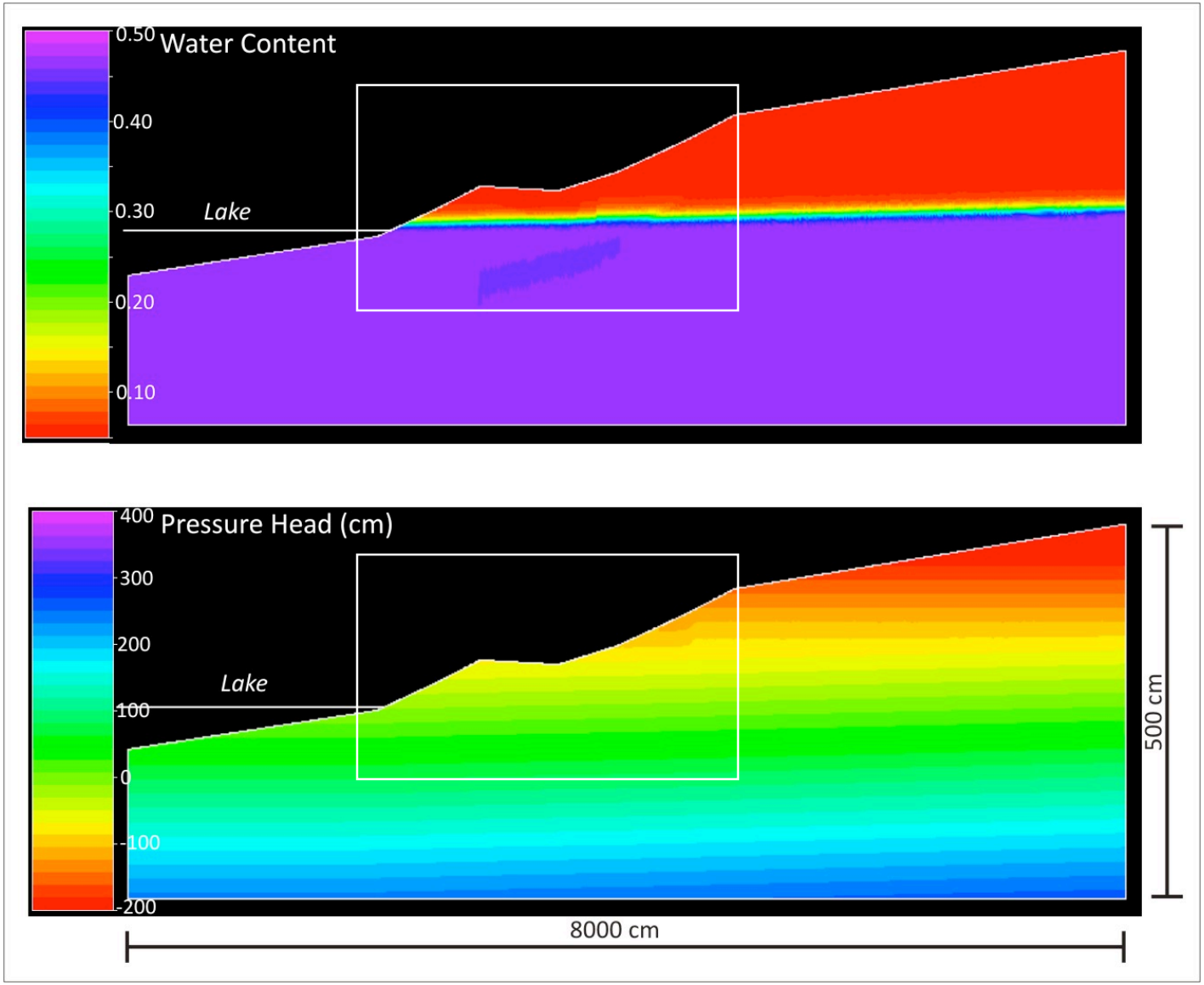

Figure 4.17.1: 2D water content and pressure head profiles for the calibrated BBS beach model. The field transect is outlined by white box.

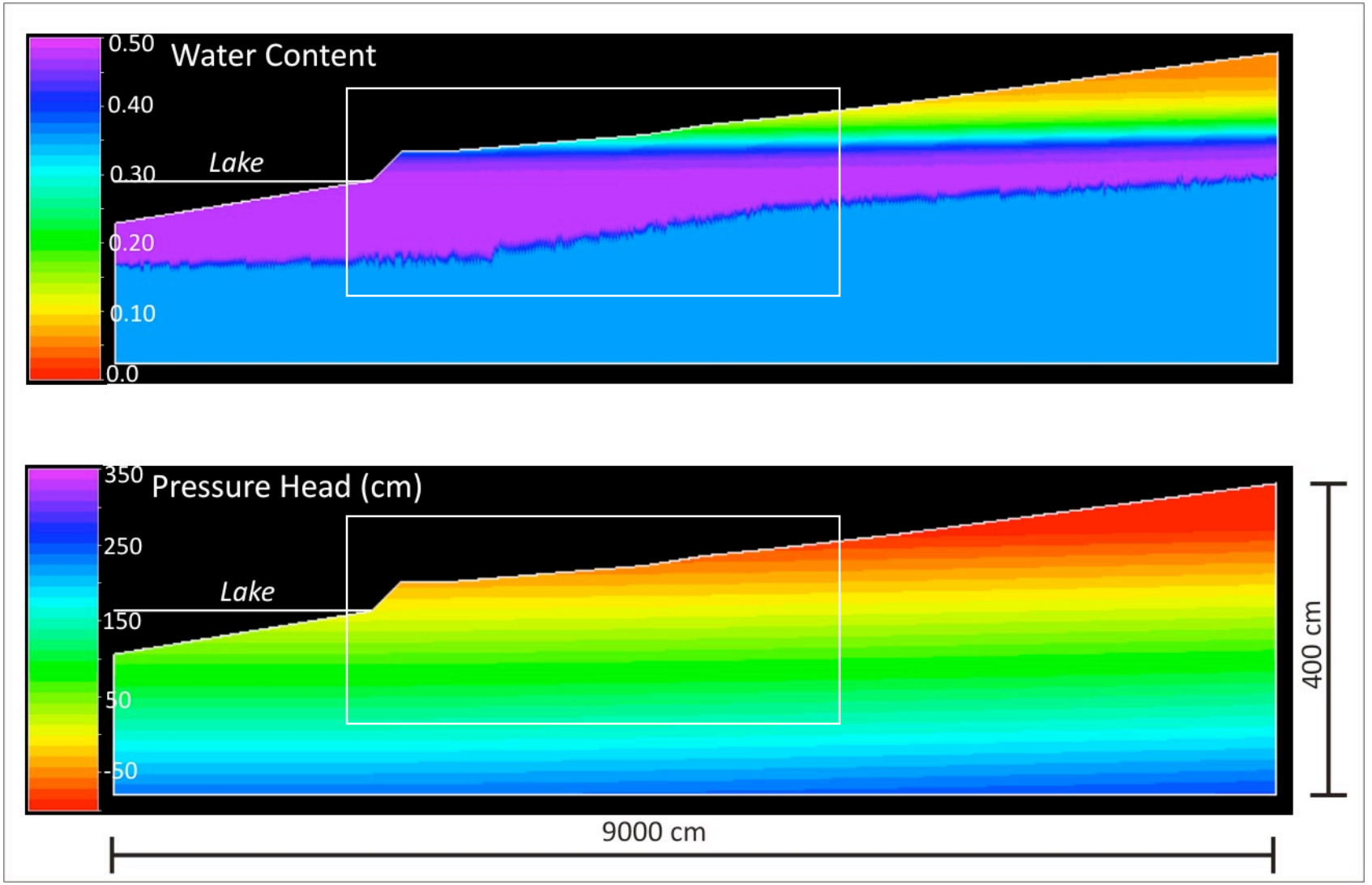

Figure 4.17.2: 2D water content and pressure head profiles for the calibrated JPB beach model. The field transect is outlined by white box.

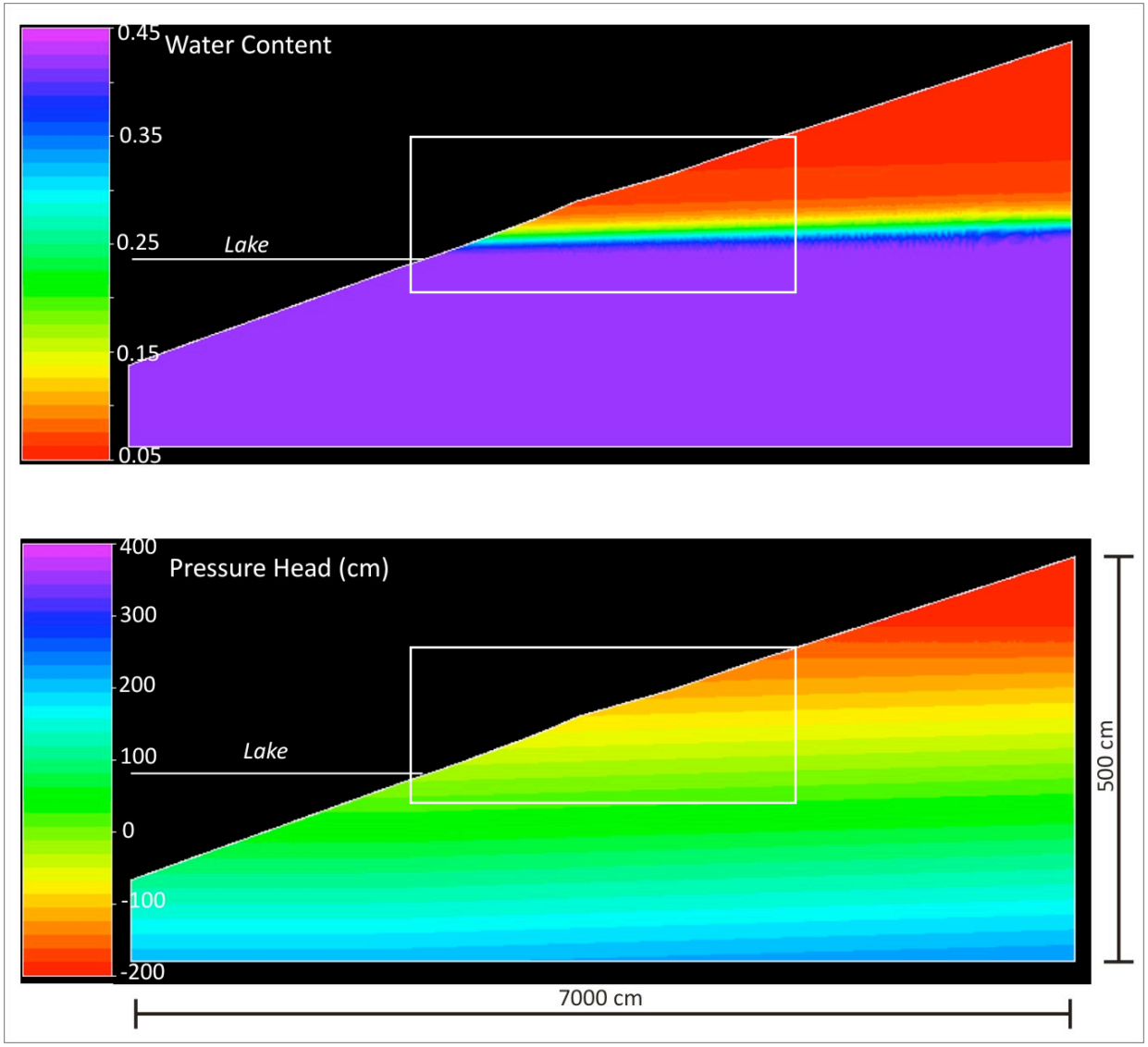

Figure 4.17.3: 2D water content and pressure head profiles for the calibrated WBN beach model. The field transect is outlined by white box.

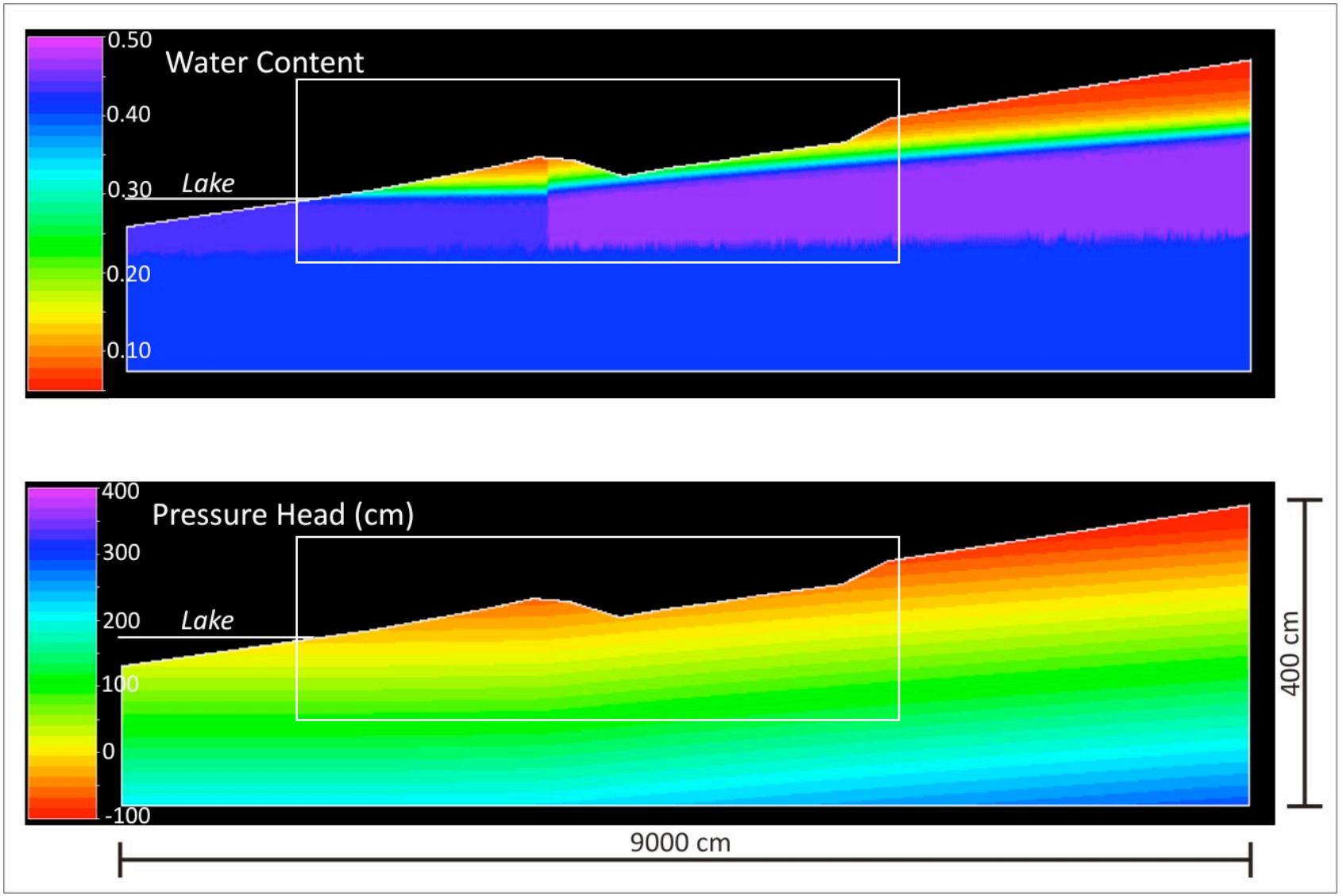

Figure 4.17.4: 2D water content and pressure head profiles for the calibrated WBS beach model. The field transect is outlined by white box.

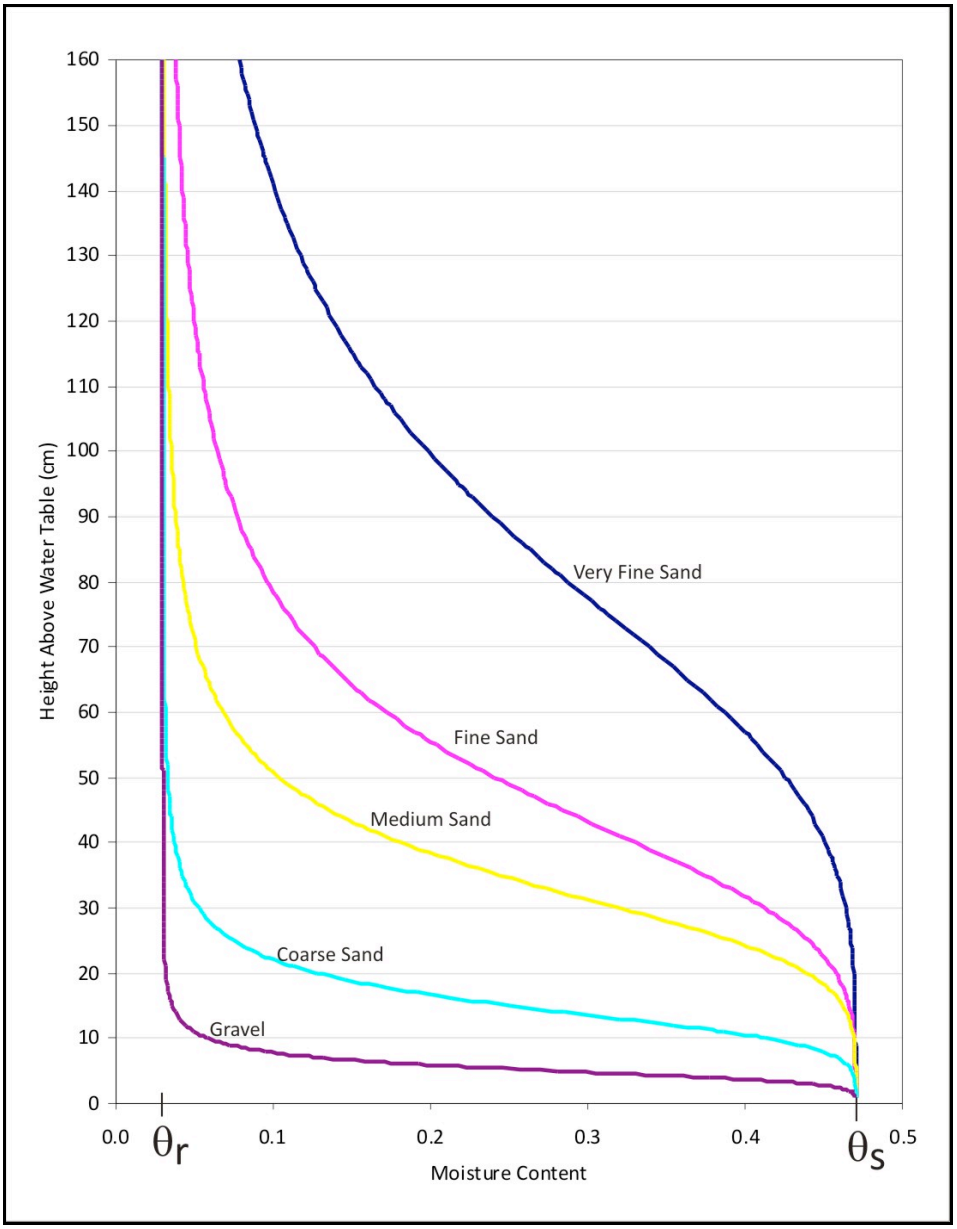

Figure 4.18: Type curve summarizing the ability of different materials (textures) to retain moisture at various heights above the water table.

5.0 BEACH MANAGEMENT ISSUES: An Investigation of Wet and Dry Beaches

Beach managers, scientists, and consultants have many questions and concerns regarding the groundwater conditions and beach quality of the beaches of the Great Lakes. The four calibrated beach models (two wet and two dry beaches) were used to explain why the wet and dry beaches exist. It is evident that wet and dry beaches are controlled by surface topography, water table depth, and also texture of the beach sand. There are numerous beach management questions that can be simulated regarding the hydrology and associated beach problems in Tiny Township and also around the Great Lakes. Focusing within the scope of this study, only a few scenarios were investigated to help answer the objectives. This section will address a few of the major concerns and influences of wet and dry beaches that are of interest to beach managers, scientists, and consultants.

5.1 Impact of Long-Term Lake Level Fluctuations on Wet and Dry Conditions

The water levels of the Great Lakes fluctuate both seasonally and long-term. Seasonal high water levels are observed in the spring/early summer and low water levels are observed during the winter (DFO, 2010), as observed in Figure 5.1. Seasonal fluctuations in the water levels for Lake Huron (including Georgian Bay) range between 20 and 40 cm (DFO, 2010). Long-term water levels of Lake Huron fluctuate over a greater range than seasonal fluctuations. For example, Lake Huron's water levels was highest in 1986 at approximately 150 cm above the International Great Lakes Datum (IGLD) (elevation = 177.5 m) and lowest in 1964 at approximately 40 cm below the IGLD (elevation = 175.58 m), or maximum historical fluctuation of almost 2 m (DFO, 2010). Although understanding the dynamics behind lake level fluctuations is not within the scope of this study, understanding how lake level fluctuations can influence or control wet and dry beaches is of

particular interest. Using HYDRUS-2D, the calibrated 2D models for Jackson Park Beach (JPB) and Woodland Beach North (WBN) in Tiny Township, were used to address the question:

- How do fluctuating lake levels influence wet and dry beach conditions on a flat-sloped beach and a steep-sloped beach comprised of fine sand or coarse sand?

5.1.1 Influence of Long-Term Lake Level Fluctuations on a Flat-Sloped Beach

The 2D model for JPB, was selected to simulate the influence of long-term lake level fluctuations on a flat-sloped beach. In addition to surface topography, beach texture was also a parameter investigated in these simulations. The inland constant head boundary in the model was replaced with a constant flux boundary to observe the water table response with texture. The constant flux boundary was set by applying a groundwater flux of 70 $cm \cdot d^{-1}$ spread vertically over 30 cm (6 nodes), to maintain the water table position consistent with field measurements below JPB in August 2009. Once the water table was consistent with field data, the original material layers (fine sand and loam) assigned in the JPB model were both replaced with one material layer for each simulation; a homogeneous fine sand material (K_{sat} = 2795 $cm \cdot d^{-1}$) and also a homogeneous coarse sand material (K_{sat} = 60072 $cm \cdot d^{-1}$). Base case simulations (*Simulations 1A, 1B*) were run to achieve steady state conditions using the new texture and boundary conditions. Once steady state conditions were reached, four hypothetical scenarios of long-term fluctuations of lake levels were applied to the JPB (fine and coarse) models by adjusting the lake level (left constant head boundary):

- *Simulation 2A: Low lake level (- 50 cm) on a fine textured, flat-sloped beach*
- *Simulation 2B: High lake level (+ 50 cm) on a fine textured, flat-sloped beach*
- *Simulation 3A: Low lake level (- 50 cm) on a coarse textured, flat-sloped beach*
- *Simulation 3B: High lake level (+ 50 cm) on a coarse textured, flat-sloped beach*

Results from the base case simulations (1A, 1B) and lake level simulations (2A, 2B, 3A, 3B) are presented in Figure 5.2a. Consistent with Crowe and Meek (2009), water tables fluctuate proportionally with lake level fluctuations, regardless of the sand texture. That is, the elevation of the lake at the shoreline determines the elevation of the water table exit point where groundwater discharges into the lake, whereas sand texture influences the hydraulic gradient of the water table below the beach. Also consistent with Meek (2007), Crowe and Meek (2009) the low saturated hydraulic conductivity of the fine textured sand results in an increased water table slope (hydraulic gradient) compared to the coarse textured scenarios which results in an essentially flat-sloped water table. Since wet and dry beaches are defined primarily by moisture contents, the resulting soil moisture retention profiles were investigated for the flat-sloped (fine and coarse) simulations, presented in Figure 5.2b. The moisture retention profiles can be applied below the entire beach because they represent the static equilibrium moisture conditions at all locations (above the water table) across the beach. Results of the simulations will be discussed with regards to the moisture profiles below the middle of each beach, at a distance of 4000 cm inland.

The water table positions of the base case are located approximately 55 cm below the surface at both beaches. At this location, both beaches exhibit different surface moisture conditions (*1A compared to 1B*), even though the water table depth is relatively consistent. The surface moisture content is approximately 20 % at the fine textured beach and approximately 5 % at the coarse textured beach. According to this study's definition of wet and dry beaches, the fine textured (flat-sloped) beach is classified as a wet beach and the coarse textured (flat-sloped) beach can be classified as a dry beach because the surface moisture contents are greater and less than 10 %, respectively. This is directly attributed to the moisture retention abilities of different materials (textures), where moisture is well retained (higher) in fine sands and poorly retained (lower) in

coarse sands, consistent with literature and results presented in *Chapter 4.0* (Schwartz and Zhang, 2003; Yang *et al.*, 2004). When the lake level is lowered by 50 cm, the position of the water table is 99 cm (2A) and 108 cm (2B) below the surface at the fine and coarse beach, respectively. In this scenario, the surface moisture contents of both beaches approach dry conditions (< 10 % moisture); 3% and 5% respectively for the fine and coarse sand. When the lake level is increased by 50 cm, the position of the water table at both beaches is very shallow; 8 cm below the beach surface. At this point, the moisture content at surface of the fine-sand beach is saturated (47 %) because it falls within the 10 cm capillary fringe. Similarly, the moisture content at the coarse beach is approaching saturation (43 %) because the top of the capillary fringe is only 3 cm below the beach surface. It is evident that the texture of the sand at a beach is the primary control of wet and dry beaches due to moisture retention via capillarity and also influencing the slope of the water table. The role of long-term fluctuations of lake levels however, indirectly influences the moisture conditions below flat-sloped (fine and coarse) beaches by controlling the elevation of the water table exit point, thus influencing the elevation of the water table below a beach. In addition, as previously stated, the surface topography of a beach influences the depth to the water table, thereby, controlling wet and dry conditions. Referring to Figure 5.2a, higher lake levels will reduce the total beach area exposed at the surface of a flat-sloped beach by encroaching onto the beach. In contrast, lower lake levels will expose more beach, thereby, increasing the overall surface.

5.1.2 Influence of Long-Term Lake Level Fluctuations on a Steep-Sloped Beach

The model for WBN was selected to simulate the influence of fluctuating lake levels on steep-sloped beaches. The role of texture was also investigated (*consistent with Section 5.1.1)*. The homogeneous fine and coarse sands used in the previous simulations were also used in the steep-

sloped beach simulations. A constant flux boundary condition was assigned to the right boundary instead of the (original) constant head boundary condition to assess for textural influences on the slope of the water table. The constant flux assigned to the right boundary was a groundwater flux of 300 $cm \cdot d^{-1}$ that was spread vertically over 30 cm (6 nodes), which yields water table positions consistent with field measurements from measurements in August 2009. Base case simulations (*Simulations 4A, 4B*) were run to achieve steady state conditions as a result of the new input parameters (texture) and boundary conditions (constant flux). Once steady state conditions were reached, four hypothetical scenarios of fluctuating lake levels were applied to the WBN (fine and coarse) models by adjusting the lake level (left constant head boundary):

- *Simulation 5A: Low lake level (- 50 cm) on a fine textured, steep-sloped beach*
- *Simulation 5B: High lake level (+ 50 cm) on a fine textured, steep-sloped beach*
- *Simulation 6A: Low lake level (- 50 cm) on a coarse textured, steep-sloped beach*
- *Simulation 6B: High lake level (+ 50 cm) on a coarse textured, steep-sloped beach*

Results from the base case simulations (4A, 4B) and lake level simulations (5A, 5B, 6A, 6B) are presented in Figure 5.3 (a). Consistent with Crowe and Meek (2009), the elevation of the water table fluctuates proportionally with fluctuating lake levels, regardless of texture or surface topography. In addition, the low saturated hydraulic conductivity assigned in the fine sand (steep-sloped) model yields a steep water table slope compared to a flat water table in the coarse sand model. It is important to recognize that the water table slope in the WBN (fine sand) model is steeper than the water table slope in the JPB (fine sand) model, although both sands textures are consistent. This observation is attributed to the different groundwater fluxes assigned to the boundaries in each model; the flux used to calibrate the JPB model is lower than the flux required to calibrate the WBN model. According to Darcy's law, a higher groundwater flux (q) directly increases

the hydraulic gradient (water table slope) in a particular texture (K_{sat}) (Freeze and Cherry, 1979). Similar to results from the flat-sloped simulations, lake level fluctuations at steep-sloped beaches only controls the position of the water table exit point, whereas, texture and groundwater fluxes influence the slope of the water table (hydraulic gradient) below the beach.

In addition, Figure 5.3b presents the resulting soil moisture retention profiles for the steep-sloped fine and coarse beach simulations. Results of the simulations will also be discussed with regards to the moisture profiles below the middle of each beach, at a distance of 4000 cm inland. The base case water table position is 90 cm below the surface in the fine sand model and 113 cm below the surface in the coarse sand model. The surface moisture contents in the base case simulations are both classified as dry conditions; 9 % and 5 % moisture in the fine and coarse beach models, respectively. These results are different compared to the base case simulations in the flat-sloped model; where the fine sand model was wet (20 %) and the coarse sand model was dry (5 %). This is because the influence of both texture and depth to the water table (pressure head) controls the moisture conditions at the surface of a beach. That is, both the fine and coarse sands do not retain high moisture contents well above the water table.

When the lake level falls by 50 cm, the elevation of water table is 123 cm below the surface of the fine beach and 163 cm below the surface of the coarse beach. Both the fine and coarse (steep-sloped) beaches exhibit similar trends in moisture content where; the surface moisture contents approach residual saturation (3 % and 5 %, respectively). Results are consistent with the flat-sloped beach simulations where low lake levels increase the depth to the water table from the surface, regardless of the surface topography. In addition, when the lake level is increased by 50 cm, the position of the water table at the fine beach is 54 cm below the surface and the water table position at the coarse beach is approximately 64 cm below the surface. Unlike the flat-sloped beach

simulation, the moisture contents at both beaches exhibit different trends, where saturation is not observed at the surface. The fine textured beach contains a surface moisture content of 23 % and the coarse textured beach contains a moisture content of 5 % (residual saturation). The depth to the water table at this steep-sloped beaches is larger compared to the depth to the water table at flat-sloped beaches, therefore, the lake level rise of 50 cm is not high enough to for the coarse sand to wick water from the water table through capillarity. The fine sand beach however, has stronger capillarity forces and therefore, a water table rise of 50 cm increases the surface moisture content above 10 % to classify the beach as wet. Furthermore, the surface moisture contents at both beaches are not at saturation because the capillary fringe does not extend beyond 10 cm above the water table for the fine sand and 5 cm above the water table for the coarse sand beach. In addition, referring to Figure 5.3a, steep-sloped beaches will not be as sensitive to higher or lower lake levels.

5.1.3 Summary: Influence of Long-Term Lake Level Fluctuations on Beaches

It is evident that the moisture conditions at beaches are controlled by three factors including: (1) beach surface topography, (2) water table depth, and (3) the texture of the sand at a beach. In addition, the role of long-term lake level fluctuations controls the elevation of the water table exit point, which in turn influences the depth of the water table below the surface of a beach. That is, the water table below a beach fluctuates proportionally with lake level fluctuations. Therefore, results from these simulations provide insight on how long-term fluctuating water levels of the Great Lakes affect whether a beach is wet or dry.

Beach managers, scientists, and consultants can therefore predict how a beach will be affected by long-term fluctuations of lake levels if the detailed texture of a particular beach, surface topography, and depth of the water table are known, assuming there is not a significant change in

the topography of the beach. For example, according to Figure 4.18 (*Chapter 4.0*) if the water levels of the Great Lakes maintained a water table approximately 50 cm below the surface of a very fine sand (flat-sloped or steep-sloped) beach, the beach would be classified as a wet beach. The surface moisture content would be approximately 45 %, which is well above the criteria for the classification of a wet beach (> 10 %). If the beach (flat-sloped or steep-sloped) is comprised of gravel, the beach would be classified as a dry beach under this scenario, because the surface moisture content would be at residual saturation (3 %). Alternatively, if the lake level was very low, as observed at Lake Huron in 1986, approximately 150 cm below the beach surface (DFO, 2010), the very-fine sand and gravel beach would be classified as dry beaches because the surface moisture contents at both beaches would be less than 10 %. Beach managers, scientists, and consultants are now better able to predict and assess which beaches of the Great Lakes are at greater risk of becoming wet and which beaches will remain dry under long-term scenarios.

5.2 Human Induced Alterations: Changing Wet Beaches into Dry Beaches

Beach profiles are altered by Aeolian sediment transport when sand is naturally eroded and deposited onto beach surfaces (Lundgren, 1986; Crowe and Milne, 2007) and also by waves, currents, storms, and ice (Horn, 2002). Human activities also result in beach profile alterations by either directly adding or removing sand from the beaches. In particular, along the shores of southern Georgian Bay and Lake Huron, the Lake Huron Centre for Coastal Conservation has implemented a dune stewardship program to conserve the sand dunes. This program involves the participation of local residents with installing sand fences and also planting natural beach grass (*Ammophila breviligulata*) to help restore the sand natural beach-dune ecosystem, wildlife habitat, and also protect shorelines from storms during high lake levels (LHCCC, 2011).

In addition, human activities have removed beach sand and altered the profiles of the beaches of the Great Lakes through bulldozing sand dunes (*see Figure 3.2b*) and also through beach grooming. These human activities have altered natural dry beaches into degraded wet beaches, as observed directly in Tiny Township at WBS. Beach managers are therefore interested in investigating and answering the following questions:

- Can the wet beaches be changed into dry beaches by adding sand onto the beach surface?
- Can the dry beaches be changed into wet beaches by removing sand from the beach surface?

5.2.1 Changing a Wet Beach into a Dry Beach

i. Adding Original (Fine Textured) Sand to the Beach Surface

It is evident from this study that wet and dry beaches are influenced by surface topography which is related to the depth to the water table. In addition, texture primarily controls the moisture retained at a beach and also influences the water table depth by inducing the hydraulic gradient (water table slope). The soil moisture retention curve (moisture content profile) from the JPB beach model was used to determine if a fine-grained wet beach can be converted into a dry beach by adding fine sand to the surface (Figure 5.4). Initially, this beach was classified as a wet beach because the mean water table depth is approximately 50 cm below the beach surface and the moisture content at the surface is 25 % (> 10 %). As observed in Figure 5.4, it is evident that the soil moisture retention curve for the fine sand retains moisture greater than 10 % up to a depth of approximately 80 cm above the water table. Under these conditions, if desirable, to convert the wet beach into a dry beach, at least 30 cm of additional fine sand is required to be added onto the beach

surface to maintain surface moisture contents less than 10 %. Due to high recreational use of the beaches and also Aeolian sediment transport of the beach sand, this study recommends at least 40 cm of additional fine sand is required to sustain dry conditions at this beach.

ii. Adding Coarse Textured Sand to the Beach Surface

Coarse sands hold less water compared to fine sands as a result of weak capillarity due to large pore spaces (Abdul and Gillham 1984; Gillham, 1984; Turner, 1993a; Debrasch *et al.*, 1999). Figure 5.5 shows the soil moisture retention curve for coarse textured sand and also a fine textured sand. It is evident that the coarse sand retains high moisture contents (>10 %) only up to a depth of 25 cm above the water table, where as, the fine sand retains high moisture contents up to a depth of approximately 80 cm above the water table. In this hypothetical scenario where the mean water table below the wet beach is 50 cm below the surface, only 1 – 2 cm of coarse sand is technically required to convert the wet beach into a dry beach. However, to sustain dry conditions, this study recommends the addition of approximately 10 cm of coarse sand added to the surface of the beach. By adding 10 cm of coarse sand to the beach, the new surface moisture content would be at residual saturation of the coarse sand (~ 5 %) compared to wet conditions from the original beach (~ 25 %). Although the water table below the dry beach would only be 60 cm below the beach surface, compared to the previous scenario (90 cm below the surface), the beach would remain dry due to the weak capillarity forces of coarse sands.

5.2.2 Restoring a Human-Altered Wet Beach into a Dry Beach

i. Adding Original (Medium Textured) Sand to Restore the Beach Surface

The soil moisture retention curve from the WBS model was used to investigate the scenario of restoring a human-altered wet beach into a dry beach. The mean grain size at this beach is

comprised of medium textured sand. Medium sands generally retain less moisture compared to fine grained sands and retain more moisture compared to coarse grained sands. The soil moisture retention curve (moisture content profile) for this wet beach is presented in Figure 5.6. The mean water table position is 37 cm below the surface of the beach and the corresponding moisture content at the surface is approximately 17 %. In order to convert this human-altered wet beach back into a dry beach, at least 20 cm of medium sand is required to be added to the surface of the beach. However, in order to sustain dry conditions, the addition of approximately 30 cm of medium sand to the surface of the beach is recommended by this study. An additional 30 cm of medium sand will increase the depth of the water table from 37 cm to 67 cm below the beach surface. As such, the medium textured sand is unable to retain moisture contents greater than 10 % at this particular height above the water table. The new surface moisture content of WBS will therefore be approaching residual saturation of the medium sand, approximately 7 % moisture. Results from this analysis therefore suggest that if the original surface of a particular wet beach remains unaltered by humans, thus the original sand was not removed from the surface, than the beach would be classified as a natural dry beach. As such, the success of the restoration of this beach to natural conditions may be highly achievable with the proper implementation and monitoring of the Lake Huron Centre for Coastal Conservation dune conservation program.

ii. Adding Coarse Textured Sand to Restore the Beach Surface

Similar to results presented in *Section 5.2.1.ii*, adding coarse textured sand is hypothesized to reduce the moisture content at a human-altered (medium textured) wet beach, due to the weak nature of coarse sands in retaining moisture by capillarity. As the water table position is 37 cm below the surface, only approximately 1 – 2 cm of coarse sand is required to change the surface

moisture content to residual saturation (~ 5 %) (Figure 5.7). Results are consistent with the fine sand scenario, confirming that coarse sands have weaker moisture retention abilities compared to fine and medium sands. Similarly, to sustain dry conditions, the addition of 10 cm of coarse sand is recommended due to heavy traffic and erosion/transport of the sand at the beaches of the Great Lakes. The new water table position would be 47 cm below the beach surface, which is a high enough elevation above the water table for the coarse sand to not hold water via capillarity.

5.3 Influences of Precipitation Events

Infiltration of precipitation is an important process to investigate because it influences groundwater recharge, the transport of contaminants, and also available water for plants (Geiger and Durnford, 2000). Infiltration at beaches has been extensively investigated in the swash zone, focusing on sediment transport and water table mounds (Grant, 1948; Turner and Masselink, 1998; Horn, 2002; Austin and Masselink, 2006). However, little research has been conducted in the backshore area of a beach specifically focusing on the moisture distribution profiles below the beach surface. When assessing the wet and dry beaches of the Great Lakes, beach managers, scientists, and/or consultants, are concerned with understanding the response of the beaches to infiltration events. In particular, with the growing concern and interest in global climate change, questions arise concerning the predictions of higher intensity and more extreme precipitations events within the Great Lakes basin (Patz *et al.*, 2008). *Will dry beaches become wet as a result of heavy precipitation (high intensity infiltration) events? Will wet beaches become saturated (instantaneous water table rise) as a result of infiltration events?* In order to assess the impact of extreme precipitation events on wet and dry conditions of beaches of the Great Lakes, the following questions were investigated:

- How do the moisture profiles respond to a very heavy rainfall event (high intensity and long duration) on fine and coarse textured (wet and dry) beaches?
- How do the moisture profiles respond to an extreme rainfall event (higher intensity and short duration) on fine and coarse textured (wet and dry) beaches?

In order to address these questions, a 1D, narrow rectangular grid was used in the HYDRUS-2D numerical model, to investigate vertical (downward) infiltration in unsaturated beach sand. Using a 1D grid provides a more simplistic method of investigating the complex process of infiltration in sands, which can directly be applied to the fundamentals of infiltration below beaches. The role of evaporation was not assessed during the simulations; instead, evaporation will be discussed in *Section 5.4.* The models were set up containing one homogeneous material layer: unsaturated fine sand (K_{fs} = 799 cm·d^{-1}) and unsaturated coarse sand (K_{fs} = 17163 cm·d^{-1}). The fine sand properties are consistent with the fine sand used in the JPB beach model and the coarse sand properties are consistent with the coarse sand used in the BBS beach model (*refer to* Chapter 4.0). Field-saturated hydraulic conductivities were assigned to the material layers ($K_{fs} = K_{sat}/3.5$) to represent unsaturated vadose zone conditions above the water table at wet and dry beaches. The rectangular grids were 1 cm wide with nodal a spacing of 0.1 cm, by 100 cm deep (and also, 75 cm, 50 cm, and 25 cm) with a nodal spacing of 0.2 cm for the fine sand grids and 0.4 cm for the coarse sand grids. A constant head boundary condition was assigned across the bottom boundary to define the water table. When assigning this boundary condition, the assumption is made that the water table does not fluctuate during the precipitation simulations. Finally, an atmospheric boundary condition was defined across the top boundary and assigned a precipitation flux during the simulations.

5.3.1 Very Heavy Rainfall Event (High Intensity and Long Duration)

During summer months, average precipitation events around southern Georgian Bay range from low to moderate rainfalls and are less than 1 $cm \cdot d^{-1}$ (NCDIA, 2011). It is unclear whether rainfall events contribute to the wet conditions at the wet beaches around the Great Lakes, therefore, an investigation of the response of these beaches to very heavy rainfall events was conducted. Furthermore, with global climate change predictions of more intense and frequent storm events, it is important for beach mangers, scientists, and consultants to understand if beaches are more at risk in becoming wet as a result of the future storms. As such, a rainfall rate selected for the high intensity and long duration (very heavy rainfall) simulations was selected based on a very heavy (above average) rain storm event that is archived in historic weather records from the National Climate Data and Information Archive. The rainfall rate of 7.4 $cm \cdot d^{-1}$ was assigned to the atmospheric boundary in HYRDUS-2D, for a duration of 3 days, with no evaporation (*see Section 5.4*). This rate was recorded from a southern Georgian Bay weather station located in Collingwood, ON, (44°30'00.00"N, 80°13'00.000"W) measured on July 31, 2000 (NCDIA, 2011). The total volume of water applied to the system under the specified rate is 22.2 cm of rain over 3 days. This simulation is similar to the intensity, but less than the total rain supplied to southern Ontario in 1954 during Hurricane Hazel, where the rate of 14.3 $cm \cdot d^{-1}$ supplied 28.5 cm of rain in 2 days (Environment Canada, 2011).

The resulting moisture content and pressure head profiles during the rain event (wetting curve) through a fine sand, with a water table 100 cm below the surface, is summarized in Figure 5.8a and through a coarse sand in Figure 5.9a. The rate of infiltration into the fine and coarse sand columns (analogous to a beach) is controlled by the saturated hydraulic conductivity and infitrability of the beach sand, the initial moisture content, gravity forces, and also due to the continuous supply of water at the surface (rainfall rate and duration) (Hillel, 1998). Simulation results are similar to

classic infiltration profiles where initially, suction gradients dominate controlling the depth of the wetting front, as is pores fill with water. At later times, the wetting front penetrates deeper in the profile as gravity forces dominate, increasing the moisture content of the sand with depth, for the duration of the infiltration event. During the rainfall event, the surface moisture contents and pressure heads for both sands remain consistent between 24 and 72 hours. This is attributed to the relatively high hydraulic conductivity and infitrability of both sands continuously moving the supplied water vertically downward throughout the profile, thus not saturating the systems. The highest moisture content reached during the fine sand simulation is 13 % which is higher than the highest moisture content reached during the coarse sand simulation, reaching 8 %. Comparing both moisture profiles, a sharp wetting front is present within the coarse sand column, compared to a shallow and more redistributed moisture profile present within the fine sand column. Fine textured materials are able to retain and redistribute the supplied water due to smaller pores and stronger capillarity abilities, compared to coarse textured soils. The nature of coarse textured sands, comprised of large pore spaces and weak capillarity forces, enables these sands to retain moisture, therefore, the wetting front moves quickly and deep into the profile during infiltration. In addition, the supplied precipitation rate at the surface is well below the field saturated hydraulic conductivity of the sands; 7.4 $cm \cdot d^{-1}$ compared to 799 $cm \cdot d^{-1}$ for the fine sand and 17163 $cm \cdot d^{-1}$ for the coarse sand, therefore, the water moves quickly throughout these systems and no surface ponding occurs, during the infiltration event.

Once the infiltration event was shut off in the models, the process of drainage and redistribution took place, where profiles are summarized in Figure 5.8b (fine sand) and Figure 5.9b (coarse sand) for water tables that were 100 cm, 75 cm, 50 cm, and 25 cm below the surface. During drainage and redistribution, the soil water continues to wick horizontally and move vertically

downward throughout the profile due to suction (capillarity) and gravity gradients. When the water table is located 100 cm below the surface, the largest response in moisture content variation was observed immediately following the precipitation event. Specifically, the moisture content at the surface of the fine sand column increased by approximately 10 % and the moisture content at the surface of the coarse sand column increased by approximately 3 % (from residual saturation). As the depth to the water table decreased, redistribution from the precipitation event is less apparent, because the moisture profiles remain consistent with their original shape.

No surface ponding or runoff occurred during these simulations, as a result of the relatively low application rate compared to the high hydraulic conductivities (K_{sat}/K_{fs}) and infitrabilities of these sands. As such, it is suggested that the fate of the precipitation upon application continues to infiltrate and redistribute downward throughout the profile, thereby recharging the water table. Further investigation of solute transport is necessary to determine whether the groundwater reaches and recharges the water table. Also evident in Figure 5.8b and 5.9b, after 480 minutes, the moisture content and pressure head profiles at all depths (100 cm, 75 cm, 50 cm, and 25 cm) appear close to their original (steady-state) conditions and return to their original conditions after less than one day.

In summary, the response of fine and coarse textured sands to very high intensity and long duration precipitation events is relatively fast. As observed, the precipitation quickly infiltrates, drains, and redistributes, potentially recharging the water table in under than one day. Therefore, it is evident that heavy rainfall events do not significantly control the wet conditions at fine and coarse beaches. In addition, regardless of the depth to the water table or the texture of the sand, high intensity precipitation events applied at rates lower than the hydraulic conductivity (K_{sat}/K_{fs}) of the

sand, will not saturate the beach or significantly alter their moisture profiles for extended periods of time.

5.3.2 Extreme Rainfall Event (Higher Intensity and Short Duration)

As observed from simulations presented in *Section 5.3.1*, the high hydraulic conductivities and infitrabilities of the Tiny Township beach sands have the ability to infiltrate large amounts of water applied at very high rainfall rates. For the extreme rainfall simulations, the rainfall rate selected and applied to both the fine and coarse sand columns (100 cm, 75 cm, 50 cm, and 25 cm) is 799 $cm \cdot d^{-1}$ (33.30 $cm \cdot hr^{-1}$) for 40 minutes or 0.02778 days. This rate is equal to the field-saturated hydraulic conductivity of the finest sand in the Tiny Township beaches (JPB), therefore, both the fine and coarse sands can infiltrate precipitation applied at this rate, without inducing surface ponding or runoff. The duration of 40 minutes was selected to supply the same amount of water (22.2 cm) as applied in *Section 5.3.1*. This rainfall rate is consistent with extreme rainfall events in southern Ontario and is less than the highest rainfall rate recorded in Toronto on June 15, 2008 at a rate of 42.66 $cm \cdot hr^{-1}$ (TWFC, 2011).

In addition, for the coarse sand simulations, an additional application rate of 0.5 $cm \cdot d^{-1}$ was applied to the model for the duration of one day prior to the extreme rainfall event. One of the consequences of these extreme application rates onto soils near residual water contents is numerical solution problems (Lebeau and Konrad, 2010). As such, one way to alleviate these numerical problems is to precede the extreme event with a short term and low application rate to the soil.

Moisture content and pressure head results are presented in Figure 5.10a (fine sand) and Figure 5.11a (coarse sand) summarizing the vertical (downward) migration of the wetting front

during the extreme rainfall event. Unlike the wetting fronts during the heavy rainfall and long duration simulations (*Section 5.3.1*), sharp wetting fronts are visible in both the fine and coarse sand simulations. The profiles are similar to classic infiltration profiles where the wetting front migrates downward towards the water table. The steepness of the wetting fronts differ between sands, where the fine sand has a shallow wetting front and the coarse sand has a sharp wetting front. The fine sand also becomes nearly saturated at the surface (~ 45 %) during the 40 minute application, where as, the coarse sand only reaches a maximum moisture content of 19 % at the surface. The coarse sand does not approach saturation due to the higher hydraulic conductivities of coarse sands and the nature of large pore spaces, allowing water to quickly fill and also drain pores.

Following the infiltration event, the process of drainage and redistribution took place and is summarized in Figure 5.10b, c, and Figure 5.11b. Figure 5.10b and Figure 5.10c are expressed as two figures because they exhibit different wetting profiles during the precipitation event. For example, the models with the shallower water tables (75 cm, 50 cm, and 25 cm) become nearly saturated (~ 46 %) throughout the entire profile as a result of the precipitation event. In contrast, the model with the deepest water table (100 cm) does not become approach saturation evenly throughout the profile. In the coarse sand simulations, saturation did not occur when the water table was closer to the surface, therefore, the resulting moisture and pressure head profiles are summarized in one figure (Figure 5.11b).

Results indicate that higher intensity storms have a greater affect on saturating a fine sand beach if the water table is close to the surface (≤ 75 cm). Coarse sand beaches are not at risk of becoming saturated during extreme rainfall events, as these sands have a higher ability to intake surface water compared to fine sands. As seen in the figures, it is evident that moisture contents at the surface for both sands become lower as the wetting front drains towards the water table and

redistributes throughout the profiles. Similar to the very heavy rainfall simulations, the moisture profiles approach to their original (steady-state) conditions after 480 minutes in both sands.

In summary, the simulations presented in both *Section 5.3.1* and *5.3.2* show the response of different sands (fine and coarse) wetting and draining back to static conditions under different rainfall scenarios. It is evident that extreme (and heavy) rainfall events that apply water to the surface of a beach at a rate less or equivalent to the hydraulic conductivity of the sand, only affects the moisture conditions for short time periods (< 1 day). Results are generally consistent regardless of the texture of the sand, depth of the water table, and also duration of the precipitation event. In addition, it is evident that the long term sustainable infiltration rates without observing flooding at these beaches is equal to the hydraulic conductivity times the unit gradient. As such, the high hydraulic conductivities of the beaches of the Great Lakes are an excess of violent precipitation rates during hurricanes, and therefore, it is unlikely that flooding the beach sands will occur. Furthermore, results also confirm that the wet beaches of the Great Lakes are not the result of extreme precipitation events due to the nature and the fast response of the sands in infiltrating, redistributing, and also draining surface water.

5.4 Influence of Evaporation

Evaporation of water in porous media describes the water-to-gas exchange process between a soil and the atmosphere (Lehman *et al.*, 2008). Evaporation rates are controlled by temperature and humidity, where highest rates of evaporation occur under high temperatures and low humidity (Lehman *et al.*, 2008). Under these conditions, evaporation from porous media (e.g. sand) is highest during the summer season around the Great Lakes. During hot summer days, the temperature of the surface sand at the beaches of the Great Lakes can be very hot. In fact, the

temperatures of the sands at beaches in general, can reach up to 40 to 60°C (Maun, 2009). These hot sands can even burn feet when walking along the beach (*personal communication* Crowe, 2011). High temperatures (and low humidity) are found to promote high evaporation rates (Lehman *et al.*, 2008). During the field work for this thesis, and subsequent observations, the moisture conditions of the wet beaches (JPB and WBS) and dry beaches (BBS and WBN) did not appear to be affected by temperatures; both types of beaches exist on the same very hot days.

As such, beach managers, scientists, and consultants are interested in understanding how evaporation rates influence the moisture conditions at a beach. *Will high evaporation rates dry out the wet beaches in Tiny Township? After a rainfall, where does the water go; does it infiltrate or is it lost by evaporation?* To address these questions concerning evaporation at the Tiny Township beaches, the following simulation was investigated:

- How does a high evaporation rate on a hot summer day, affect the moisture profiles following a very heavy rainfall event?

A high evaporation rate was selected from Lehman *et al.* (2008) and was applied to the 100 cm fine sand column used in the simulations in *Section 5.3.1*. The range of evaporation rates presented in Lehman *et al.* (2008) for fine and coarse quartz sands under a high temperature (28°C) and low humidity (31 %) is of 2 to 9 $mm \cdot d^{-1}$, therefore, the high rate of 0.9 $cm \cdot d^{-1}$ was selected. In this simulation, evaporation started immediately following the very heavy and long duration rainfall event. Results are presented in Figure 5.12, showing the effect of evaporation on a fine sand beach with the water table 100 cm below the surface. The overall shape of the moisture content profiles remain consistent with Figure 5.8b, with the exception of the moisture contents at the surface and just below the surface; the upper moisture contents are lower in Figure 5.12a. It is evident that evaporation only influenced the moisture contents in the upper centimeters of sand (< 10 cm),

causing the surface sand to quickly approach residual moisture (3 %). This also lowers the pressures (high suctions) at the surface (Figure 5.12b) to approximately -1200 cm. The low pressures at the surface of the sand column are the result of the strong capillarity forces, wicking the residual moisture in between the sand grains, when evaporation is acting on the surface (Hellwig, 1973).

In addition, Figure 5.12c is a plot of the hydraulic head versus height above the water table. This plot shows the direction of the groundwater flux when evaporation is acting on the surface, following the infiltration event. Inflection points are present on the hydraulic head curves, where both upward and downward groundwater flow is present (as indicated by arrows in Figure 5.12c). The upward flux is induced by the process of evaporation drawing out moisture from the sand (following the rain event). Upward flow exists because the hydraulic head above the inflection point is lower than the hydraulic head at the inflection point. Because hydraulic head is the driving force for groundwater flow, flow proceeds upwards and out of the column. Similarly, below the inflection point, the hydraulic head is lower than the hydraulic head at the inflection point. As a result, groundwater flow is downward, thus continuously draining through the profile following the rain event.

In addition, at 480 minutes, the moisture content near the surface approaches residual saturation, at a very low pressure (approximately - 1200 cm) or very high suction. As a result the simulation did not continue to run. This is because after 480 minutes, the water that infiltrated into the profile from the rain event moved deep into the profile and as such, the forces of evaporation were not high enough to draw out moisture held tightly in between sand grains by suction (capillarity). Note that vapour transport is not simulated in HYDRUS-2D.

In summary, following a very heavy rainfall event, the process of evaporation induces upward (vertical) groundwater flow, only influencing shallow depths below the surface of a beach (<

10 cm). In addition, the process of drainage (downward flow) and redistribution at lower depths (> 10 cm) remains unaffected by evaporation. Furthermore, the influence of evaporation inducing vertical flow, only proceeds until pore pressures (or suction forces) exceed the forces of evaporation. HYDRUS-2D does not allow flow to reduce moisture contents below residual content. Due to the high moisture retention abilities of the sands at wet beaches compared to the relatively weak forces of evaporation, high evaporation rates will not influence the moisture profile well below the surface (> 10 cm) of a beach.

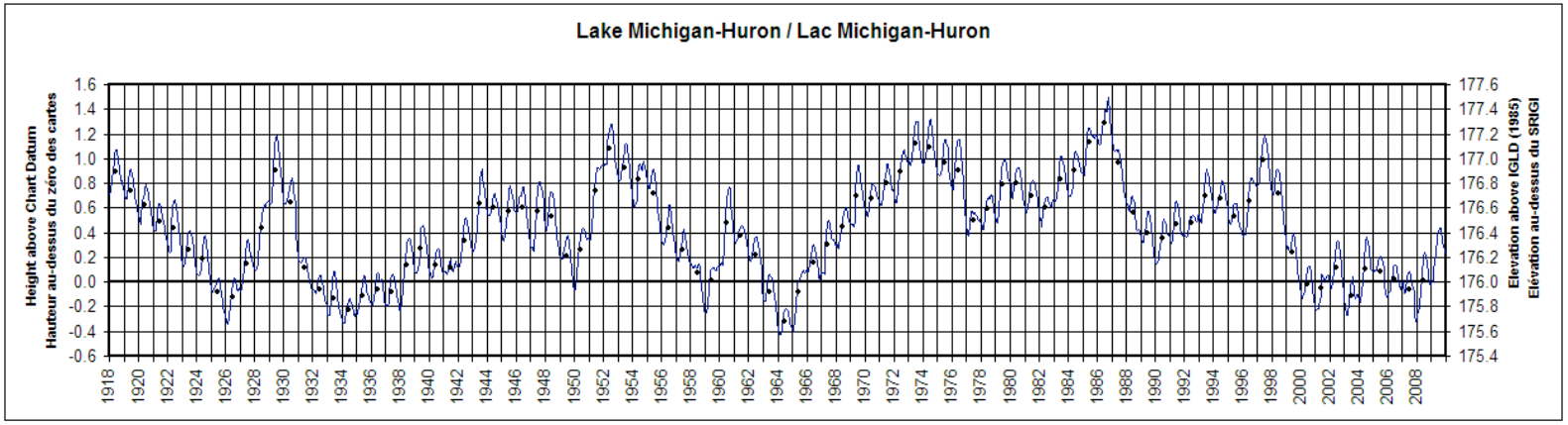

Figure 5.1: Seasonal and long-term lake level fluctuations (1918 – 2008) of Lake Huron (including Georgian Bay) (DF0, 2010).

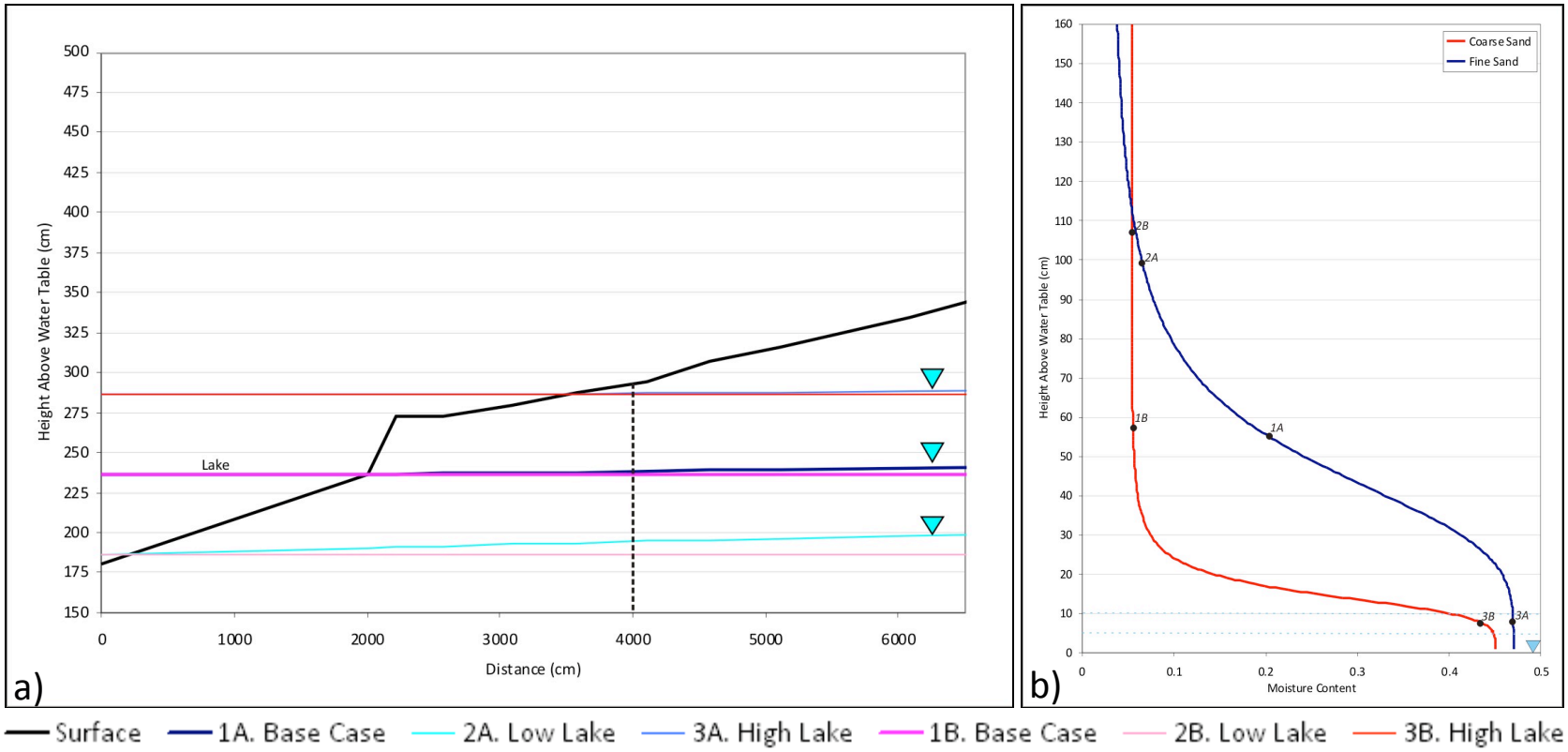

Figure 5.2: (a) Water table positions fluctuate proportionally with the lake below a flat-sloped beach for fine (A) and coarse (B) sands. The slope of the water table (hydraulic gradient) is influenced by texture (K_{sat}). (b) Moisture content profile at position 4000 cm as indicated in (a). Relative surface elevations for a specified water table position are indicated.

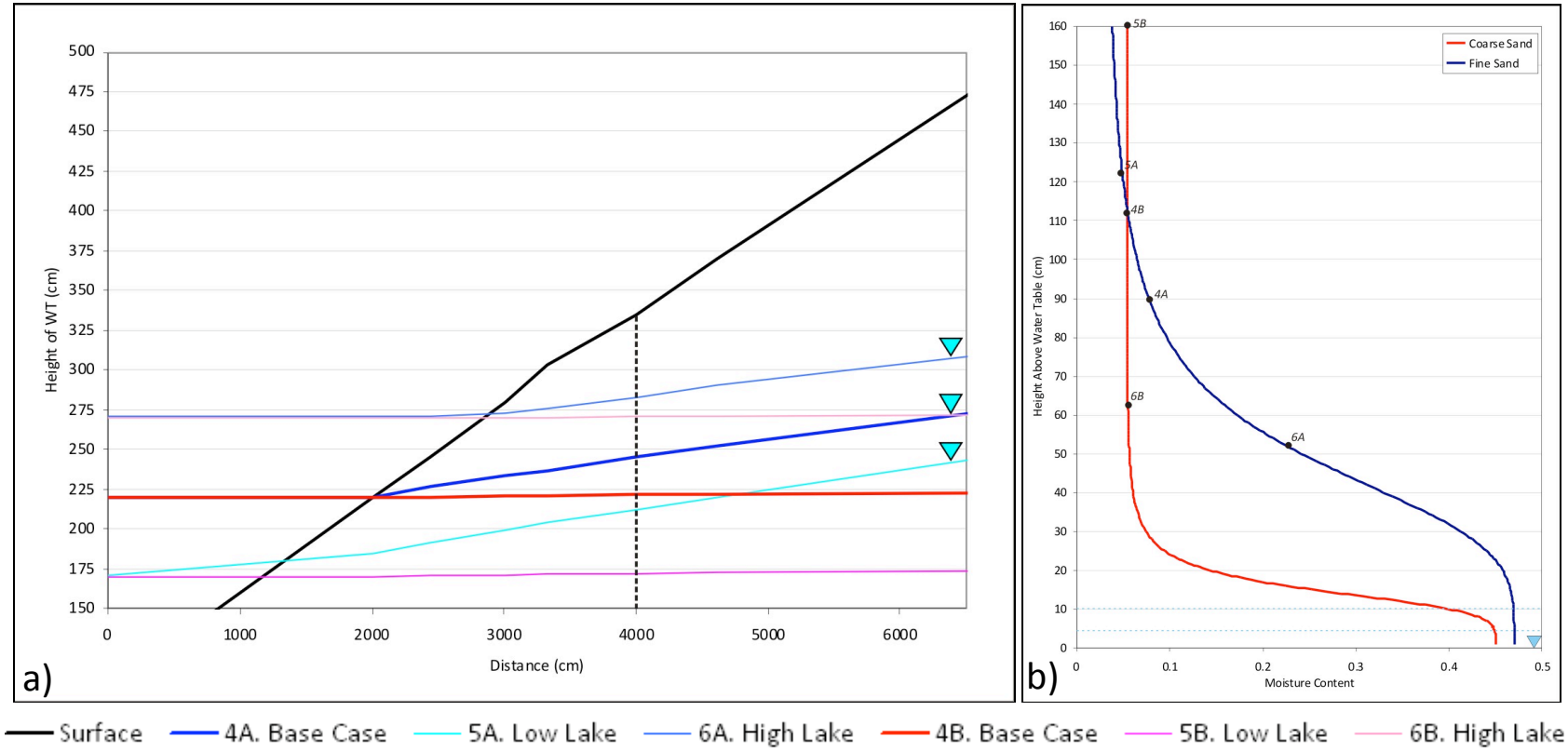

Figure 5.3: (a) Water table positions fluctuate proportionally with the lake below a steep-sloped beach comprised of fine (A) and coarse (B) sands. The slope of the water table (hydraulic gradient) is influenced by texture (K_{sat}). (b) Moisture content profile at position 4000 cm as indicated in (a). Relative surface elevations for a specified water table position are indicated.

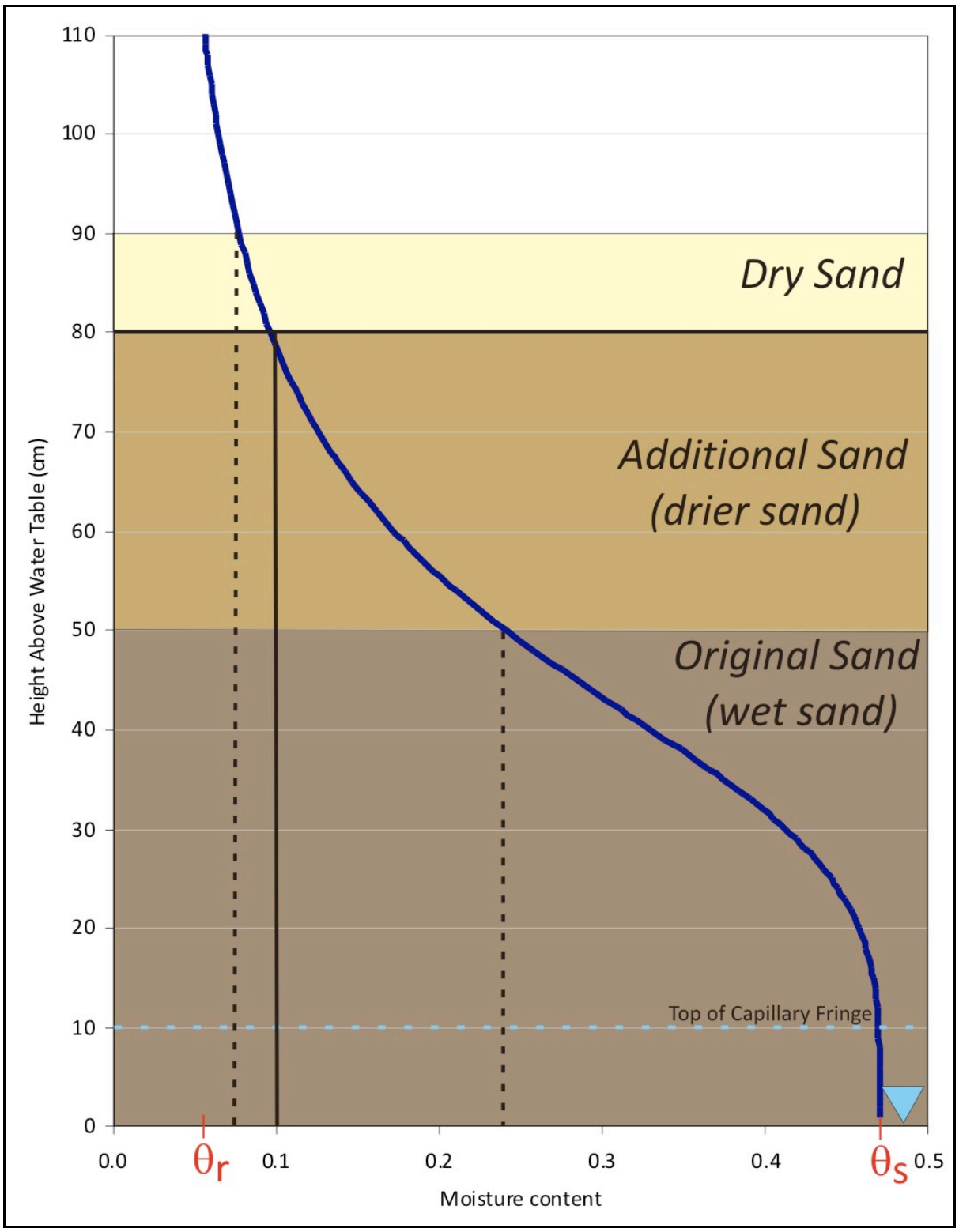

Figure 5.4: Converting a fine-textured, wet beach into a dry beach by adding 40 cm of fine sand to the surface.

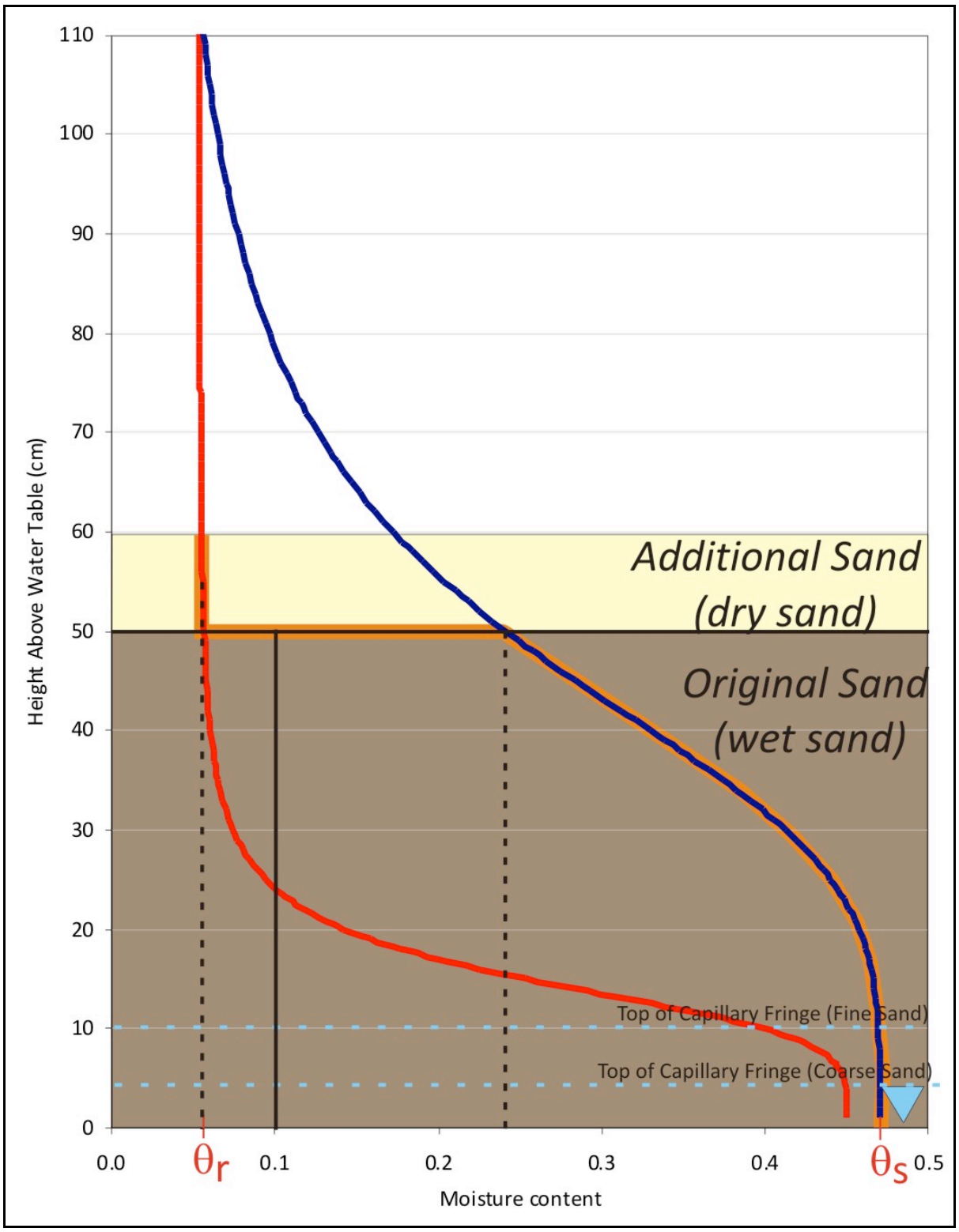

Figure 5.5: Converting a fine-textured wet beach into a dry beach by adding 10 cm of coarse sand to the surface. The resulting moisture content profile is highlighted in **orange**.

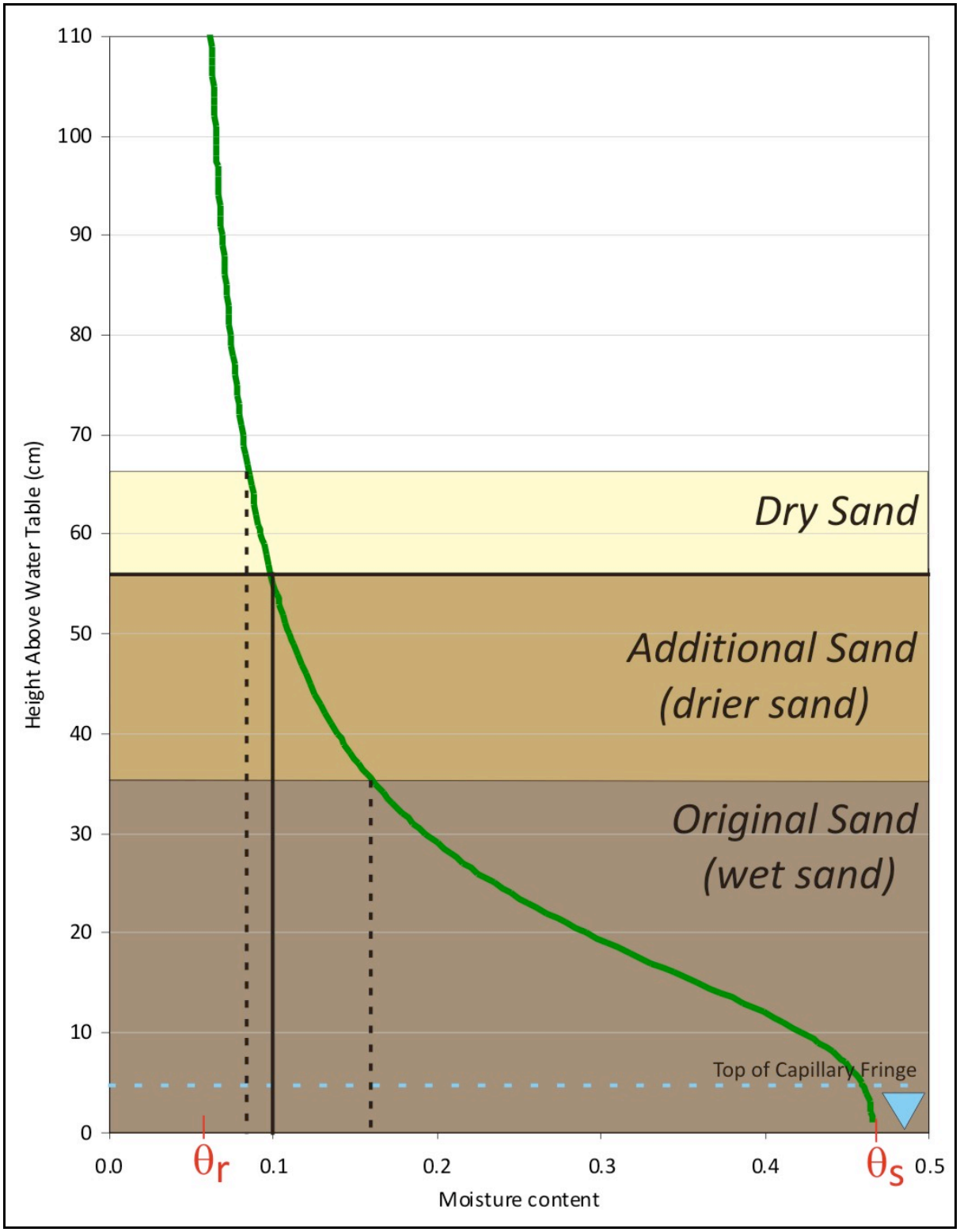

Figure 5.6: Restoring a human-altered wet beach (medium-textured) into a natural dry beach by adding 30 cm of medium sand to the surface.

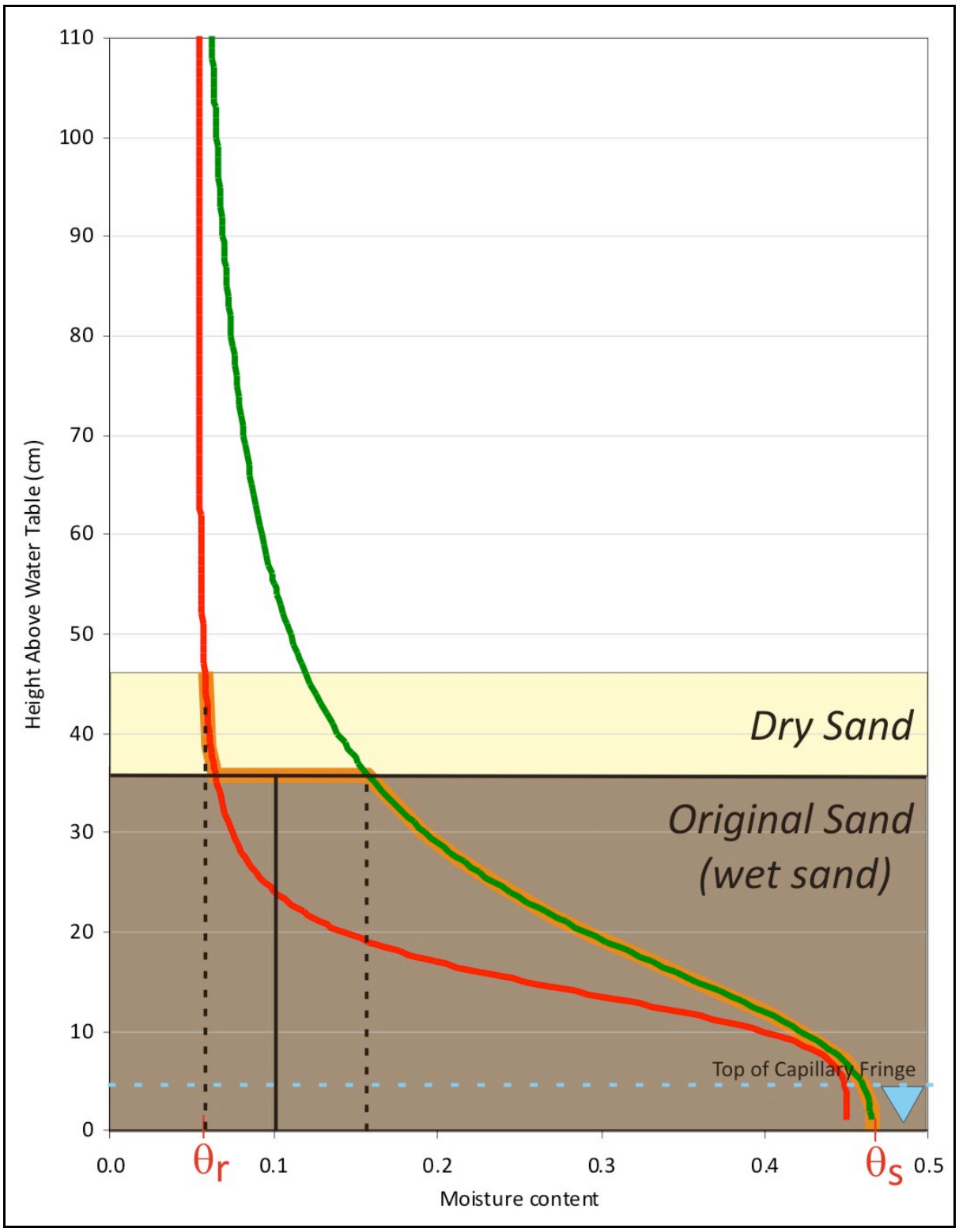

Figure 5.7: Restoring a human-altered wet beach (medium-textured) into a dry beach by adding 10 cm of coarse sand. The resulting moisture content profile is highlighted in **orange**.

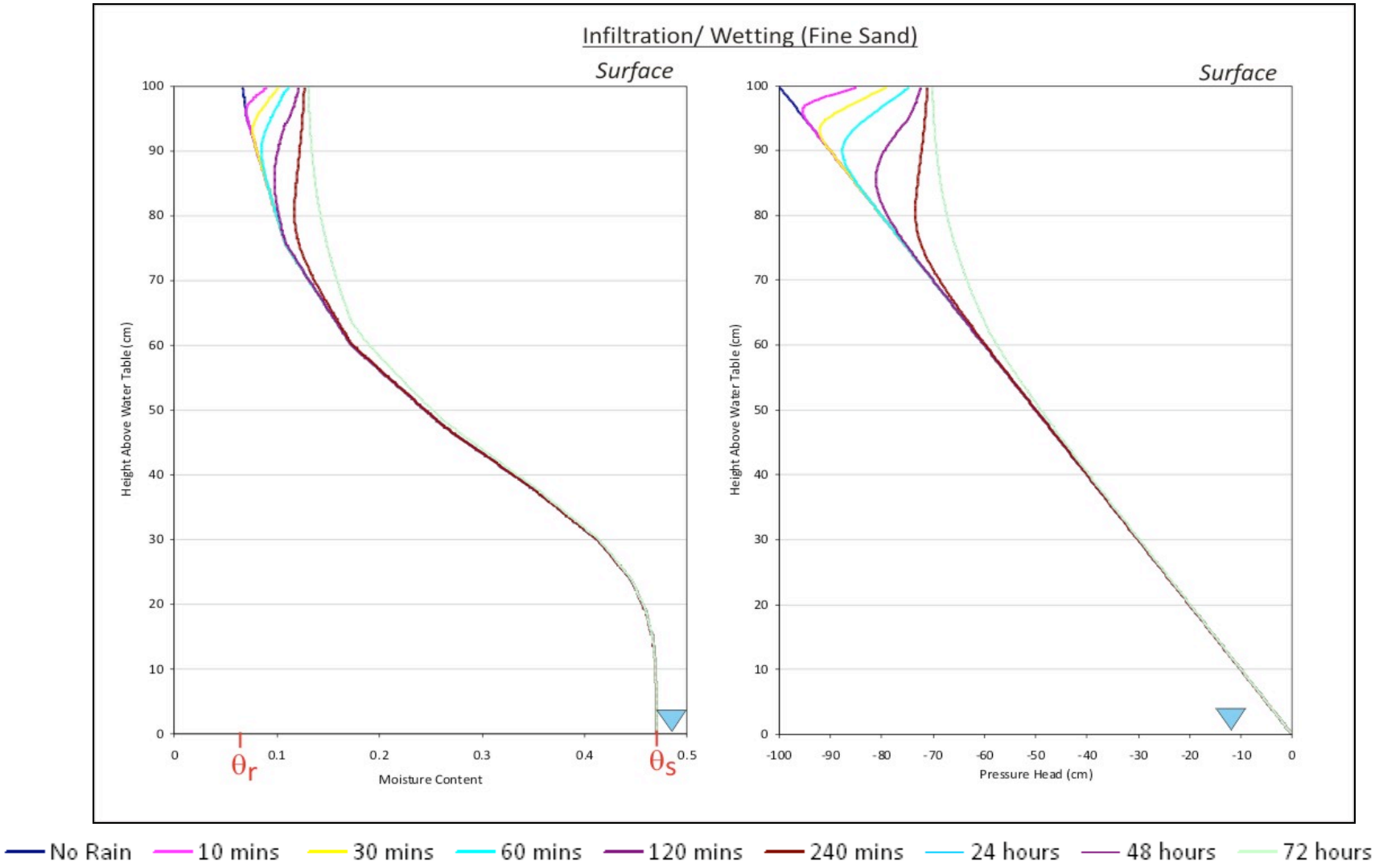

Figure 5.8a: High intensity and long duration wetting front profiles (moisture content (left) and pressure head (right)) during the infiltration of precipitation into a fine sand column**. 22.2 cm of precipitation applied for 3 days at a rate of 7.4 cm·d^{-1}.**

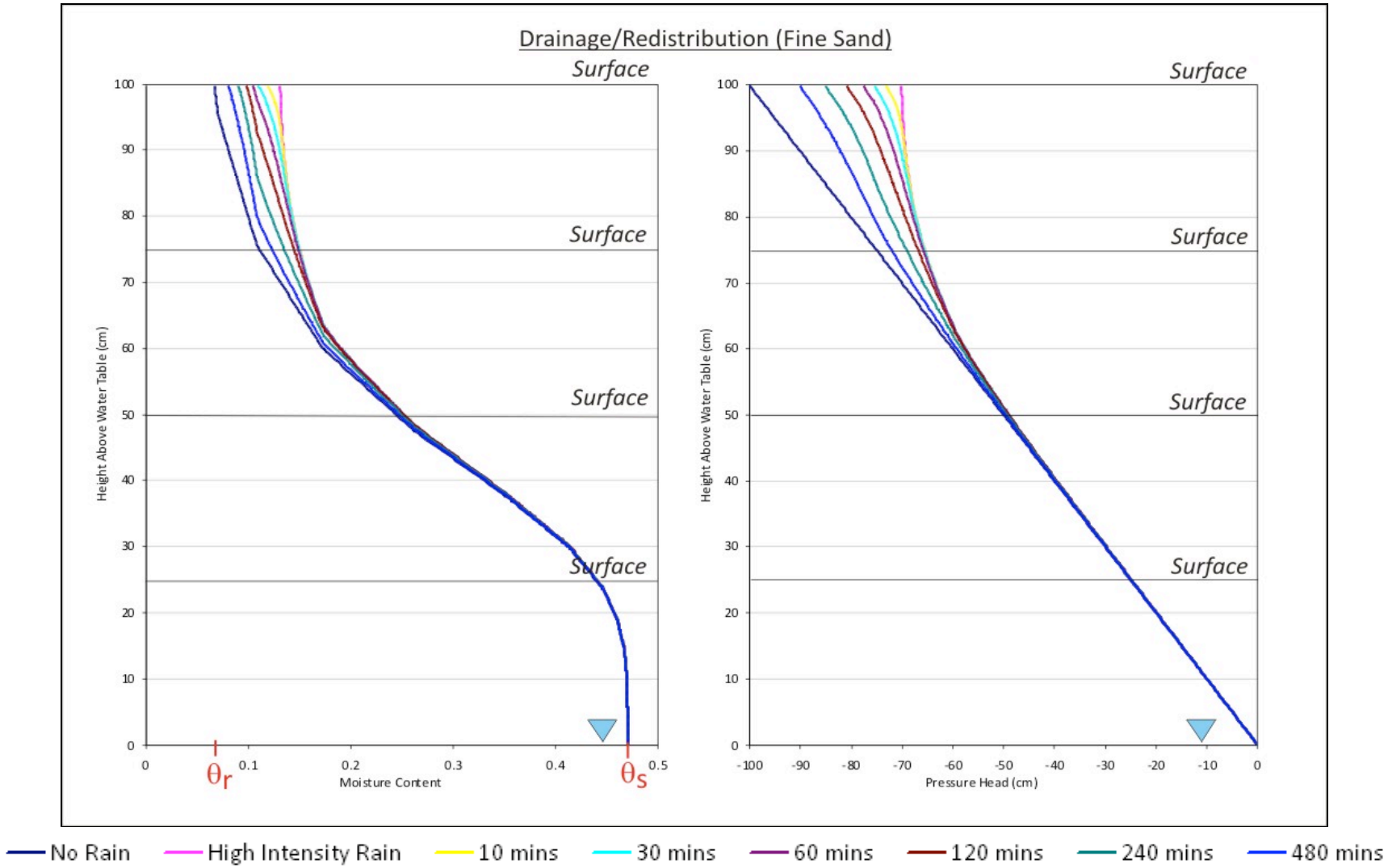

Figure 5.8b: Drainage and redistribution curves (moisture content (left) and pressure head(right)) following a high intensity and long duration infiltration event through a fine sand with a water table 100 cm, 75 cm, 50 cm, and 25 cm below the surface. **22.2 cm of rain applied for 3 days at a rate of 7.4 cm·d^{-1}.**

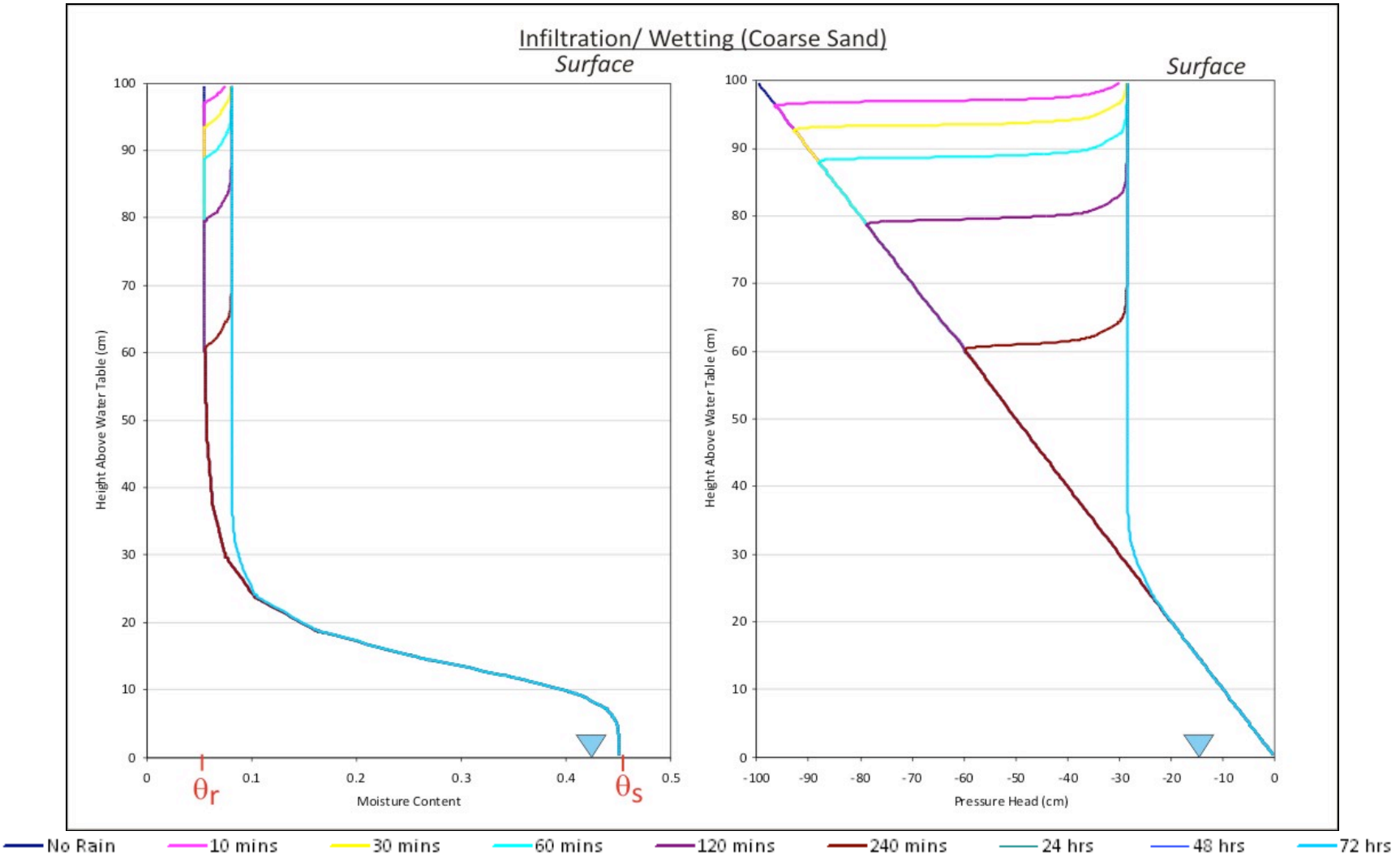

Figure 5.9a: High intensity and long duration wetting front profiles (moisture content (left) and pressure head (right)) during the infiltration of precipitation into a coarse sand column**. 22.2 cm of precipitation applied for 3 days at a rate of 7.4 cm·d^{-1}.**

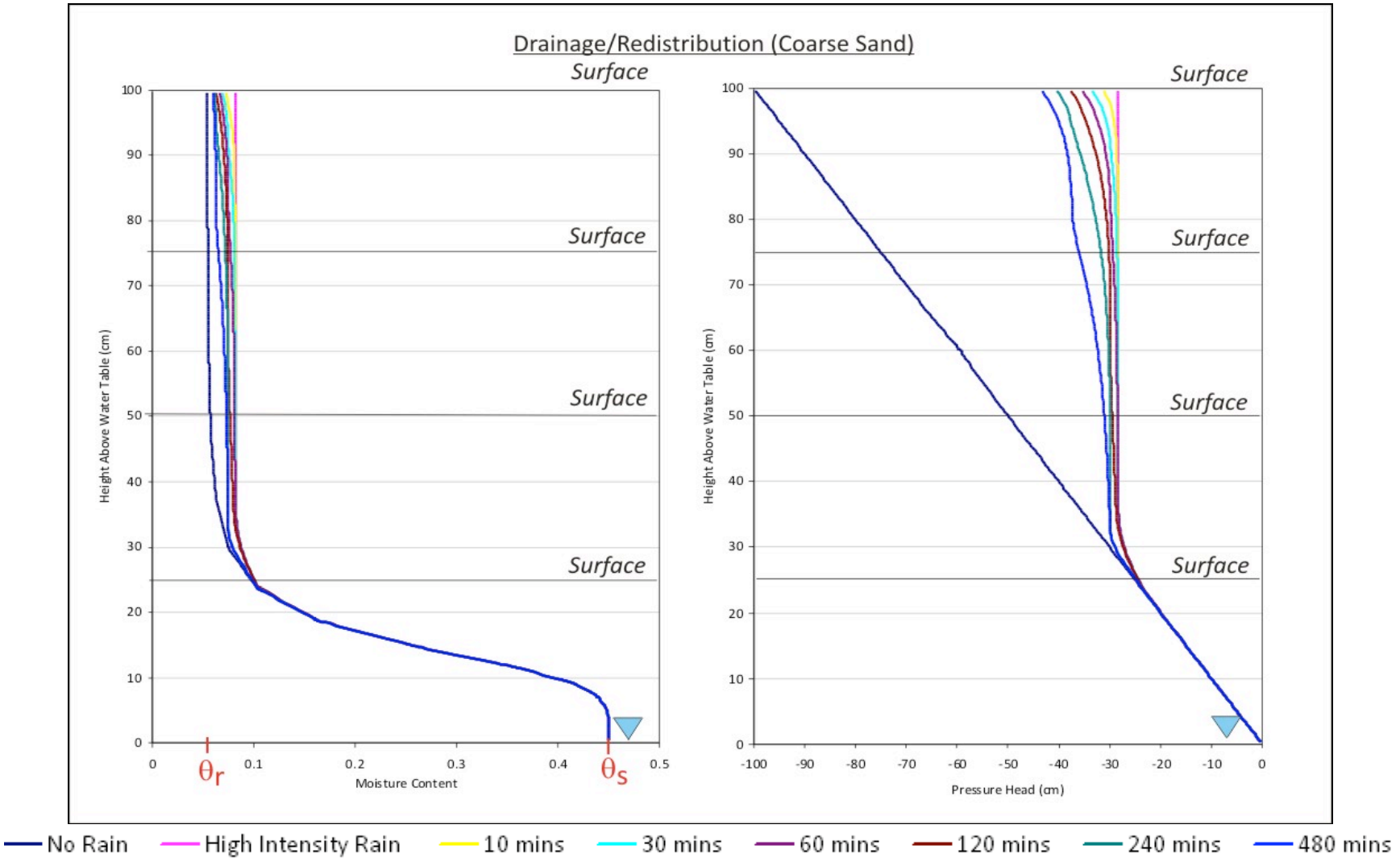

Figure 5.9b: Effect of precipitation rate on the moisture content (left) and pressure head (right) below coarse sand beaches with a water table 100 cm, 75 cm, 50 cm, and 25 cm below the surface. **22.2 cm of rain applied for 3 days at a rate of 7.4 cm·d^{-1}**.

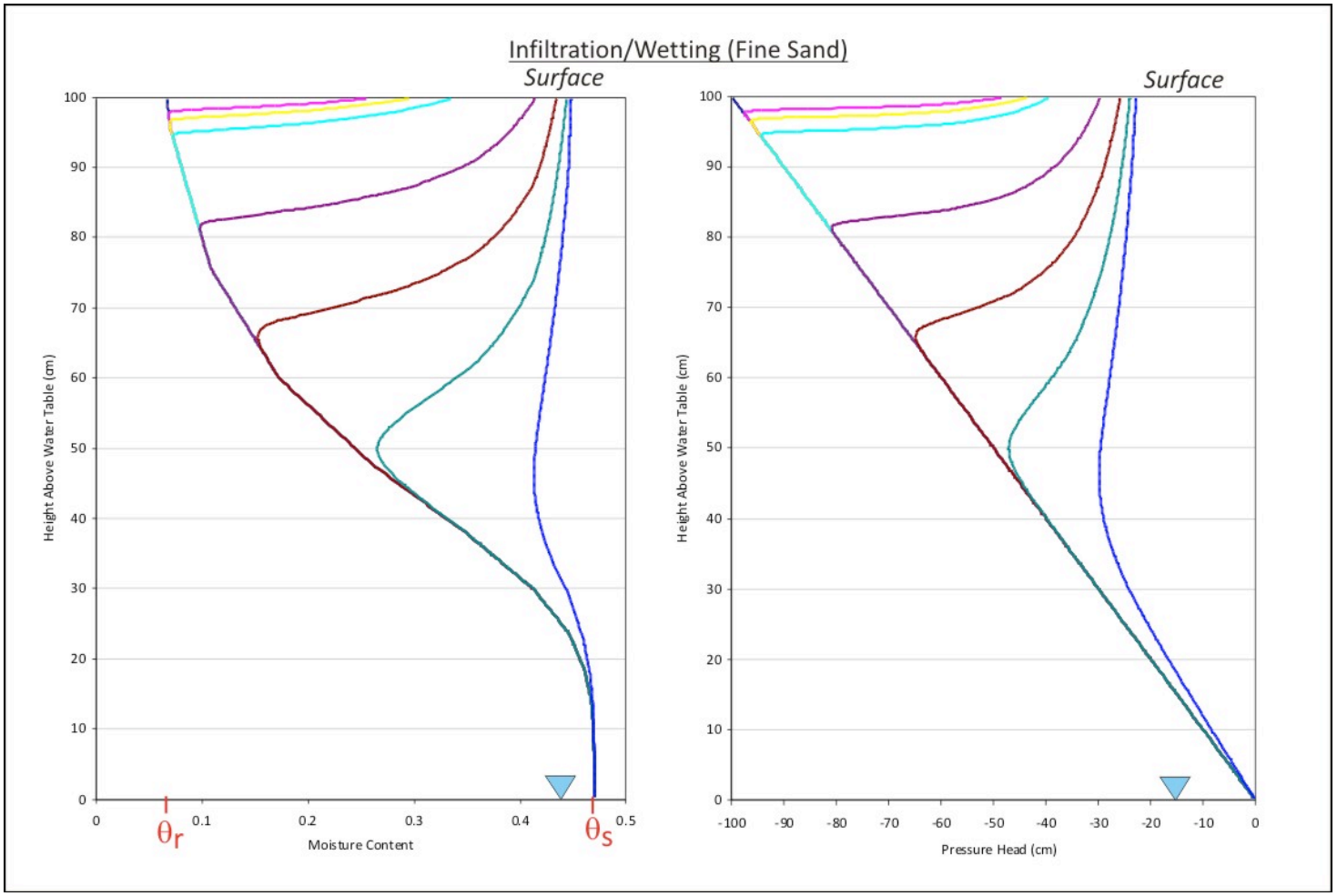

Figure 5.10a: Higher intensity and short duration wetting front profiles (moisture content and pressure head) during the infiltration of precipitation into a fine sand column**. 22.2 cm of precipitation applied for 40 minutes (0.02778 days) at a rate of 7.4 cm·d^{-1}.**

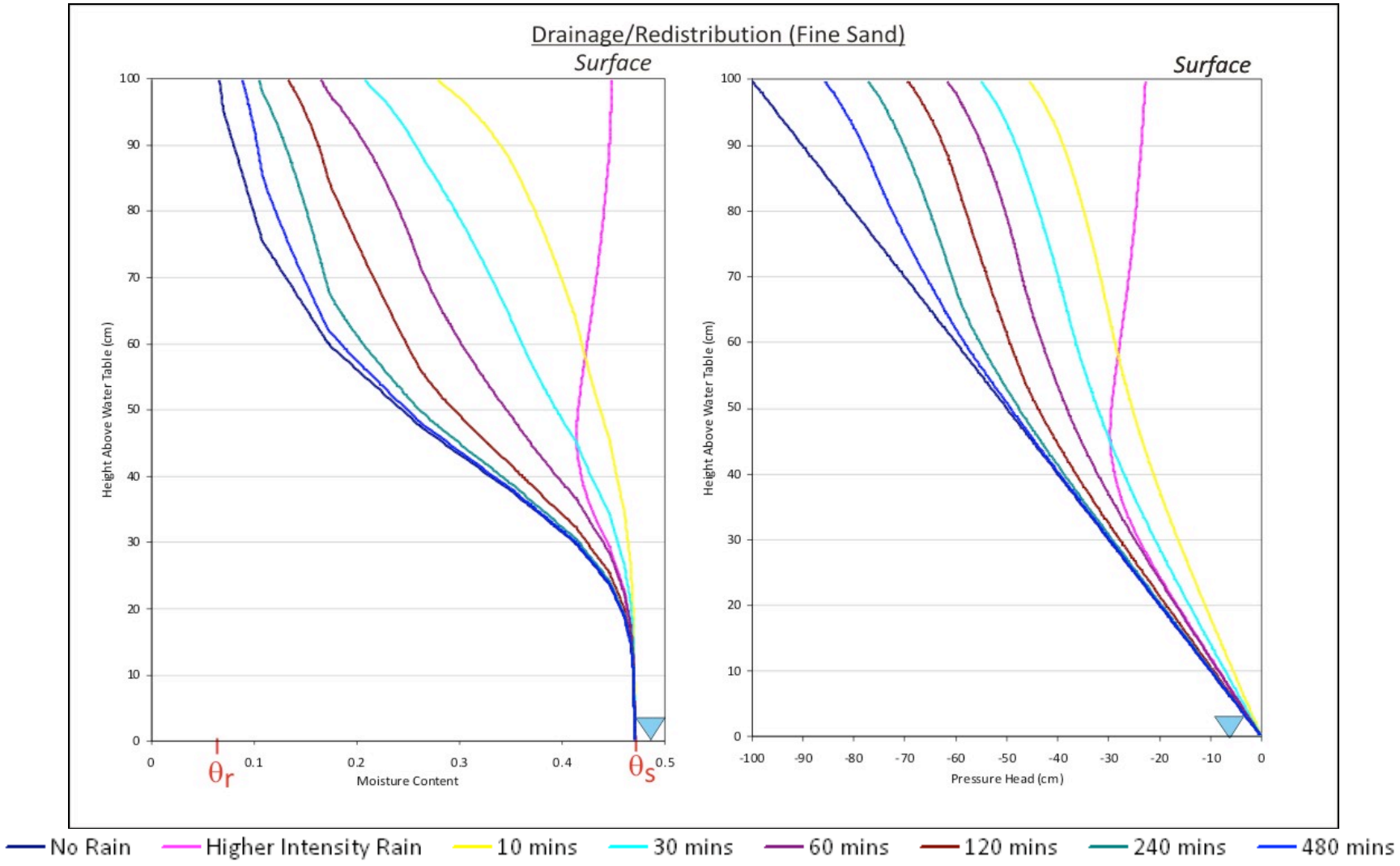

Figure 5.10b: Effect of precipitation rate on the moisture content and pressure head below fine sand beaches with a water table 100 cm below the surface. **22.2 cm of rain applied for 40 minutes at a rate of 799 cm·d^{-1}**.

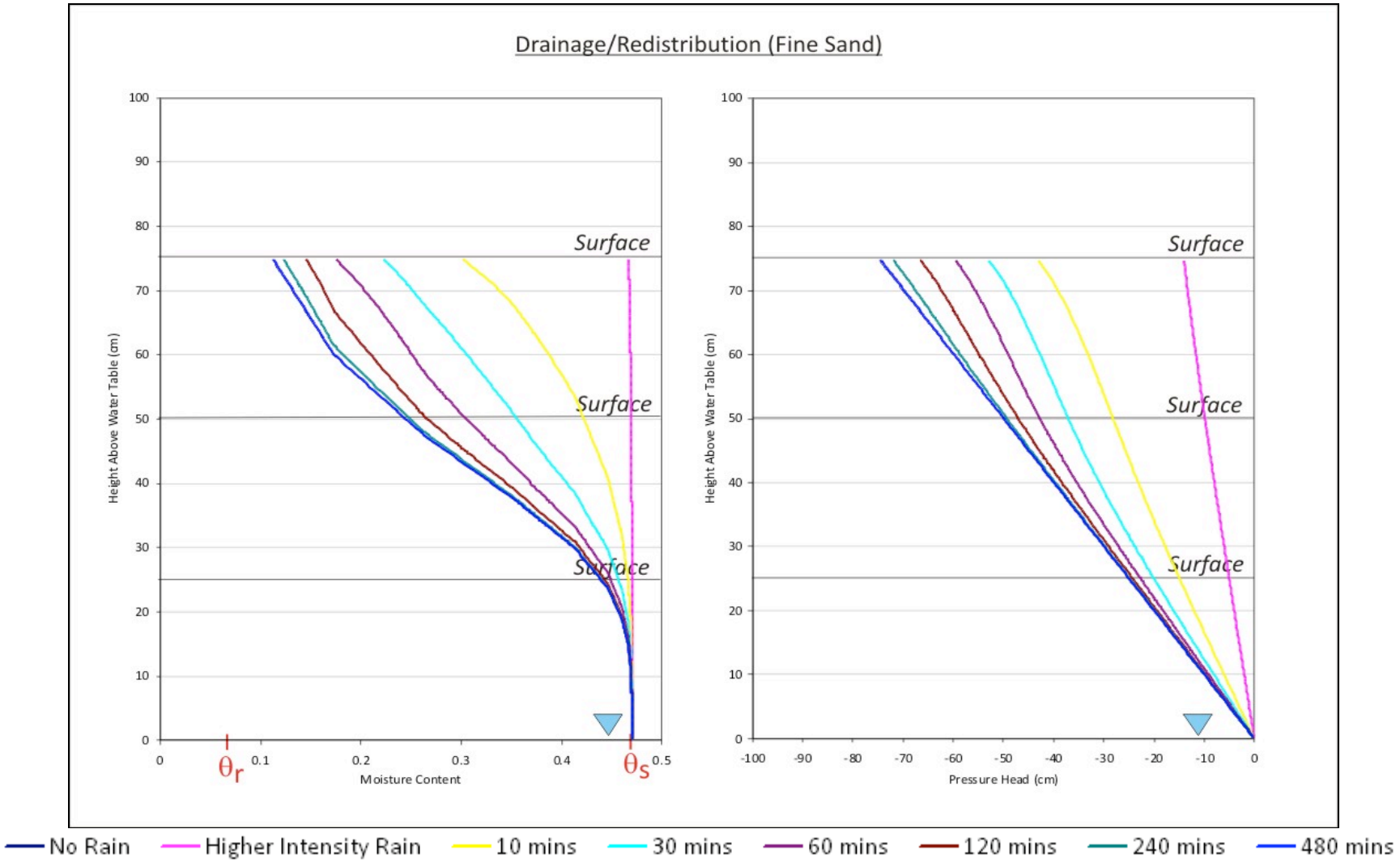

Figure 5.10c: Effect of precipitation rate on the moisture content and pressure head below fine sand beaches with a water table 75 cm, 50 cm, and 25 cm below the surface. **22.2 cm of rain applied for 40 minutes at a rate of 799 cm·d^{-1}**.

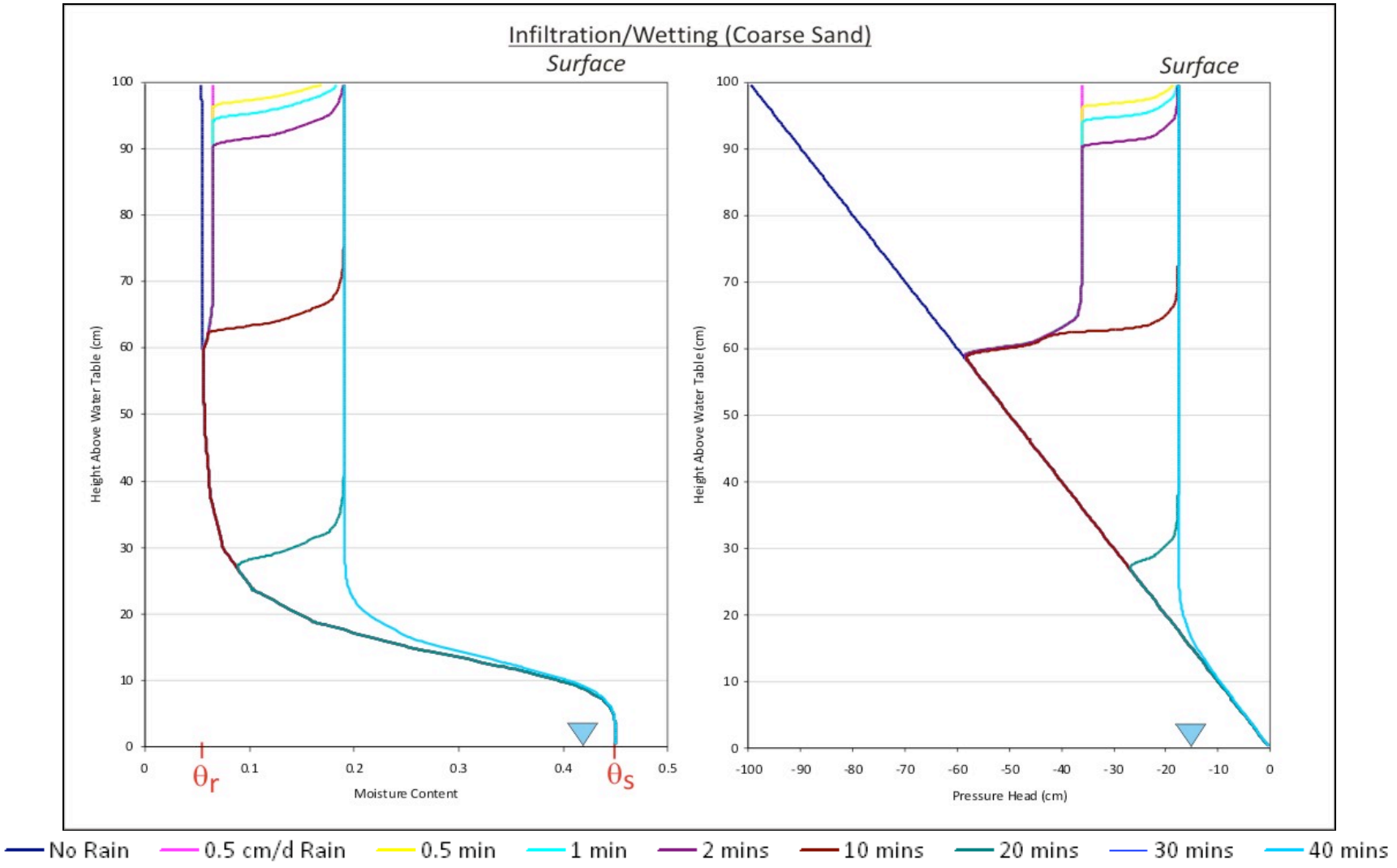

Figure 5.11a: Higher intensity and short duration wetting front profiles (moisture content and pressure head) during the infiltration of precipitation into a coarse sand column**. 22.2 cm of precipitation applied for 40 minutes at a rate of 799 cm·d^{-1}.**

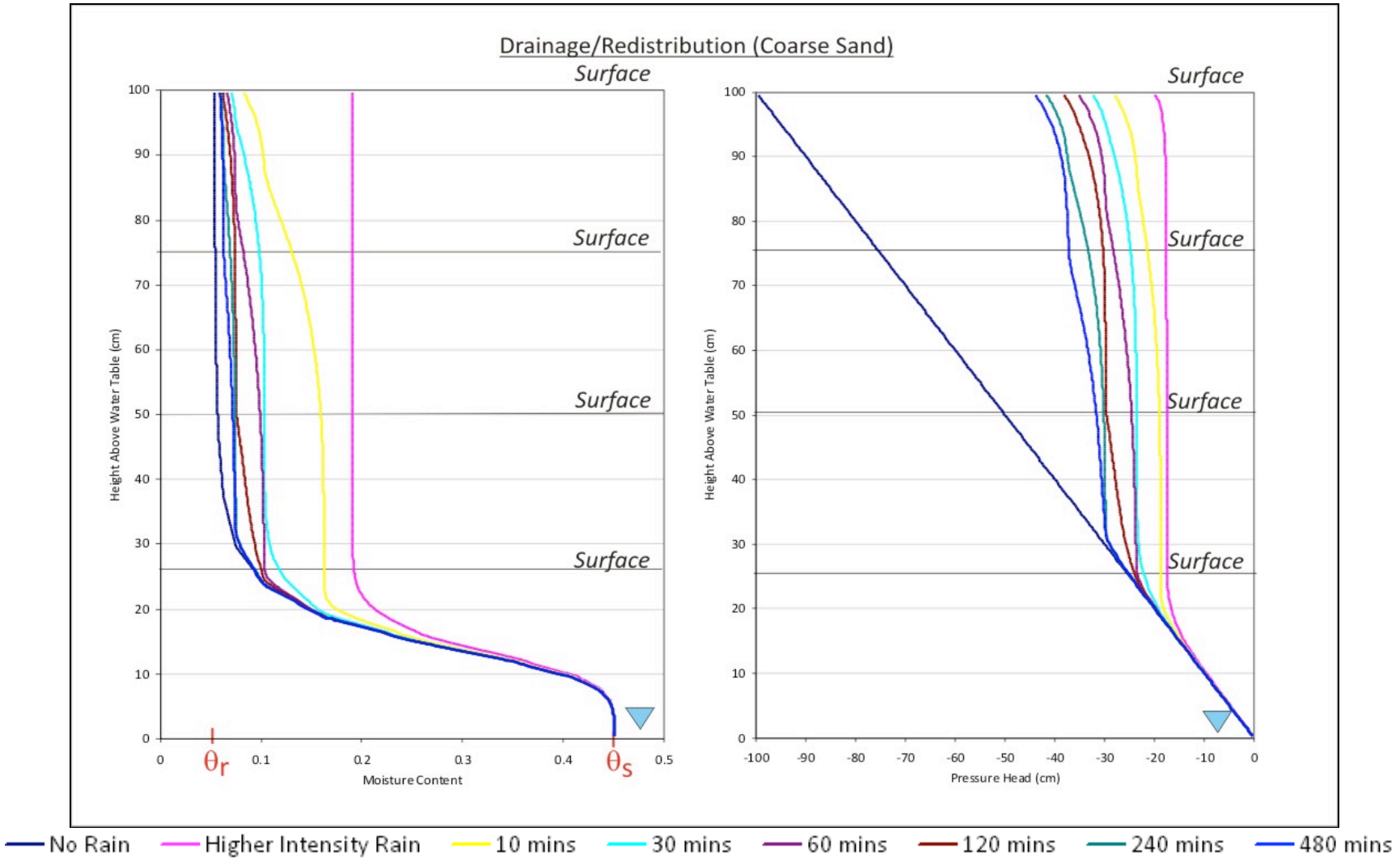

Figure 5.11b: Effect of precipitation rate on the moisture content and pressure head below coarse sand beaches with a water table 75 cm, 50 cm, and 25 cm below the surface. **22.2 cm of rain applied for 40 minutes at a rate of 799 cm·d^{-1}**.

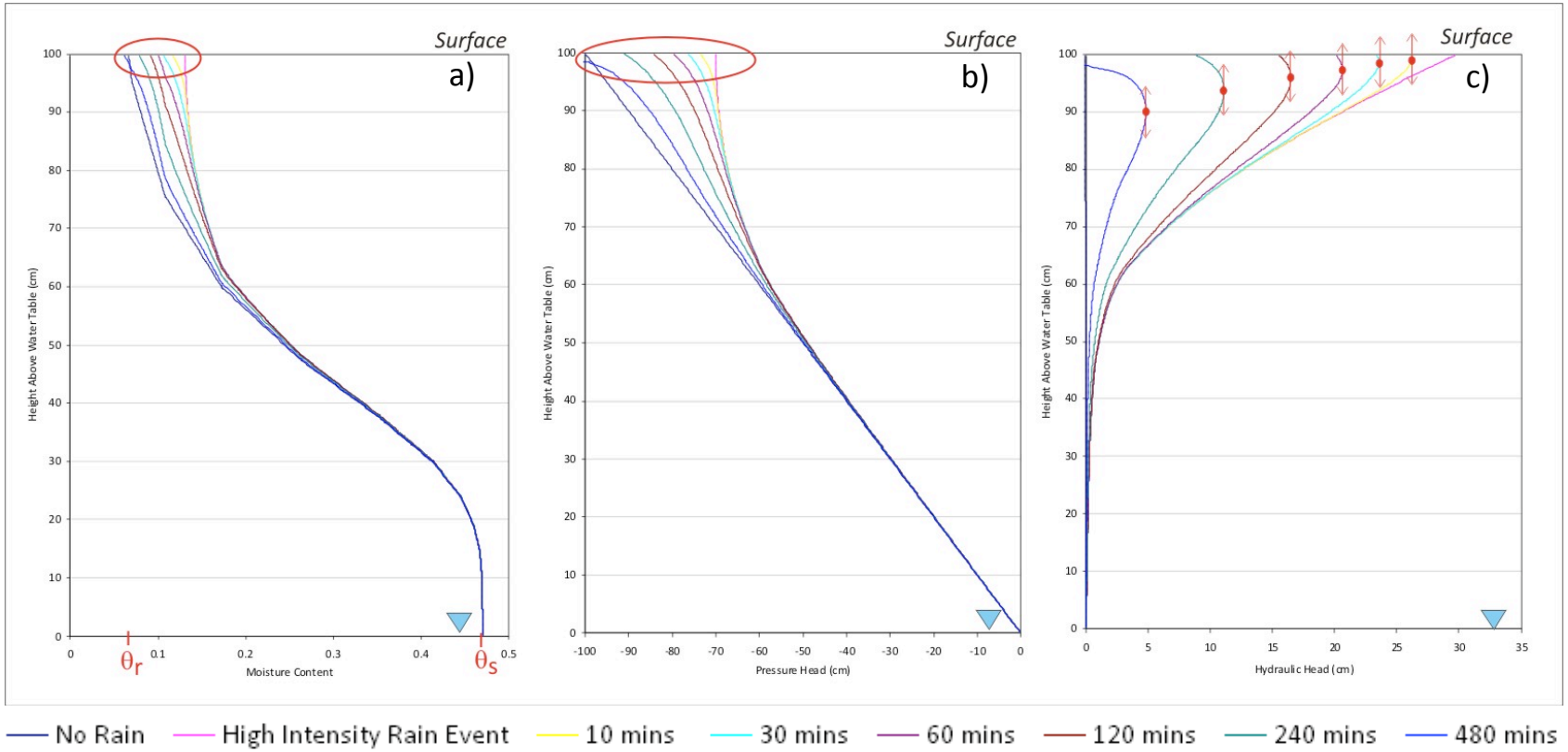

Figure 5.12: Effect of low evaporation rates after a long precipitation event on (a) moisture content, (b) pressure head, and (c) hydraulic head profiles below a fine sand beach with a water table 100 cm below the surface. **0.9 cm.d^{-1} of evaporation following 22.2 cm of rain applied for 3 days at a rate of 7.4 cm·d^{-1}.**

6.0 CONCLUSIONS, IMPLICATIONS, AND FUTURE RECOMMENDATIONS

6.1 Conclusions

Recreational beaches of the Great Lakes play a critical role in the quality of life for local residents and beach goers. They also contribute to the economic and environmental health of the Great Lakes region. Several persistent problems have, and continue to, been observed at the beaches of the Great Lakes, causing the quality of the beaches to deteriorate. Beach problems including: elevated levels of *E. coli*, invasive and non-native vegetation, iron staining, loss of sand, and increasing wet conditions have been observed at numerous beaches.

The purpose of this study was to investigate the physical and hydrological factors that control wet and dry beaches, in order to explain why these beaches exist along the shores of the Great Lakes. A wet beach is defined herein as a natural or degraded beach comprised of wet conditions (high moisture contents, > 10 %) at and well below the surface. Wet beaches often exhibit shallow water tables (< 50 cm), flat surface elevations, and invasive and non-native vegetation on the surface of the beach (e.g. *Phragmites*, sedges, rushes, cattails). Dry beaches are defined herein as natural beaches that are comprised of dry conditions (low moisture contents, < 10 %) at and well below the surface. Dry beach typically have deep water tables (> 50 cm), and contain sand dunes on the leeward side of the beach with natural vegetation on the dunes (e.g. beach grass). Four beaches were investigated in Tiny Township, along the shores of southern Georgian Bay, including Balm Beach south, Jackson Park Beach, Woodland Beach north, and Woodland Beach south. The objective of this thesis was addressed through a combination of field, laboratory, and modelling analyses.

Results from this study showed that there are three primary interconnected factors that control the wet or dry conditions at a particular beach, including: (1) texture of the beach, (2) depth to the water table, and (3) ground surface elevation (topography).

1. Texture is the primary factor controlling the moisture conditions present at a beach. Finer grained sands (wet beaches) have strong capillarity forces as a result of small pore spaces (smaller grains), and consequently have a higher capillary rise and greater abilities to retain moisture well above the water table. This includes a thicker capillary fringe (tension saturated zone) above the water table. Coarser grained sands (dry beaches) have weak capillarity forces as a result of large pore spaces (larger grains), therefore, have a low capillary rise and retain less moisture well above the water table. Although textures vary between beaches, the hydraulic conductivities (K_{fs} and K_{sat}) of the beach sands only vary by less than one order of magnitude. As such, wet and dry beaches are able to infiltrate and drain water (applied at the surface) quickly throughout the vadose zone towards the water table and also move groundwater quickly within the saturated zone towards the lake.
2. Depth to the water table is controlled by the elevation of the lake, elevation of the ground surface, and also the texture of the beach sand. The depth to the water table influences the moisture conditions at a beach by through its association with the position of the top of the capillary rise (above the water table) with respect to the surface of the beach. Wet beaches contain shallow water tables (close to the surface) and dry beaches contain deep water tables.
3. Ground surface elevation (topography) influences the thickness of sand above the water table at a beach and depth to the water table. Lower surface elevations (flat-sloped, wet beaches) retain more moisture at and well below the surface of the beach and higher surface elevations (steep-sloped, dry beaches) retain less moisture at and well below the surface of the beach.

According to the results from the field, laboratory, and modelling analyses, the four beaches of Tiny Township were classified based on the three factors that control the conditions present at beaches.

1. Balm Beach South is a natural dry beach because it is comprised of low moisture contents (< 10 %) at and well below the surface of the beach, coarse grained sands, a deep water table (> 50 cm), a steep-sloped surface, sand dunes on the leeward side of the beach, and has not been altered by human activities.
2. Jackson Park Beach is a natural wet beach because it is comprised of high moisture contents (> 10 %) at and well below the surface of the beach, fine grained sands, a shallow water table (< 50 cm), a flat-sloped surface, contains invasive and non-native vegetation on the surface of the beach, and has not been altered by human activities.
3. Woodland Beach north is a natural dry beach because it is comprised of low moisture contents (< 10 %) at and well below the surface of the beach, fine grained sands with a deep water table (> 50 cm), a steep-sloped surface, sand dunes on the leeward side of the beach, and has also not been altered by human activities.
4. Woodland Beach South is a degraded wet beach because it is comprised of high moisture contents (> 10 %) at and well below the surface of the beach, medium grained sands, a shallow water table (< 50 cm), a flat-sloped surface, and contains invasive and non-native vegetation across the surface of the beach. In addition, the surface of the beach has been subjected to human induced changes (i.e. bulldozing sand dunes, removing sand, installing break walls, etc.) therefore, this beach no longer resembles the dry conditions as it once did; similar to its neighboring beach, Woodland Beach North.

In addition, this study used the numerical model HYDRUS-2D to provide insight into beach management scenarios, investigating: (1) the influence of long-term lake level fluctuations, (2)

human induced changes by adding or removing sand, and the influence of (3) Precipitation events and (4) evaporation on the moisture conditions at beaches.

1. Long-term lake level fluctuations influence the depth of the water table below a beach by controlling the position of the point of groundwater discharge (interface between the water table and the lake). Beaches with shallow water tables and also fine sands are at greater risk of flooding or becoming wetter, under very high lake levels. Beaches with steep slopes, deep water tables, and also coarse sand are at less risk of flooding or becoming wet under very high lake levels.
2. Human induced changes by adding sand to a beach can convert wet beaches into dry beaches by adding sand to the surface of a beach in order to lower the depth of the water table from the surface. The amount of sand required depends on its texture; less coarse grained sand, because of its low moisture retention properties (~ 10 cm), is required than fine grained sand (> 40 cm). In addition, human activities that remove the sand from a beach (e.g., bulldozing sand dunes and beach sand) will convert natural dry beaches into degraded wet beaches because these activities lower the ground surface close to the water table.
3. Precipitation events, including high intensity rainfalls, do not have a significant impact on influencing the long-term moisture conditions at a beach. The high hydraulic conductivities of sand, allows surface water to quickly infiltrate, drain, and redistribute below the surface, towards the water table. Precipitation events will not convert dry beaches into wet beaches.
4. Evaporation, including high rates, only influences the moisture contents at the surface and just below the surface (< 5 cm) at wet and dry beaches; the moisture contents approach residual saturation. Evaporation induces an upward flux less than ~ 10 cm below the surface of a beach;

however, the moisture contents within this zone (< 10 cm) do not fall below 10 % moisture. As such, evaporation will not convert wet beaches into dry beaches.

This study successfully in determined why wet and dry beaches exist along southern Georgian Bay. Beach managers, scientists, and consultants can now use the results from this study and the calibrated beach models to better understand the conditions beaches and to also predict which beaches of the Great Lakes are at high risk of becoming wet under various natural and human-impacted scenarios.

6.2 Implications

Results from this study address public concerns regarding why the quality of the beaches along the shores of the Great Lakes are deteriorating. Natural wet beaches will always remain wet because of shallow water tables, fine sand, and naturally flat sloped surfaces, regardless of lake level changes. Degraded wet beaches were once dry beaches that have been converted as a result of increased and unrestricted residential development and human induced profile changes. As a result, along with natural wet beaches, the degraded wet beaches are promoting persistent beach problems that are deteriorating the quality of the beaches of the Great Lakes. It is therefore important to minimize or prevent the destruction of beaches by implementing beach restoration programs and also strict regulations against beach profile alterations.

For example, wet conditions are suitable conditions for the growth of vegetation across the beach, including invasive and non-native species (e.g. *Phragmites*, sedges, and rushes). If these conditions persist, wet beaches may be converted into marshes or wetlands. In addition, the wet conditions and sustainable growth of vegetation will attract geese and gulls to the beaches. This could lead to additional sources of *E. coli* being directly supplied to the surfaces of the beach (via

fecal material), increasing risk of contamination of *E. coli* to the groundwater and the lake, and consequently increasing the frequency of beach closures.

6.3 Future Recommendations

The high infiltration rates and differing water retention characteristics of beach sands are such that future field and modeling studies should address the implications for solute transport and pathogen mobility at beaches. In addition, the conditions at wet beaches are suggested to promote and sustain the growth of invasive vegetation on the surface of the beach. Increased growth of vegetation will supply organic matter to the beaches. Organic matter retains high volumes of moisture and also provides suitable conditions for the survival of *E. coli*. In addition, the complex rooting system provided by the invasive vegetation, will create large macropores and furrows below the beaches. This may increase the transport of contaminants (*E. coli*) to the groundwater below. Future field studies investigating the influence of vegetation on the wet and dry beaches should be investigated.

7.0 REFERENCES

Abdul A.S., and Gillham R.W., 1984. Laboratory Studies of the Effects of the Capillary Fringe on Streamflow Generation. Water Resources Research. 20 (6): 691-698.

Albright W.H, Gee G.W., Wilson G.V., and Fayer M.J., 2002. Alternative Cover Assessment Project Phase I Report. Division of Hydrologic Sciences: Desert Research Institute, University and Community College System of Nevada. Publication No. 41183.

Alm E.W., Burke J., and Hagan E., 2006. Persistence and Potential Growth of the Fecal Indicator Bacteria Escherichia coli, in Shoreline sand at Lake Huron. Journal of Great Lakes Research, 32, 401-405.

American Geological Institute (AGI), 1962. Dictionary of Geological Terms. Dolphin Books Doubleday and Company Inc. Garden City, NY, US.

Anderson M.P., and Woessner W.W., 1992. Applied Groundwater Modelling: Simulation of Flow and Advective Transport. Academic Press. San Diego, NY, US.

Austin M.J., and Masselink G., 2006. Swash-Groundwater Interaction on a Steep Gravel Beach. Cntinental Shelf Research. 26, 2503-2519.

Baird A.J., Mason T., and Horn D.P., 1998.Validation of the Boussinesq Model of Beach Groundwater Behaviour. Marine Geology. 148, 55-69.

Baird A.J. and Horn D.P., 1996. Monitoring and Modelling Groundwater Beahviour in Sandy Beaches. Journal of Coastal Research. 12(3): 630-640.

Bear J., 1979. Dynamics of Fluids in Porous Media. American Elsevier Publishing Company. New York, NY, US.

Beversdorf L.J., Bornstein-Forst S.M., and McLellan S.L., 2006. The Potential for Beach Sand to Serve as a Reservoir for Escherichia coli and the Physical Influences on Cell Die-Off. Journal of Applied Microbiology, 102, 1372-1381.

Brady N.C., and Weil R.R., 2002. The Nature and Properties of Soils, Thirteenth Edition. Prentice Hall. Upper Saddle River, NJ, US.

Cartwright N., Baldock T.E., Nielsen P., Jeng D.S., and Tao L., 2006. Swash-Aquifer Interaction in the Vicinity of the Water Table Exit Point on a Sandy Beach. Journal of Geophysical Research. 111 (C09035), doi:10.1029/2005JC003149.

Chapman L.J. and Putnam D.F., 1984. The Physiography of Southern Ontario 3rd Edition. Ontario Geological Survey Special Volume 2.

Cheng X., and Anderson M.P., 1993. Numerical Simulation of Groundwater Interaction with Lakes Allowing for Fluctuating Lake Levels. Ground Water. 31(6), 929-933.

Cherkauer, D.S., and McKereghan, P.F., 1991, Groundwater Discharge to Lakes: Focusing in Embayments: Ground Water, 29 (1), 72-80.

Chiu A.C.F., Zhu W., and Chen X., 2009. Rainfall Infiltration Pattern in an Unsaturated Silty Sand. Journal of Hydrologic Engineering. 14 (8): 882-886.

County of Simcoe, 2009. Simcoe County Maps. On-line: http://maps.simcoe.ca/EasyMap/Index.html.

Crowe A.S., and Meek G.A., 2009. Groundwater Conditions beneath Beaches of Lake Huron, Ontario, Canada. Journal of Aquatic Ecosystem Health and Management. 12 (4), 444-445.

Crowe A.S. and Milne J., 2007. Relationship between Natural and Degraded Beach Ecosystems and E. coli Levels in Groundwater below Beaches of the Great Lakes, Canada. Proceedings of the XXXV International Association of Hydrogeologist Congress – Groundwater and Ecosystems. Libson, Portugal, September 11-21, 2007.

Crowe A.S., Shikaze S.G., and Ptacek C.J., 2004. Numerical Modelling of Groundwater Flow and Contaminant Transport to Point Pelee Marsh, Ontario, Canada. Hydrological Processes. 18, 293-314.

Dane J.H., and Topp, G.C., 2002. Soil Science Society of America (SSSA) Book Series 5: Methods of Soil Analysis Part 4: Physical Methods. SSSA Inc. Madison, WI, US.

Darke I., and McKenna-Newman C., 2008. Field Study of Beach Water Content as a Guide to Wind Erosion Potential. Journal of Coastal Research. 24(5): 1200-1208.

Davis R.A., and Fitzgerald D.M., 2004. Beaches and Coasts. Blackwell Publishing. Malden, MA, US.

Debrasch J.M., Parnell K.E., Hume T.M., and Dolphin T.J., 1999. The Capillary Fringe and the Water Table in an Intertidal Estuarine Sand Flat. Estuarine, Coastal and Shelf Science. 48, 215-222.

Decagon Devices, 2009. Minidisk Infiltrometer (MDI) User's Manual, Version 9. Pullman, WA, US.

Department of Fisheries and Oceans Canada (DFO), 2010. Hourly Water Level Data – Central and Artic Region. Canadian Hydrographic Service. On-line: http://www.waterlevels.gc.ca/C&A/gs_selection_e.html.

Dincer T., Al-Murgin A., and Zimmermann U., 1973. Study of the Infiltration and Recharge through the Sand Dunes in Arid Zones with Special Reference to the Stable Isotopes and Thermonuclear Tritium. Journal of Hydrology. 23, 79-109.

Dunn A.M., and Silliman S.E., 2003. Air Entrapment in the Vicinity of the Water Table. Ground Water. 41(6): 729-734.

Emery K.O., and Foster J.F., 1948. Water Tables in Marine Beaches. Journal of Marine Research. 7 (3), 644-654.

Environment Canada, 2011. Hurricane Hazel Storm Information. Weather and Meterology. On-Line: http://www.ec.gc.ca/ouragans-hurricanes/default.asp?lang=En&n=5C4829A9-1.

Freeze R.A., and Cherry J.A., 1979. Groundwater. Prentice Hall Inc. Englewood Cliffs, NJ, US.

Fetter C.W., 1999. Contaminant Hydrogeology, Second Edition. Prentice Hall Inc. NJ, US.

Garder R., and McLaren S., 1999. Infiltration and Moisture Movement in Coastal Sand Dunes, Stuland, Dorset, U.K.: Preliminary Results. Journal of Coastal Research. 15 (4), 936-949.

Geiger S.L., and Durnford D.S., 2000. Infiltration in Homogeneous Sands and a Mechanistic Model of Unstable Flow. Soil Science Society of America. 64, 460- 469.

Gillham R.W., 1984. The Capillary Fringe and Its Effect on Water-Table Response. Journal of Hydrology. 67, 307-324.

Gourlay, M.R., 1992. Wave set-up, wave run-up and beach water table: Interaction between surf zone hydraulics and groundwater hydraulics. Coastal Engineering, 17, 93-144.

Grant U.S., 1948. Influence of the Water Table on Beach Aggregation and Degradation. Journal of Marine Research. 7 (3), 655-678.

Hegge B.J., and Masselink G., 1991. Groundwater –Table Responses to Wave Run-up: An Experimental Study from Western Australia. Journal of Coastal Research. 7(3), 623-634.

Hellwig D.H.R., 1973. Evaporation of Water From Sand, 2: Diurnal Variations. Journal of Hydrology. 18, 109-118.

Hillel D., 1982. Introduction to Soil Physics. Academic Press. Orland, FL, U.S.

Hillel D., 1998. Environmental Soil Physics. Academic Press, San Diego, CA, U.S.

Horn D.P., 2002. Beach Groundwater Dynamics. Geomorphology. 48, 121-146.

Horn D.P., 2006. Measurements and Modelling of Beach Groundwater Flow in the Swash Zone: A Review. Continental Shelf Research. 26, 622-652

Horn D.P., and Walton S.M., 2007. Spatial and Temporal Variations of Sediment Size on a Mixed Sand and Gravel Beach. Sedimentary Geology. 202: 509-528.

Hunt R.J., Haitjema H.M., Krohelski J.T., and Feinstein D.T., 2003. Simulating Groundwater-Lake Interactions: Approaches and Insights. Groundwater. 42 (2): 227-237.

International Joint Commission (IJC) Report, 2011. Fifteenth Biennial Report on the Great Lakes Water Quality. http://www.ijc.org/rel/boards/watershed/15biennial_report_web-final.pdf.

Jackson D.W.T., and Cooper J.A.G., 1999. Beach Fetch Distance and Aeolian Sediment Transport. Sedimentology, 46, 517-522.

Jackson N.L., Horn D.P., Spalding V., and Karl F.N., 1999. Changes in Beach Water Table Elevation During Neap and Spring Tides on a Sandy Estuarine Beach, Delaware Bay, New Jersey. Estuaries. 22(3B): 753-762.

Jeng D.S., Seymour B.R., Barry D.A., Li L., and Parlange J.-Y., 2005. New Approximation for Free Surface Flow of Groundwater: Capillarity Correction. Advances in Water Resources. 28, 1032-1039.

Kasenow M., 2002. Determination of Hydraulic Conductivity from Grain Size Analysis. Water Resources Publications, Littleton, CO, US.

Lebeau M., and Konrad J.M., 2010. A New Capillary and Thin Film Flow Model for Predicting the Conductivity of Unsaturated Porous Media. Water Resources Research. 46, 12554-12569.

Lehman P., Assouline S., and Or D., 2008. Characteristic Lengths Affecting Evaporative Drying of Porous Media. Physical Review E 77. 056309, 1-15.

Lake Huron Centre For Coastal Conservation (LHCCC), 2011. Beach and Dune Stabilization with Sand Fencing and Vegetation. On-Line: http://lakehuron.ca/index.php?page=beach-and-dune-stabilization-with-sand-fencing-and-vegetation.

Li L., Barry D.A., Parlange J.Y., and Pattiaratchi C.B., 1997. Beach Water Table Fluctuations due to Wave Run-up: Capillarity Effects.Water Resources Research. 33, 935-945.

Li L., Barry D.A, Stagnitti F., Parlange J.-Y., and Jeng D.S., 2000. Beach Water Table Fluctuations Due to Spring-Neap Tides: Moving Boundary Effects. Advances in Water Resources. 23, 817-824.

Lundgren L., 1986. Environmental Geology. Prentice-Hall. Englewood Cliffs, NJ, US.

Luthin J.N., and Miller R.D., 1953. Pressure Distribution in Soil Columns Draining into the Atmosphere. Soil Science Society of America. 329-333.

Marinas M., 2009. Effects of Disconnected Entrapped Air on Hydraulic Conductivity in the Presence of Water Table Fluctuations. M.Sc. Thesis, School of Geography and Earth Sciences, McMaster University, Hamilton, Ontario, CAN.

Maun M.A., 2009. The Biology of Coastal Sand Dunes. Oxford University Press. Oxford, NY, US.

Meek G.A., 2007. Transport and Persistence of E. coli in the Swash Zone at Amberly Beach, Lake Huron, Ontario, Canada. M.Sc. Thesis, School of Geography and Earth Sciences, McMaster University, Hamilton, Ontario, CAN.

National Climate Data Information Archive (NCDIA), 2011. Historical Weather and Climate Data.Environment Canada. On-Line: http://climate.weatheroffice.gc.ca/Welcome_e.html.

Neba B., Boufadel M.C., and Weaver J., 2002. The Role of Capillary Forces in Steady-State and Transient Seepage Flows. Ground Water. 40 (4): 407-415.

Nielsen P., 1990. Tidal Dynamics of the Water Table in Beaches. Water Resources Research. 26 (9), 2127-2134.

Nielsen P., 1999. Groundwater Dynamics and Salinity in Coastal Barriers. Journal of Coastal Research. 15 (3): 732-740.

Nielsen P., and Perrochet P., 2000. Water Table Dynamics Under Capillary Fringes: Experiments and Modelling. Advances in Water Resources. 23, 503-515.

Oblinger A., and Anthony E.J., 2008. Surface Moisture Variations on a Multibarred Macrotidal Beach: Implications for Aeolian Sand Transport. Journal of Coastal Research. 24 (5):1194-2003.

Odong J., 2007. Evaluation of Empirical Formulae for Determination of Hydraulic Conductivity based on Grain-Size Analysis. American Journal of Science. 3(3): 54-60.

Parlange J.Y., 1987. A Capillarity Correction for Free Surface Flow of Groundwater. Water Resources Research. 23 (5): 805-808.

Patz J.A., Vavrus S.J., Uejio C.K., and McLellan S.L., 2008. Climate Change and Waterborn Disease Risk in the Great Lakes Region of the U.S. American Journal of Preventive Medicine. 35(5):451-458.

Philip J.R., 1956a. The Theory of Infiltration: 1. the Infiltration Equation and its Solution. Soil Science. 83, 345-357.

Philip J.R., 1956b. The Theory of Infiltration: 2. the Profile of Infinity. Soil Science. 83, 435-448.

Rassam D., Simunek J., and van Genuchten M.Th., 2003. Modelling Variably Saturated Flow with HYDRUS-2D, 1st edition. ND Consult, Brisbane, AUS.

Reineck H.E., and Singh I.B., 1980. Depositional Sedimentary Environments, Second Edition. Springer-Verlag. Berlin Heidelberg, NY, US.

Reynolds W.D., and Elrick D.E, 1987. A Laboratory and Numerical Assessment of the Guelph Permeameter Method. Soil Science. 144: 282-299.

Robertson W.D., Cherry J.A., and Sudicky E.A., 1991. Ground-Water Contamination from Two Small Septic Systems on Sandy Aquifers. Ground Water. 29(1): 82-92

Rocha D., Abbasi F., and Feyen J., 2006. Sensitivity Analysis of Soil Hydraulic Properties on Subsurface Water Flow in Furrows. Journal of Irrigation and Drainage Engineering. 132 (4): 418-424.

Romano C.G., Frind E.O., and Rudolph D.L., 1999. Significance of Unsaturated Flow and Seepage Faces in the Simulation of Steady-State Subsurface Flow. Ground Water. 37 (4):625-632.

Ronen D., Scher H., and Blunt M., 2000. Field Observations of a Capillary Fringe Before and After a Rainy Season. Journal of Contaminant Hydrology. 44, 103-118.

Rubin J., Stenhardt R., and Reiniger P. 1964. Soil Water Relations During Rain Infiltration: II. Moisture Content Profiles During Rains of Low Intensities. Soil Science Society of America Proceedings. 28 (1): 1-5.

Schwartz F.W., and Zhang H., 2003. Fundamentals of Groundwater. John Wiley and Sons Inc. New York, NY, US.

Silliman S.E., Berkowitz B., Simunek J., and Van Genuchten M.Th., 2002. Fluid Flow and Solute Migration within the Capillary Fringe. Ground Water. 40 (1): 76-84.

Simunek J., Sejna M., and van Genuchten M.Th., 1999. The HYDRUS-2D Software Package for Simulating the Two-Dimensional Movement of Water, Heat, and Multiple Solutes in Variably Saturated Media, Version 2.0, IGWMC-TPS-53B, International Groundwater Modelling Center, Colorado School of Mines. Golden, CO, US.

Skalbeck J.D., Kinzelman J.L., and Mayer G.C., 2010. Fecal Indicator Organism Density in Beach Sands: Impact of Sediment Grain Size, Uniformity, and Hydrologic Factors on Surface Water Loading. Journal of Great Lakes Research. 36, 707-714.

Soil Moisture Equipment Corp (SMEC), 1993. Guelph Permeameter 2800K1 Operating Instructions. Sanata Barbara, CA, US.

Solutions Direct, 2011. Bulk Densities of Pulverized Materials in Freely Poured Condition. On-line: http://www.solutionsdirect.com/test-sieves-technical-specifications.html.

Song J., Chen X., Cheng C., Wang D., Lackey S., and Xu Z., 2009. Feasibility of Grain-Size Analysis Methods for Determination of Vertical Hydraulic Conductivity of Streambeds. Journal of Hydrology. 375 (3, 4): 428-437.

Stephens D.B., 1996. Vadose Zone Hydrology. Lewis Publishers, Florida, US.

Tan S.B.K., Shuy E.B., and Chua L.H.C., 2007. Effects of Meteorological and Hydrogeological Factors on Gross Recharge Percentage at Unconfined Sandy Aquifers with an Equatorial Climate. Hydrological Processes, 21, 2493-2503.

Teo H.T., Jeng D.S., Seymour B.R., Barry D.A., and Li L., 2003. A New Analytical Solution for Water Table Fluctuations in Coastal Aquifers with Slopping Beaches. Advances in Water Resources. 26, 1239-1247.

Toronto Weather Forecast and Climate (TWFC), 2011. Hurricane Ike and Southern Ontario. TorontoForcast.com. On-Line: http://klmweather.org/weatherblog/page/2/.

Townley L.R., and Trefry M.G., 2000. Surface Water-Groundwater Interaction Near Shallow Circular Lakes: Flow Geometry in Three Dimensions. Water Resources Research. 36(4): 935-949. 2003

Trenhaile, A.S., 2004. Geomorphology A Canadian Perspective, Second Edition. Oxford University Press, CAN.

Trenhaile, A.S., 2007. Geomorphology A Canadian Perspective, Third Edition. Oxford University Press, CAN.

Turner I., 1993a. The Total Water Content of Sandy Beaches. Journal of Coastal Research. 15, 11-26.

Turner I., 1993b. Water Table Outcropping on Macro-Tidal Beaches: A Simulation Model. Marine Geology. 115, 227-238.

Turner I., 1993c. Beachface Permeability, the Groundwater Effluent Zone and Intertidal Profiles of Macro-tidal Beaches – A Conceptual Model. In THOMS, M. (editor), Catchments and Coasts of Eastern Australia. Department of Geography, University of Sydney, Monograph Series, 5, 88-99.

Turner I.L., and Masselink G., 1998. Swash Infiltration-Exfiltration and Sediment Transport. Journal of Geophysical Research. 103 (C13): 30813-30824.

Turner I.L. and Nielsen P., 1997. Rapid Water Table Fluctuations within the Beachface: Implications for Swash Zone Sediment Mobility. Coastal Engineering. 32, 45-59.

Tymchak M.P., and Torres R., 2007. Effects of Variable Rainfall Intensity on the Unsaturated Zone Response of a Forested Sandy Hillslope. Water Resources Research. 43, W06431, doi:10.1029/2005WR004584.

Ullman W.J., Chang B., Miller D.C., and Madsen J., 2003. Groundwater Mixing, Nutrient Digenesis, and Discharges Across a Sandy Beachface, Cape Henlopen, Delaware (USA). Estuarine, Coastal and Shelf Sciences. 57, 539-552.

Vukovic M., and Soro A., 1992. Determination of Hydraulic Conductivity of Poros Media from Grain-Size Composition. Water Resources Publications, Littleton, CO, US.

Wang X.P., Cui Y., Pan Y.X., Li X.R., Yu Z., and Young M.H., 2007. Effects of Rainfall Characteristics on Infiltration and Redistribution Patterns in Revegetated-Stabilized Desert Ecosystems. Journal of Hydrology. 358, 134-143.

Wang X.P., Li X.R., Xiao H.L., Berndtsson R., and Pan Y.X., 2008. Effects of Surface Characteristics on Infiltration Patterns in an Arid Shrub Desert. Hydrological Processes. 21. 72-79.

Whitman R.L., and Nevers M.B., 2003. Foreshore Sand as a Source of Escherichia coli in Nearshore Water of a Lake Michigan Beach. Applied and Environmental Microbiology, 69, 5555-5562.

Wiggs G.F.S., Baird A.J., and Antherton R.J., 2004. The Dynamic Effects of Moisture on the Entrainment Transport of Sand by Wind. Geomorphology, 59, 13-30.

Yang Y., and Davidson-Arnott R.G.D., 2005. Rapid Measurement of Surface Moisture Content on a Beach. Journal of Coastal Research, 21, 447-452.

Yang H., Rahardjo H., Leong E.C., and Fredlund D.G., 2004. Factors Affecting Drying and Wetting Soil-Water Characteristic Curves of Sandy Soils. Canadian Geotechnical Journal. 41, 908-920.

APPENDIX 1

Table 1A.1: Water table and surface elevations for the Tiny Beaches, August 2009

Location	Distance from Reference Point (m)	Beach Surface Elevation (m)	Depth to Water Table (m)	Water Table Elevation (m)
Balm Beach South				
Lake	0.000	98.522	0.000	98.522
Hole 1	4.740	98.893	0.407	98.486
BBS1	8.250	99.194	0.666	98.528
BBS2	14.490	99.133	0.534	98.599
BBS3	19.260	99.389	0.741	98.648
BBS4	24.450	99.775	1.091	98.684
Hole 6	28.670	100.140	1.438	98.702
Dune Surf.	33.820	100.546	--	--
Jackson Park Beach				
Lake	46.590	97.861	0.000	97.861
Hole 1	44.370	98.235	0.379	97.856
Hole 2	40.840	98.233	0.369	97.864
JPB1	35.720	98.297	0.414	97.883
Hole 4	30.810	98.372	0.469	97.903
JPB2	25.575	98.445	0.510	97.935
Hole 6	20.770	98.576	0.605	97.971
JPB3	15.520	98.664	0.649	98.015
JPB4	5.730	98.850	0.746	98.104
Woodland Beach North				
Lake	50.350	97.704	0.000	97.704
Hole 1	45.950	97.950	0.185	97.765
WBN1	40.320	98.301	0.538	97.763
WBN2	37.050	98.530	0.724	97.806
WBN3	30.300	98.853	1.014	97.839
Hole 5	24.250	99.300	1.429	97.871
Woodland Beach South				
Lake	47.700	97.679	0.000	97.679
Hole 1	38.400	98.126	0.425	97.701
WBS1	34.850	98.250	0.537	97.713
Hole 3	31.950	98.216	0.468	97.748
WBS2	27.950	97.998	0.217	97.781
Hole 5	24.250	98.100	0.245	97.855
WBS3	20.550	98.190	0.279	97.911
Hole 7	16.800	98.291	0.300	97.991
WBS4	11.950	98.440	0.356	98.084
Hole 9	6.600	98.754	0.513	98.241

(Table 4.1 (continued) in Appendix 1 containing the water table depths and beach surface elevations from October 2009 and November 2010)

Table 1A.1: Water table and surface elevations for the Tiny Beaches, October 2009

Location	Distance from Reference Point (m)	Beach Surface Elevation (m)	Depth to Water Table (m)	Water Table Elevation (m)

Balm Beach South				
Lake	0.000	98.254	0.000	98.254
Hole 1	3.220	99.631	0.262	99.369
BBS1	7.800	99.279	0.957	98.322
BBS2	13.430	99.176	0.829	98.347
BBS3	17.210	99.361	0.998	98.363
BBS4	23.730	99.882	1.485	98.397
Hole 6	--	--	--	--
Jackson Park Beach				
Lake	55.13	97.555	0.000	97.555
Hole 1	46.57	97.969	0.322	97.647
Hole 2	--	--	--	--
JPB1	35.84	98.313	0.686	97.627
Hole 4	--	--	--	--
JPB2	27.68	98.443	0.624	97.819
Hole 6	--	--	--	--
JPB3	7.63	98.612	0.678	97.934
JPB4	5.73	98.877	0.774	98.103
Woodland Beach North				
Lake	--	--	--	--
Hole 1	--	--	--	--
WBN1	--	--	--	--
WBN2	--	--	--	--
WBN3	--	--	--	--
Hole 5	--	--	--	--
Woodland Beach South				
Lake	54.92	97.199	0	97.199
Hole 1	40.61	97.964	0.583	97.372
WBS1	34.77	98.297	0.509	97.431
Hole 3	--	--	--	--
WBS2	27.94	98.088	0.591	97.497
Hole 5	--	--	--	--
WBS3	20.49	98.171	0.866	97.662
Hole 7	--	--	--	--
WBS4	12.13	98.446	0.592	97.863
Hole 9	--	--	--	--

Table 1A.1 (continued): Water table and surface elevations for the Tiny Beaches, November 2010

Location	Distance from Reference Point (m)	Beach Surface Elevation (m)	Depth to Water Table (m)	Water Table Elevation (m)
Balm Beach South				
Lake	--	--	--	--
Hole 1	--	--	--	--
BBS1	--	--	--	--
BBS2	--	--	--	--
BBS3	--	--	--	--
BBS4	--	--	--	--
Hole 6	--	--	--	--

Jackson Park Beach				
Lake	72.180	97.384	0.000	97.384
Shoreline	72.180	97.384	0.000	97.384
Hole 1	64.980	97.507	0.063	97.444
Hole 2	49.080	97.676	0.135	97.541
Hole 3	39.030	98.232	0.605	97.627
JPB1	29.580	98.358	0.636	97.722
Hole 5	--	--	--	--
JPB2	21.880	98.541	0.729	97.812
Hole 7	--	--	--	--
JPB3	14.380	98.666	0.738	97.928
JPB4	5.730	98.852	0.837	98.015
Woodland Beach North				
Lake	--	--	--	--
Hole 1	--	--	--	--
WBN1	--	--	--	--
WBN2	--	--	--	--
WBN3	--	--	--	--
Hole 5	--	--	--	--
Woodland Beach South				
Lake	50.300	97.148	0.000	97.148
Shoreline	50.300	97.148	0.000	97.148
Hole 1	47.800	97.469	0.170	97.299
WBS1	38.650	98.049	0.663	97.386
Hole 3	--	--	--	--
WBS2	29.650	98.209	0.762	97.447
Hole 5	--	--	--	--
WBS3	22.200	98.211	0.642	97.569
Hole 7	--	--	--	--
WBS4	12.150	98.454	0.660	97.794
Hole 9	3.200	99.109	0.960	98.149

APPENDIX 2

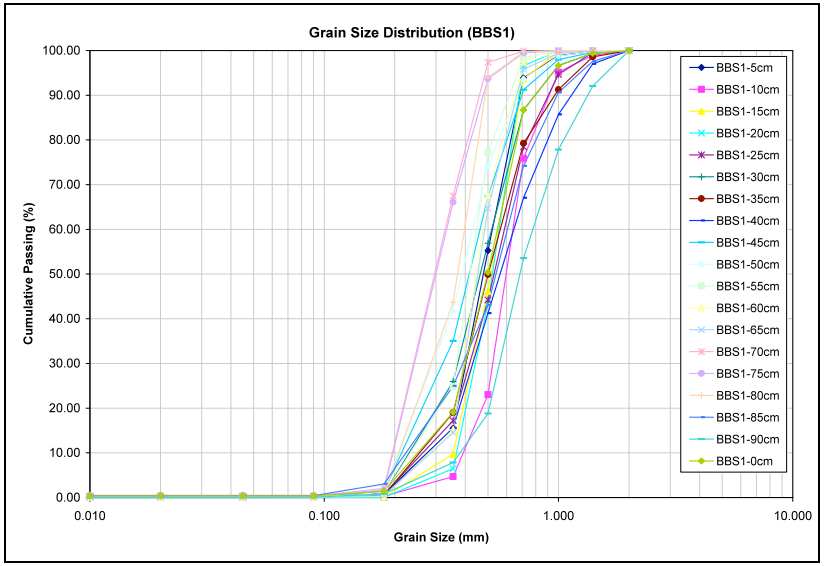
Grain Size Distribution (BBS1)
Cumulative Passing (%)
Grain Size (mm)
BBS1-5cm
BBS1-10cm
BBS1-15cm
BBS1-20cm
BBS1-25cm
BBS1-30cm
BBS1-35cm
BBS1-40cm
BBS1-45cm
BBS1-50cm
BBS1-55cm
BBS1-60cm
BBS1-65cm
BBS1-70cm
BBS1-75cm
BBS1-80cm
BBS1-85cm
BBS1-90cm
BBS1-0cm

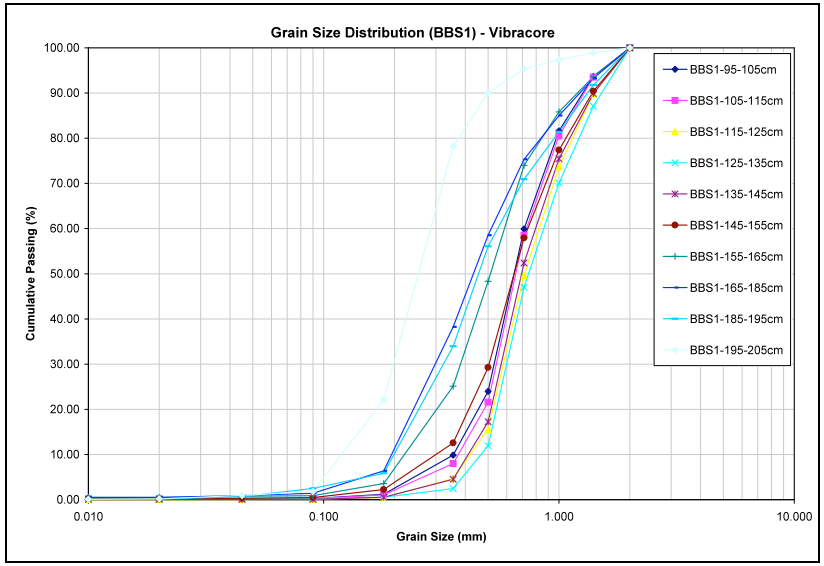
Grain Size Distribution (BBS1) - Vibracore
Cumulative Passing (%)
Grain Size (mm)
BBS1-95-105cm
BBS1-105-115cm
BBS1-115-125cm
BBS1-125-135cm
BBS1-135-145cm
BBS1-145-155cm
BBS1-155-165cm
BBS1-165-185cm
BBS1-185-195cm
BBS1-195-205cm

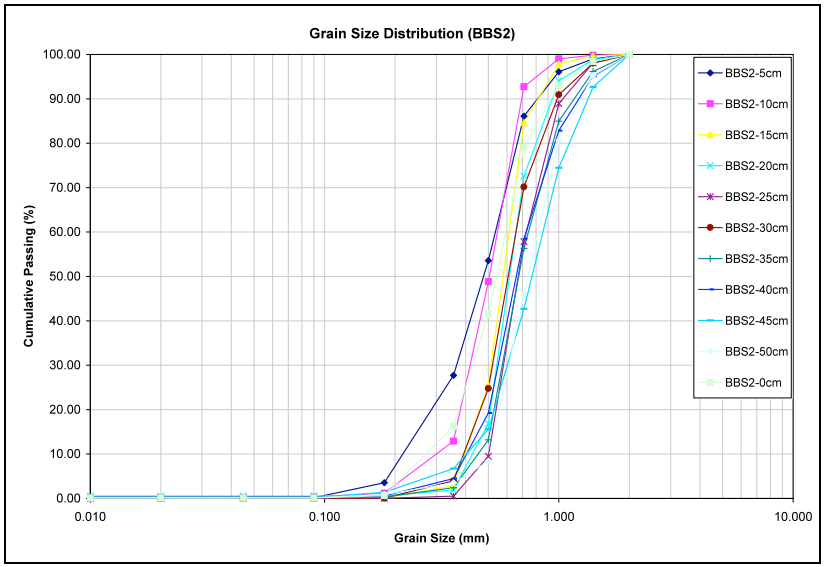
Grain Size Distribution (BBS2)
Cumulative Passing (%)
Grain Size (mm)
BBS2-5cm
BBS2-10cm
BBS2-15cm
BBS2-20cm
BBS2-25cm
BBS2-30cm
BBS2-35cm
BBS2-40cm
BBS2-45cm
BBS2-50cm
BBS2-0cm

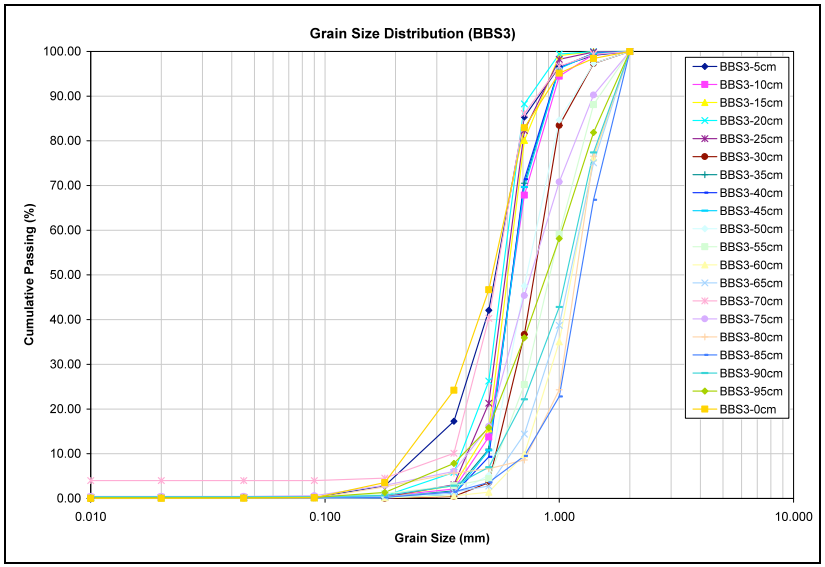
Grain Size Distribution (BBS3)
Cumulative Passing (%)
Grain Size (mm)
BBS3-5cm
BBS3-10cm
BBS3-15cm
BBS3-20cm
BBS3-25cm
BBS3-30cm
BBS3-35cm
BBS3-40cm
BBS3-45cm
BBS3-50cm
BBS3-55cm
BBS3-60cm
BBS3-65cm
BBS3-70cm
BBS3-75cm
BBS3-80cm
BBS3-85cm
BBS3-90cm
BBS3-95cm
BBS3-0cm

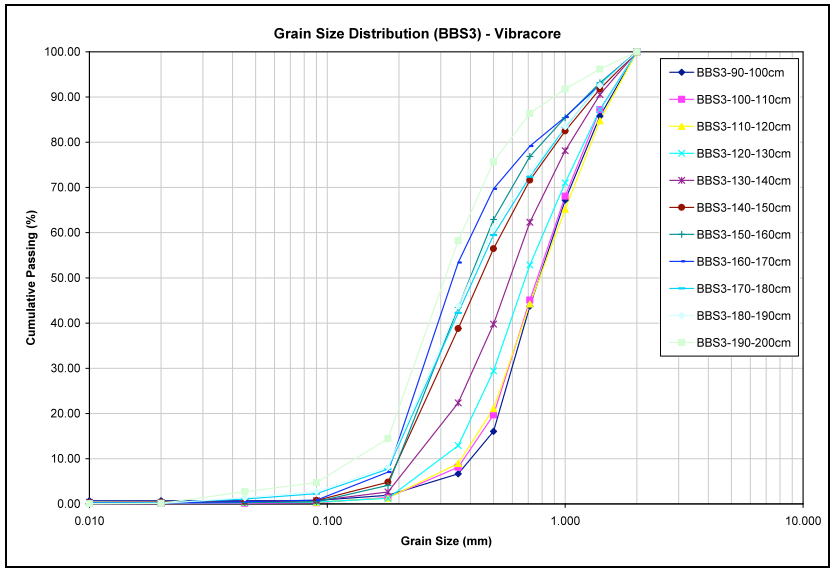
Grain Size Distribution (BBS3) - Vibracore
Cumulative Passing (%)
Grain Size (mm)
BBS3-90-100cm
BBS3-100-110cm
BBS3-110-120cm
BBS3-120-130cm
BBS3-130-140cm
BBS3-140-150cm
BBS3-150-160cm
BBS3-160-170cm
BBS3-170-180cm
BBS3-180-190cm
BBS3-190-200cm

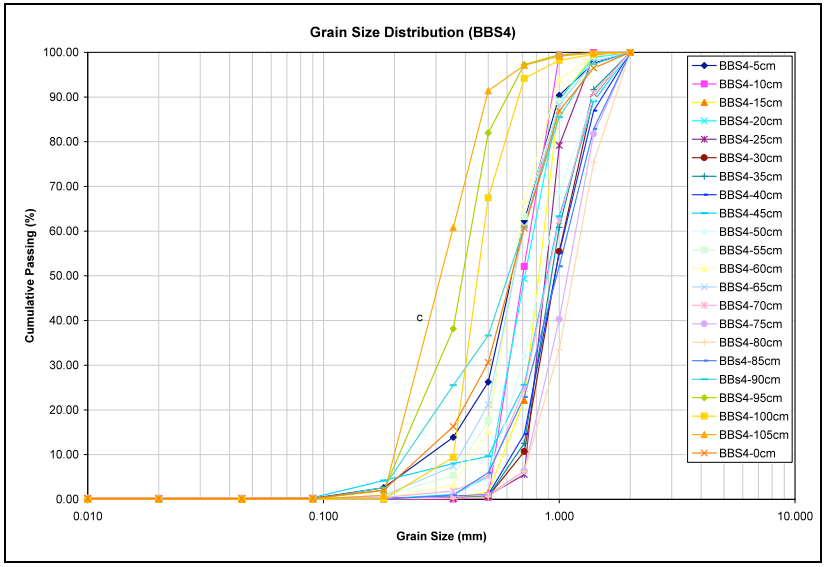
Grain Size Distribution (BBS4)
Cumulative Passing (%)
Grain Size (mm)
BBS4-5cm
BBS4-10cm
BBS4-15cm
BBS4-20cm
BBS4-25cm
BBS4-30cm
BBS4-35cm
BBS4-40cm
BBS4-45cm
BBS4-50cm
BBS4-55cm
BBS4-60cm
BBS4-65cm
BBS4-70cm
BBS4-75cm
BBS4-80cm
BBs4-85cm
BBs4-90cm
BBS4-95cm
BBS4-100cm
BBS4-105cm
BBS4-0cm

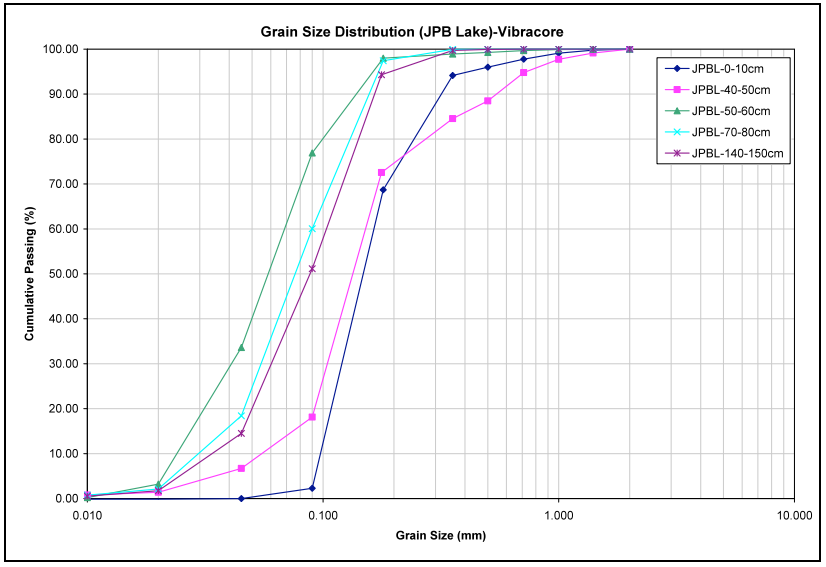
Grain Size Distribution (JPB Lake)-Vibracore
Cumulative Passing (%)
Grain Size (mm)
JPBL-0-10cm
JPBL-40-50cm
JPBL-50-60cm
JPBL-70-80cm
JPBL-140-150cm

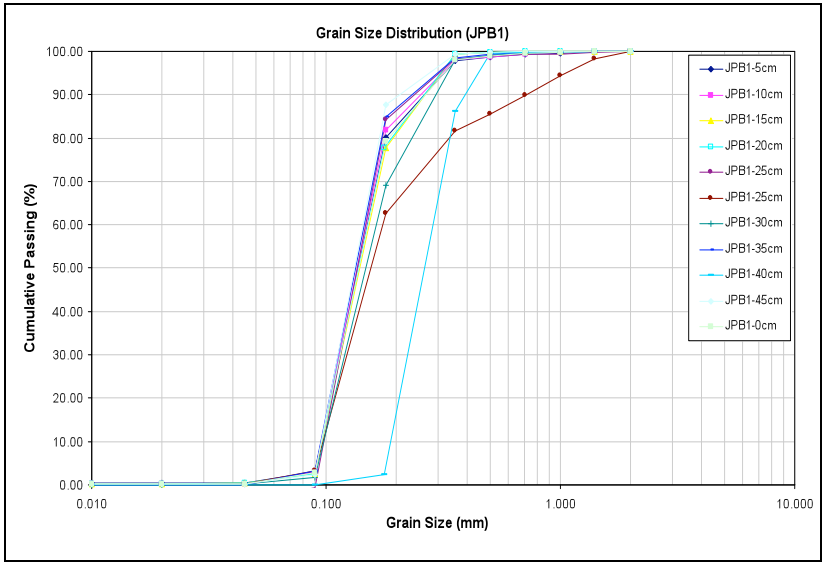
Grain Size Distribution (JPB1)
Cumulative Passing (%)
Grain Size (mm)
JPB1-5cm
JPB1-10cm
JPB1-15cm
JPB1-20cm
JPB1-25cm
JPB1-25cm
JPB1-30cm
JPB1-35cm
JPB1-40cm
JPB1-45cm
JPB1-0cm

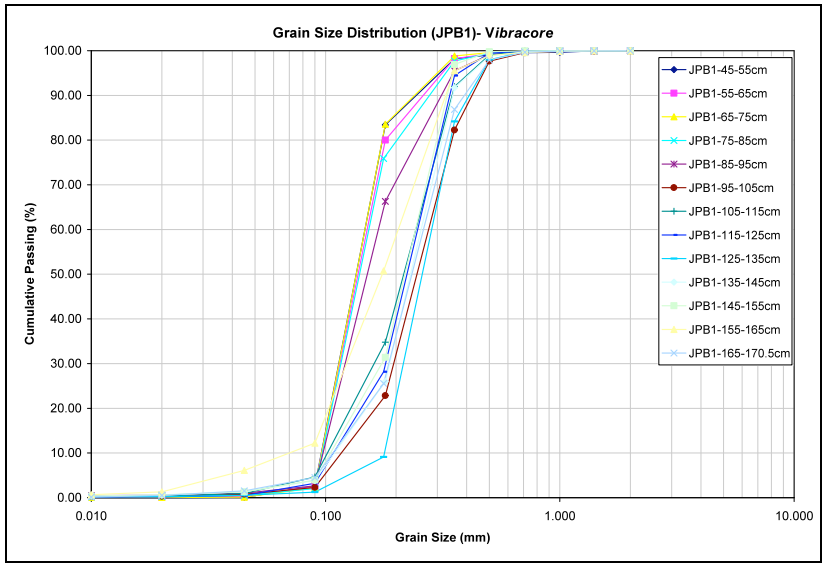
Grain Size Distribution (JPB1)- Vibracore
Cumulative Passing (%)
Grain Size (mm)
JPB1-45-55cm
JPB1-55-65cm
JPB1-65-75cm
JPB1-75-85cm
JPB1-85-95cm
JPB1-95-105cm
JPB1-105-115cm
JPB1-115-125cm
JPB1-125-135cm
JPB1-135-145cm
JPB1-145-155cm
JPB1-155-165cm
JPB1-165-170.5cm

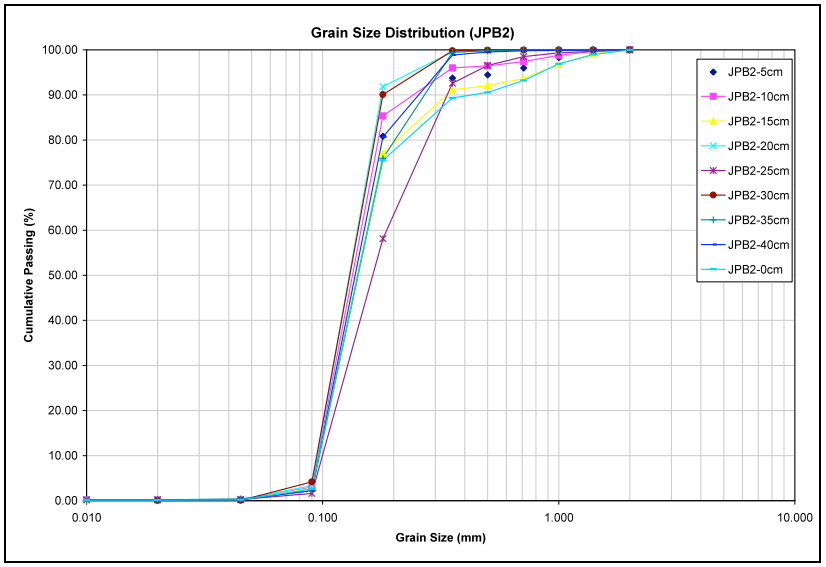
Grain Size Distribution (JPB2)
Cumulative Passing (%)
Grain Size (mm)
JPB2-5cm
JPB2-10cm
JPB2-15cm
JPB2-20cm
JPB2-25cm
JPB2-30cm
JPB2-35cm
JPB2-40cm
JPB2-0cm

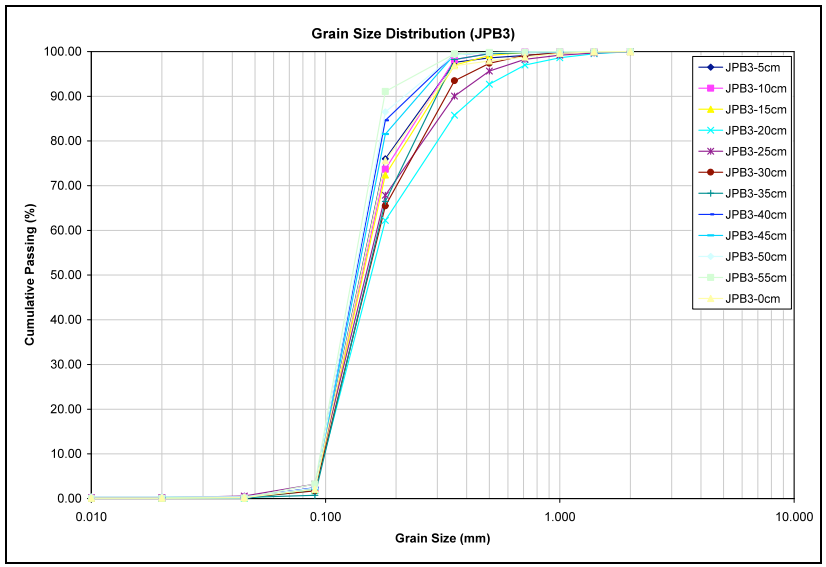
Grain Size Distribution (JPB3)
Cumulative Passing (%)
Grain Size (mm)
JPB3-5cm
JPB3-10cm
JPB3-15cm
JPB3-20cm
JPB3-25cm
JPB3-30cm
JPB3-35cm
JPB3-40cm
JPB3-45cm
JPB3-50cm
JPB3-55cm
JPB3-0cm

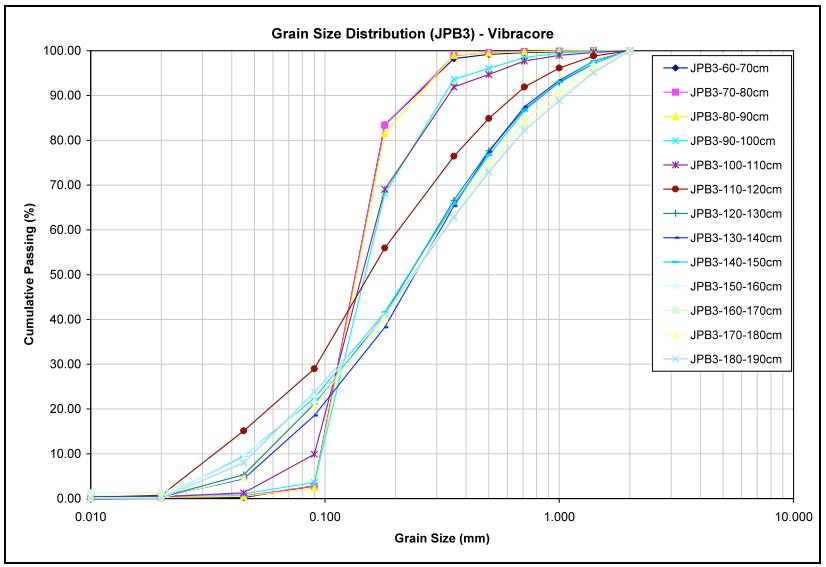
Grain Size Distribution (JPB3) - Vibracore
Cumulative Passing (%)
Grain Size (mm)
JPB3-60-70cm
JPB3-70-80cm
JPB3-80-90cm
JPB3-90-100cm
JPB3-100-110cm
JPB3-110-120cm
JPB3-120-130cm
JPB3-130-140cm
JPB3-140-150cm
JPB3-150-160cm
JPB3-160-170cm
JPB3-170-180cm
JPB3-180-190cm

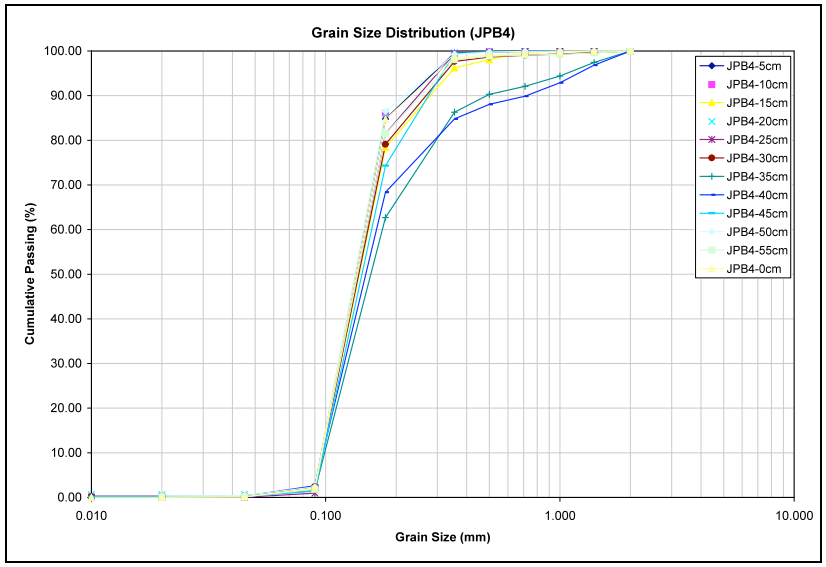
Grain Size Distribution (JPB4)
Cumulative Passing (%)
Grain Size (mm)
JPB4-5cm
JPB4-10cm
JPB4-15cm
JPB4-20cm
JPB4-25cm
JPB4-30cm
JPB4-35cm
JPB4-40cm
JPB4-45cm
JPB4-50cm
JPB4-55cm
JPB4-0cm

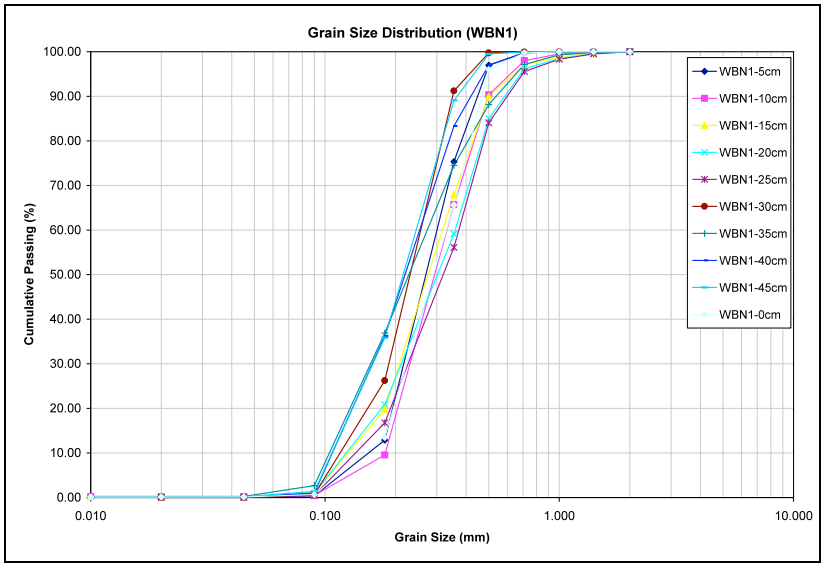
Grain Size Distribution (WBN1)
Cumulative Passing (%)
Grain Size (mm)
WBN1-5cm
WBN1-10cm
WBN1-15cm
WBN1-20cm
WBN1-25cm
WBN1-30cm
WBN1-35cm
WBN1-40cm
WBN1-45cm
WBN1-0cm

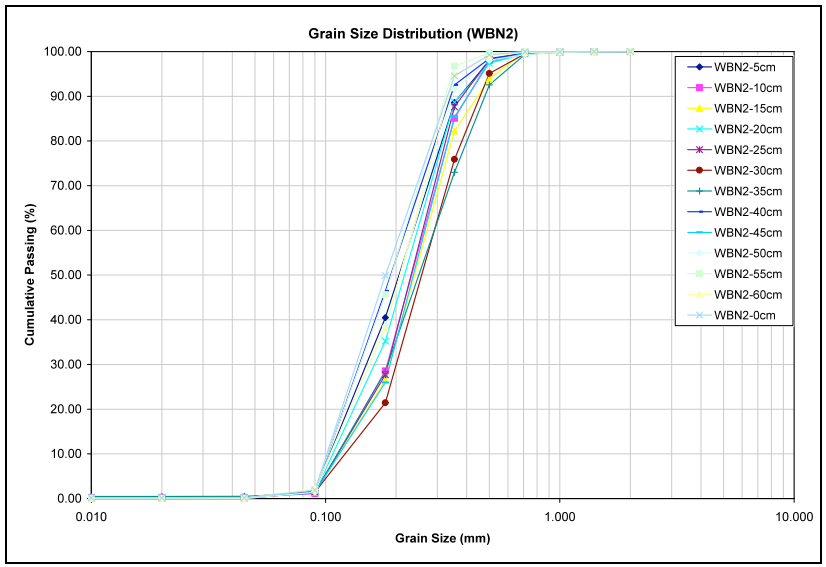
Grain Size Distribution (WBN2)
Cumulative Passing (%)
Grain Size (mm)
WBN2-5cm
WBN2-10cm
WBN2-15cm
WBN2-20cm
WBN2-25cm
WBN2-30cm
WBN2-35cm
WBN2-40cm
WBN2-45cm
WBN2-50cm
WBN2-55cm
WBN2-60cm
WBN2-0cm

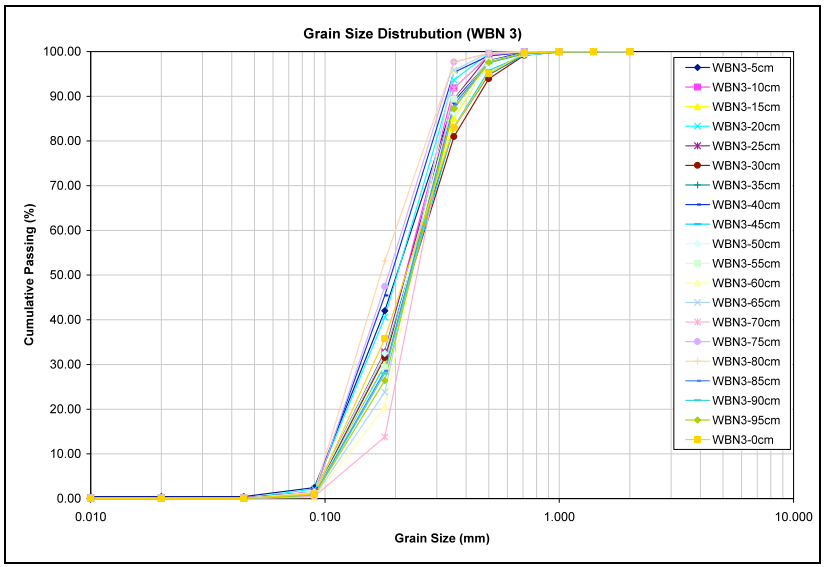
Grain Size Distrubution (WBN 3)
Cumulative Passing (%)
Grain Size (mm)
WBN3-5cm
WBN3-10cm
WBN3-15cm
WBN3-20cm
WBN3-25cm
WBN3-30cm
WBN3-35cm
WBN3-40cm
WBN3-45cm
WBN3-50cm
WBN3-55cm
WBN3-60cm
WBN3-65cm
WBN3-70cm
WBN3-75cm
WBN3-80cm
WBN3-85cm
WBN3-90cm
WBN3-95cm
WBN3-0cm

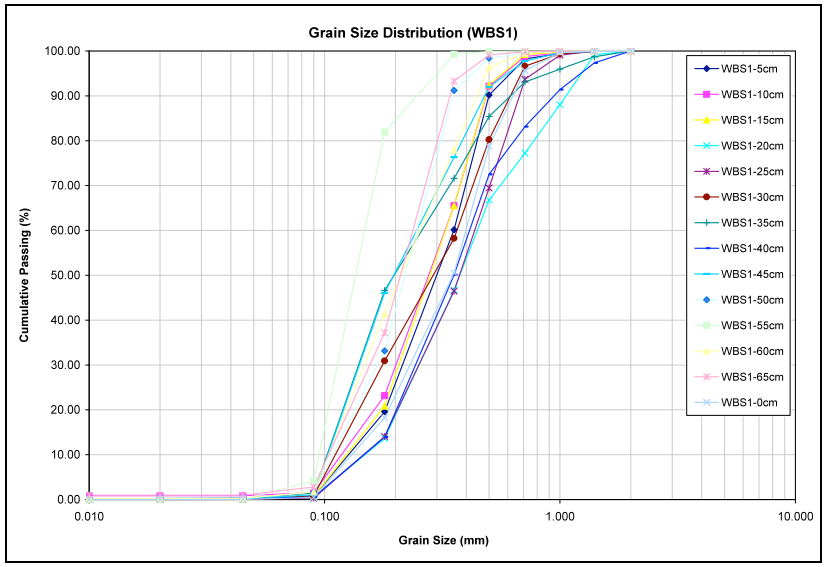
Grain Size Distribution (WBS1)
Cumulative Passing (%)
Grain Size (mm)
0.010
0.100
1.000
10.000
WBS1-5cm
WBS1-10cm
WBS1-15cm
WBS1-20cm
WBS1-25cm
WBS1-30cm
WBS1-35cm
WBS1-40cm
WBS1-45cm
WBS1-50cm
WBS1-55cm
WBS1-60cm
WBS1-65cm
WBS1-0cm

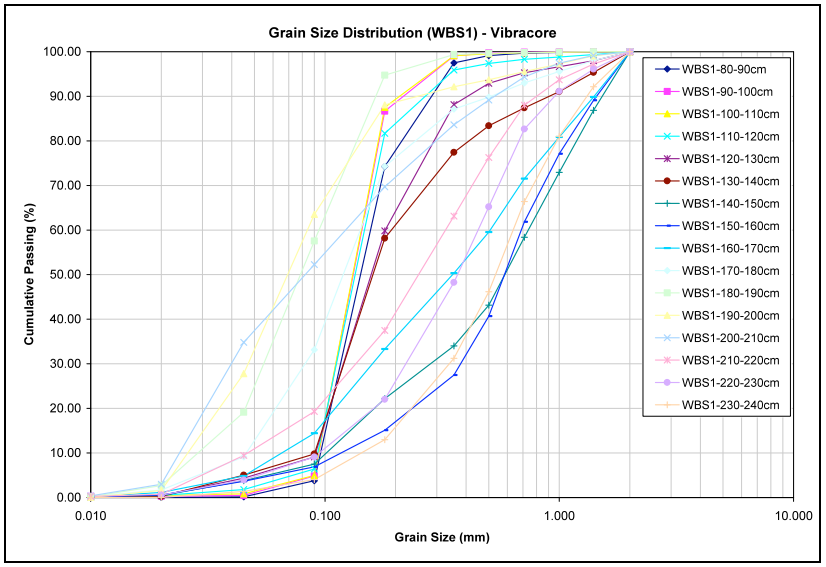
Grain Size Distribution (WBS1) - Vibracore
Cumulative Passing (%)
Grain Size (mm)
0.010
0.100
1.000
10.000
WBS1-80-90cm
WBS1-90-100cm
WBS1-100-110cm
WBS1-110-120cm
WBS1-120-130cm
WBS1-130-140cm
WBS1-140-150cm
WBS1-150-160cm
WBS1-160-170cm
WBS1-170-180cm
WBS1-180-190cm
WBS1-190-200cm
WBS1-200-210cm
WBS1-210-220cm
WBS1-220-230cm
WBS1-230-240cm

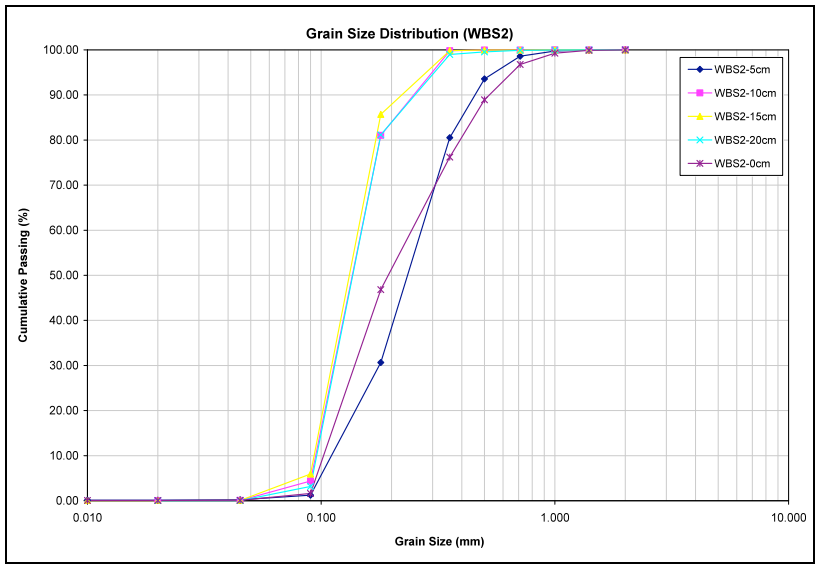
Grain Size Distribution (WBS2)
Cumulative Passing (%)
Grain Size (mm)
0.010
0.100
1.000
10.000
WBS2-5cm
WBS2-10cm
WBS2-15cm
WBS2-20cm
WBS2-0cm

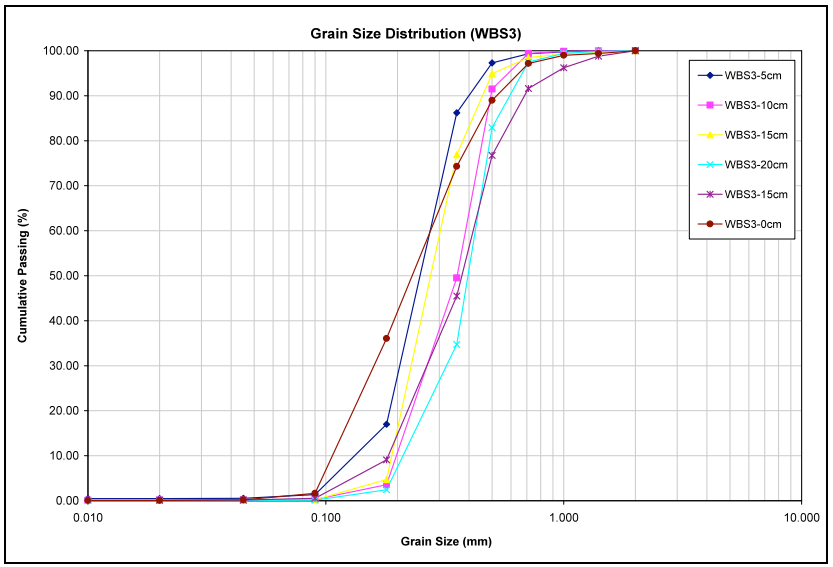
Grain Size Distribution (WBS3)
Cumulative Passing (%)
Grain Size (mm)
0.010
0.100
1.000
10.000
WBS3-5cm
WBS3-10cm
WBS3-15cm
WBS3-20cm
WBS3-15cm
WBS3-0cm

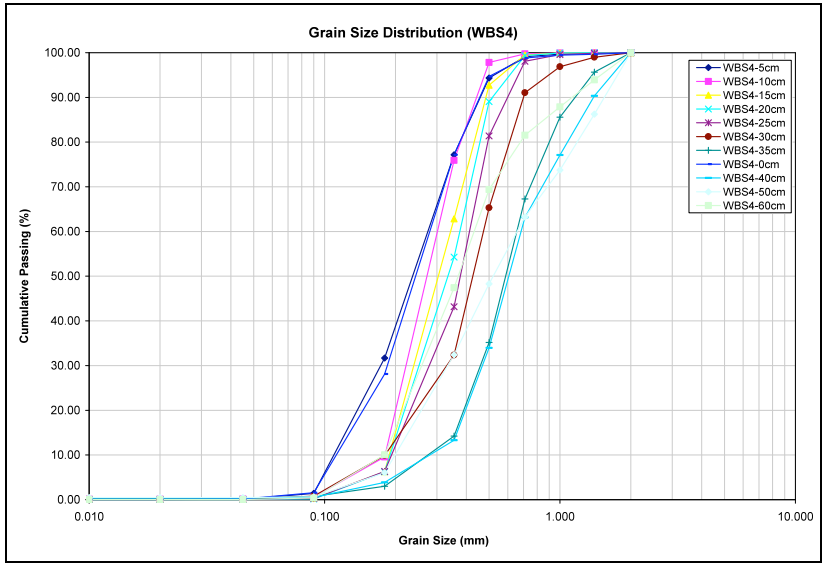
Grain Size Distribution (WBS4)
Cumulative Passing (%)
Grain Size (mm)
0.010
0.100
1.000
10.000
0.00
10.00
20.00
30.00
40.00
50.00
60.00
70.00
80.00
90.00
100.00
WBS4-5cm
WBS4-10cm
WBS4-15cm
WBS4-20cm
WBS4-25cm
WBS4-30cm
WBS4-35cm
WBS4-0cm
WBS4-40cm
WBS4-50cm
WBS4-60cm

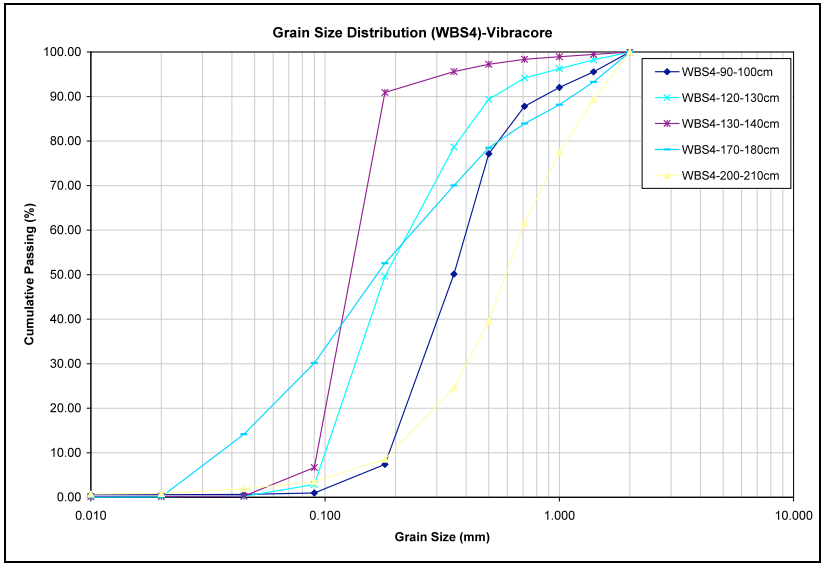
Grain Size Distribution (WBS4)-Vibracore
Cumulative Passing (%)
Grain Size (mm)
0.010
0.100
1.000
10.000
0.00
10.00
20.00
30.00
40.00
50.00
60.00
70.00
80.00
90.00
100.00
WBS4-90-100cm
WBS4-120-130cm
WBS4-130-140cm
WBS4-170-180cm
WBS4-200-210cm

Table 2A.1: Results from the structural analysis of the Tiny Township beaches, August 2009

Balm Beach south

Depth from Surface (cm)	Volumetric Moisture Content (%)		Porosity	Bulk Density (g/cm^3)
	Short Core Method	TDR Method		
BBS1				
0	0.25	--	0.37	1.68
5	0.58	4.2	0.40	1.58
10	4.74	5.8	0.46	1.43
15	4.61	7.5	0.48	1.38
20	5.71	8.3	0.46	1.43
25	5.61	8.6	0.47	1.41
30	5.85	9.7	0.45	1.45
35	7.89	9.8	0.46	1.44
40	5.38	9.7	0.45	1.46
45	7.86	14	0.47	1.41
50	26.67	24.1	0.41	1.56
55	28.52	26.5	0.44	1.50
60	31.44	38.2	0.45	1.45
65	34.20	48.8	0.44	1.47
BBS2				
0	0.26	--	0.37	1.66
5	0.30	6.2	0.37	1.67
10	5.75	8.6	0.46	1.43
15	3.95	7.5	0.45	1.45
20	5.02	6.8	0.44	1.47
25	4.28	8.4	0.47	1.41
30	5.05	10	0.47	1.41
35	10.02	12.9	0.45	1.46
40	18.26	30.9	0.43	1.51
45	28.30	40.1	0.40	1.59
50	30.28	42.6	0.41	1.58
BBS3				
0	2.13	--	0.40	1.58
5	4.11	8.7	0.48	1.38
10	4.29	6.8	0.48	1.37
15	4.59	6.6	0.46	1.43
20	4.67	8.4	0.46	1.43
25	2.82	7	0.48	1.39
30	2.39	5.6	0.52	1.28
35	2.92	4.9	0.48	1.38
40	2.91	6.3	0.52	1.28
45	5.20	9.3	0.48	1.37
50	7.55	12.8	0.49	1.35
55	10.87	17.4	0.45	1.45
60	21.96	37.8	0.42	1.54
BBS4				
0	0.79	--	0.42	1.54

5	2.11	6.1	0.45	1.47
10	4.16	6.5	0.45	1.46
15	1.98	7.3	0.48	1.37
20	3.98	7.5	0.48	1.37
25	4.51	8.2	0.46	1.42
30	3.85	6.2	0.48	1.38
35	2.00	5.9	0.46	1.42
40	2.06	8	0.47	1.40
45	5.43	7.7	0.46	1.43
50	2.48	7.9	0.46	1.44
55	2.86	7.3	0.49	1.35
60	3.80	9.1	0.46	1.43
65	3.35	9.1	0.48	1.38
70	6.79	7.6	0.43	1.51
75	2.68	6.3	0.48	1.38
80	2.44	6.2	0.49	1.36
85	1.85	7.3	0.50	1.32
90	7.03	27.5	0.47	1.41
95	28.93	34.4	0.42	1.53
100	32.88	42.1	0.41	1.56
105	34.35	45.7	0.42	1.54

Jackson Park Beach

Depth from Surface (cm)	Volumetric Moisture Content (%)		Porosity	Bulk Density (g/cm^3)
	Short Core Method	TDR Method		
JPB1				
0	32.04	--	0.40	1.58
5	31.64	41.40	0.41	1.57
10	32.01	40.70	0.42	1.54
15	34.40	43.20	0.40	1.59
20	34.26	41.50	0.46	1.43
25	39.79	43.40	0.39	1.62
JPB2				
0	12.41	--	0.45	1.46
5	24.25	10.00	0.43	1.51
10	30.69	29.70	0.41	1.56
15	33.62	24.10	0.40	1.60
20	32.56	36.80	0.42	1.52
25	35.10	34.50	0.40	1.59
30	35.97	41.20	0.38	1.65
35	38.79	43.60	0.42	1.54
40	40.05	47.00	0.42	1.54
JPB3				
0	3.44	--	0.43	1.52
5	17.99	2.90	0.43	1.51
10	20.32	3.00	0.44	1.49
15	28.55	21.60	0.40	1.59
20	26.63	23.60	0.39	1.61

25	39.44	30.60	0.46	1.43
30	37.95	37.50	0.45	1.46
35	32.57	33.40	0.45	1.47
40	30.92	39.60	0.42	1.54
45	34.35	42.20	0.42	1.54
50	38.41	47.70	0.40	1.58
JPB4				
0	4.10	--	0.45	1.46
5	11.69	12.10	0.48	1.38
10	12.25	14.50	0.53	1.25
15	16.08	18.60	0.49	1.35
20	23.00	20.50	0.47	1.41
25	26.64	27.50	0.48	1.38
30	29.15	25.00	0.41	1.56
35	21.52	30.50	0.50	1.32
40	26.82	34.50	0.43	1.51
45	31.90	31.90	0.44	1.48
50	35.82	44.20	0.45	1.46
55	36.13	41.40	0.44	1.49
60	38.57	47.80	0.46	1.43

Woodland Beach north

Depth from Surface (cm)	**Volumetric Moisture Content (%)**		**Porosity**	**Bulk Density (g/cm3)**
	Short Core Method	**TDR Method**		
WBN1				
0	6.34	--	0.46	1.43
5	6.24	9	0.42	1.53
10	8.64	12.8	0.37	1.66
15	13.03	10.5	0.45	1.47
20	15.06	14.5	0.40	1.58
25	14.42	15	0.44	1.48
30	28.22	26.9	0.37	1.68
35	29.11	28.9	0.42	1.53
40	32.60	42.8	0.40	1.58
45	33.37	43.1	0.41	1.56
0	11.92	12.3	0.41	1.56
WBN2				
5	9.92	7.3	0.42	1.53
10	7.51	7.6	0.39	1.60
15	9.25	9.7	0.41	1.55
20	7.88	--	0.40	1.58
25	9.58	10.7	0.43	1.50
30	10.78	11	0.43	1.52
35	11.51	14.5	0.43	1.51
40	25.84	29.2	0.40	1.58
45	27.56	26.9	0.40	1.60
50	28.90	37.3	0.38	1.63
55	31.84	37.9	0.41	1.56

60	32.93	39.1	0.40	1.58
WBN3				
0	12.32	6.4	0.44	1.48
5	10.78	12.6	0.39	1.60
10	13.87	--	0.42	1.53
15	18.91	12.4	0.38	1.63
20	22.01	11.1	0.44	1.49
25	8.87	11.6	0.42	1.53
30	6.01	9.4	0.40	1.58
35	6.34	9.6	0.41	1.58
40	8.64	9	0.41	1.57
45	7.45	10.1	0.47	1.40
50	6.34	10.8	0.42	1.54
55	9.68	12.8	0.39	1.61
60	12.05	12.9	0.43	1.52
65	16.00	21.3	0.44	1.48
70	18.00	22.6	0.46	1.43
75	26.92	34	0.40	1.60
80	28.22	35.8	0.45	1.47
85	15.79	40.4	0.33	1.77
90	32.74	39.9	0.39	1.61
95	33.88	42.2	0.42	1.53

Woodland Beach south

Depth from Surface (cm)	Volumetric Moisture Content (%)		Porosity	Bulk Density (g/cm3)
	Short Core Method	TDR Method		
WBS1				
0	0.40		0.38	1.65
5	6.72	6.9	0.42	1.52
10	6.90	11.1	0.48	1.38
15	19.65	12.6	0.41	1.56
20	12.62	14	0.45	1.45
25	12.00	14.7	0.45	1.46
30	18.38	18.7	0.45	1.47
35	34.05	41.8	0.39	1.62
40	26.47	27.2	0.46	1.43
45	34.83	32.8	0.41	1.55
50	34.92	43.6	0.38	1.63
55	37.75	48.5	0.38	1.63
WBS2				
0	33.24		0.37	1.68
5	29.48	33.1	0.38	1.65
10	33.39	45.3	0.37	1.66
15	33.98	46.8	0.36	1.70
20	39.18	46.5	0.39	1.61
WBS3				
0	27.87		0.38	1.65
5	28.14	30.2	0.39	1.63

10	27.63	31.3	0.44	1.49
15	29.23	37.6	0.36	1.69
20	35.44	41.7	0.40	1.60
25	--	45.3	--	--
WBS4				
0	20.79	--	0.40	1.59
5	21.15	19.9	0.42	1.54
10	19.85	18.5	0.43	1.51
15	26.65	20.4	0.41	1.56
20	28.15	23.4	0.42	1.54
25	30.25	32.7	0.44	1.49
30	30.91	38.4	0.44	1.49
35	30.22	41.5	0.37	1.68

APPENDIX 3

Figure 3A.1: Grain size distribution curves for Guelph Permeameter grab samples (■ , ▲ , X) compared to August 2009 field samples (◆)

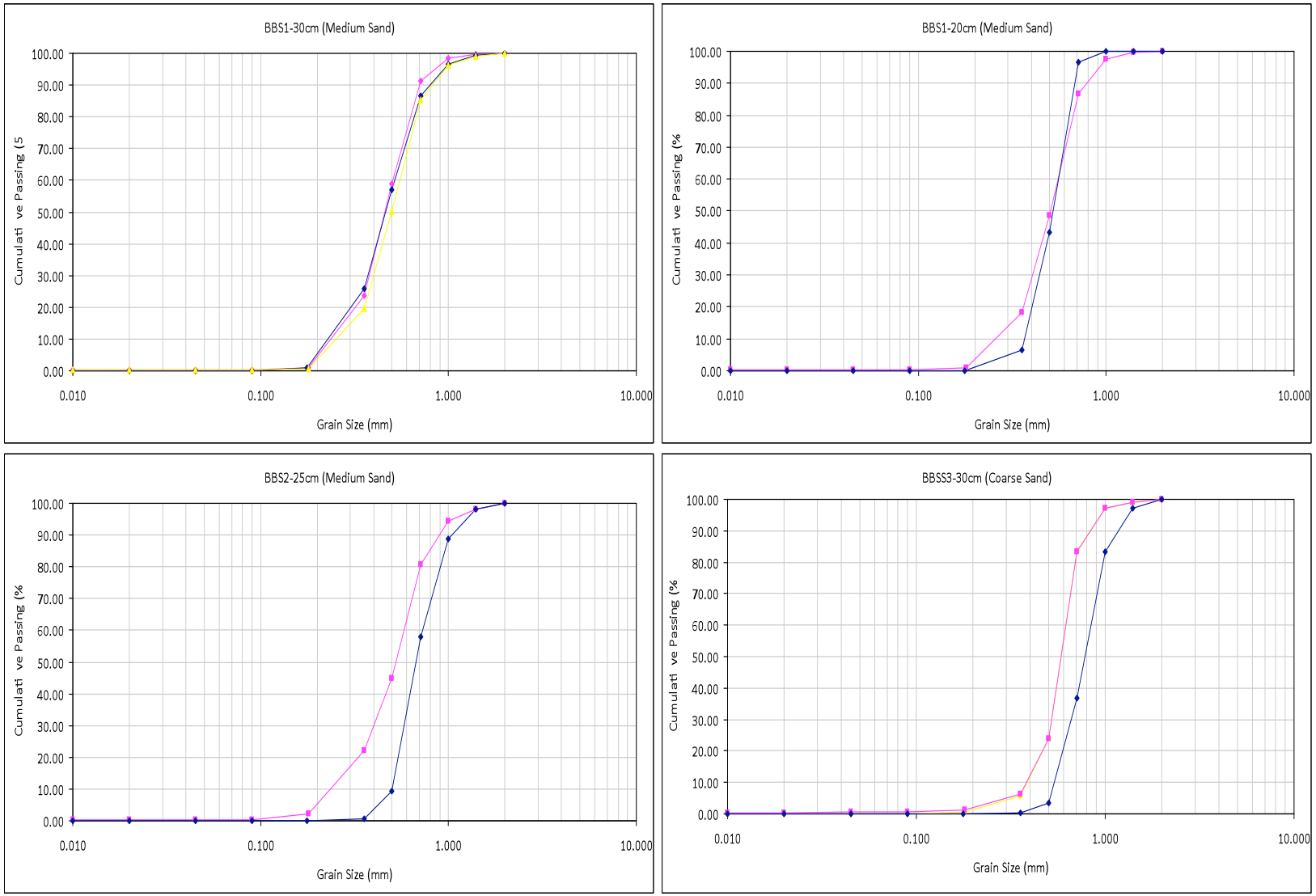

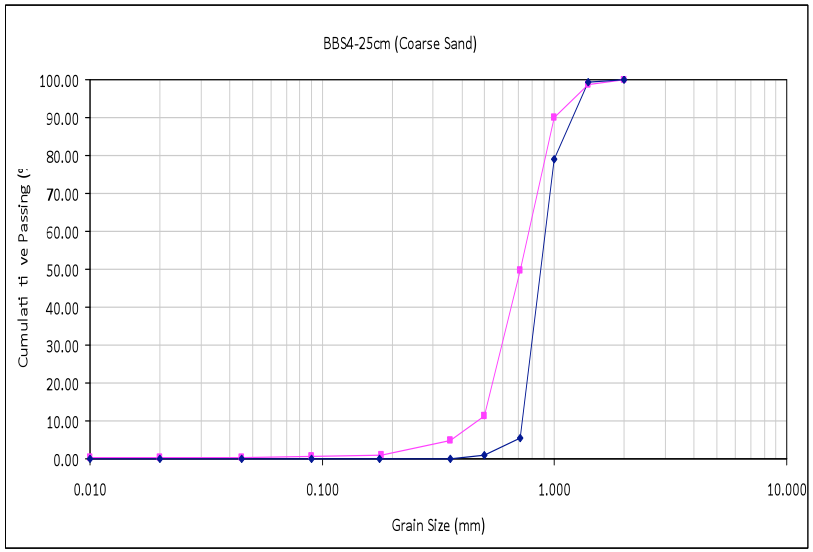
BBS4-25cm (Coarse Sand)
Cumulati ti ve Passing (%
100.00
90.00
80.00
70.00
60.00
50.00
40.00
30.00
20.00
10.00
0.00
0.010
0.100
1.000
10.000
Grain Size (mm)

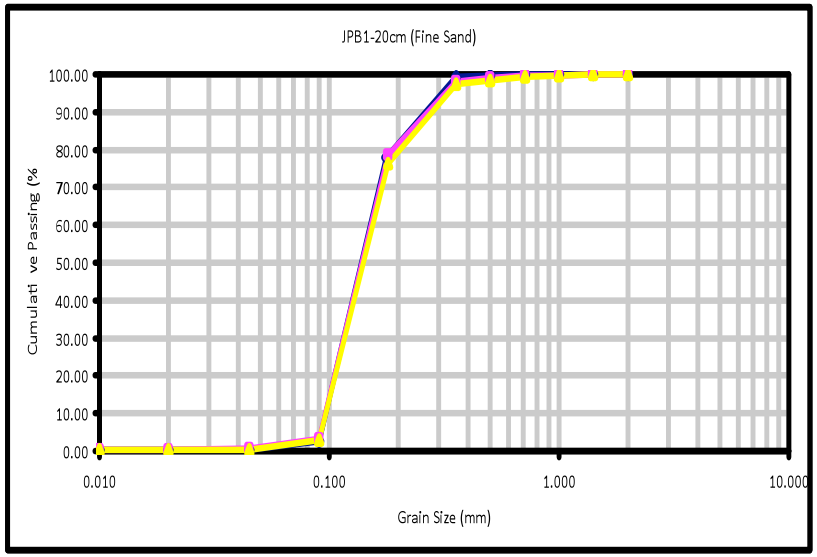
JPB1-20cm (Fine Sand)
Cumulati ve Passing (%
100.00
90.00
80.00
70.00
60.00
50.00
40.00
30.00
20.00
10.00
0.00
0.010
0.100
1.000
10.000
Grain Size (mm)

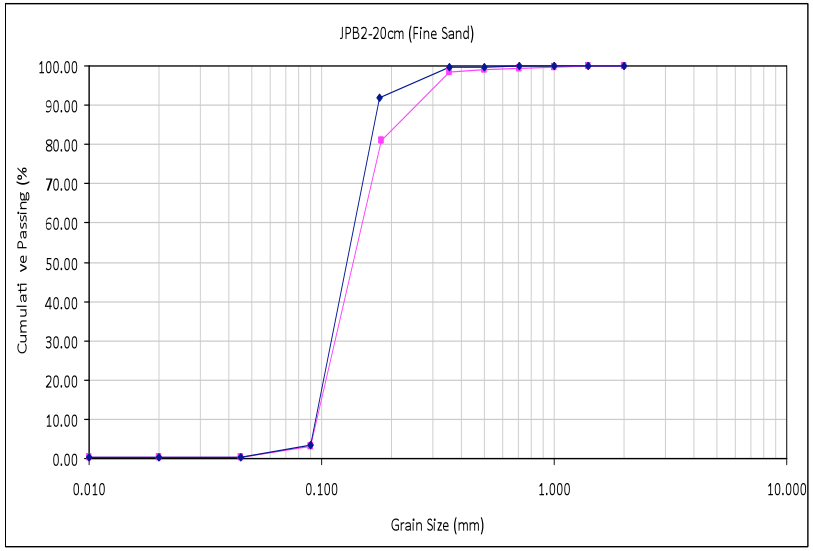
JPB2-20cm (Fine Sand)
Cumulati ve Passing (%
100.00
90.00
80.00
70.00
60.00
50.00
40.00
30.00
20.00
10.00
0.00
0.010
0.100
1.000
10.000
Grain Size (mm)

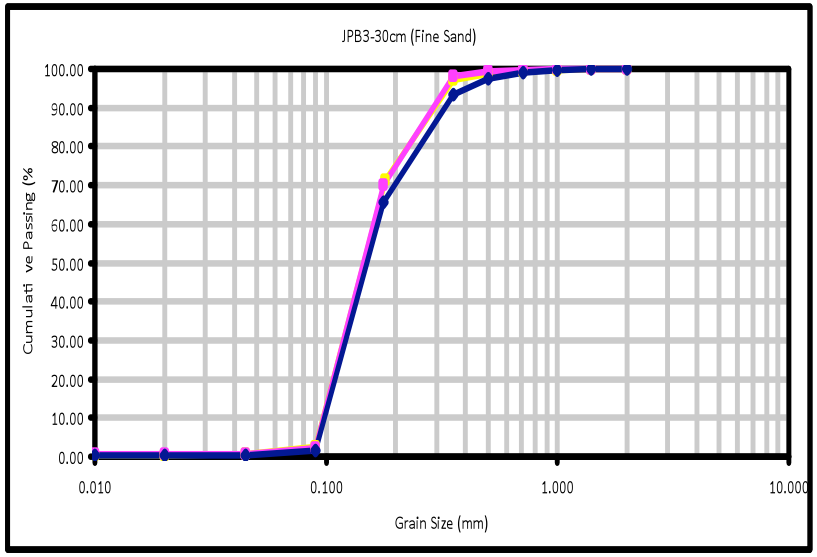
JPB3-30cm (Fine Sand)
Cumulati ve Passing (%
100.00
90.00
80.00
70.00
60.00
50.00
40.00
30.00
20.00
10.00
0.00
0.010
0.100
1.000
10.000
Grain Size (mm)

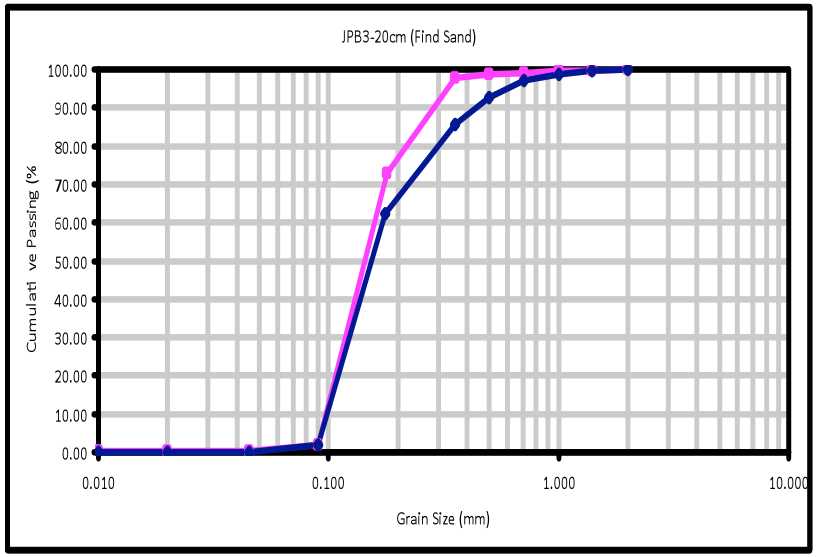
JPB3-20cm (Find Sand)
Cumulati ve Passing (%
100.00
90.00
80.00
70.00
60.00
50.00
40.00
30.00
20.00
10.00
0.00
0.010
0.100
1.000
10.000
Grain Size (mm)

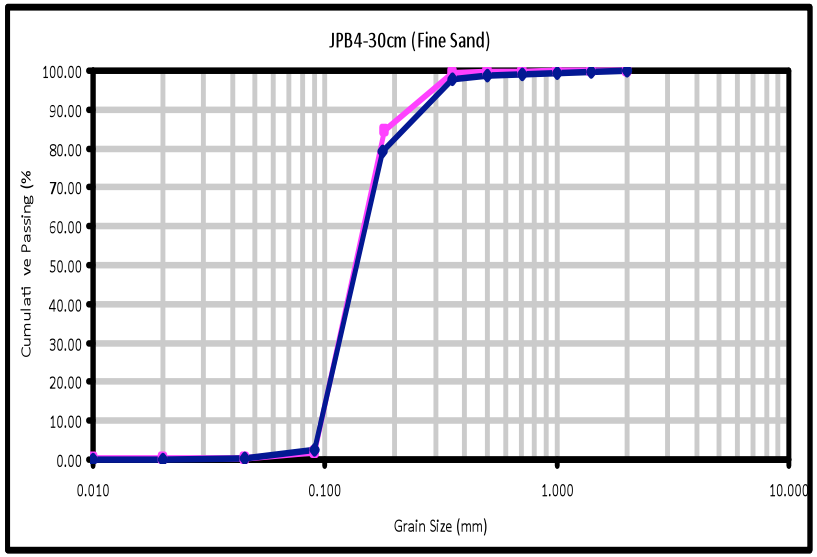
JPB4-30cm (Fine Sand)
Cumulati ve Passing (%
100.00
90.00
80.00
70.00
60.00
50.00
40.00
30.00
20.00
10.00
0.00
0.010
0.100
1.000
10.000
Grain Size (mm)

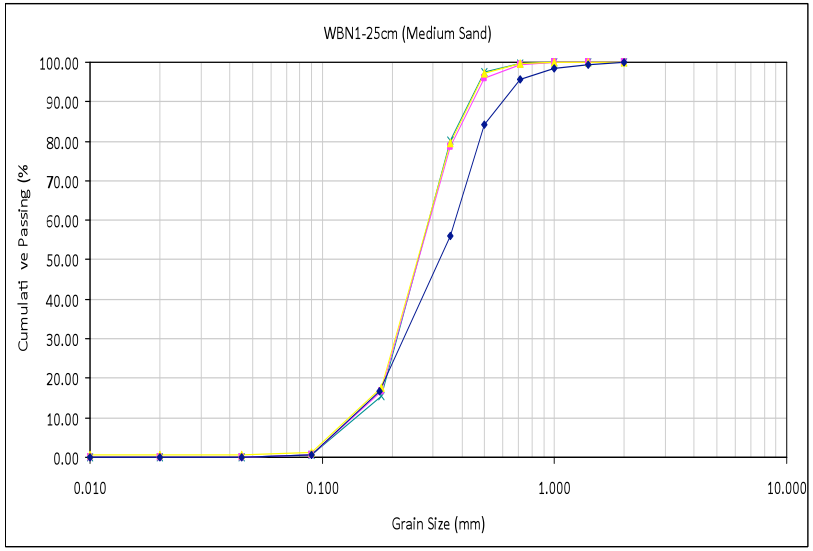
WBN1-25cm (Medium Sand)
Cumulati ve Passing (%
100.00
90.00
80.00
70.00
60.00
50.00
40.00
30.00
20.00
10.00
0.00
0.010
0.100
1.000
10.000
Grain Size (mm)

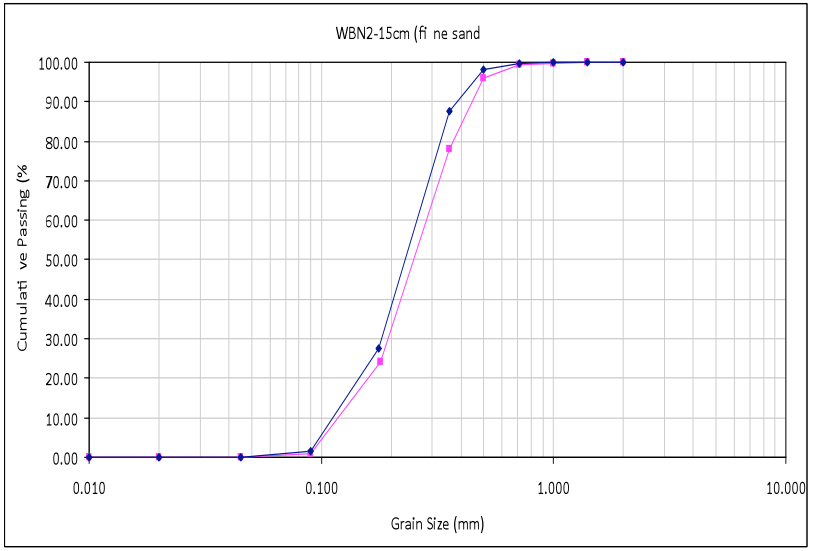
WBN2-15cm (fi ne sand
Cumulati ve Passing (%
100.00
90.00
80.00
70.00
60.00
50.00
40.00
30.00
20.00
10.00
0.00
0.010
0.100
1.000
10.000
Grain Size (mm)

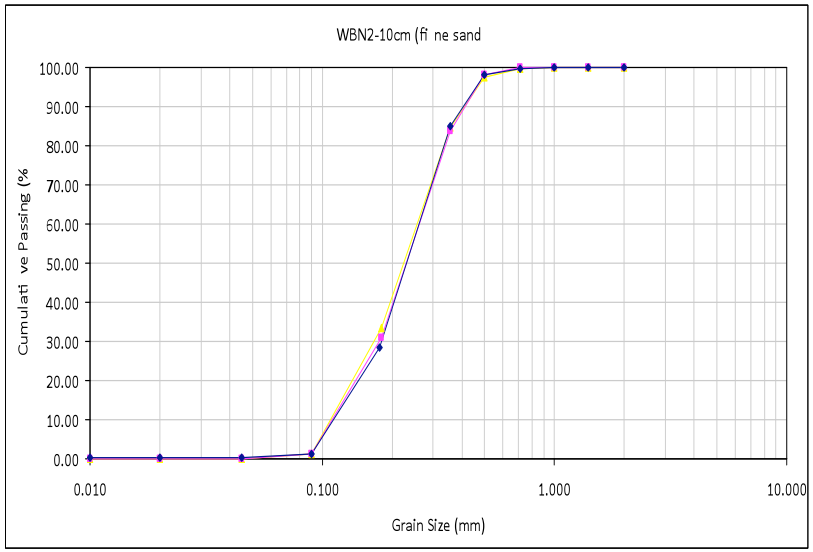
WBN2-10cm (fi ne sand
Cumulati ve Passing (%
100.00
90.00
80.00
70.00
60.00
50.00
40.00
30.00
20.00
10.00
0.00
0.010
0.100
1.000
10.000
Grain Size (mm)

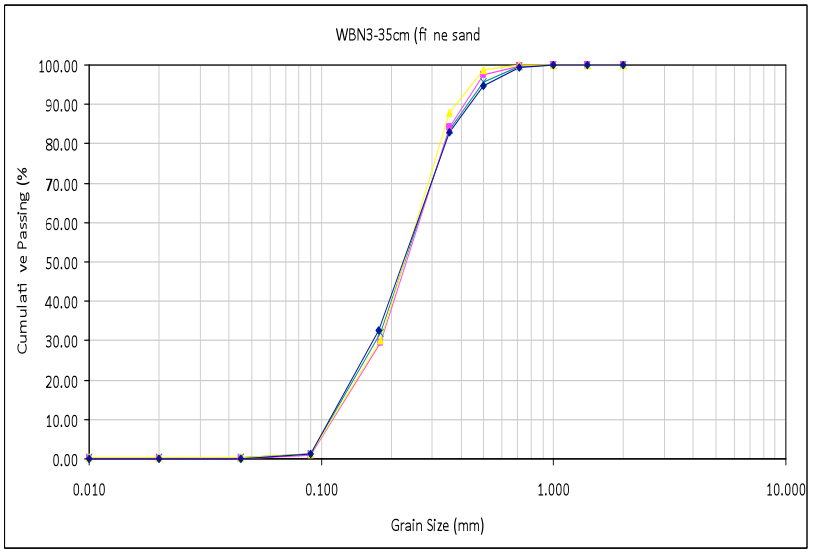
WBN3-35cm (fi ne sand
Cumulati ve Passing (%
100.00
90.00
80.00
70.00
60.00
50.00
40.00
30.00
20.00
10.00
0.00
0.010
0.100
1.000
10.000
Grain Size (mm)

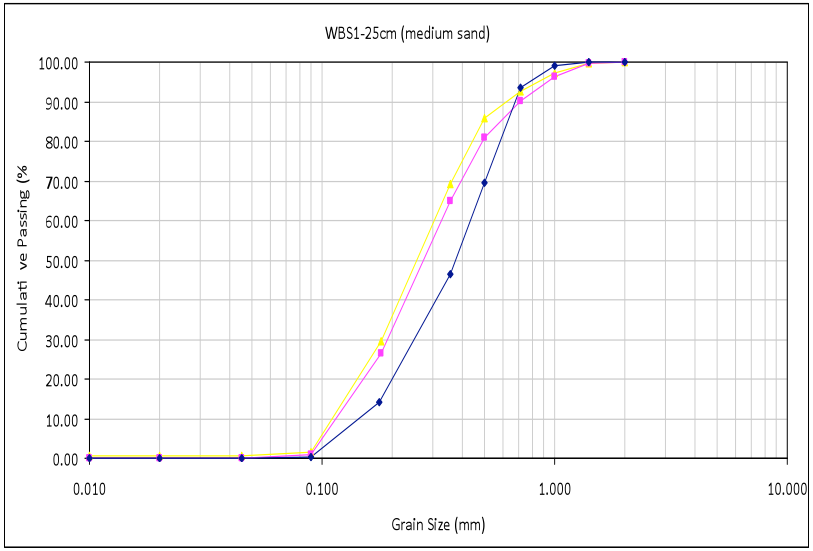
WBS1-25cm (medium sand)
Cumulati ve Passing (%
100.00
90.00
80.00
70.00
60.00
50.00
40.00
30.00
20.00
10.00
0.00
0.010
0.100
1.000
10.000
Grain Size (mm)

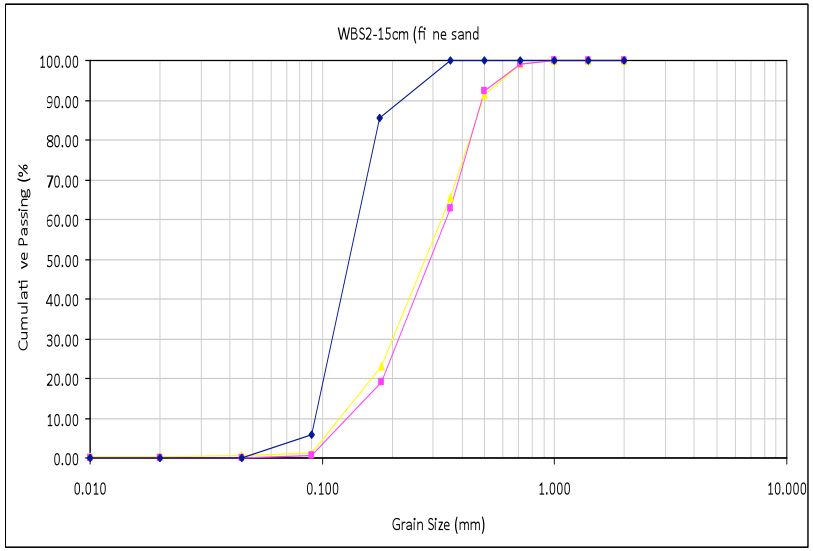
WBS2-15cm (fi ne sand
Cumulati ve Passing (%
100.00
90.00
80.00
70.00
60.00
50.00
40.00
30.00
20.00
10.00
0.00
0.010
0.100
1.000
10.000
Grain Size (mm)

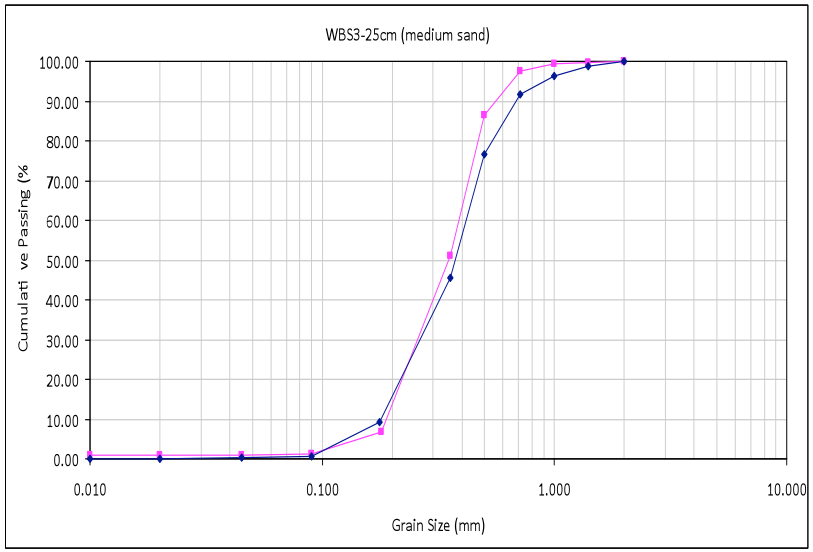
WBS3-25cm (medium sand)
Cumulati ve Passing (%
100.00
90.00
80.00
70.00
60.00
50.00
40.00
30.00
20.00
10.00
0.00
0.010
0.100
1.000
10.000
Grain Size (mm)

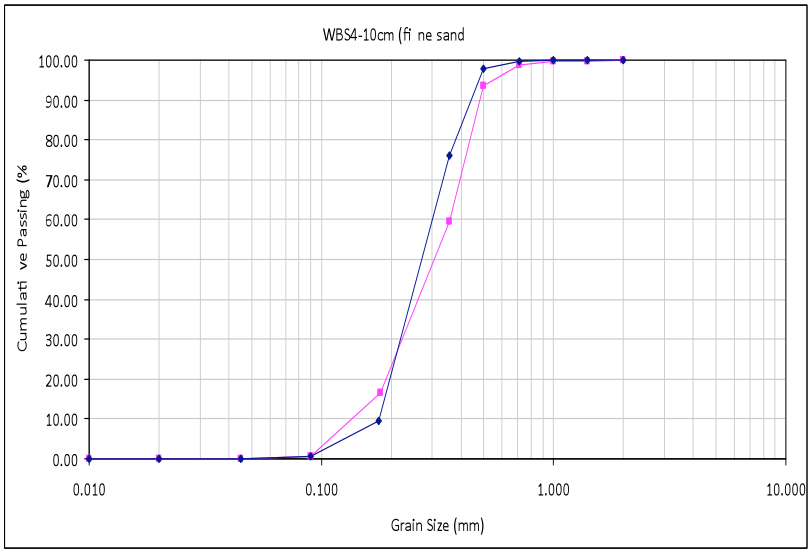
WBS4-10cm (fi ne sand
Cumulati ve Passing (%
100.00
90.00
80.00
70.00
60.00
50.00
40.00
30.00
20.00
10.00
0.00
0.010
0.100
1.000
10.000
Grain Size (mm)

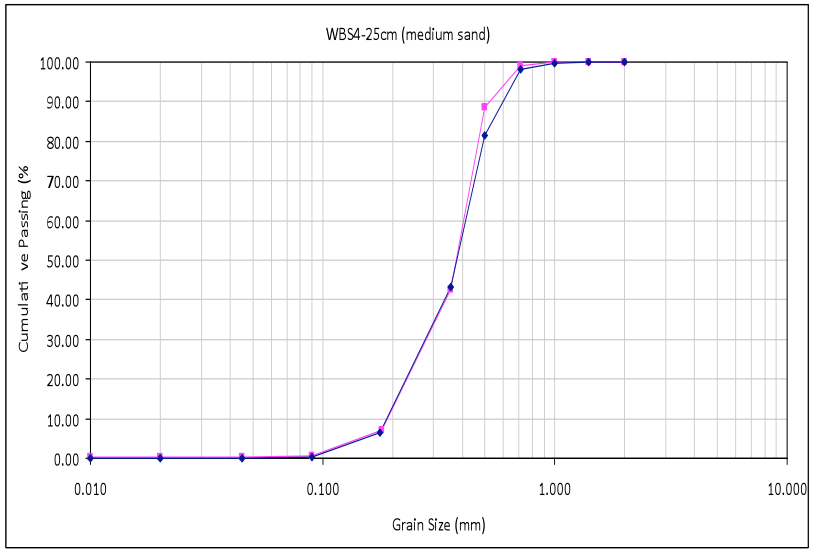
WBS4-25cm (medium sand)
Cumulati ve Passing (%
100.00
90.00
80.00
70.00
60.00
50.00
40.00
30.00
20.00
10.00
0.00
0.010
0.100
1.000
10.000
Grain Size (mm)

Table 3A.1: Single-factor ANOVA test on the statistical significant difference between measured field-saturated hydraulic conductivities between beaches.

Critical Value = 3.88				
	BBS (n = 7)	JPB (n = 7)	WBN (n = 7)	WBS(n = 7)
BBS		***14.001**	***12.049**	***10.22**
JPB			2.801	3.781
WBN				1.209
WBS				

- **Statistically significantly different**

Table 3A.2: Single-factor ANOVA test on the statistical significant difference between the Guelph Permeameter method (K_{fs}) and the Empirical Methods (K_{sat})

Critical Value = 3.912					
	Guelph Permeameter (Kfs) (n = 30)	Hazen (Ksat) (n= 30)	Slitcher (Ksat) (n= 30)	Beyer (Ksat) (n= 30)	Kozeny-Carman (Ksat) (n= 30)
Guelph Permeameter (Ksat)		0.257	***5.828**	0.35	2.445
Hazen (Ksat)			***6.086**	0.607	2.188
Slitcher (Ksat)				***5.479**	***8.273**
Beyer (Ksat)					2.795
Kozeny-Carman (Ksat)					

- **Statistically significantly different**

Table 3A.3: Single-factor ANOVA test on the statistical significant difference between the adjusted Guelph Permeameter method (K_{sat}) and the Empirical Methods (K_{sat})

Critical Value = 3.912					
	Guelph Permeameter (Kfs) (n = 30)	Hazen (Ksat) (n= 30)	Slitcher (Ksat) (n = 30)	Beyer (Ksat) (n = 30)	Kozeny-Carman (Ksat) (n = 30)

Guelph Permeameter (Ksat)		***7.610**	***13.610**	***8.217**	***5.422**
Hazen (Ksat)			***6.086**	0.606	2.188
Slitcher (Ksat)				***5.479**	***8.294**
Beyer (Ksat)					2.795
Kozeny-Carman (Ksat)					

- **Statistically significantly different**

Table 3A.4: Single-factor ANOVA testing the statistical significant difference among modified empirical methods in predicting the field saturated hydraulic conductivities at the Tiny Township beaches

Critical Value = 4.199				
	Hazen-Calibrated (n= 4)	Slitcher-Calibrated (n= 4)	Beyer-Calibrated (n= 4)	Kozeny-Carman-Calibrated (n= 4)
BBS		0.0459	0.0289	0.0336
JPB			0.0747	0.0624
WBN				0.0123
WBS				

*** Statistically significantly different**

APPENDIX 4

Table 4A.1: Calibrated (best fit) water table positions compared to measured field data

Location (model x-coordinate)	Field Surface (model y-coordinate)	Field Water Table (model y-coordinate)	Calibrated Water Table (model y-coordinate)
Balm Beach South			
Lake (2000)	252	252	252
Hole1 (2474)	289	248	254
BBS1 (2825)	319	252	259
BBS2 (3449)	313	260	260
BBS3 (3926)	339	265	265
BBS4 (4445)	378	269	269
Hole6	414	270	270
Boundary (8000)			280
Jackson Park Beach			
Lake (2000)	236	236	236
Hole1 (2220)	273	235	237
Hole2 (2575)	273	236	237
JPB1 (3087)	280	239	239
Hole4 (3578)	287	240	240
JPB2 (4102)	294	243	243
Hole6 (4582)	307	246	244
JPB3 (5107)	316	251	247
JPB4 (6086)	335	260	250
Boundary (9000)			265
Woodland Beach North			
Lake (2000)	220	220	220
Hole1 (2440)	245	226	224
WBN1 (3003)	280	266	226
WBN2 (3330)	303	231	230
WBN3 (4005)	335	234	233
Hole5 (4610)	380	237	237
Boundary (7000)			248
Woodland Beach South			
Lake (2000)	233	233	216
Hole1 (2930)	262	219	218
WBS1 (3285)	275	221	220
Hole3 (3575)	271	224	223
WBS2 (3975)	250	228	229
Hole5 (4345)	261	236	234
WBS3 (4715)	269	241	240
Hole7 (5090)	279	245	245
WBS4 (5750)	294	258	255
Hole9 (6110)	325	274	260
Boundary (9000)			297 (q = 92cm/day)

[1]Measurement error during field collection, [2]High water level due incoming storm, [3]High water level possibly as a result of a localized low K_{sat} layer due to man-induced alteration of the beach